Vehicle-based modelling of traffic

Theory and application to environmental impact modelling

vorgelegt von
Nils Gustaf Eissfeldt
aus Aachen

Köln 2004

Berichterstatter: Prof. Dr. Rainer Schrader
Priv.-Doz. Dr. Andreas Schadschneider

Tag der mündlichen Prüfung: 14.06.2004

"Verba volant, scripta manent."

"Computers are useless. They can only give you answers."
Pablo Picasso (1881-1973)

"I have made this (letter) longer, because I have not had the time to make it shorter."
Blaise Pascal (1623-1662)

Contents

List of Figures

Abstract

This dissertation addresses vehicle-based approaches to traffic flow modelling. Having regard to the inherent dynamic nature of traffic, the investigations are mainly focused on the question, how this is captured by different model classes. In the first part, the dynamics of a microscopic car-following model (SKM), presented in [113], is studied by means of computer simulations and analytical calculations. A classification of the model's behaviour is given with respect to the stability of high-flow states and the outflow from jam. The effects of anticipatory driving on the model's dynamics is explored, yielding results valid in general for this model class. In the second part, a new approach is introduced based on queueing theory. It can be regarded as a microscopic implementation of a state-dependent queueing model, using coupled queues where the service rates additionally depend on the conditions downstream. The concept is shown to reproduce the dynamics of free flow and wide-moving jams. This is demonstrated by comparison with the SKM and real world measurements. An analytical treatment is given as well. The phenomena of boundary induced phase transitions is further addressed, giving the complete phase diagrams of both models. Finally, the application of the queueing approach within simulation-based traffic assignment is demonstrated in regard to environmental impact modelling.

Kurzzusammenfassung

In dieser Arbeit werden fahrzeugbasierte Verkehrsflussmodelle behandelt. Angesichts der dynamischen Natur von Straßenverkehr steht dabei der Aspekt im Vordergrund, wie diese in unterschiedlichen Modellansätzen wiedergegeben wird. Im ersten Teil der Arbeit wird die Dynamik eines mikroskopischen Fahrzeugfolgemodells (SKM) [113] mit Hilfe von analytischen Methoden und Simulationen untersucht. Das Modellverhalten wird anhand der Stabilität der Hochflusszustände und des Flusses aus dem Stau klassifiziert. Der Einfluss von Antizipation auf die Modelleigenschaften wird anhand eines erweiterten SKM untersucht. Die Resultate sind auf andere Fahrzeugfolgemodelle übertragbar. Im zweiten Teil wird ein neuer Modellansatz eingeführt. Dieser kann als mikroskopische Implementierung eines zustandsabhängigen Warteschlangenmodells betrachtet werden. In diesem sind aufeinanderfolgende Warteschlangen miteinander derart gekoppelt, dass ihre Bedienzeiten vom Zustand beider Warteschlangen abhängen. Dieser Ansatz erlaubt die Modellierung von rückwärtslaufenden Staus, wie durch eine analytische Behandlung des Modells sowie durch Simulationsvergleiche mit dem SKM und Realdaten gezeigt wird. Zusätzlich wird in der Arbeit das Phänomen randinduzierter Phasenübergänge behandelt und die Phasendiagramme beider Modelle werden abgeleitet. Die Arbeit schließt mit der Einbettung des Warteschlangenmodells in die Methode der simulationsbasierten dynamischen Verkehrsumlegung und zeigt die praktische Anwendbarkeit des Modelles anhand der Untersuchung verkehrsbedingter Umweltbelastungen.

Chapter
1

Introduction

It is a fact that daily traffic volumes continuously increase. And the situation will not change in regard to the predicted growth of transportation of goods and business traffic. Todays traffic volumes already virtually exceed the existing road infrastructure, in particular in conurbations. The resulting bottlenecks lead to congestion which is not only affecting the people wasting their time standing inside a jam. Congested road networks do, moreover, cause economic costs and have a strong impact on humans and environment. Due to financial and spatial restrictions, the possibilities of a further increase of road infrastructure are limited. Therefore, strategies are necessary which allow for a more efficient use of existing capacities by redistribution of traffic streams and demand.

The instruments of intelligent transportation systems (ITS) aim at an optimal redistribution of traffic demand by providing information about the traffic conditions inside a network, and active traffic control, besides other objectives. To this end, simulation models of traffic flow play an important role in order to obtain a net-wide description of the traffic state, based on local measurements, and to allow for the prediction of the future state, at least in short-term. Moreover, such models can be used for the testing and evaluation of ITS measures before they are implemented in practice. An important methodical framework in this context is given by dynamic traffic assignment (DTA) (see section 4.3). DTA predicts route choice, network flows, link travel times and route travel costs on a given transportation network with a given travel demand. Again, models of traffic flow can be seen as one principle component of DTA.

These models have to meet the requirement that the dynamic properties of traffic streams and bottlenecks are modelled properly, in order to obtain a valid representation of the traffic patterns which result from the given demand. If individual information about routes or the control of individual traffic behaviour by means of ITS measures are addressed, a modelling based on vehicles is favourable. The same is true for the modelling of environmental impacts of traffic streams, because the amount of emitted pollutants by cars depends not only on mean traffic

volumes but depends moreover strongly on dynamic effects as congestion and single vehicular dynamics.

That is the point where this work starts. Within a collaboration with meteorologists [164] a model chain was to be built up which is able to compute the impact situation in respect of air pollution taking into account the impacts of street traffic (see appendix B). Starting the project, it was intended to use a sequence of models in order to compute emission inventories of traffic flow in the following way: In a first step, the route choice of a given traffic demand is computed by means of DTA, using a computationally very efficient model based on queueing theory [59, 60]. In a second step, the individual trips computed in the DTA step are simulated by means of a microscopic car-following model (SKM,[112, 113]) which yields a dynamic description of traffic situations appropriate for the computation of emission inventories.

Using the described procedure, difficulties arise from the fact, that the calibration of model parameters has not to be done only for the two models themselves, which is already a tedious task. Moreover, the representation of dynamic bottlenecks and congested periods has to be captured similar in both models. This is in particular important, if oversaturated network flows occur, which is frequently the case for the network[1] under consideration. Otherwise, *gridlocking* can lead to incompatibilities between the two models, to name just a main problem which has been encountered.

Therefore, it is not very far fetched to try the computation of emissions within the DTA, skipping the second step. However, investigations of the simple queueing approach in use have shown, that an appropriated description of traffic dynamics is not given, *i.e.*, there is no backward propagation of jams and throughputs at bottlenecks tend to be too high. These findings are also true for many approaches used in traffic flow modelling based on traditional queueing theory (see appendix A).

The main objective of this work is, in consequence of the above findings, the introduction of a vehicle-based model of traffic flow by means of queueing theory, which is able to describe the dynamics of traffic states on a detailed level without sacrificing computational efficiency needed in DTA.

Besides, the discussion strongly focuses on the investigation of dynamic properties of microscopic models, due to their importance not only for application purposes. It is a challenging task to understand the dynamics of traffic which can be seen as complex system of many interacting particles driven far from equilibrium. Within this context, there are many open questions related to the understanding of the basic mechanisms that are responsible for traffic flow breakdown. In order to explore where the models in use nowadays fail in their description and which

---

[1]The main road network of the city of Cologne including the highway ring enclosing the city.

properties are essential in regard to the reproduction of empirical findings, it is important to well understand their inner working. This can obviously not done in general in this work. Therefore, only some of the given aspects are addressed for the microscopic car-following model SKM and the queueing approach introduced here.

This work is organised as follows:

Chapter 2 gives the definition of the microscopic car-following model SKM, besides a short review of microscopic model approaches and empirical findings. Its dynamic properties are discussed in detail. The SKM is extended in respect to anticipatory driving and the consequences of this extension in regard of the model's dynamics are investigated. The chapter closes with investigations of boundary induced phase transitions within both model variants.

In chapter 3, the application of traditional queueing theory to traffic flow is discussed focusing on their ability to capture the dynamics of traffic streams. A new approach is presented which can be regarded as a microscopic implementation of state-dependent queueing systems, using coupled queues where the service rates additionally depend on the conditions downstream. Its properties are investigated in great detail, including the comparison with the SKM and the computation of vehicular emissions.

The modelling of network flows within the new approach are studied in chapter 4. The role of the model within DTA is further discussed before results of environmental impact modelling are presented which stem from the collaboration described above.

The main results of this work are summarised in chapter 5.

Microscopic Car-Following Models

2.1 Microscopic models of traffic flow

Researchers from widely varying disciplines, such as transportation engineering, civil engineering and physics, have utilised different techniques to study traffic interaction and movement. This wide interest originates from the necessity to understand the nature of traffic streams in order to allow a more efficient use of existing road capacities. Besides this practical point of view it is a challenging task to understand the complex dynamics of traffic which can be seen as a complex system of many interacting particles driven far from equilibrium.
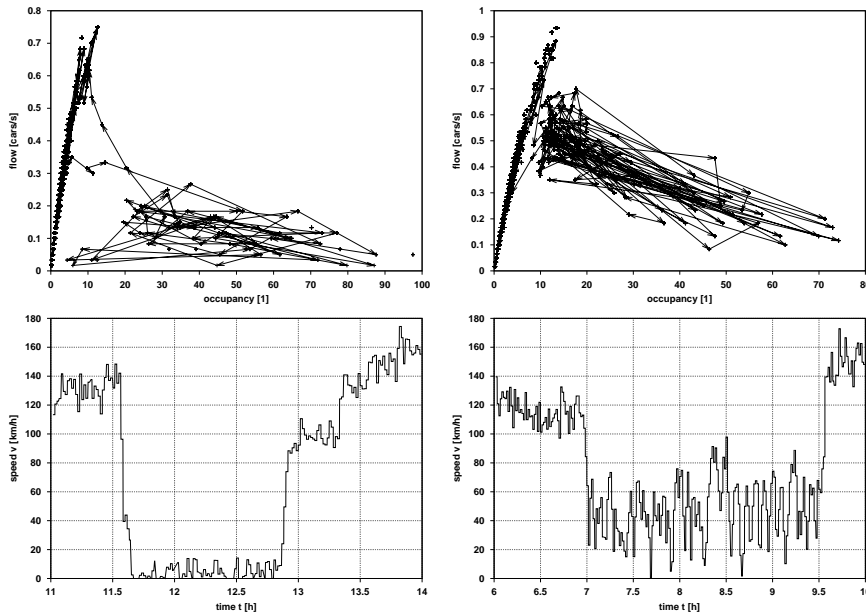
This work focuses on microscopic models of traffic flow. It is therefore necessary to introduce the most important terms and properties of traffic flow before starting the discussion of specific models.

2.1.1 Empirical properties of traffic flow

Numerous empirical data of highway traffic have been obtained, which demonstrate the existence of qualitatively different dynamic states (or phases). It is still under discussion, how many states exist in traffic flow and how the measurements have to be interpreted. Many researchers tend to believe that three dynamic phases, distinct from each other, are observed on highways: *free flow*, *traffic jam* and *synchronised traffic* [76, 91, 108]. The last two traffic states are frequently referred to as *congested flow*. In the measurements one finds moreover that the complexity in traffic flow is related to certain transitions between the basically different types of traffic [90, 101]. The following description of traffic states partially follows [103].

Typical quantities used to characterise traffic states are

- the density ρ, which gives the number of cars in a certain section of a road,

- the velocity v and
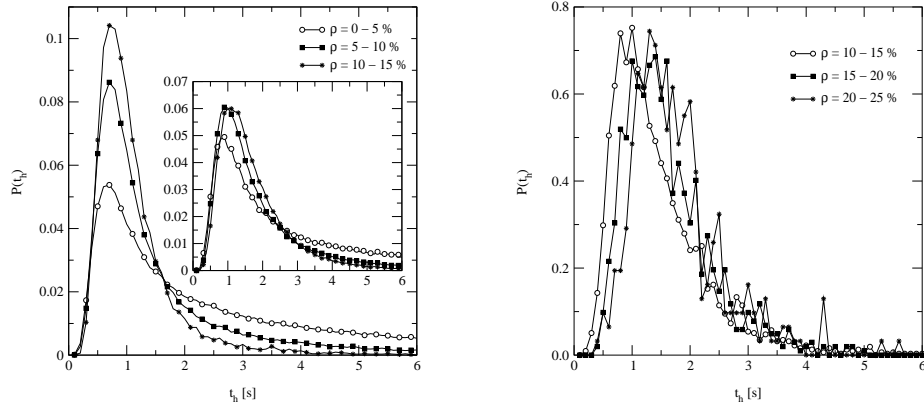
Figure 2.1   Flow-density relations (*top*) and time-series of the velocity (*bottom*) measured on highways in Germany. The figures are taken from [108] and slightly modified [178]. The arrows indicate the direction of time. **Left**: Wide moving jam. **Right**: Synchronised flow.

   - the flow q, which gives the number of cars that pass a cross-section during
     a specific time slice. The maximum possible flow at a specific cross-section
     is also referred to as *capacity* of the cross-section.

These quantities are usually measured at detector loops by means of time averages. Note that the velocity and the flow can be measured at a cross-section (*i.e.*, locally), whereas the density is a spatial quantity which has to be approximated (*e.g.*, the hydrodynamical relation $\langle\rho\rangle = \langle q\rangle\langle 1/v\rangle$ can be used if stationary flow is assumed). The representation of the measured flow versus the density is called *flow-density relation* or *fundamental diagram* (FDR), see figure 2.1.

In the regime of *free flow* all vehicles can move according to their individual maximum velocity and interactions between vehicles occur rarely. The average velocity of this state is, therefore, quite large. Free-flow states are found at low densities in the FDR. They form the *low-density branch* and the flow grows more or less linear with the density.

If the density grows up to a critical value, the free-flow state becomes unstable and breaks down to congested flow. Note that nothing will be said here about the mechanism of breakdown. In the regime of congested flow the velocities are rather small. In figure 2.1 one can clearly see that in the congested state two different

Figure 2.2 Distribution of the time-headways measured on highways in Germany for the free flow (*left*) and synchronised flow (*right*). The figures are taken from [108].

types of behaviour can be distinguished.

In traffic jams (or *wide moving jams*) vehicles form compact structures which possess two fronts separated by a region of negligible velocity and flow. The width of these structures is much larger than its fronts at the upstream and downstream ends where the speed of vehicles changes sharply. The structures move against the direction of traffic flow, *i.e.*, upstream. One finds a line with negative slope in the FDR, *i.e.*, the flow decreases with increasing density. This line is called *high-density branch* of the FDR. The intersection of this branch with the low-density branch gives the *outflow from jam*. The size of this flow is an intrinsic property of jams and this flow is stable [100]. Besides this, jams can be characterised by the propagation velocity of the downstream front and their density.

In *synchronised traffic* the velocity is considerably smaller than in free flow but the flow can still have large values, see figure 2.1.

The name of this phase stems from the observation that the time-series of measurements on different lanes are highly correlated. However, this is also true for wide moving jams. The German expression 'zähfließender Verkehr' is more suited to describe the situation. In the FDR one observes irregular patterns, *i.e.*, there is no functional relationship between density and flow as for the other two traffic states.

The relation between ρ and q in the FDR can be used to give a helpful measure in order to identify the three traffic states in time-series of loop detector data. If one addresses the cross-correlation $c(\rho, q)$ between flow and density, $c \approx 1, 0, -1$

holds for free flow, synchronised flow and wide moving jams, respectively[140].

In figure 2.1 one can see a region $\rho_f \leq \rho \leq \rho_c$ in which the free flow and congested flow coexist (*cf.* also figure 2.5). For densities $\rho < \rho_f$ laminar traffic flow is always stable, whereas traffic is always found in the congested state for $\rho > \rho_c$. In the intermediate density regime traffic can be in one of the two states. The states on the free-flow branch in this density regime are also called *high-flow states*. Disturbances of these states can lead to a breakdown onto the high-density branch. In most observations one finds that the system can only recover back to the low-density branch passing the density ρ_f. This is called *hysteresis* which typically occurs in connection with phase transitions of first order. Note that figure 2.1 gives an example of a differing behaviour (see also discussion on *p.* 38). Further note that the flow q_f at density ρ_f equals the outflow from jam which is smaller than the maximum flow $q_c = q(\rho_c)$. The finding $q_f < q_c$ is referred to as *capacity drop* in literature.

The measures discussed so far are quantities averaged over time. A more detailed characterisation of traffic states can be obtained by means of microscopic measurements from single-vehicle data [108]. One important microscopic variable is the *time-headway* between two consecutive cars. The time-headway τ_h is given by the time which elapses between two vehicles passing a detector. If one assumes a constant velocity v of the vehicles, $\tau_h v$ equals the (spatial) headway or *gap g* between the vehicles. Figure 2.2 shows typical time-headway distributions found in free and synchronised flow. In the free flow, the distributions within different density regimes show a maximum which is independent of density. Note the existence of very short time-headways. In contrast, the distributions in synchronised flow have a maximum that is much broader and less pronounced. Its position depends significantly on the density. For further details see [103, 106, 108].

2.1.2   Microscopic model approaches

In principle, there exist two different approaches to model traffic flow: *microscopic* and *macroscopic* ones. Whereas in microscopic models different vehicles and their velocities (or further state variables) can be distinguished, in macroscopic models only aggregated variables as density, velocity and flow are considered.

Macroscopic models are usually based on methods found in hydrodynamics and gas-kinetic models of physics. They widely use partial differential equations to describe the relation between the aggregated quantities. Models of that kind are not addressed in this work. A comprehensive overview can be found in [73, 74].

In contrast, the movement of individual vehicles along a road is modelled in great detail in microscopic approaches. The interaction between two consecutive cars is considered explicitly. Since in these models cars follow each other the

term *car-following model* is often used. A short categorisation of microscopic car-following models is given in the sequel. Extensive reviews of microscopic models can be found in [33, 134] and references therein.

Differential equations

If one assumes that the motion of a vehicle v is governed exclusively by the vehicle in front and further that the following car adopts the velocity of its predecessor $\tilde{v}$ (in order to avoid collisions), the dynamic can be described by means of an ordinary differential equation [146],

$$\frac{dv(t)}{dt} = \frac{\tilde{v}(t) - v(t)}{\tau},$$
(2.1)

with τ being a relaxation time. However, no cluster effects can be modelled by (2.1). This drawback can be overcome by the introduction of a finite reaction time Δt which leads to the description as delayed differential equation [28],

$$\frac{dv(t)}{dt} = \left.\frac{\tilde{v}(t) - v(t)}{\tau}\right|_{t-\Delta t}.$$
(2.2)

The delay takes into account that a driver does not react instantaneously to the actions of her predecessor. Many such models have been proposed in the fifties, an overview is given in [21].

Newer approaches as the widely used optimal-velocity model [9, 11] and the intelligent-driver model [172, 173] also belong to this class of models.

Cellular automata

Cellular automata are dynamic models in which space, time and state variables are discrete. Discrete space consists of a regular grid of cells of length Δx where each cell can either be empty or occupied by a vehicle. Besides its position on the grid the state of each vehicle is determined by its velocity. The velocity is an integer number and gives the number of cells that the vehicle can jump per time step. Before a car is moved, its current velocity is determined respecting the position of its predecessor to guarantee collision-free motion. All cells are updated in discrete time steps Δt. Due to the exclusive local interaction between vehicles, cellular automata approaches are well suited for large-scale simulations of traffic networks.

The first model of that class, which was proposed in the context of modelling traffic flow, is the well-known Nagel-Schreckenberg model (NaSch) [133]. It is a stochastic model that incorporates imperfections of driving using a noise term

p_{brake} in the update rules:

1. Acceleration: $\quad v(t+\Delta t) \quad \leftarrow \quad \min\{v_{\mathrm{max}}, v(t)+1\}$

2. Deceleration: $\quad v(t+\Delta t) \quad \leftarrow \quad \min\{v(t+\Delta t), g\}$

3. Randomisation: $\quad v(t+\Delta t) \quad \leftarrow \quad \max\{v(t+\Delta t)-1, 0\}$

$\qquad\qquad\qquad\qquad\qquad\qquad$ with probability p_{brake}

4. Motion: $\qquad\quad\; x(t+\Delta t) \quad \leftarrow \quad x(t)+v(t+\Delta t)$

g is the distance to the vehicle in front (measured in cells), v_{max} the maximum velocity (discretised in units of $\Delta x/\Delta t$). A *parallel update scheme* is used, *i.e.*, steps 1 through 3 are executed for each vehicle before all cars are together moved. Despite its simplicity, the model reproduces empirical FDR and spontaneous clustering quite well.

Further extensions of the model have been proposed to obtain better agreement to empirical findings. The NaSch model with velocity-dependent randomisation (VDR) discriminates different levels of noise which depend on the current velocity of a vehicle [14]. If the randomisation is chosen such that the escape of vehicles from a jam is delayed, *metastable states* (which are strongly connected to the existence of a capacity drop and hysteresis, see *p.* 19) and phase separation between jams and free flowing vehicles exist. The delayed escape from a jam is also called *slow-to-start*.

If further interactions among vehicles are taken into account, such as anticipation (*cf.* section 2.3) and an increased interaction horizon, even empirical single-vehicle data can be reproduced with cellular automata models. Long ranged interactions can be introduced by means of a brake light if drivers inside the interaction horizon react on brakings of the leading vehicle. The brake light version of the NaSch model (BL) was first introduced in [104, 105].

A detailed discussion about the dynamic properties and the behaviour with respect to empirical findings of different variants of cellular automata based on the NaSch model can be found in [103, 106].

Coupled maps

In models which belong to the class of coupled maps, time is discrete (Δt) and the dynamics of the model is represented by discrete transformations (*map*). In models of traffic flow the maps depend on the state variables of the vehicles. In contrast to cellular automata, the state variables do not have to be discrete. If only interactions between two consecutive cars are taken into account the typical

structure of such models is

$$
\begin{aligned}
v_{t+\Delta t}^{\nu} &= \mathrm{map}_{\nu}(g_t^{\nu}, v_t^{\nu}, \tilde{v}_t) \\
x_{t+\Delta t}^{\nu} &= v_{t+\Delta t}^{\nu} + x_t^{\nu} \Delta t.
\end{aligned}
\tag{2.3}
$$

Depending on the update scheme, the velocity of each car ν is updated according to its map in a first step. The calculated velocity is then used to move the vehicle to its new position. The microscopic car-following models which are further discussed in this chapter belong to this model class.

2.2 Car-following model by Krauß (SKM)

The following discussion focuses on a specific car-following model which is referred to as SKM. On the one hand certain aspects of its dynamics are investigated as well as the effects of anticipatory driving and open boundary conditions.The findings of different model classes, as given in the original work, is revisited in light of recent results. On the other hand this model will be used as a reference during the later discussion of approaches to traffic modelling based on queueing theory.

2.2.1 Dynamical equations

The SKM [112, 113, 114] is based on an approach by Gipps [62] and considers the braking distance of individual cars. Its connection to the NaSch model is investigated in [115].

Starting with the assumption of safe driving, an update scheme can be formulated as coupled map. In the SKM the state variables, *i.e.*, space and velocity, are continuous. In order to formulate the model's equations three basic assumptions have been made, namely,

- that the vehicles travel without colliding,
- that the vehicles do not travel faster than a maximum velocity v_{max}, and
- that the acceleration a and the deceleration b of a vehicle are bounded.

A safety conditions can be derived given the assumption of collision-free driving. Assume one car (driver-vehicle unit) with velocity v is following another car (driving with velocity $\tilde{v}$) within a distance g. Here, g is the free space between vehicles, *i.e.*, the distance between the cars at positions x, $\tilde{x}$ minus the cars' length l_{car}. Safety, *i.e.*, collision-free motion is guaranteed if

$$
d(v) + \tau v \leq d(\tilde{v}) + g
\tag{2.4}
$$

holds, with $d(v)$ being the braking distance needed to stop when driving with velocity v and τ a finite reaction time. When braking with constant deceleration $b > 0$, *resp.* $-b \leq dv/dt$, the braking distance is given by $d(v) = v^2/(2b)$. Equation (2.4) then leads to

$$v_{\text{safe}}(\tilde{v}, g) = -b\tau + \sqrt{b^2\tau^2 + \tilde{v}^2 + 2bg}. \tag{2.5}$$

In order to complete the definition of the model's dynamics it is assumed that each car moves at the highest velocity compatible with the assumptions. Within each time step Δt each car is updated after calculating its v_{safe} according to the following scheme,

$$
\begin{aligned}
v_{\text{des}} &= \min\{v_t + a\Delta t, v_{\text{safe}}, v_{\text{max}}\} \\
v_{t+\Delta t} &= \max\{v_{\text{des}} - \eta\varepsilon a, 0\} \\
x_{t+\Delta t} &= x_t + v_{t+\Delta t}\Delta t.
\end{aligned}
\tag{2.6}
$$

The update (2.6) is done in parallel, *i.e.*, after the velocity update of all cars they are all moved at once. The random fluctuation of strength $\eta\varepsilon a$ is introduced to mimic deviations from the optimal driving strategy given by v_{safe}. η is a random number uniformly distributed in the interval $[0, 1]$ and the parameter ε determines the fluctuation strength in units of a. Microscopic jam nuclei are generated mainly from this noise. Once generated, they can evolve into macroscopic jams independent of noise. Therefore, with $\varepsilon = 0$ the jammed phase vanishes and the rich structure of the model's dynamics disappears (*cf.* slow-to-start behaviour of the SKM, *p.* 15).

It should be noted that the formulation of v_{safe} in (2.5) differs from that given in [113] [1]. The reason is primarily due to the calculation of the update scheme (2.6) becoming more simple. However, its structure meant, we could not find a analytical proof for collision-free driving (as it is possible for the original formulation). But extensive simulations with $\tau \geq \Delta t$ neither gave the merest hint of collisions nor was a crucial difference in the model's dynamics found. The condition $\tau \geq \Delta t$ means that safe driving is possible, if the "true" reaction time, *i.e.*, one time step, is smaller or equal to the reaction time each driver assumes.
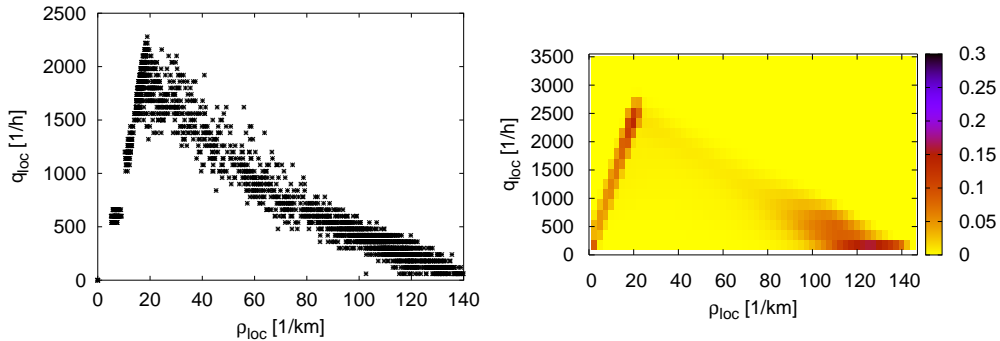
2.2.2   Characteristics of the model

Macroscopic properties

In order to investigate the properties of traffic flow models one frequently uses *periodic boundary conditions*, *i.e.*, a one-lane loop. Figure 2.3 shows a typical

---

[1]In the original work $v_{\text{safe}} = \tilde{v} + 2b(g - \tilde{v})/(v + \tilde{v} + 2b\tau)$ is used.

Figure 2.3 **Left**: FDR of the SKM with periodic boundary conditions. At each global density the loop is initialised homogeneously with 1000 cars. Density and flow are measured locally (virtual detector) after the system becomes stationary. **Right**: Probability of $(\rho_{\text{loc}}, q_{\text{loc}})$. The probability distribution is computed by averaging over simulations at different global densities. Measurements are taken in the stationary state only.

FDR of the SKM. The figure is generated using a periodic system which is initialised homogeneously at different densities. At each global density the update scheme (2.6) is iterated for 50000 time steps. In order to analyse the results, the first half of each simulation is discarded to let transients die out and the system reach a stationary state. In the steady state mean density $\langle \rho \rangle$, mean velocity $\langle v \rangle$ and flow $\langle q \rangle$ are measured at a fixed location using 60 s intervals for sampling (*virtual detector*). The *local density* for a car n passing the detector is defined as

$$\rho_{\text{loc}} = 1/(g_n + l_{\text{car}}). \tag{2.7}$$
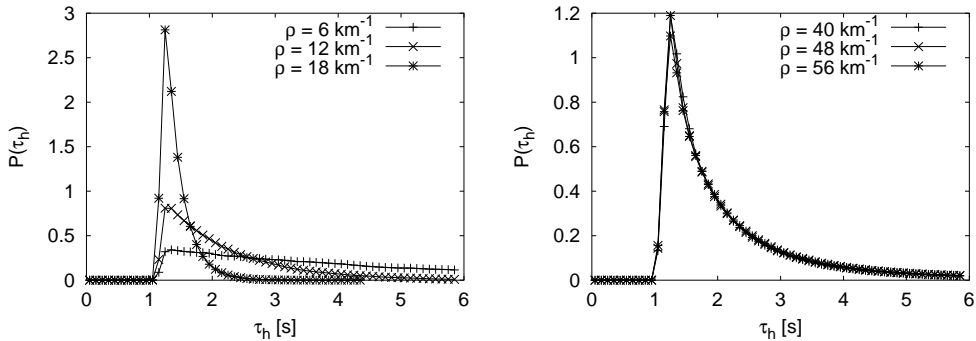
The parameters used are

$$
\begin{array}{lll}
a = 2 \; m/s^2 & b = 8 \; m/s^2 & v_{\max} = 35 \; m/s \\
\varepsilon = 1 & l_{\text{car}} = 7 \; m & \tau = \Delta t = 1 \; s.
\end{array} \tag{2.8}
$$

These parameters are closely related to the real world. Note that the parameter $-b$ has the meaning of a lower bound for the braking ability of cars which hardly occurs in the simulations. Typically, the deceleration of the cars has values around $-1.6 \; m/s^2$.

With respect to these parameters, jam formation (wide moving jams) and high-flow states exist in the SKM as can be seen in figure 2.3 [2]. The existence of the capacity drop indicates *slow-to-start* behaviour. Note that there is no explicit

---

[2]Due to the local measurement the high-flow states cannot be seen so clearly as in the case of global measurements (*cf.* figure 2.18).

Figure 2.4   Time headway distribution of the SKM under free-flow conditions (*left*) and in the congested state (*right*). The parameters used are given by (2.8).

rule introducing this effect. It results from the asymmetry in the randomisation process for low speeds. This is due to the fact that negative gaps and velocities are not allowed in the model. Since the stability of jams is directly related to the fact that the outflow from a jam is smaller than the maximum possible flow [97], macroscopic jams can be observed in the SKM.

In the closed system the congested state coexists with the free-flow state for densities $\rho \geq \rho_f$ ($\rho_f \approx 20 km^{-1}$ in figure 2.3). Already at this point of the discussion it is clearly stated that the SKM only possesses two states of traffic, namely free flow and wide moving jams. Time-series at a fixed density in the regime of coexistence alternately display free-flow and congested states. Intermediate points in figure 2.3 stem from sampling periods in which a jam front crosses the virtual detector. The existence of solely two states can also be seen from the distribution of local densities and flows (see figure 2.3).

Time-headway distribution

Several empirical studies have analysed single-vehicle data from counting loops [10, 108, 110, 140, 170]. Such measurements provide information about the microscopic structure of traffic streams. The investigation of the corresponding observable in stochastic traffic flow models can, therefore, justify their quality.

The *time-headway* is the microscopic analogue of the inverse flow. In real data, it is simply determined by the time difference $\tau_h = t_{\nu-1} - t_\nu$ between the different times t two cars pass an observer. As the SKM has a time step of $\Delta t = 1$ s, a different approach has to be used to measure the time-headway. This is done by using the relation

$$\tau_h = g/v. \tag{2.9}$$

The closed loop still serves as the computer experimental setup. It is initialised at different densities and the time-headway distribution is measured after an appropriate relaxation time (≈ 30000 time steps). The parameters used are given by (2.8).

In figure 2.4 the time-headway distribution of the free-flow phase at different global densities is presented. Empirical investigations show (*cf.* figure 2.2) that in the free flow extremely small time-headways exist ($\tau_h^{min} \approx 0.2\ s$). Moreover, the maximum of the distributions, and its shape at short time-headways are independent of the density [108, 140, 170].

Figure 2.4 shows that the SKM is not able to reproduce such small temporal headways in the free-flow phase. There exists a sharp cut-off at $\tau_h \approx \Delta t = 1\ s$, *i.e.*, the model's dynamics leads to $v_{t+\Delta t} \leq g_t$. The maximum of the distributions is located at $\tau_h \approx 1.3\ s$. In the free flow one finds $\langle v \rangle \approx 34\ m/s$ which corresponds to $\langle g \rangle \approx 41.5\ m$.

The time-headway distributions in the congested state are almost independent of the density. The exponential decay of the distribution results from the fact that for large headways cars can be regarded as virtually independent from each other, implying a Poissonian distribution. Unlike reality the peak is fixed and not as broad. Their maximum is also located at $\tau_h \approx 1.3\ s$, which is close to real world measurements. Since the maximum of the distributions is independent of the global density in the SKM, one can conclude that the model owns a fix point in its dynamics.

Optimal velocity curve

Neglecting fluctuations, the *optimal velocity curve* (OVC) of the SKM can be analytically derived. The OVC gives the relation between velocity and headway and is helpful in order to characterise the microscopic structure of the traffic phases [108, 140, 170].
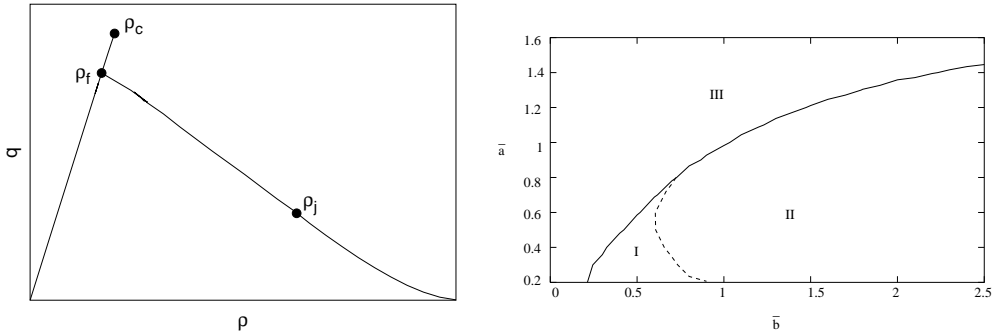
The OVC of the SKM results from its safety condition (2.5), *i.e.*,

$$v_{\text{safe}} = -b\tau + \sqrt{b^2\tau^2 + \tilde{v}^2 + 2bg} = \tilde{v}. \tag{2.10}$$

Equation (2.10) is solved by $\tilde{v} = g/\tau$, therefore, the OVC of the SKM reads

$$V_{\text{opt}}^{\text{SK}}(\rho) = \min\left\{ \frac{1}{\tau}\ \left(\frac{1}{\rho} - \frac{1}{\rho_{\text{max}}}\right), v_{\text{max}} \right\}. \tag{2.11}$$

From (2.11) it follows that $\tau_h^{\text{sk}} \equiv \tau$ for the deterministic case ($\varepsilon = 0$). The OVC confirms the previous result. Time-headways smaller than Δt cannot be modelled by the SKM as $\tau \geq \Delta t$ is required due to safety constraints. As fluctuations lead to $\langle v \rangle < v_{\text{max}}$, $\tau_h^{\text{SK}} \geq \tau$ holds in general.

Figure 2.5 **Left**: Sketch of a FDR with high-flow states. ρ_f, ρ_j are the densities in the outflow region of a jam and inside a jam, respectively. The high-flow branch of the FDR becomes unstable above density ρ_c.
Right: The model classes of the SKM in the $(\bar{a}, \bar{b})$-plane and $\bar{v} = 3$, $\bar{l}_{\mathrm{car}} = 1, \varepsilon = 1$ as given in [113].

Model classes

The SKM has been designed to reproduce the empirical findings in *traffic jams*. These are [90, 92, 100]:

- Traffic jams can even develop and exist in the absence of any obstacle.

- The outflow from jams is stable and not maximal.

- The outflow from jams and the velocity of the downstream front do not depend on the inflow conditions.

- There is a density regime with non-unique FDR (*cf.* $\rho_f \leq \rho \leq \rho_c$ in figure 2.5). Depending on the initial conditions either high-flow states are displayed by the model or states which belong to the high-density branch.

- The transition between free flow and congestion is a phase transition of first order [101].

These properties are displayed by the model for a certain range of parameters but the SKM shows an even richer behaviour.

In [113] three classes of qualitatively different behaviour are found depending on the parameters a and b. Note that parameters given in the plots are dimensionless (as well as in the discussion if appropriate), *i.e.*, length and time are rescaled by means of $l_{\mathrm{car}} = 7.5m$ and $\Delta t = 1s$, respectively. Rescaled parameters are indicated by use of $\bar{\cdot}$. This is primarily done in order to faciliated a comparison with the original diagrams.

Class I (macroscopic phase separation)

The limit of low acceleration and low deceleration ($\bar{b} \ll 1, \bar{a}/\bar{b} \approx 1$) belongs to this class where jam formation is modelled correctly within the meaning of the properties given above. The FDR shows a capacity drop and a jam nuclei can, therefore, evolve into a macroscopic jam (given that the outflow from a jam is stable). For the same reason the growing of jams is quasi-deterministic in this model class and the jamming transition is a phase transition of first order.

Class II (spontaneous structure formation)

In the limit of high deceleration ($\bar{b} \rightarrow \infty$) there exist a separation into regions of high and low densities. However, these structures do not grow to arbitrary size and the jamming transition is no phase transition. The FDR does not show a capacity drop. The dynamics has much in common with the NaSch model.

Class III (no structure formation at all)

In the limit of high acceleration ($\bar{a} \rightarrow \bar{v}_{\max}, \bar{b} \approx 1$) there is no structure formation at all in the model's dynamics.
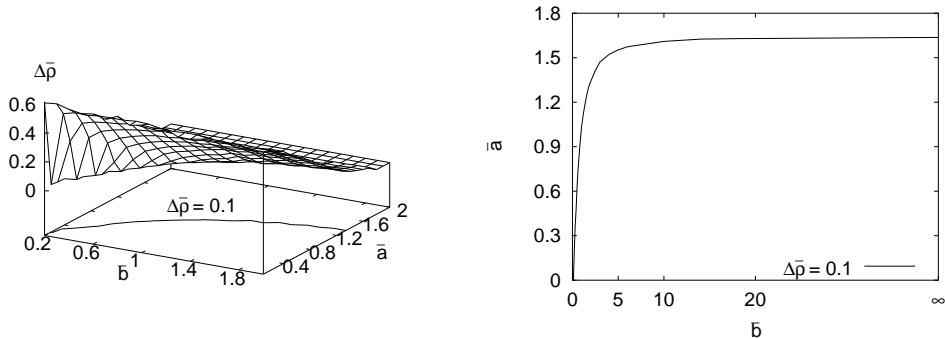
With respect to the full parameter plane ($\bar{a}, \bar{b}$) the model classes[3] are given in [113] as shown in figure 2.5. There, the parameters $v_{\max}$, l_{car} and ε were fixed to $22.5\,m/s$, $7.5\,m$ and 1, respectively. In order to characterise the behaviour, three quantities are of importance, namely the densities ρ_f, ρ_c and ρ_j (*cf.* figure 2.5).

In Class III models, $\Delta\rho = \rho_j - \rho_f \approx 0$ holds, whereas $\Delta\rho > \rho_{\mathrm{thresh}}$ holds for Classes I and II. ρ_{thresh} is a constant considerably larger than zero. Following the reasoning in [113] the Class I and Class II models can be distinguished by means of the existence of high-flow states, *i.e.*, $\rho_c > \rho_f$. Moreover, it is assumed that these states are truly *metastable*, *i.e.*, that they vanish in the thermodynamic limit of infinite system size.

As long as the capacity drop exists for a specific pair of parameters ($\bar{a}, \bar{b}$), macroscopic jams occur in the model. It is then found in the SKM that the outflow of jam is stable. With respect to the transition between Class I and Class II, it is assumed in [113] that the vanishing of metastable states goes along with an unstable outflow. In that case, the propability to find stopped vehicles at densities ρ_f becomes unequal to zero. Indeed, this criterion is used to deduce the boundary in the ($\bar{a}, \bar{b}$)-plane between Class I and Class II models. Note that, if these arguments were right, the dynamics of Classes I and II would correspond the VDR and NaSch, respectively. However, investigations in [131] show that the existence of

---

[3]The term classes refers to the definitions listed above in the following.

Figure 2.6   **Left**: In order to identify parameters $(\bar{a}, \bar{b})$ for which the SKM displays structre ($\Delta\bar{\rho} = \bar{\rho}_j - \bar{\rho}_f \geq 0.1$) a loop with 5000 cars is used. The other paramters are fixed to $\bar{v} = 3$, $\bar{l}_{\mathrm{car}} = 1$ and $\varepsilon = 1$. Measurments are made for 10^4 time steps after relaxation of the system for $3 \cdot 10^4$ time steps at density ρ_{sim}. **Right**: Line in the $(\bar{a}, \bar{b})$-plane between models without structure and models which display structre formation.

high-flow states and the stability of the outflow from jam are independent properties of stochastic microscopic traffic flow models.
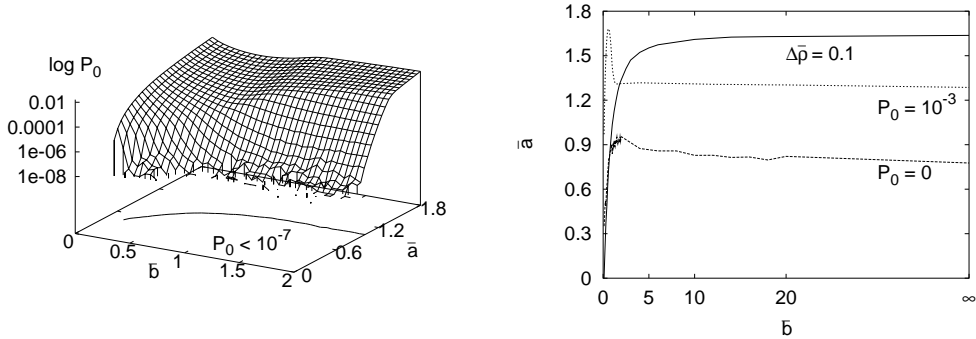
It was doubtful that the dynamics of the SKM in Class I behaves similarly to the VDR and investigations on the stability of the high-flow states showed a different behaviour than that expected. Accordingly, the model classes as given in [113] are revisited in the following.

First of all, the border in the $(\bar{a}, \bar{b})$-plane between models with and without structure formation is determined again (*border to structure*). To this end, the same setup as in the original work is used.

Scanning the $(\bar{a}, \bar{b})$-plane, the density ρ_{sim} is identified in an iterative process. At this density the system possesses the same number of cars in the free-flow and the congested state. Initial conditions had a *homogeneous state* in which all cars have the same distance, $g(0) = 1/\rho - l_{\mathrm{car}}$ and $v(0) = \min\{g, v_{\mathrm{max}}\}$.

The ratio of jammed cars to free-flowing cars is measured after an appropriate relaxation time by means of the following criterion: A car is considered to be jammed, if more than half of the n neighbours (including the car itself, $n = 5$ in the following) have a velocity below $v_{\mathrm{max}}/2$. This threshold is reasonable with respect to the bimodal distributions of the velocities and the gaps which are found in systems with a global density where the free-flow state coexists with the congested state. As shown in [85] this criterion is still applicable in the case of a non-vanishing overlap between the two maxima of these distributions.

Finally, in the system initialised with ρ_{sim}, the densities ρ_f and ρ_j are determined by averaging there out the gaps in front of free-flowing and jammed cars,

Figure 2.7   **Left**: Probability P_0 to find stopped cars in the outflow from a mega-jam. The parameters are the same as for figure 2.6 and the method to determine P_0 is described in the text. **Right**: The lines in the $(\bar{a}, \bar{b})$-plane with $\Delta\bar{\rho} = 0.1$, $P_0 = 0$ and $P_0 = 0.001$.

respectively. Figure 2.6 shows the findings which are in complete agreement with the original ones. In order to distinguish models with structure formation from those without, $\Delta\bar{\rho} = 0.1$ is used. Additionally, the border of structure is extrapolated to $\bar{b} \to \infty$ using cuts along $\bar{b} = [1, 1.2, ..., 2, 4, ..., 20, \infty]$. In the case $\bar{b} \to \infty$, the safety conditions (2.5) reduces to the well-known condition from the NaSch model,

$$\lim_{b\to\infty} \left(-b\tau + \sqrt{b^2\tau^2 + \tilde{v}^2 + 2bg} \right) = g/\tau. \tag{2.12}$$

At values $\bar{b} > 20$ the function is parallel to the $\bar{b}$-axis with $\bar{a} \approx 1.64$. It is clear that there is a bound for the acceleration beyond the system always stays homogeneous. If $\bar{a}$ is no longer small with respect to $\bar{v}_{\max}$, almost all perturbations can heal out in one time step given the high acceleration possible [85].

However, it was not possible to reproduce the transition line between Class I and Class II models as given in [113]. The original work states that the probability P_0 of finding stopped cars ($v = 0$) in the state ρ_f is only non-vanishing for Class II models (see arguments above). Using $P_0 < 0.001$ as criterion, the transition line between the two model classes was determined as shown in figure 2.5.

In order to reinvestigate the transition line between Classes I and II three different setups are used:

a) For each pair $(\bar{a}, \bar{b})$ a system is initialised with the homogeneous state at density ρ_f. ρ_f is the density in the free flow measured in the simulations to determine $\Delta\rho$. Two different setups for the loop are used, namely, a fixed length ($2000\, l_{\mathrm{car}}$) and a fixed number of cars (1000). Both setups give the same results. After relaxation of 10^4 time steps, P_0 is measured over 10^6 time steps. Note that this is the method used in [113].

b) For each pair $(\bar{a}, \bar{b})$ the complete FDR of the closed system is generated. The density ρ_f is determined by the intersection of the low-density and the high-density branch. Again, the homogeneous state with density ρ_f is relaxed for 10^4 time steps and P_0 is subsequently measured over 10^6 time steps.

c) An infinitely large *mega-jam* $(g(0) = 0, v(0) = 0)$ is fixed at the left boundary of an open system. The system has a fixed length of $L_S = 10^4\,m$. Due to the slow-to-start behaviour, the probability to have stopped cars is non-vanishing at the downstream front of the mega-jam. Therefore, P_0 is measured $10\,m$ away from that front. Again, the system is simulated for 10^6 time steps and each value P_0 is the average of five simulations. This method is similar to the setup used in [131] to investigate the interface dynamics.

The findings for the outflow from the mega-jam are shown in figure 2.7. It is worth noting this was also found in the other two setups, namely, that P_0 decreases steeply with decreasing $\bar{a}$. The line below P_0 vanishes is almost a parallel to the $\bar{a}$-axis with $\bar{a} \approx 0.8$, independent of the parameter $\bar{b}$. This differs significantly from figure 2.5. Moreover, below that line, high-flow states always exist in the SKM.
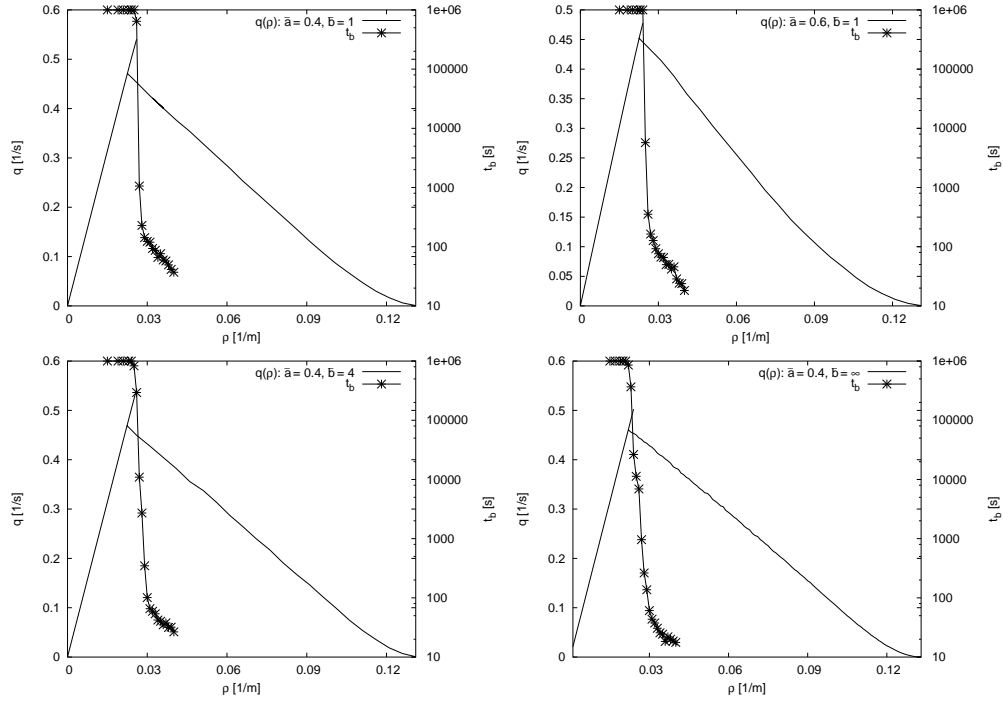
In figure 2.8 four FDR are shown for pairs of $(\bar{a}, \bar{b})$ which all belong to Class II and should, therefore, not display high-flow states. Additionally, the *time to breakdown* t_b is given for these sets of parameters. This concept has been introduced in [88, 131] in order to investigate the stability of high-flow states and needs further explanation.

The time to breakdown $t_b(\rho)$ gives the number of time steps needed to observe a stopped car in a system that has been initialised in the homogeneous state at density ρ. If the high-flow states are *metastable*, the time to breakdown decreases with increasing system size[4] and it increases with decreasing density. The transition from homogeneous flow to the congested state is in that case very similar to the gas-liquid transition.

However, for the SKM a different behaviour is found in the parameter range presented above. There, the *high-flow states* are stable. Stable high-flow means that the strong, intrinsic fluctuations of the model are insufficient to cause a transition into the congested regime (possible explanations of this phenomena are given in [131]). Indeed, that is what is found here. For example, for $(\bar{a}, \bar{b}) = (0.4, 1.0)$ the breakdown time grows three orders of magnitude from $\rho = 27\,km^{-1}$ to $\rho = 26\,km^{-1}$, and from $\rho = 22\,km^{-1}$ up to $\rho = 26\,km^{-1}$ both branches are stable within 10^6 time steps (see figure 2.8). For $(\bar{a}, \bar{b}) = (0.4, \infty)$ there is still a rapid growth in the breakdown time but there is no longer a divergence. From this, one can conclude that there is a transition from stable high-flow states to metastability with increasing braking capability $\bar{b}$.

---

[4]In the limit $L_S \to \infty$ metastable high-flow states vanish.

Figure 2.8 FDR and breakdown time for different sets of parameters $(\bar{a}, \bar{b})$, the other parameters are equal to figure 2.5. Each loop is initialised homogeneously with 5000 cars. The FDR is measured globally after an appropriate relaxation time. The breakdown times are means over 10 realisations, each lasting for 10^6 time steps.

With respect to the stability of the homogeneous state one would expect the following dependencies:

a) $a = const.$, increasing b

With increasing b the safe velocity increases and converges to $v_{\mathrm{safe}} = g/\tau$, *cf.* (2.12). For high b the braking capability is bounded by $v_{\max}$. The mean deceleration of the cars increases. Therefore, with increasing b the high-flow states become more unstable.

b) $b = const.$, increasing a

It is self-evident that the stability of high-flow states decreases with increasing a, due to the fact that the number of interactions needed to stop a car is $\propto v_{\max}/(\varepsilon a)$ and fluctuations in the model's dynamics are $\propto a$.

These assertions can be clearly found in figure 2.7 and figure 2.8. Note that the strong dependence of P_0 on a is also visible in the corresponding plot in [113] (not shown).
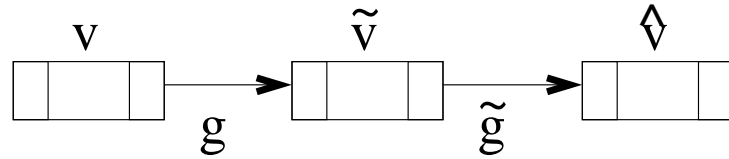
Of further note is that the initialisation of the system with a homogeneous state in a different way, namely, $g(0) = 1/\rho - l_{\mathrm{car}}$ and $v(0) = 0$, leads to reduced breakdown times and a strong increase in its variance. This is due to the slow-to-start behaviour of the model's dynamics. In the case of $\bar{b} \to \infty$ high-flow states are no longer found. Moreover, once stopped cars exist in a loop at global density ρ_f, the number of stopped vehicles will in general not reach zero again. This may explain why in [113] no capacity drop was found for Class II models and there was a non-vanishing probability to find stopped cars within this regime of parameters.

In light of these findings and [88, 131], it can be said that the picture given in [113] was incomplete. The new findings for the model, namely $\Delta\rho$ and P_0, are presented in figure 2.7. Within a certain parameter range, the SKM exhibits stable high-flow states. Their stability decreases with increasing a and b. However, breakdown times are still quite high where noise levels a are low. Especially, the distinction of Class I and Class II models based on the existence of metastable states is not possible below a certain value for a. The transition line where the stable high-flow states change to become truly metastable did not reveal itself here in detail. Given that the different phases are obtained by variations of continuous parameters, the determination of this transition line is computationally expensive and, due to the fast growth of the breakdown time in a small interval of densities, good numerical results are difficult to obtain. The computations of P_0 suggest that for all parameter sets (a, b) with $\Delta\bar{\rho} \geq 0.1$ and $\bar{v} = 3$, $\varepsilon = 1$ the outflow from jam is stable in the SKM. With increasing a its stability decreases. This was also found in [131] where specific sets of parameters were investigated with a huge amount of computational power. Within those parameter ranges where there is an observable capacity drop, the SKM displays a real phase transition of first order, from free flow to congestion.

In the following, only sets of parameters will be used where the SKM displays true macroscopic phases. For these parameters the dynamics of the SKM really differs from the VDR model, because the latter shows truly metastable high-flow states and an unstable outflow from jam [131].

2.3   Investigations of anticipatory driving

In the model described above, each car accounts only for the car in front of it in order to deduce its optimal driving strategy. That assumption is obviously unrealistic, particularly in dense traffic situations. In fact, drivers try to avoid strong accelerations and abrupt braking by considering the future movement of all cars within their interaction horizon. For example, a driver who approaches the end of a queue of cars, reduces her speed significantly before fully braking becomes necessary in order to avoid a crash. This is also true for situations where traffic is

Figure 2.9 Representation of the variables $v, g, \tilde{v}, \tilde{g}, \hat{v}$. All cars are considered to have equal length l_{car}.

still flowing. The drivers try to estimate the velocity of preceding cars for future times in order to determine their driving strategy. This behavioural component of driving is called "anticipatory driving" in literature.

Anticipation has been successfully introduced as a major component of cellular automata approaches, in order to obtain more consistency with microscopic observables such as time-headways or follow-the-leader behaviour, and to model synchronised states of traffic [86, 104]. It is obvious that the anticipation of future movement leads to an increase in streets' capacities by reducing the safe time-headways between consecutive cars. Furthermore, the free flow-phase is stabilised by a decrease of speed variance. It can be said, therefore, that this mechanism is necessary if real world traffic data is to be reproduced [103]. An understanding of the effects anticipation has on the dynamics of traffic flow is, therefore, essential to obtain more realistic models of traffic, as well as to investigate the use of automated driving systems.

In [119] the effects of several anticipation schemes have been investigated with respect to cellular automaton models of traffic flow. The results obtained were in agreement with the findings in [52], namely, that anticipation enables the formation of stable platoons of cars and leads to an increase in the capacity depending on the strength of anticipation.

In order to get a better understanding of the changes in the model's dynamics as a consequence of anticipatory driving, this strategy is introduced into the SKM via next-nearest-neighbour interactions. The effects of this driving strategy are explored by simulation, as well as by analytical calculations. Leaping ahead, it is said that, by virtue of anticipation, the system organises the headways of the cars in an alternating structure which allows for the small time-headways observed in reality. As will become clear from the following discussion, most of the results found should be at work in other models too (*cf.* [103, 119]).

2.3.1 SKM with anticipation (SKA)

In order to bring anticipation into the model the update scheme is modified by an intermediate step: Each driver predicts the worst-case strategy v_{anti} her predecessor will choose in the next time step. Assuming there is a car in front of the

predecessor within a distance $\tilde{g}$ driving with velocity $\hat{v}$ (see figure 2.9), then

$$v_{\text{anti}} = \max\{\tilde{v}_{\text{des}} - \varepsilon a, 0\} \tag{2.13}$$

with

$$\tilde{v}_{\text{des}} = \min\{\tilde{v} + a, \tilde{v}_{\text{safe}}(\hat{v}, \tilde{g}), v_{\text{max}}\}. \tag{2.14}$$

The calculated v_{anti} is then used in order to determine the safe velocity. Therefore, the safety condition (2.4) is restated on the assumption that the leading car chooses $\tilde{v}_{t+\Delta t} \geq v_{\text{anti}}$ as its driving strategy,

$$d(v) + \tau v + \gamma_c(v, \tilde{v}) \leq d(v_{\text{anti}}) + v_{\text{anti}}\tau + g. \tag{2.15}$$

The function $\gamma_c(v, \tilde{v})$ has been introduced to take account of "unexpected" fluctuations in the predecessor's driving behaviour. Then, the new expression (2.15) leads to a new expression of the safe velocity,

$$
\begin{aligned}
v_{\text{safe}} = \quad & - \quad b\tau \\
& + \quad \sqrt{b^2\tau^2 + v_{\text{anti}}^2 + 2b(g + v_{\text{anti}}\tau - \gamma_c(v, \tilde{v}))}.
\end{aligned} \tag{2.16}
$$

In the following,

$$\gamma_c(v, \tilde{v}) = \min\{v_{\text{anti}}\tau, g_c\} \tag{2.17}$$

is chosen where g_c is constant. In that, $g + v_{\text{anti}} - \gamma_c(v, \tilde{v})$ can be interpreted as an effective gap g_{eff}, where (2.17) forces $g_{\text{eff}} \geq g$. The idea of the effective gap is similar to the cellular automaton model in [104] (BL). The major difference is that in the modified SKM anticipation enters the model by velocity and the effective gap (*cf.* equation (2.16)), whereas in the BL it enters the model solely via the latter.
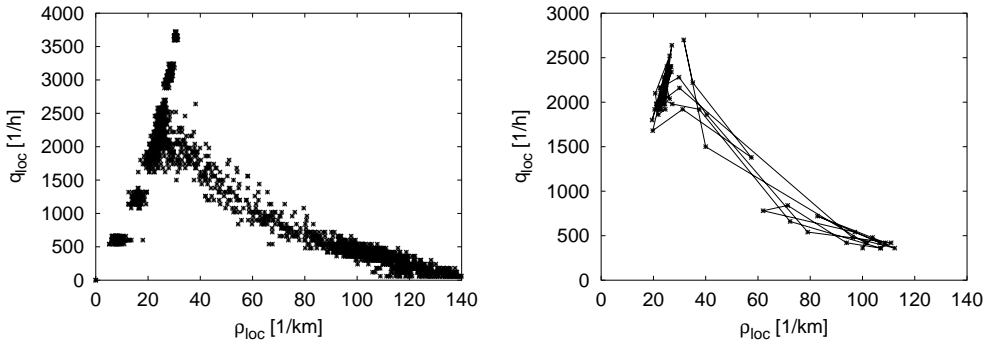
As well as the new definition of v_{safe}, the update scheme (2.6) is used. The modified SKM is referred to as SKA in the following.

2.3.2 The role of anticipation

In the following, the SKA is compared with the original model by means of computer simulations. For this purpose the same fixed set of parameters is used that was previously used in section 2.2,

$$
\begin{aligned}
a &= 2 \ m/s^2 & b &= 8 \ \ m/s^2 & v_{\text{max}} &= 35 \ m/s \\
\varepsilon &= 1 & g_c &= 1 \ m & l_{\text{car}} &= 7 \ \ m.
\end{aligned} \tag{2.18}
$$

$\tau = \Delta t = 1s$ is chosen again as time scale. Given these parameters, the formation of jams (wide moving jams), and stable high-flow states exist in the corresponding SKM (*cf.* section 2.2).

Figure 2.10   **Left**: FDR of the SKA with periodic boundary conditions. At each density the loop is initialised homogeneously with 1000 cars. Density and flow are measured locally (virtual detector) after the system becomes stationary. **Right**: Sequence of measurements at fixed density $\rho = 35km^{-1}$. In that density regime the free-flow state and the congested state coexist.
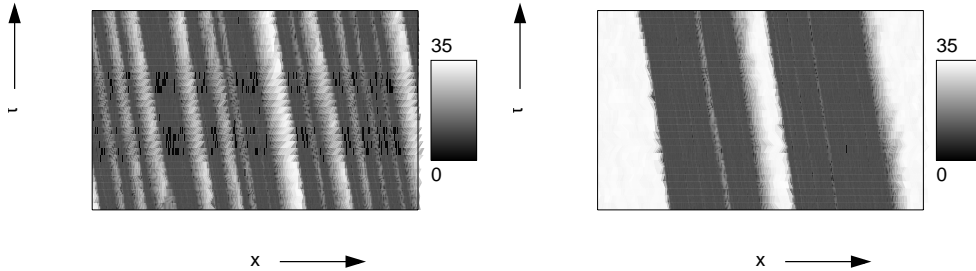
Macroscopic properties

Firstly, the model's behaviour is compared to the SKM with respect to the macroscopic observables density and flow, as well as with the observable states of traffic. For this purpose, periodic boundary conditions are used again, and the observables are measured by a virtual detector after relaxation of the system. As sampling, intervals of $60s$ are used.

Comparing the FDR of the SKA (see figure 2.10) with the SKM, they both display high-flow states and a capacity drop at intermediate densities. The effective slow-to-start behaviour of the SKM is, therefore, not changed by introducing next-nearest-neighbour interactions. Moreover, the "optimised" driving strategy leads, in fact, to a stabilisation of the high-flow branch towards higher densities, as stated above.

As already seen for the SKM, the congested state coexists with the free-flow state for densities $\rho \geq 20km^{-1}$ in the closed system. Time-series of a virtual detector at a fixed density in that regime, therefore, alternately display free-flow and congested states (see figure 2.10). At densities where the homogeneous free-flow state is unstable, small clusters of cars are generated due to intrinsic fluctuations. Eventually, the number of jams decreases until only one jam remains (see figure 2.11). Recalling the argumentation in [113], the jamming transition in the SKA is a phase transition and one finds a phase-separated system at equilibrium using periodic boundary conditions.

The next comparison undertaken between the models pertains to the classification of stochastic traffic flow models as given in [131] (*cf.* discussion in sec-
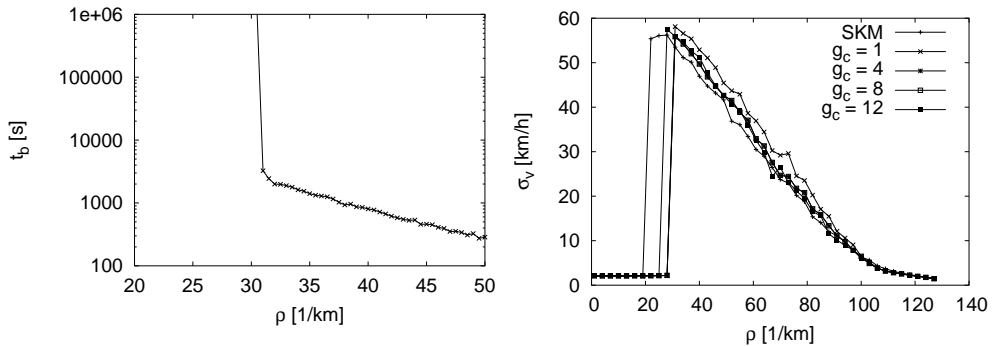
Figure 2.11   Space-time diagram for a typical evolution of the SKA. Each car is coloured by its current velocity in units m/s. Initially, there are a lot of small jams (*left*) that coagulate into a double jam state (*right*). However, when waiting for a very long time, only one wide moving jam remains.

tion 2.2.2). In figure 2.12 the time to breakdown is plotted against the system's density. For each simulation run a system with 5000 cars was initialised homogeneously. The values presented are means of 20 realisations per density. Simulations were stopped after 10^6 time steps, if the initial state did not break down. As can be seen, the time to breakdown diverges at $\rho_c \approx 31 km^{-1}$, *i.e.*, homogeneous states corresponding to $\rho < \rho_c$ are *absolutely stable*. These states represent the high-flow branch (see figure 2.10) and, therefore, the SKA owns the same type of stability as the SKM does.

The observations presented so far show that the SKA possesses a *stable high-flow branch*, similar to the SKM, and allows for higher flows compared to the latter model. Microscopically, this is due to smaller time-headways which nevertheless permit safe driving. With respect to the velocity, its standard deviation is an indicator of the efficiency in traffic flow. High standard deviations of the speed indicate that drivers experience frequent speed changes which in turn lead to an increased probability of traffic breakdown [119]. In figure 2.12 the standard deviation of the speed for different values of g_c is shown.

Compared to measurements the anticipatory driving strategy leads to unrealistic high, attainable flows (with respect to non-automated driving). This is also a known feature for some extensions of the NaSch model [106]. Even though such states only appear for special initial conditions, *i.e.*, highly ordered, homogeneous configurations, modifications are necessary to apply it to reasonable applications. However, it remains a different question whether these flows can be attained in a realistic setting with macroscopic disturbances arising from lane-changing, on- and off-ramps, *etc.*. Further, by introducing diversified driver behaviour, this may

Figure 2.12 **Left**: The average time to breakdown t_b for the SKA. **Right**: Standard deviation of speed against the system's density for the SKM and SKA (using different values for g_c).

lower the maximum flow to realistic values. For example, this may be done using a distribution $p(\tau)$ for the parameter τ, so each driver has her individual τ drawn from that distribution. Another way of doing this would be to increase g_c.
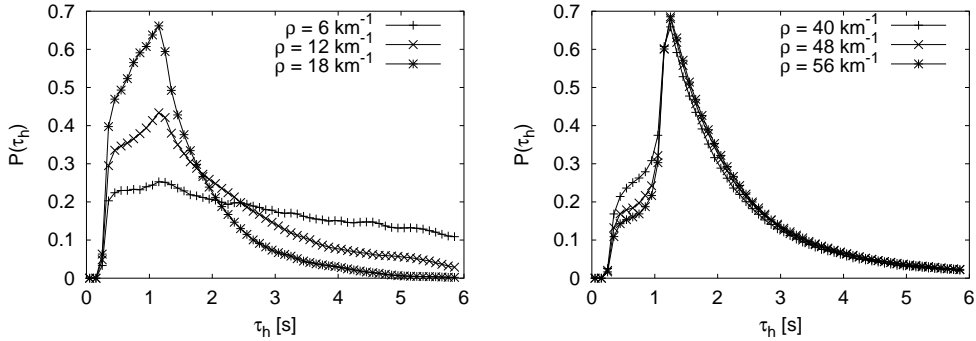
Apart from these unrealistic high flows, it can be concluded that the overall macroscopic properties of the SKA under periodic boundary conditions (*i.e.*, the FDR, the spontaneous jam formation and the existence of compact jams) are similar to the corresponding SKM.

Time-headway distribution

After the macroscopic comparison of the SKA with the SKM its microscopic structure is investigated. The closed loop still serves as the computer experimental setup to analyse time-headways (2.9). It is initialised at different densities and the time-headway distribution is measured after transients died out. In figure 2.13 the time-headway distribution of the free flow phase at different densities is presented together with the distributions of the congested phase.

With respect to the free flow phase, the SKA shows a different structure than the SKM (*cf.* figure 2.4). The peaks of the distributions are much broader and headways noticeably smaller than $1s$ exist, as in empirical observations. The figure also shows that the distributions at short time-headways are independent of the density. However, the broadness of the peaks is not found in real world observations. The occurrence of short time-headways stems from the introduction of the velocity anticipation. Drivers can optimise their gap to the leading vehicle, since they have an idea about its future behaviour. Smaller gaps at $v \approx v_{\max}$ than in the SKM are, therefore, possible.

Moreover, the broadness of the peaks indicates that in the SKA a range of headways to the car in front can be taken by cars driving at $v \approx v_{\max}$, *i.e.*,

Figure 2.13   Time-headway distribution for the SKA under free-flow conditions (*left*) and in the congested state (*right*). Headways smaller than $1s$ at high densities stem from the free-flow state (their share decreases with increasing density).
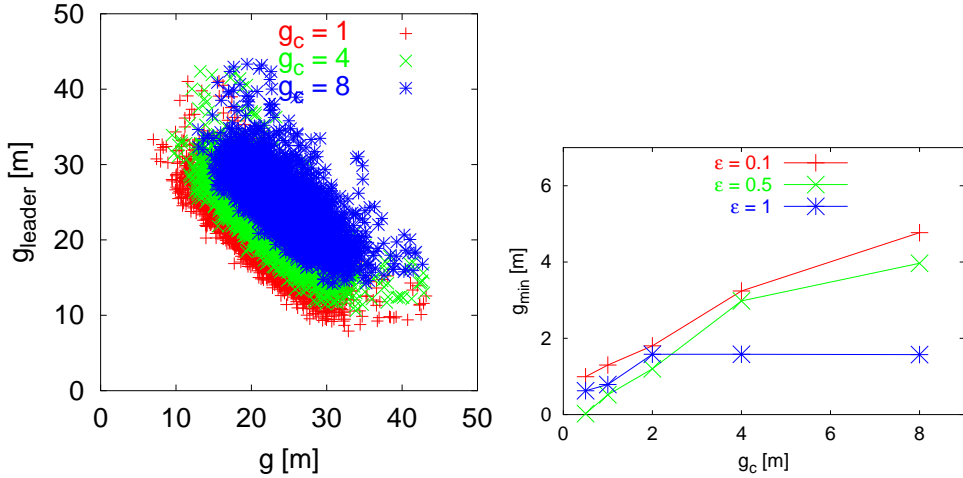
the fixed-point in the car-following dynamics is not such strong as in the SKM. With increasing density the peak in the distribution becomes more and more pronounced and shifts towards smaller time-headways. The position of the peak corresponds to the mean gap, given by the initial conditions, $\langle g \rangle = 1 / \rho - l_{\mathrm{car}}$. Moving towards higher densities along the free-flow branch of the FDR, the possible range of gaps between cars decreases.

Comparing the time-headway distributions of the congested state, these are almost independent of the density, as in the SKM. In addition to the appearance of $\tau_h \leq 1s$, these also agree quantitatively. The occurrence of small time-headways is due to the experimental setup. In the closed loop the system is separated into two phases, one wide moving jam and a region of free-flow (see figure 2.11). As demonstrated before, time-headways smaller than $1\,s$ can be found in the free-flow phase. Therefore, cars that are not in the congested state generate these time-headways. Given that the number of cars in the free-flow phase decreases with increasing density the weight of small time-headways also reduces. From this, one can conclude that with respect to the dynamics inside jams, both models behave similarly.

Optimal velocity curve

The OVC of the SKA confirms the latter finding. The OVC is derived from the condition

$$\hat{v} = v_{\mathrm{safe}} = \tag{2.19}$$
$$- b\tau + \sqrt{b^2\tau^2 + v_{\mathrm{anti}}^2 + 2b(g + v_{\mathrm{anti}}\tau - \gamma_c)},$$

Figure 2.14   **Left**: The simulations performed with the stochastic version of the SKA and for different values of g_c are in qualitative agreement with (2.30). **Right**: Minimal gap found in simulations of the loop, taking different values for g_c and ε.

with

$$v_{\text{anti}} = -b\tau + \sqrt{b^2\tau^2 + \hat{v}^2 + 2b\tilde{g}}. \tag{2.20}$$

With respect to (2.17) two cases have to be distinguished.

In the case of $v_{\text{anti}} > g_c$, *i.e.*, $\gamma_c = g_c$, equation (2.19) is solved by $\hat{v}\tau = (g + \tilde{g} - g_c)$ and the OVC reads

$$V_{\text{opt}}^{\text{f}}(\rho) = \min\left\{\frac{2}{\tau}\left(\frac{1}{\rho} - \frac{1}{\rho_{\text{max}}} - \frac{g_c}{2}\right), v_{\text{max}}\right\}, \qquad v_{\text{anti}} > g_c. \tag{2.21}$$

If $v_{\text{anti}} < g_c$, *i.e.*, $\gamma_c = v_{\text{anti}}\tau$, the known expression of the SKM (2.11) follows,

$$V_{\text{opt}}^{\text{j}}(\rho) = V_{\text{opt}}^{\text{SK}}, \qquad v_{\text{anti}} < g_c. \tag{2.22}$$

2.3.3   Follow-the-leader behaviour

Finally, the differences in the follow-the-leader behaviour between the two models is investigated. For this purpose, a chain of 1000 cars is used that follows the first car whose speed is fixed to $V \leq v_{\text{max}}$. The system is initialised by all cars standing ($g(0) = v(0) = 0$). The lead car accelerates until the constant velocity V is reached. Measurements commence if $x \geq 10000 \cdot V$ holds for the last car of the chain. It can be assumed that the system then reached a stationary state.

Before presenting the simulation results, this set-up is analysed more closely. To this end, only the case of deterministic motion is regarded. Thus, all speeds can be eliminated to yield an update equation exclusively for the gaps. In order to keep the equations concise, the following notation is adopted: If a quantity is labelled with a prime $'$, it means the following time step $t + \Delta t$. Otherwise, quantities are taken at the current time step t. For the same reason, $\tau = 1$ is used in the following.

Assuming a lead car driving at constant speed $v_0 = V$, the behaviour of the SKM is then determined by the equations

$$
\begin{aligned}
v' &= v = -b + \sqrt{b^2 + V^2 + 2bg} \\
g' &= g = g + V - v'
\end{aligned}
\tag{2.23}
$$

Equation (2.23) has a *fixed-point* at $v^* = V$ and $g^* = V$. Since this result can be extended to the full chain of cars, it follows that

$$
g_{n+1} = g_n.
\tag{2.24}
$$

The lower index denotes the position n of a car in the chain.

The result explains the independence of the peak in the time–headway distribution at low densities (cf. figure 2.4). Moreover, it can be concluded that the intrinsic fluctuations of the SKM are not able to allow the dynamics to escape from the fixed-point. It is worth saying that the robustness of the fixed-point in continuous car-following models is hard to overcome in general which causes problems with regard to modelling the synchronised state.

As next, the same situation is investigated for the SKA. Again, the lead car drives constantly with $v_0 = V$, which is also v_{anti} for the first following car. Having regard to the deterministic case, that car then drives with $v_1^* = V$ and with constant headway $g_1^* = g_c$. This is because

$$
v_1' = -b + \sqrt{(b + V)^2 + 2b(g_1 - g_c)}
\tag{2.25}
$$

and
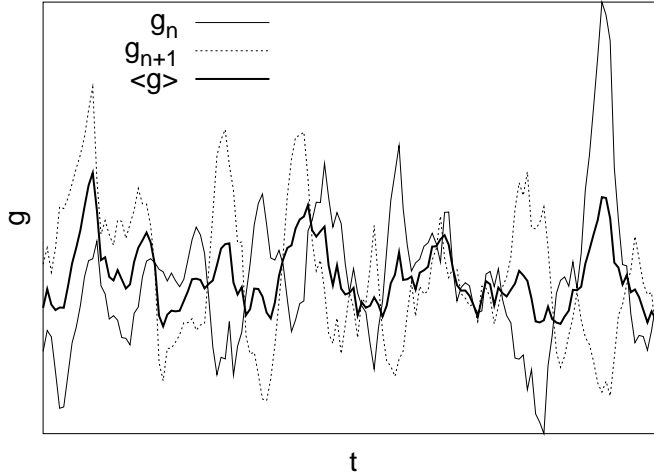
$$
g_1' = g_1 + V - v_1',
\tag{2.26}
$$

whose fixed-point $g_1' = g_1 \equiv g_1^*$ is just g_c.

For the second car this procedure can be carried out to give

$$
g_2' = b + V + g_2 - \sqrt{b^2 + V^2 + 2bg_2},
\tag{2.27}
$$

where the stationary state of the first car $v_1^* = V$ and $g_1^* = g_c$ has been assumed. This equation has a simple fixed-point, namely $g_2^* = V$. Obviously, $v_2^* = V$ holds likewise.

Figure 2.15 Typical time-series of the gaps between two consecutive cars in the follow-the-leader behaviour of the SKA. The leading cars drives at $V = 15ms^{-1}$. The mean gap $\langle g \rangle = (g_n + g_{n+1})/2$ hardly varies, because the two cars share a common gap $\propto 1/\rho$. The two gaps between three consecutive cars are anti-correlated.

For the third car the computation leads to

$$
\begin{aligned}
g_3' &= b + V + g_3 \\
&- \sqrt{b^2 - 2bg_c + V^2 + 2bg_2 + 2bg_3},
\end{aligned}
\tag{2.28}
$$

and $g_3^* = g_c, v_3^* = V$. Expressed generally, the latter equation reads

$$
\begin{aligned}
g_{n+1}' &= b + V + g_{n+1} \\
&- \sqrt{b^2 - 2bg_c + V^2 + 2bg_n + 2bg_{n+1}},
\end{aligned}
\tag{2.29}
$$

resulting in the following expression for the stationary state $g_n' = g_n, v_n = V$:

$$
g_{n+1} = -g_n + g_c + V.
\tag{2.30}
$$

The result (2.30) shows that the gaps of the n–th and $(n+1)$–th car are asymptotically anti-correlated. In figure 2.14 time-series g_n vs. g_{n+1} are shown for different values of g_c. With increasing g_c, the corresponding straight line moves away from the origin, thereby causing the corresponding flow to decrease.

The result helps understand the plateau structure found in the time-headway distribution of the SKA at low densities (cf. figure 2.13). With respect to (2.30), the two time-headways of three consecutive cars equal the bounds of the interval

$[g_c/V, 1]$. In the simulation, the lower bound of the interval scarcely occurs due to fluctuations. These fluctuations are not able to drive the system away from the fixed-point, comparably to the SKM. However, in the SKA, three consecutive cars share a common gap given by the mean density, but the share between g_n and g_{n+1} is not fixed. Fluctuations allow two cars to exchange their role in the common structure, *i.e.*, if a cars approaches the car in front, its car behind will enlarge the headway and vice versa. This leads to characteristic oscillations in the time-series of the gaps as shown in figure 2.15.

Before correlations of observables in the models are investigated in more detail, the role of g_c is further explained. With respect to equation (2.30) one may ask why the anti-correlation does not lead to states with $g < 0$.

Assume that a car $n + 1$ has closed in on its predecessor n. Recalling (2.29), the gap g_{n+1} develops as
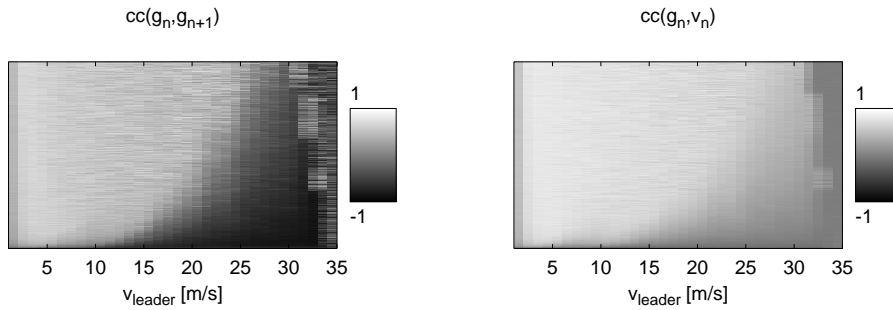
$$
\begin{aligned}
g'_{n+1} &= b + V + g_{n+1} \\
&\quad - \sqrt{b^2 - 2bg_c + V^2 + 2bg_n + 2bg_{n+1}}.
\end{aligned}
$$

Setting $g_{n+1} = g$ and $g_n \approx V$, the following approximation of g'_{n+1} holds,

$$
\begin{aligned}
g'_{n+1} &= b + V + g - \sqrt{(b+V)^2(1 + \frac{2b}{(V+b)^2}(g - g_c)} \\
&\approx b + V + g - |b + V| \left(1 - \frac{b}{(V+b)^2}(g - g_c)\right) \\
&= \left(1 - \frac{b}{V+b}\right) g + \frac{b}{V+b} g_c. \tag{2.31}
\end{aligned}
$$

Equation (2.31) shows that once $g_n = V = const$, g tends to become zero. But, this decrease is finally stopped at g_c. A car that starts with $g < g_c$ is drawn towards g_c, which is the fixed-point. Having regard to fluctuations, safe driving can, therefore, not be assured setting $g_c = 0$. If one determines the minimal gap that occurs in simulations of the model, depending on the fluctuations' strength ε and g_c, this becomes more clear. It can clearly be seen in figure 2.14 that the minimal gap increases with increasing g_c. The dependence on ε is not as explicit. This results from the fact that ε enters twice into the model's equations. On the one hand, it acts similar to the ε in the SKM (*cf.* equation (2.6)), on the other hand it is also used to determine v_{anti}. With respect to the collision-free motion in the SKA, a minimal g_c^* can, therefore, always be found for a specific set of parameters which guarantees safe driving, if $g_c \geq g_c^*$ is chosen. However, g_c^* cannot be given analytically. It has to be determined by means of numerical simulations.

Finally, a closer look at the correlation functions between the gaps and the velocities completes the discussion of the effects on the system state due to an-

Figure 2.16 Correlation functions $c_1(g, g)$ (*left*) and $c_0(g, v)$ (*right*) for the follow–the-leader setup in the SKA. The value for each car is indicated by the colour. The cars are sorted along the y-axis with increasing car number n.

ticipation. The correlation function of two arbitrary observables ξ and χ at car n, $n + \Delta n$, respectively, used in the following is given by

$$c_{\Delta n}(\xi_n, \chi_{n+\Delta n}) = \frac{\langle(\xi_n - \langle\xi_n\rangle)(\chi_{n+\Delta n} - \langle\chi_{n+\Delta n}\rangle)\rangle}{\sigma_\xi^n \sigma_\chi^{n+\Delta n}} \qquad (2.32)$$

In (2.32) σ_ξ^n stands for the standard deviation of the observable ξ taken at car n.

In figure 2.16 the correlation functions $c_1(g, g)$ and $c_0(g, v)$ are shown. In contrast to the SKM[5] there exist a platoon of cars behind the leading car in the SKA which displays a strong anti-correlation between two consecutive gaps, *cf.* equation (2.30). Note that this structure is even not destroyed if the lead car drives with velocities fluctuating symmetrically around around $\langle v_{\text{leader}}\rangle$. In the regime of strong anti-correlation, $c_0(g, v) \approx 0$ is found, *i.e.*, a car is free to choose a gap g independently of the velocity of the car in front. Therefore, this state is reminiscent of synchronised flow [90, 91, 92]. However, further exploration of the simulated data shows that the velocity only displays fluctuations of strength $a/2$ around the mean speed $\langle v_{\text{leader}}\rangle$. Thus, anticipation alone cannot generate synchronised states.

2.4 Open boundary conditions

The investigation of periodic boundary conditions (PBC) is valuable in order to understand the bulk properties of a dynamic model. However, in the context of street traffic one obviously deals with open systems, *e.g.*, a segment of street

---

[5] $c_1(g, g) \approx 1$. The same holds for $c_0(g, v)$.

between two ramps or two intersections. There it is the present travel demand which determines the in- and outflow of such a segment, as well as the flows may be restricted by traffic lights or speed limits. In contrast to closed systems the density of the segment is no longer conserved. Therefore, the understanding of the effects open boundaries have on the model's dynamics is essential with regard to real world applications of traffic flow models.

2.4.1 Boundary induced phase transitions

Moreover, physics teaches us that dynamic systems can display *boundary induced phase transitions* under *open boundary conditions* (OBC) [116]. With respect to this phenomena the class of *driven lattice gases* (DLG) plays an important role [116, 158]. In these models a lattice is connected to particle reservoirs at its boundaries and the particles have a preferred direction of motion. The NaSch model and its variants can be seen as special realisations of driven lattice gases, as well as the SKM (however, having continuous state variables).

One famous example is the so-called *total asymmetric simple exclusion process* (TASEP) which has been studied extensively, so that even exact results exist [45, 53, 61, 150, 159]. In this model particles enter the system (*left boundary*) with a probability α and leave the system (*right boundary*) with probability β. Particles then move site by site (from left to right) with a transition rate p and are subjected to hard-core repulsion, *i.e.*, a particle can only jump into a free site. Its FDR displays one maximum (as the NaSch) and an unique relation between density and flow. With respect to PBC, there is only one phase to be observed. Using OBC, however, the model shows a surprisingly rich *phase diagram* depending on the inflow and outflow rates.

In principle, one can distinguish between three different phases. Namely, the *low-density phase*, the *high-density phase* and the *maximum current phase* [150], which are separated by phase transitions. In the first two phases, the flow in the system q_{sys} is only dominated by the inflow rate α and outflow rate β, respectively, whereas the limiting factor on the flow is the bulk rate p in the latter phase. The representation of these phases within the (α, β)-plane is called phase diagram.

There exists a rather general, phenomenological theory of boundary induced phase transitions for models with unique FDR [4, 67, 109, 148] which allows the phases in the open system to be predicted considering the FDR of the closed system. Applying this theory, the flow Q in the open system is related to the FDR $q(\rho)$ of the periodic system by an *extremal principle*

$$
\begin{aligned}
Q &= \max_{\rho \in [\rho_\beta, \rho_\alpha]} q(\rho) \quad \text{for } \rho_\alpha > \rho_\beta, \\
Q &= \min_{\rho \in [\rho_\alpha, \rho_\beta]} q(\rho) \quad \text{for } \rho_\alpha < \rho_\beta.
\end{aligned}
\tag{2.33}
$$

ρ_α and ρ_β are effective densities at the left and right boundary, respectively. They are closely related to the flow rates α and β. The principle implies that two models with different microscopic dynamics but unique FDR always have the same phase diagram for OBC. Therefore, the phase diagram of the NaSch model is qualitatively the same as the one of the TASEP [147, 156].

In contrast, traffic flow shows *branched* FDR, *i.e.*, within a certain regime of densities the homogeneous flow can coexist with the congested state. It is on the one hand interesting to verify whether the extremal principle (2.33) is still valid for such systems. On the other hand, it is worth understanding whether open boundaries give rise to phases which are not bulk phases (PBC) or whether the order of transitions between phases changes due to OBC.

One class of models with non-unique FDR is given by the VDR. In [5] a VDR model with $v_{\max} = 1$ is investigated. It displays metastable high-flow states. Due to its simplicity, an analytical description of the phases is possible. In principle, one finds the same phases as in the TASEP, but the microscopic structure of the phases is different. For finite system sizes L_S, there is a maximum current phase which vanishes in the limit $L_S \to \infty$. The findings concur with the extremal principle.

VDR models with $v_{\max} > 1$ are investigated in [13, 167]. The phase diagram of these models shows the free-flow and jammed phase together with a *phase of high flow* which corresponds to the maximum current phase. However, as for $v_{\max} = 1$ the microscopic structure of the jammed phase differs from the TASEP. The model reveals a special structure which can be characterised as *striped patterns*. This structure seems to be generic for DLG with metastability. In [13], these structures are investigated in great detail. The system states of the open system can all be explained by means of the microscopic structures. Note that for the models with branched FDR all system states of the periodic system can be related to the open system. In this sense, the extremal current principle is fulfilled also. Additionally, there exist states of high flow which cannot be related to the FDR of the periodic system. The corresponding *high-flow phase* is dominated by one large jam alternating with periods of free flow. The latter periods give rise to the overall high flow. The observed effect in the high-flow phase can be traced back to the metastability of the models leading to local cluster effects [98]. A more detailed explanation can be found in [13]. Note that the systems investigated in [13] are short (500 cells) and the stochastic component in the movement of the cars is relatively weak. This explains why the effects of metastability can be readily observed. In the thermodynamic limit the high-flow states would vanish and the phase diagram (and phases) of the NaSch and VDR would be equal.

Before presenting the results for the SKM with OBC some further aspects are given why these investigations are important in order to obtain a better understanding of the models [178]. Since real world measurements are always made in

open systems, they are important for the calibration and validation of traffic flow models. Moreover, the understanding of the relation between the microscopic dynamics and phases in presence of OBC may help to establish the connection of the microscopic description with the macroscopic by FDR. As mentioned before, there is still an ongoing discussion about the number of phases that may exist in traffic [24, 41, 76, 93]. With respect to OBC and microscopic models, it can even be seen as open question whether the observed features are bulk properties or boundary induced. A similar statement can be made for the transitions between phases. For example, the assumption that the *hysteresis loop* can only be run through in one direction is challenged by the findings in [174, 187]. In light of OBC it seems natural to assume that the hysteresis loop can be cycled in both directions. Moreover, there is much evidence [140, 147] that non-equilibrium phase transitions occur in traffic flow on highways which are triggered by capacity restrained states in the vicinity of on- and off-ramps. So, there may well be different phases and phase transitions but they may as well be generated by the boundaries and not by the bulk dynamics. The details of the bulk dynamics may solely be able to change the order of the phase transitions observed for OBC [178].
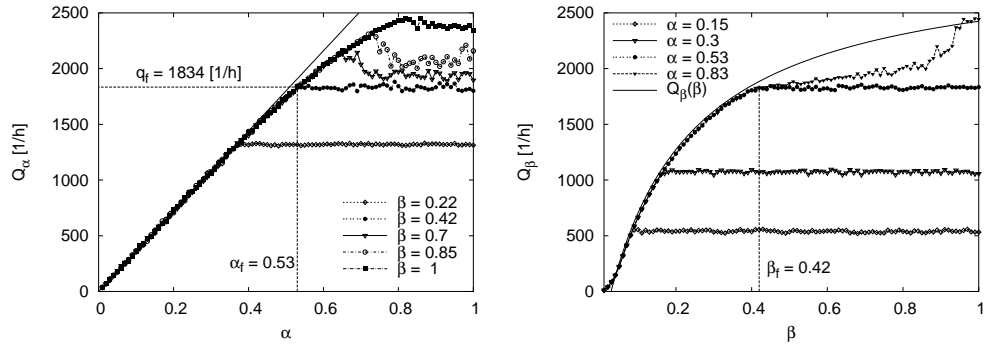
2.4.2 SKM with open boundaries

In the following discussion, the SKM is investigated by means of numerical simulations, using OBC. The parameters chosen are,

$$
\begin{array}{lll}
a = 2 \; m/s^2 & b = 8 \;\; m/s^2 & v_{\max} = 35 \;\; m/s \\
\varepsilon = 1 & l_{\mathrm{car}} = 7 \;\; m & \tau = \Delta t = 1 \; s,
\end{array}
\tag{2.34}
$$

i.e., stable, high-flow states exist in the periodic system and the model displays macroscopic phases. The FDR of the periodic system is given in figure 2.18. For the parameters the outflow from jam and maximum flow are $(\rho_f, q_f) = (15 \, km^{-1}, 1834 \, h^{-1})$ and $(\rho_c, q_c) = (20 \, km^{-1}, 2445 \, h^{-1})$, respectively. As will become clear, the findings of the metastable VDR [13] can be transferred to this case. However, as may be expected, the high-flow phase in regard to OBC is noticeably more stable. Transitions between the phases are also considered and compared to the SKA in section 2.4.3.

The SKM has already been investigated in the open system [137, 138] and, in principle, the expected behaviour was evidenced. Three phases, namely free-flow, jam and high-flow phase, were found and the system states were in agreement with the extremal principle (2.33). However, the high-flow phase was only be observed where there was no restriction imposed upon the outflow of the system. Therefore, the transition to the high-flow phase could not be investigated numerically. Moreover, an artificial phase diagram was found for one of the insertion strate-

Figure 2.17 **Left**: Inflow Q_α for different conditions at the exit of the system. Flows that exceed q_f are found for $\alpha > 0.53$, $\beta > 0.42$. The inserted line is $\propto \alpha$. **Right**: Outflow Q_β for different inflows. Also shown is $Q_\beta(\beta)$ where $\tau_\beta = 1.2\,s$ and $l_\beta = 9.77\,m$ are obtained by fitting (2.35).

gies used in [138]. Two problems were encountered due to the applied boundary conditions:
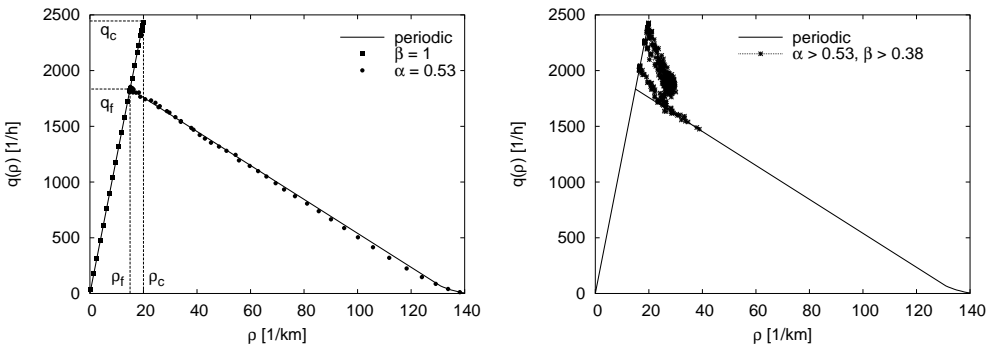
- The use of the standard insertion rule (insert a car with probability α, if the first 'site' is not occupied) does not allow all states along the high-flow branch of the FDR to be reached. In fact, the inflow significantly decreased with increasing α for $\alpha > 0.6$ and was even lower than the outflow from jam (*overfeeding*).

- If the outflow is modelled by blocking the exit with probability β, strong perturbations are introduced into the system at its exit. This leads to the problem that the high-flow phase is destroyed as soon as the probability of having a block is unequal to zero. Note that this strategy is appropriate for models of NaSch type because the braking ability in these models is not bounded.

It is known from [32, 31, 81] that special boundary conditions can have a large influence on the phase diagram, possibly even leading to a violation of the extremal principle.

In order to confirm the findings in [138], and to clarify the transitions between the phases, new boundary rules are established. As usual, cars enter the system at the left boundary and move to the right, where there is the exit of the open system.

Left boundary (entry)

The choice of the input strategy is crucial in order to permit an investigation of the entire spectrum of possible system states. As seen earlier, the use of the standard

Figure 2.18 **Left**: System states for $\beta = 1$ (open exit) and $\alpha = \alpha_f$ (inflow equals q_f). All states of the periodic FDR can be related to the open system. **Right**: For inflows greater than q_f high-flow states occur in the open system that can not be found in the periodic one. For these states $\alpha > \alpha_f$ and $\beta > \beta^* = 0.38$ holds.

insertion rule leads to overfeeding and the high-flow states immediately break down. Because several time steps are needed to reach v_{max} again, flows that exceed the outflow from jam are scarcely reached. An appropriate rule, therefore, has to be able to mimic the highly ordered high-flow states, at least for undisturbed right boundaries. In these states $\langle g \rangle \gtrsim \langle v \rangle$ and $\langle v \rangle = v_{max} - a/2$.

The method used to generate homogeneous states at the left boundary is similar to the method used in [13]. A short segment of length $L_\alpha \geq v_{max}\Delta t + l_{car}$ is linked to the entry and its state is updated in each time step of the simulation. In the first step it is flushed completely, *i.e.*, if there is a car inside the segment, it is removed from it. In the second step, a new car is inserted into the segment with probability α and initial velocity v_{max}. Its position is calculated according to the position of the first car in the open system. The position of the inserted car is chosen such that the gap is at least $g_{min} = v_{max}$ and the distance to the open system is minimal.

Therefore, with open right boundaries, the inflow Q_α to the system increases linearly with α until it snaps off for flows above the outflow from jam q_f. This is due to a slight *overfeeding* because for the stochastic model $\langle g \rangle > \langle v \rangle$ holds. After the inflow reaches a maximum, one finds a plateau which is determined either by the restricted outflow from the system or by the overfeeding effect. For the given parameter set, Q_α is shown in figure 2.17. $Q_\alpha = q_f$ for $\alpha_f = 0.53$ and the maximum flow q_c is reached at $\alpha_c = 0.83$ with an open right boundary.

Right boundary (exit)

The outflow from the open system is determined by the right boundary. Instead of using a block, a segment of $L_\beta = 0.1\,L$ linked to the right boundary. In order to change the outflow, a restriction is imposed on the velocity by setting $v_\beta = \beta v_{\max}$. After a short relaxation time this affects the outflow from the system. For the deterministic case, the relation is determined by (2.11) leading to $Q_\beta = v_\beta/(\tau v_\beta + l_{\mathrm{car}})$. In the stochastic case this becomes, in principle,

$$Q_\beta = \frac{\langle v_\beta \rangle}{\tau_\beta \langle v_\beta \rangle + l_\beta} \qquad \text{where}$$

$$\langle v_\beta \rangle = \beta v_{\max} - a/2, \tag{2.35}$$
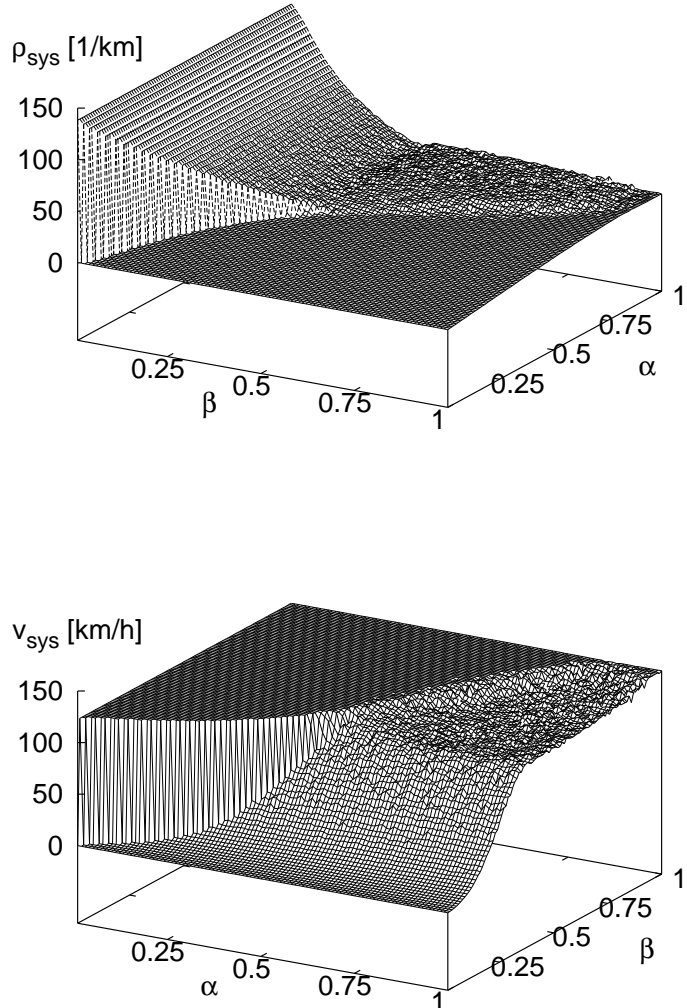
because [113] $\langle g \rangle = \tau_\beta \langle v \rangle + l_\beta$ with $\tau_\beta > \tau$, $l_\beta > l_{\mathrm{car}}$. As long as the possible outflow does not exceed the inflow into the system, this rule, therefore, allows a continuous scaling of the outflow. Note that this boundary condition is closely related to the effects one finds at on- and off-ramps.

The dependency (2.35) is displayed in figure 2.17 together with measurements of Q_β. At low densities small deviations from (2.35) are found due to the slow-to-start behaviour. If the inflow exceeds q_f, the system's flow is lower than that given by (2.35) if $\beta_f > 0.42$. In this case, the reduction of velocity at the exit affects the high-flow states. However, this perturbation is not strong enough to lead to an overall breakdown in the system because of the stability of these states. Note that for the open system ($\beta \gtrsim 0.95$) and maximum inflow, flows complying with (2.35) are reached again.

Open system
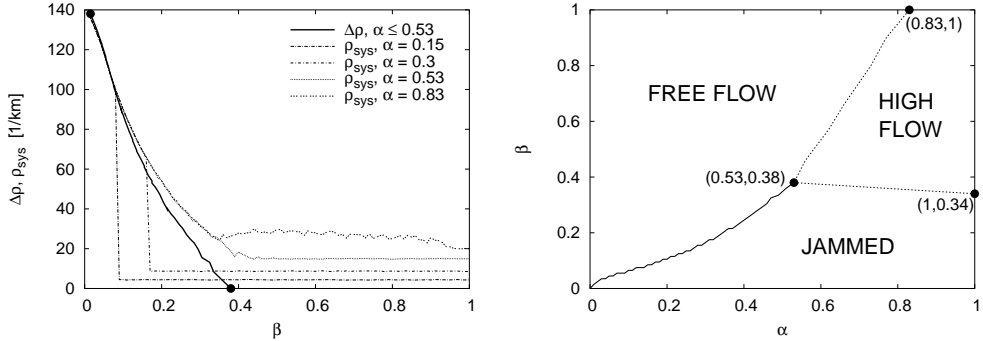
Using the rules given above, an open system of length $L_S = 10^4\,m$ is simulated, screening the (α, β)-plane with step-size 0.01. The system is always relaxed for $2 \cdot 10^5$ time steps before the measurements start. After that time, all simulated systems became stationary, which can easily be checked: In the stationary state, the inflow and the outflow of the system are equal. Presented quantities are time averages over $2 \cdot 10^4$ time steps. The in- and outflow are measured immediately at the entry and the exit, respectively. The corresponding densities and speeds at the boundaries of the system are measured within a $100\,m$ segment. Mean densities ρ_{sys} and speeds v_{sys} in the middle of the system are measured within a $200\,m$ segment. Now, the most relevant results of these simulations are presented. Noteworthy is that the dependency of the in- and outflow are non-linear with respect to α and β.

In figure 2.18 the macroscopic system states measured in the open system are compared to the FDR of the periodic system. One finds that the extremal principle

Figure 2.19   **Top**: System density of the open system. Note that the axis of α and β were interchanged for better presentation. **Bottom**: System velocity of the open system.

(2.33) is also fulfilled for the SKM. The complete FDR of the periodic system can be traced back to the open system. In order to obtain the complete high-density branch, one has to choose a proper inflow, *i.e.*, equal to the outflow from jam ($\alpha = 0.53$). Moreover, one finds high-flow states that do not exist in the closed system. For parameters (α, β) where these states are found, at least one of the

Figure 2.20 **Left**: System densities along $\alpha = const.$. For $\alpha < \alpha_f$, one finds a jump $\Delta\rho$ in these functions which is also displayed. For $\beta \to 0.38$, $\Delta\rho$ vanishes. If inflows exceed q_f, the function $\rho_{\text{sys}}(\beta)$ becomes continuous, showing a discontinuity in its derivative. **Right**: Phase diagram of the SKM. The solid line represents the transition from the free-flow phase to the jammed one and is of first order. The transitions to the high-flow phase are of second order. Their transition lines are indicated by dashed lines.

border densities is inside the interval $\rho_f \leq \rho_{\alpha,\beta} \leq \rho_c$, *i.e.*, the flow $q(\rho_{\alpha,\beta})$ is not well defined with respect to the periodic system. The microscopic structure of these high-flow states explains how flows greater than those within the periodic system are reached (see below).

Before deriving the phase diagram of the SKM from the simulation results, the definition of the *high-flow phase*, as used in the following, is given. Frequently, one uses this term for system states where $q_{\text{sys}} > q_f$. In that case, the high-flow phase simply spans a rectangle in the phase diagram. For the given parameters, this would be the plane represented by $\alpha \geq \alpha_f = 0.53$, $\beta \geq \beta_f = 0.42$. However, using an order parameter to determine the transitions between the phases, slightly different border lines defining the high-flow phase are found. The reasons for this will become clear, but for the moment just note that there are also states with $q < q_f$ which do not exist in the periodic system. It is observed that a transition to the high-flow phase always occurs (by means of an appropriate order parameter), if system states are obtained which do not have a counterpart in the periodic system. Only these states are, therefore, regarded as states of the high-flow phase in the following.

Figure 2.19 shows the density and velocity measured in the middle of the system. Three regions are clearly distinguishable. The region in which density and velocity are high *resp.* low, corresponds to the jammed phase. In the free-flow phase the density is low and the velocity is given by $v_f \approx v_{\max} - a/2$. Lastly, there is a region where the density is slightly greater than in the free-flow phase.

Here the velocity is also high, but lower than v_f. The latter region is the high-flow phase.

Along lines of constant $\alpha \leq 0.53$, one observes a non-vanishing jump $\Delta\rho$ whose size decreases with increasing α. For specific values of α, the system density on β is displayed in figure 2.20, together with the size $\Delta\rho$. The jump $\Delta\rho \to 0$ for $\beta \to \beta^* = 0.38$. If $\Delta\rho$ is used as an order parameter, the *phase transition* from the free-flow phase to the jammed phase is identified to be of first order [55].

For $\alpha \geq \alpha_f$, the system density over β is continuous but displays a jump in its derivative indicating a phase transition of second order [55], *cf.* figure 2.20. A fully automated determination of the transition points (α, β) is complicated by the present fluctuations of the densities in the high-flow phase and would require further numerical efforts. The transitions lines defining the high-flow phase which are given in the *phase diagram*, figure 2.20, were, therefore, determined "by eye". With regard to the displayed profiles of $\rho_{\mathrm{sys}}(\beta)$ and $\alpha = const$, the discontinuity in the derivative of ρ_{sys} is clearly visible. The same is true for the corresponding profiles of $\rho_{\mathrm{sys}}(\alpha)$ and $\beta = const$.
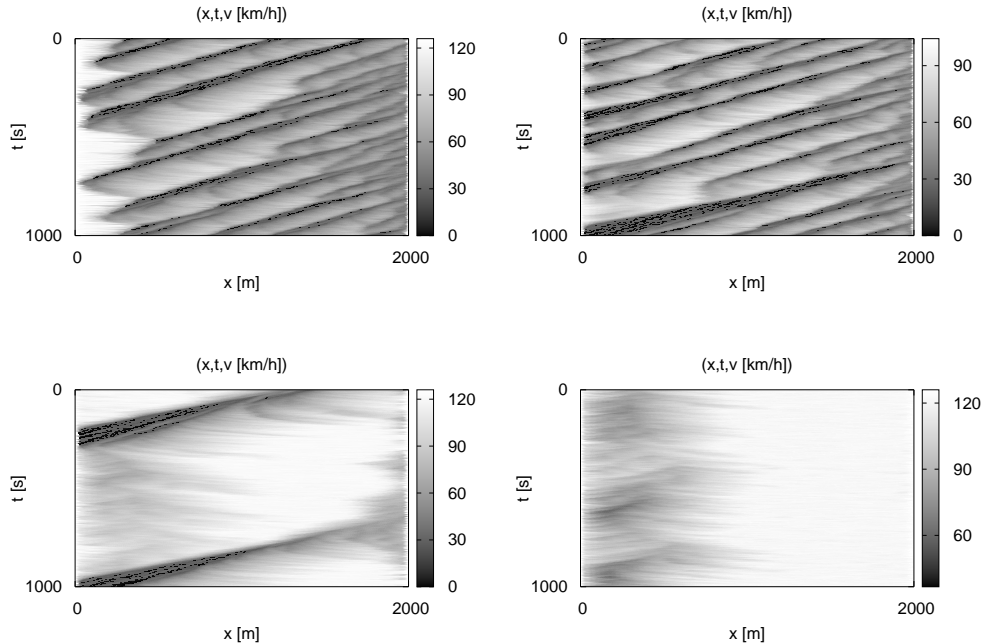
In order to attenuate the lack of mathematical rigour, the results were checked again, using the velocity v_{sys}, *cf.* figure 2.19. The profiles of the velocity with constant α were processed as follows. Firstly, the profiles were smoothed because a fit to a functional relation was otherwise impossible due to the fluctuations in the data points. To this end, the weighted sum of each data point and its neighbours was calculated. After, the derivative of each profile, $dv/d\beta$, was computed and fitted against functions of the type $(\beta_c - \beta)^\gamma$. The value β_c gives the transition point. The values for β_c, which resulted from the fitting procedure, compare to the values determined before, *i.e.*, the ones plotted in figure 2.20. For the critical exponent, $\gamma \approx 0.5$ was found. The profiles with $\beta = const$ were processed in the same way, and the results confirmed the earlier findings for the transition line.

An alternative representation of the phase diagram is obtained, using the inflow Q_α and outflow Q_β instead of α and β. The transformation of the above results can be done using the inverse of $Q_\alpha(\beta = 1)$ and $Q_\beta(\alpha = 0.83)$ from figure 2.17. Recall that these flow depend on α and β in a non-linar way. Using this representation, it can be seen that the system always displays flows which that can be maintained by both boundaries.

With respect to the microscopic structure of the phases (shown in figure 2.21) the findings concur with [13].

Inside the free-flow phase either no perturbations exist at the system's exit or small micro-jams are generated there. However, since the inflow into these jams is smaller than their outflow, they dissolve immediately (not shown).

In the jammed phase there are several jams inside the system which are generated by perturbations at the right boundary. While travelling backward through

Figure 2.21   **Top**: Space-time diagrams inside the jammed phase. *Left*: $(\alpha, \beta) = (0.4, 0.2)$ (Jam-I). *Right*: $(\alpha, \beta) = (1.0, 0.2)$ (Jam-II). **Bottom**: Space-time diagrams inside the high-flow phase. *Left*: $(\alpha, \beta) = (0.8, 0.5)$. *Right*: $(\alpha, \beta) = (0.9, 0.9)$.

the system, they do not grow considerably because their outflow equals their inflow as this is feeded by another jam. Note that the merging of two subsequent jams is also possible if they were generated close to each other. According to the definitions given in [13] it is possible to distinguish the behaviour inside the jammed phase on the following basis: The jams either all dissolve before reaching the entry or restart growing close to it. In [13] this is termed as Jam-I phase and Jam-II phase, respectively. Given that compact jam clusters alternate with free-flow regions in these two phases, their microscopic structure is referred to as *striped pattern*.

An example of a Jam-I phase is given in figure 2.21 with $(\alpha, \beta) = (0.4, 0.2)$. In this case, if a jam is closest to the entry, its outflow exceeds the inflow at its upstream front provided by the left boundary. The jam dissolves mostly before the left boundary is reached.

In the Jam-II phase, *e.g.*, $(\alpha, \beta) = (1.0, 0.2)$, the exact opposite occurs. Inflows into the system are greater than the outflow from jam and, therefore, a jam closest to the entry even grows. When the jam reaches the entry, the insertion of

new cars is suppressed until the jam has dissolved. The findings show that the striped structure should be present in all models that display phase separation in the periodic system.

In the high-flow phase it is also possible to distinguish between two different behaviours.

The first type of behaviour is given in the case where the outflow is almost unrestricted, *e.g.*, $(\alpha, \beta) = (0.9, 0.9)$. Thus, no perturbations are introduced at the system's exit. If α exceeds α_f, small perturbations can exist in the vicinity of the left boundary due to overfeeding effect, however, healing out very quickly. Most of the time the flow in the system is, therefore, not affected at all, *i.e.*, the high-flow states inserted at the left boundary reach the exit.
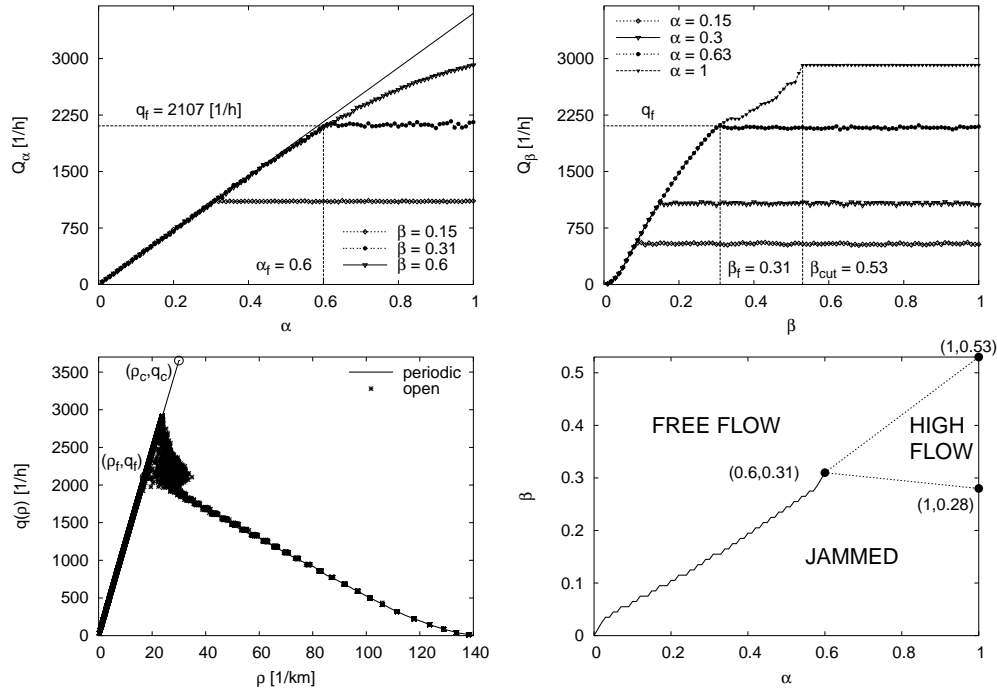
If the right boundary affects the flow, *e.g.*, $(\alpha, \beta) = (0.8, 0.5)$, the striped structure is found again. However, in the case of the high-flow phase, the system is mainly dominated by one single large jam. Periods of unrestricted high flow alternate with periods where the flow is determined by the outflow from jam. If the system size is small enough, the time periods of high flow have an integral part in the overall system flow, *cf.* [13].

To complete the discussion, a short comment is made with respect to applications of the preceding findings to real world traffic. The influence of OBC on the system state show that controlling in- and outflows can have an effect on optimising traffic streams. An example of flow optimisation by inflow control is provided by the famous experiments at the Lincoln and Holland Tunnels in New York [64, 79]. Other than the reduction of fluctuations, the effect ramp metering has on flow stabilisation can also be discussed in light of boundary induced phase transitions.

2.4.3   SKA with open boundaries

The investigations performed for the SKM with OBC are repeated for the model with anticipation. Concise results are presented because the findings are the same as those for the model without anticipation. This again shows that anticipation only gives rise to more stable high flows and allows for shorter time-headways, whereas the overall dynamic nature of the model remains unchanged. Using OBC, the same phases as in the SKM are found and the order of phase transitions also remains unchanged. The same is true for the microscopic structure of the phases.

The same methods and the same set of parameters used for the SKM were used for the simulations. Additionally, g_c is fixed to $1\,m$. It is evident from figure 2.22 that the maximum flow of the periodic system ($q_c = 3653\,h^{-1}$ at $\rho_c = 30\,km^{-1}$) is not reached in the open system. This is due to the special structure of the high-flow states (*cf.* section 2.3), which is not mimicked by the insertion strategy. The outflow from jam ($q_f = 2107\,h^{-1}$ at $\rho_f = 17\,km^{-1}$ in the periodic system) is

Figure 2.22 **Top**: In- and outflow of the system (SKA). *Left*: Inflow Q_α for different conditions at the exit of the system. Flows that exceed q_f are found for $\alpha > 0.6$, $\beta > 0.31$. *Right*: Outflow Q_β for different inflows. If $\beta > 0.53$, the inflow is no longer affected by the right boundary.
Bottom: Extremal principle and phase diagram (SKA). *Left*: Comparison of the states found in the periodic and the open system. All states of the periodic FDR can be related to the open system. *Right*: Phase diagram of the SKA. The solid and dashed lines represent phase transitions of first and second order, respectively. For $\beta > 0.53$, only the free-flow phase exists in the open system.

found for $\alpha_f = 0.6$ ($\beta = 1$) and, accordingly, $\beta_f = 0.31$ ($\alpha = 1$). The value of β_f is lower than for the SKM which indicates that the right boundary has a weaker impact on the system here. This is related to the fact that the drivers anticipate the velocity of their predecessors. Moreover, for $\beta > 0.53$, the right boundary has no further influence on the system. This is because the inflow does not reach all possible states along the high-flow branch of the FDR. Note that, due to the fact that two consecutive cars share a common gap in this model, equation (2.35) is not valid here.

Figure 2.22 also compares the states of the open system to the states of the periodic one. It is found that the extremal principle is fulfilled for the SKA. More-

over, the *phase diagram* of the SKA is given ($\beta > 0.53$ not shown. For these values only the free-flow phase is present). The transition lines between the different phases are determined using the same methods as before. For the critical exponent of the transition from jammed to high-flow one obtains again $\gamma \approx 0.5$ (using the velocity profiles).

2.5   Conclusion

The discussion in this chapter focused on the dynamic properties of a specific microscopic car-following model, the SKM. The investigations of the macroscopic states together with their time-headway distributions and optimal velocity curve complete the discussion of the model as given in [113].

The model displays different classes of dynamic behaviour depending on the parameters chosen. With regard to model classes where structure formation is found, the classification is reviewed in light of recent findings [131]. In contrast to traffic flow models based on cellular automata, the SKM possesses high-flow states which are stable against intrinsic fluctuations of the model. It is shown that there is a transition to metastable high-flow states, if the braking ability grows to infinity. However, in contrast to the assumptions of the original work [113], high-flow states are always observed, if the strength of fluctuations is not too high ($\bar{a} \leq 0.8$ for the parameter sets investigated in section 2.2.2). For all (investigated) parameter sets which belong to the class of models with structure formation a stable outflow from jam is found.

Anticipation is shown to be an important component in microscopic car-following models in order to obtain more consistency with empirical findings. This driving strategy is introduced into the SKM using next-nearest-neighbour interactions. The effects in regard to the model's dynamics are investigated in great detail, by simulations as well as by analytical calculations. It is found that anticipation leads to a stabilisation of the flow in dense traffic and is responsible for the occurrence of very small time-headways, as found in reality, whereas the other dynamic properties remain unchanged. It is shown that the mechanism behind works by coupling three cars together. As a consequence, they share their two respective headways which become anti-correlated. Because the given arguments are rather general, this mechanism is present in any traffic flow model that works with anticipation.

The presence of fixed-points in the dynamics of both models is further explored. These fixed-points are shown to be rather stable, therefore, considerable changes in the dynamic equations of the models are necessary, in order to allow the modelling of synchronised flow.

Other than the investigations of periodic boundary conditions, the phase diagram of both models is investigated in open systems. It is shown that the models with stable high-flow states, fulfill an extremal principle [109, 148], which relates the properties of the periodic system with the open system in a very general way. Besides the free-flow and jammed phase, a high-flow phase occurs. The microscopic structures which are found within the phases are similar to the ones which are found in empirical observations [76, 93, 173]. The introduction of appropriate boundary conditions further allows the investigation of the transition between the phases. It is shown that the transition between the free-flow and jammed phase is of first order, whereas the transitions into the high-flow phase are of second order. Together with the findings in [13], it can be concluded that the presented phase diagrams and the microscopic structure of the phases are generic for microscopic car-following models which exhibit a branched flow-density relation and phase separation.

Mesoscopic Modelling Based On Queueing Theory

3.1 Traffic flow modelling by queueing approaches

Microscopic car-following models certainly allow for the detailed representation of individual driving behaviour within simulation [52, 105, 172, 182]. For example, the drivers' assumptions about safe driving enter straightforwardly into the model's formulation as seen in chapter 2.

For many applications, such a detailed view of driving dynamics has to be weighted against computational efficiency, or is even not needed. For example, as pointed out in [59, 60], in regard to the simulation-based solution of the traffic assignment problem, an approach is favourable, which is based on individual vehicles and models the car-following behaviour solely on a coarse level. Such models are called *mesoscopic*, because of their intermediate position between microscopic and macroscopic approaches. Model approaches where individual cars are moved according to mean densities on street segments, as in DYNEMO [160], or queueing models [2, 35, 59, 72, 84, 127, 175] where vehicles or traffic volumes are moved without modelling the dynamics inside the segments, can be regarded as typical examples for mesoscopic traffic flow models.

From the perspective of queueing theory, the *links* of a network (*i.e.*, a part of a road which starts and ends at an intersection *resp.* a node) are represented as a queue or a sequence of queues. Cars that enter a queue have to wait at least for the *free-flow travel time*, necessary to pass the correspondent distance, before they are allowed to leave it. The transmission of a car to the next queue on its path is further affected by the *queueing discipline*, the *capacity* and the *storage capacity* of the link. Note that terms frequently used in the context of queueing theory are introduced in appendix A.

The following discussion starts with the presentation of different queueing

models in the context of traffic flow modelling, found in literature. This discussion focuses on the applicability of these models in regard to the computation of travel times and environmental impacts of traffic within the frame of *dynamic traffic assignment* (DTA). This framework is further described in section 4.3, but for the discussion of the models just note that the following requirements are desirable for a mesoscopic traffic flow model, having regard to the applications addressed in this work:

- The model should display traffic states distinct from each other. In this respect, the existence of two traffic phases, namely free flow and congested traffic, is already sufficient for many applications in urban networks.

- In particular, traffic inhomogeneities should be modelled properly, *e.g.*, traffic jams should move backwards.

- Modelling should be based on individual car-driver units in order to allow the tracking of vehicles on their individual routes and the representation of different vehicle classes.

- In order to reach the high computational performance, needed for simulation-based traffic assignment, the movement of the vehicles should be based on preferably large spatial units.

- Macroscopic properties of the flow, as the FDR, should result from the microscopic properties of the model.

- The model should allow the computation of the dynamics of traffic streams with preferably high temporal resolution, needed to determine environmental impacts.

It is further pointed out, why most approaches of queueing theory fail in regard to the above requirements. A new approach is, therefore, introduced in section 3.2, which is mainly motivated by microscopic traffic flow modelling. Its dynamics and properties are discussed in detail, including comparisons to the SKM. Whereas the discussion of the new approach is focused on periodic systems in this chapter, network flows and applications to environmental impact modelling are addressed in chapter 4.

3.1.1   Stationary, state-dependent and transient queues

The framework of classical queueing theory is introduced in appendix A and its application to traffic flow modelling is discussed in the following. Note in advance that, although the modelling of processes in queueing theory is motivated microscopically, system's properties are described taking a macroscopic perspective. To put it differently, the description of traffic flow using classical (stationary) queueing theory [65, 121] focuses rather on the connection of FDR with relevant

characteristics of traffic systems [71, 72, 175] than on the details of individual car motion. Nevertheless, it is worthy to understand, where these approaches can be used *resp.* where they fail, in regard to the modelling of traffic flow, because of their sound theoretical foundation.

In terms of queueing theory, each link of a street network is regarded as a service device operating at a certain *service rate* which corresponds to the *capacity* of the link, *i.e.*, maximum throughput in $[veh./h]$ which can be maintained. Queues of cars, *i.e.*, *congestion*,occur in the system, whenever the current demand exceeds the capacity of a service. In consequence, vehicles queue up in front of the service device, and experience additional waiting times before being served. The total time a vehicle spends on a link, therefore, equals the sum of the waiting time due to congestion and the service time. Queueing theory then permits the calculation of *waiting times* and *queue lengths* which result from the service and arrival rates, the degree of saturation and the queueing discipline (*cf.* appendix A).

Steady-state solution of a M/G/1-queue

In the following, the basic procedure describing traffic flow by queueing theory is demonstrated. For simplicity, solely the case of stationary flow is considered. The discussion follows [71], where traffic flow is described in terms of a M/G/1 queueing model, using first-in-first-out queueing discipline (*FIFO*).

Assume that the road is divided into pieces of length $1/\rho_{\max}$ ($\approx 8\,m$), with $\rho_{\max}$ being the density inside jams. Each of these pieces is regarded as a queue. A car driving under free-flow conditions, passes the queue within the time $1/(\rho_{\max} v_{\max})$, and the corresponding *service rate*, *i.e.*, the flow, is $\mu = \rho_{\max} v_{\max}$. Moreover, if the traffic density is given by ρ, cars arrive at the queue with the *arrival rate* $\lambda = \rho\, v_{\max}$.

However, the service may as well be busy when a car arrives at the queue. Thus, queueing occurs leading to additional waiting times. It can easily be argued that the resulting waiting time is independent from the description of the queueing process, given stationarity [71, 72]. To be more precise, it does not change the result whether one either assumes that cars are batched immediately in front of the service (*i.e.*, a queue can hold more than one car), or if the queue spatially extends backwards. Thus, a description as queue with unlimited storage capacity is appropriate.

In order to proceed, further assumptions about the arrival of vehicles and the service are necessary. If it is assumed that the interarrival times are exponentially distributed with mean $1/\lambda$, and, furthermore, that the service times are generally distributed with mean $1/\mu$ and standard deviation σ, traffic is described by means of a M/G/1 queue. In this case, the *Pollaczek-Khintchine formula* (A.11) holds, which relates the mean queue length $\langle Q_L \rangle$ and the degree of saturation

$\eta_q = \rho/\rho_{\max}$ (also called *utilisation*),

$$\langle Q_L \rangle = \eta_q + \frac{\eta_q^2 + \lambda^2 \sigma^2}{2(1 - \eta_q)}. \tag{3.1}$$

Combining this result with *Little's formula* for the waiting time, $W = \langle Q_L \rangle / \lambda$, yields

$$W = \frac{1}{v_{\max}\,\rho_{\max}} + \frac{(\rho/\rho_{\max})^2 + v_{\max}^2\,\rho^2\,\sigma^2}{2v_{\max}\,\rho(1 - \rho/\rho_{\max})}. \tag{3.2}$$

Thus, the mean speed of the system, $v = 1/(\rho_{\max} W)$, reads

$$v(\rho) = \frac{2v_{\max}(\rho_{\max} - \rho)}{2\rho_{\max} + \rho(\beta^2 - 1)}, \tag{3.3}$$

with $\beta = \sigma v_{\max}\rho_{\max}$. Equation (3.3) implies that, due to queueing, the maximum speed $v_{\max}$ cannot be maintained but is reduced according to the derived speed-density relation. This result does not only hold for the queue of length $1/\rho_{\max}$, but for the entire road. This is valid, because the density ρ has to pertain to the speed given by (3.3) everywhere in the system given stationarity. Note that this further implies that perturbations spread instantaneously over the entire system.

Further note that equation (3.3) means that the travel time t_{tr} on a link solely depends on its density ρ. The resulting function corresponds to the functional type Davidson proposed [44],

$$t_{tr} = t_{tr}^0 \left(1 + c\frac{q}{q_{\max} - q} \right) = t_{tr}^0 \left(1 + c\frac{\eta_q}{1 - \eta_q} \right), \tag{3.4}$$

where t_{tr}^0, q and $q_{\max}$ are the free-flow travel time, the current flow on the link and the capacity, respectively. The parameter c has to be estimated from field measurements. Equation (3.4) is derived from a M/M/1 queueing model, which results from (3.3) and $\beta \to 1$. The travel time (3.4) diverges as $q \to q_{\max}$ *resp.* $\eta_q \to 1$, whereas this is not found in reality. Moreover, for all flow levels below capacity, two corresponding travel time values are found due to the existence of different traffic states [132].

State-dependent queues

Observations of street traffic show that the vehicles' speed on a road segment is strongly influenced by the the current density. Therefore, it is natural to give up the assumption of fixed service rates, *i.e.*, the assumption of a constant speed for the vehicles travelling the queue. If a function for the service rate is used which

depends on the number of cars on the link, the terminology of state-dependent queueing theory is addressed. Most approaches found in literature assume stationary traffic conditions (in order to allow analytical investigations). For example, traffic flow is described by means of a state-dependent G/G/1 queue in [175]. A more comprehensive description in terms of M/G/N/N queues is given in [84]. The details of the model and its application to describe traffic systems is given in detail in appendix A. For the current discussion, the following remarks are noteworthy:

The consideration of a decreasing service rate due to an increasing utilisation of a queue aims to improve the drawbacks of approaches presented before. But, the state-dependent description also leads to a travel time functions solely depending on the density inside the queue. If such travel time functions are used to implement the microscopic counterpart of state-dependent queueing models (see *p.* 56), this does not yield an appropriate dynamics of jams, however. Besides this major drawback, it is stated in [84] that already the computation of small networks using state-dependent queues needs enormous computational efforts with respect to computation times. Thus, the simulation of large street networks, as addressed in this work, is beyond the scope of these approaches. Finally note that, in order to construct such models, assumptions about traffic flow, as the speed density relation $v(\rho)$, are necessary, whereas this work aims an description where macroscopic characteristics of traffic result from the microscopic dynamics of the model.

Consideration of non-stationarity

The descriptions of traffic flow given above all assume stationarity. However, in regard to the dynamic nature of traffic, the dependence on time has to be considered. This is pointed out more clearly in [183]. For example, it is known from measurements that traffic demand can exceed capacities for a finite time interval. In approaches which assume stationarity, however, queue lengths and delays grow to infinity in that case, *cf.* equation (3.4). Another drawback stems from the fact that the duration of peak periods, encountered in practice, is usually not long enough for the queues to settle down to a stationary state.

One possible way to deal with these problems is an approach, which switches continuously from the stationary description to a deterministic one, with increasing utilisation. In appendix A it is shown that a deterministic description of the queueing process is appropriate if the system reaches the regime of oversaturation. In the TRANSYT model [183] (and references therein) this is implemented by means of sheared delay formulae. The model can be used to predict queues and delays of road traffic at individual junctions and small areas of traffic control, however, a treatment of large networks seems to be difficult within this approach.

Besides, there is also a framework for the description of non-stationary queueing systems [65], called *transient* queues. In [72] this is related to traffic systems using transient M/M/1 queueing systems. The resulting expression for the velocity in the system can not be given in closed form. Similar to (3.3) it is given by

$$v(\rho, t) = \frac{1/\rho_{\max}}{w(\rho, t, i)}, \qquad (3.5)$$

where $w(\rho, t, i)$ is the mean waiting time per vehicle. This waiting time has to be calculated by numerical integration, and depends on the system's density ρ, the initial queue length i, and time t. The initial queue length is supposed to include all the relevant history of the system and t is the time that has elapsed since then. Besides the additional time dependence, resulting travel times are still functions solely depending on the density inside the queue [72]. Moreover, the need for numerical integration only allows for the efficient treatment of single links.

Transformation into a microscopic queueing model

The focus of the presented works is clearly on the description of uninterrupted traffic flow and its embedding into the general concepts of queueing theory. These approaches are valuable and successfully used in order to describe single road links or single intersections in regard to the estimation of performance measures under different traffic conditions, see [84, 175] *e.g.*. However, for the purpose of microscopic modelling of net-wide traffic, these approaches have shortcomings which are mainly related with the absence of different traffic states in a rigour sense. This is further demonstrated now.

The implications of the above results, with respect to microscopic modelling, can be investigated by means of an implementation of simple queueing networks in the following fashion:

A road link of length L_S is regarded. It is divided into a sequence of queues, each with spatial length L. The single queues, which compose the link, will frequently be referred to as *segment* in this work. Each segment possesses the same maximum *storage capacity*, $N = L \rho_{\max}$. A travel time is assigned to each car which enters a segment. This travel time may either be constant or depends on the the current density inside the segment. Moreover, the movement of the cars from segment to segment obeys FIFO. For simplicity, periodic boundary conditions are used, and the system is initialised by one dense traffic jam of N_S cars, *i.e.*, the global system density is $\rho_{\text{glo}} = N_S/L_S$. It is known from the discussion in chapter 2 that the initialised jam, eventually, either dissolves for $\rho_{\text{glo}} < \rho_f$ or moves backward through the system, if the global density is above ρ_f. If the travel

time functions, resulting from queueing theory were right, similar behaviour is expected for the implemented microscopic counterpart of queueing systems, at least for stationary conditions (which are given for the periodic system after a sufficient relaxation time elapsed).

Several functional dependencies for the travel time were applied, but even non-linear travel time functions, as
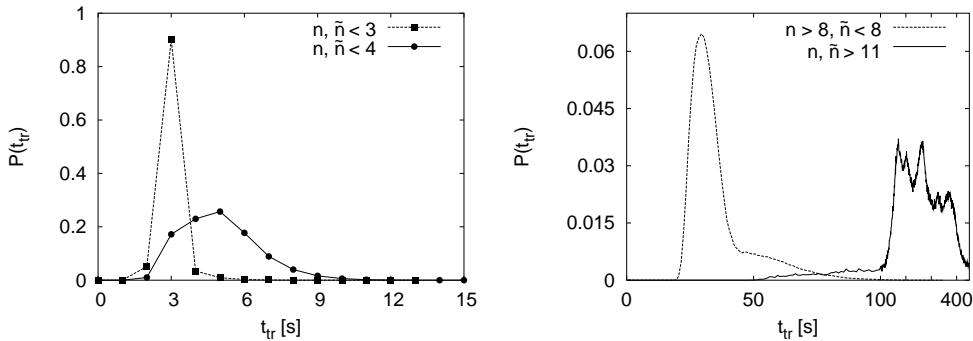
$$t_{\mathrm{tr}}(\rho) \propto 1 + \frac{1}{1 - \rho/\rho_{\max}}, \tag{3.6}$$

with ρ being the density inside the segment which is entered by the car, were not able to generate backward moving jams. Either the jams dissolved, even for $\rho_{\mathrm{glo}} > \rho_f$, or their downstream front stayed fixed at the position where it was initialised.

The reason for this behaviour stems from the fact that, even if a queue is considerably crowded, its dynamics does not differ from an almost empty one. Therefore, there is no distinction between the free-flow state and the congested one. Furthermore, the finding of jam fronts staying at a fixed position indicates that in queueing approaches all queued cars instantaneously take over a place which is opened downstream by a car leaving the jam.

The findings do not change if travel time functions are used that, additionally, depend on the density $\tilde{\rho}$ of the segment in front, *i.e.*, $t_{\mathrm{tr}} = t_{\mathrm{tr}}(\rho, \tilde{\rho})$. These functions were generated in the following way: A SKM is modelled on a loop and parameters were chosen as in (2.8), therefore, stable jams exist. This system was simulated at different densities and the travel time function $t_{\mathrm{tr}} = t_{\mathrm{tr}}(\rho, \tilde{\rho})$ was sampled by using a virtual fragmentation of the system into spatial intervals of $L = 100\,m$. Using this travel time function in the implementation of a microscopic queueing model, as given above, backward moving jams were not found. In parts, the initialised jams were even not stable at all.

Figure 3.1 shows the distribution of travel times from the above experiment for different traffic situations. The travel times are narrowly peaked around $L/v_{\max}$ inside the pure free flow, because the cars do not mutually influence their motion. If cars are considered that approach the upstream front of a jam, the distribution of travel times becomes broader and its mean slightly shifts towards greater travel times. This finding reflects that cars already start to slow down if a queue of standing cars is approached from behind. With regard to congested conditions one can clearly see that the distribution of travel times in the outflow region of a jam considerably differs from the one found inside a jam. Both distributions are rather broad compared to the case of free-flow, *i.e.*, the standard deviation and the mean value have the same order of magnitude. Note that the observed broadness of the distributions also stems from the fluctuations present in the car-following model. Two things can be concluded in regard to congested conditions:

Figure 3.1   Distribution of travel times in the SKM for different traffic situations, obtained as described in the text. The loop is divided into virtual segments of length $L = 100\,m$ and n, $\tilde{n}$ are the number of cars inside the segment entered by the car and the following segment, respectively. **Left**: For $n, \tilde{n} < 3$, all cars are in the free-flow state, whereas $n, \tilde{n} < 4$ also includes cars approaching the upstream front of a jam. **Right**: For $n, \tilde{n} > 11$, cars are inside a jam ($P(t_{\mathrm{tr}})$ is scaled by factor 10). The other distribution belongs to cars that escape from a jam, *i.e.*, the outflow region of a jam is covered. Note also the scaling of the x-axis in comparison to the figure on the left.

  - The travel time (per unit length) inside the jam is distinct from that inside the outflow region of a jam.

  - The travel time depends strongly on the system's history. This may even include the conditions several segments upstream *resp.* downstream of the segment under consideration.

These results can be seen as a possible explanation for the finding that it is not possible to capture the dynamics by means of a travel time function, solely dependent on the densities ρ and $\tilde{\rho}$. This conclusion is further supported by the findings in [167]. In this work, travel time functions of different microscopic car-following models have been investigated for open systems. It was not possible to find a relation between travel time and density which is valid for the complete density range, *i.e.*, different traffic conditions.

In order to model backward propagating jams, it is, therefore, necessary to account for the strongly reduced flows inside a jam together with the reduced outflow from jam. For systems where traffic flow is modelled by queues, this requires a connection between the dynamics of subsequent queues. It is the author's point of view that the shortcomings in most models, representing traffic flow in terms of queueing theory, can be found in the simplification that there is no coupling between the dynamics of queues.

The discussion on traditional queueing approaches is closed with a short remark on *spill back*. Spill back is different from what was termed backward propagation of jams before. If a network of queues with finite storage capacity is considered, there may occur situations in which a queue becomes completely crowded because its inflow exceeds its outflow. Only in this case there exists an interaction with queues connected to its upstream end, because no cars can leave the latter ones as long as the queue remains completely blocked. In this sense, congestion can spread backwards over the network which is called spill back. However, this congested network state either starts to dissolve simultaneously at different queues (that is the case, if the capacity of a queue is lower than the capacities of the queues downstream). Or the downstream front of the congested network state stays fixed at the queue where spill back started and dissolution proceeds from upstream. In reality, however, jams dissolve from their downstream end.
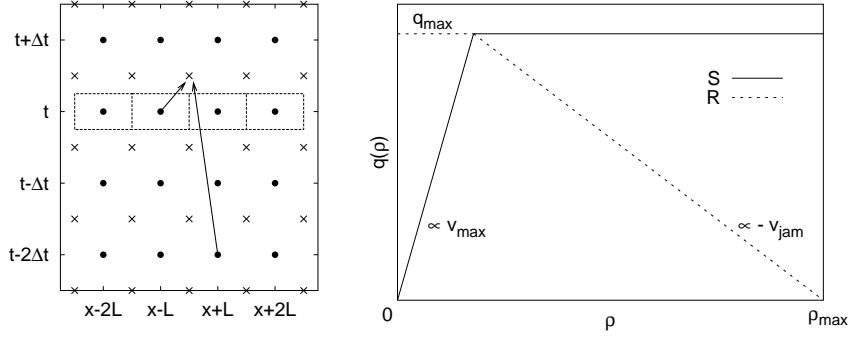
3.1.2 Approaches based on the continuity equation

The two models, presented in the following, partially use the terminology of queueing theory. Their dynamics is, however, derived on the basis of the *continuity equation*. This equation simply states conservation of vehicles within a given section of the road. The state variables of the two approaches, *i.e.*, density $\rho(x, t)$ and flow $q(x, t)$, are macroscopic which makes these models unsuitable for the vehicle-based approach to DTA. Nevertheless, they include important aspects which also play a prominent role in the new approach presented in section 3.2. As will become clear, the approaches account for the dependence of flows on the downstream traffic conditions and the fact that the speeds of density perturbations in free flow and congestion differ from each other.

Cell-Transmission Model (CTM)

The aim of the queueing model presented in [35, 36] is a description of net-wide traffic flows in order to evaluate travel times needed in DTA. The approach is based on the macroscopic description of kinematic waves on traffic highway, *i.e.*, the description in terms of the famous model of Lighthill and Whitham [123] and Richards [153] (LWR). This model was one of the first *macroscopic traffic flow models* and many later works in this area are based on it. Its dynamics is described in terms of partial differential equations,

$$
\begin{aligned}
0 &= \frac{\partial \rho(x, t)}{\partial t} + \frac{dq(\rho)}{d\rho} \frac{\partial \rho(x, t)}{\partial x}, \\
\frac{dq(\rho)}{d\rho} &= v + \rho \frac{dv(\rho)}{d\rho}.
\end{aligned}
\tag{3.7}
$$

Figure 3.2   Diagrams are taken from [38] in a modified form.
Left: Graphical representation of equations (3.8),(3.9). Dots represent the centre of a cell, the crosses symbolise the evaluation of transmitted flows between two neighbouring cells. Shown is the situation for $\ell = 2$.
Right: Triangular FDR (3.10) which determines the sending (S) and receiving (R) flow in equation (3.9).

Equation (3.7) results from the *continuity equation* $\partial_t \rho + \partial_x(v\rho) = 0$ by inserting the equilibrium flow-density relation $q(\rho)$. It describes the propagation of nonlinear kinematic waves with speed $dq/d\rho$.

Based on the works of Newell [141], the differential equations of kinematic theory are approximated by a set of difference equations for the flow. In these, the current state of the system is updated in discrete time steps of size Δt. The road is divided into cells[1] of length L. Usually, $L = v_{max} \Delta t$ is chosen (see below). In each time step the inflow to a cell, *i.e.*, the *transmitted flow*, is calculated depending on the conditions inside its neighbouring cells and its own state. That is where the name Cell-Transmission Model comes from.

If the centre of a cell is denoted by x, and $\rho(t, x)$ is the average density estimated for this cell at time t, conservation of vehicles requires

$$\rho(x, t + \Delta t) = \rho(x, t) - \frac{\Delta t}{L} \left[q_\ell \left(x + \frac{L}{2}, t + \frac{\Delta t}{2} \right) - q_\ell \left(x - \frac{L}{2}, t + \frac{\Delta t}{2} \right) \right] \quad (3.8)$$

In (3.8) the flows q_ℓ are evaluated at the upstream and downstream border of each cell, see figure 3.2. They are determined by

$$q_\ell \left(x + \frac{L}{2}, t + \frac{\Delta t}{2} \right) = \min \left\{ S\left[\rho(x, t) \right], R\left[\rho(x + L, t - \ell\Delta t) \right] \right\}, \quad (3.9)$$

where S and R are the *sending* and *receiving flow*, respectively. The flows S and R are given according to an unimodal flow-density relation $q(\rho)$ which is an input

---

[1]simply another name for a segment

of the model. In figure 3.2, S and R are pictured for a linear FDR. In that case, S and R can be described by just a few parameters, namely, v_{max}, q_{max} and v_{jam}. The latter parameter gives the slope of the high-density branch. With these parameters, the unimodal FDR reads

$$q(\rho) = \min\left\{v_{\mathrm{max}}\,\rho,\, q_{\mathrm{max}},\, v_{\mathrm{jam}}(\rho_{\mathrm{max}} - \rho)\right\} \qquad 0 \le \rho \le \rho_{\mathrm{max}}. \qquad (3.10)$$

The parameter ℓ is called the *lag* of the model. In the original formulation, as given in [35], it is set to $\ell = 0$, *i.e.*, the flows S, R are evaluated at the same time. In that case, maximum accuracy of the approximative update scheme is obtained for the choice [38]

$$\Delta t = L / \left| q(\rho) \right|_{\mathrm{max}}. \qquad (3.11)$$

$\left| q(\rho) \right|_{\mathrm{max}}$ is the maximum of the two wave speeds in the given FDR. In traffic streams the free-flow speed $\left| v_{\mathrm{max}} \right|$ is usually larger than the speed of density waves $\left| v_{\mathrm{jam}} \right|$. Thus, for the linear case $\left| q(\rho) \right|_{\mathrm{max}} = v_{\mathrm{max}}$. This result was already used above with respect to the choice of L. The meaning of (3.11) is that perturbations cannot cross several cells within one time step. Thus, it is ensured that the flow between two cells is exclusively given by their sending and receiving flows.
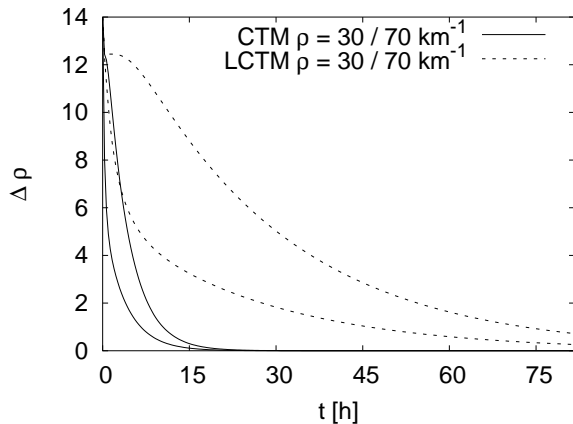
In order to improve the approximation quality of the CTM (in regard to the LWR model), it is advantageous to evaluate the sending and receiving flows at different time steps [38], if $\left| v_{\mathrm{max}} \right| \gg \left| v_{\mathrm{jam}} \right|$ (as given in traffic streams). It is shown in [38] that $\ell \neq 0$ requires

$$\ell \approx 0.5\left[\frac{L}{\Delta t \,\left| v_{\mathrm{jam}} \right|} - 1\right] \qquad (3.12)$$

in order to achieve maximum accuracy (because of $\ell \in \mathbb{N}$, next nearest integer is chosen in simulations). Condition (3.12) states that a perturbation originating in cell x at time t can only influence the transmitted flow after having reached the upstream border of that cell. The corresponding lag, obviously, depends on the cell's length L and the backward wave speed v_{jam}.

The effect of a lag, $\ell \neq 0$, is demonstrated by means of a simulation of a compact jam inside a loop. The loop consists of 100 cells, each $100\,m$ long. The chosen parameters are $\rho_{\mathrm{max}} = 140\,km^{-1}$, $v_{\mathrm{jam}} = -15\,km/h$ and $v_{\mathrm{max}} = 120\,km/h$. According to (3.11) $\Delta t = 3\,s$ is used. The same temporal discretisation is used for the lagged CTM, leading to $\ell = 3$ according to (3.12).

Figure 3.3 shows the dissolution of the initialised jam over time. In the long run the jam dissolves in both models, however, this happens considerably faster in the CTM. Recalling that the models are approximations of the LWR, the simulation results demonstrate that the lagged CTM yields an enhanced accuracy in this respect. Analytically this is shown in [38].

Figure 3.3   Simulation of a single jam on the loop with the CTM ($\ell = 0$) and lagged CTM with $\ell = 3$. $\Delta\rho$ is a measure for the difference between the maximum and minimum density per cell, found in the simulated system. For the CTM this quantity decreases considerably faster than for the lagged CTM, which indicates that jam motion is more stable in the latter one.

The fact that jams always dissolve in the cell-transmission approaches is meaningless for the applicableness of the model in real world simulations, because this happens on very large time scales. For example, comparisons between measured data and the simulations of the corresponding situation are made in [22], using the CTM with $\ell = 0$. Fairly good agreement was achieved and the error made by the CTM was comparable to the one made by microscopic car-following models.

Due to the macroscopic approach the CTM is not suitable for the vehicle-based simulations addressed in this work, although the model performs very well in respect to traffic dynamics as well as computational efficiency. Even origin-destination relationships can be simulated by the CTM using turning probabilities [36, 118]. However, in order to track individual drivers and their routes, a representation of discrete car-driver-units is necessary. Unfortunately, the model only works as intended if the transmitted flows (3.9) are numerically represented by real numbers. The attempt of a direct transfer of the CTM into a modified cell-transmission update scheme, describing the motion of discrete vehicles, did not yield stable, backward propagating jams.

Section-based queueing-theoretical model

In [75] a queueing model is proposed that tries to avoid the discretisation of links into small segments in order to yield numerical efficiency. The dynamics of cars

is modelled on *sections*. A section may start/end at intersections or on- and off-ramps, which is then identical to what was called link before. However, a link may also be divided into several sections if there exist spatial inhomogeneities, as changes in the number of lanes or a gradient. This is done because such inhomogeneities usually trigger traffic congestion [77, 101]. For each section the continuity equation implies

$$q_{\mathrm{a}}^{i+1}(t) = q_{\mathrm{d}}^{i}(t) + q_{\mathrm{r}}^{i}(t). \tag{3.13}$$

q_{a}, q_{d} and q_{r} are the flows that arrive at the upstream end of a section, depart from its downstream end, and enter or leave the system due to on- and off-ramps, respectively. The latter flow is either externally given or specified in terms of turning probabilities. Sections are numbered in ascending order, *i.e.*, the downstream end of section i equals the upstream end of section $i + 1$. Note the similarity to the CTM.

In order to determine the flows at the common border of two consecutive sections a discrete update scheme is formulated with step size Δt. Since the complete model [75] needs quite a few assumptions and equations, only the principles are illustrated in the following.

In each time step q_{d}^{i} is determined depending on the traffic conditions of the sections i and $i + 1$. To this end, a state variable s is assigned to each section which can either be free, partially congested (there is a queue of cars which length is smaller than the length of the section) or completely congested. The state of a section is determined according to the current queue length on the section (which is tracked during the update procedure) and the in- and outflows of previous time steps. Three cases have to be distinguished in order to compute q_{d}^{i}:

i) If the upstream section i is free and the downstream one $i + 1$ is not in the partially congested state, $q_{\mathrm{d}}^{i}(t)$ is given by $q_{\mathrm{a}}^{i}(t - L^{i}/v_{\mathrm{max}}^{i})$. Given the length L^{i} of the section, $L^{i}/v_{\mathrm{max}}^{i}$ just gives the travel time a car needs to cross the section in free-flow conditions.

ii) If the downstream section $i+1$ is completely congested, $q_{\mathrm{d}}^{i}(t)$ is determined by the outflow from the downstream section at time $t - L^{i}/(\tau_{h}\,\rho_{\mathrm{max}})$. If τ_{h} is the average time headway, this condition states that a perturbation at the exit of the downstream section needs a finite time to reach its upstream border.

iii) In all other cases the departure flow is mainly given by outflow from jam.

The consideration of different propagation velocities of perturbations within free and congested regions, together with the analytical treatment of the jam fronts, leads to a numerically robust update scheme. The model approach is able to describe the hysteretic breakdown of traffic flow and to reproduce typical congestion patterns [75].

3.1.3 Vehicle-based queueing approaches

The modelling of the movement of single vehicles plays an important role in the context of DTA and ITS (*Intelligent Transportation Systems*), because the tracking of individual drivers in the network is necessary for certain applications. Compared to microscopic car-following models, queueing-theoretical based approaches allow for a noticeable increase of numerical efficiency. If important aspects of traffic flow are included the latter methods are favourable to the above applications, especially in regard to online-implementations.

The concept of space-time queues

In [8, 126, 127] a link-based queueing model with discrete vehicle movement is introduced. It solely calculates the points in time where a vehicle crosses a node on its path through the network. The movement of cars is deterministic. Congestion occurs due to conflicts of vehicle trajectories which can arise at crossings and the merging or diverging of cars at ramps.

Each link is characterised by its maximum velocity $v_{\max}^i$, length L^i and maximum storage capacity $N^i = L^i/l_{\mathrm{car}}$. The entry time t^ν and exit time t_{exit}^ν of each vehicle ν at a link are given by
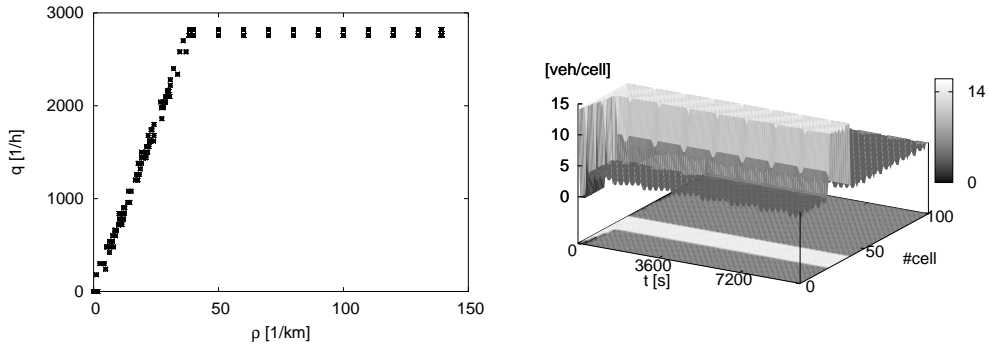
$$
\begin{aligned}
t^\nu &= \max\left\{ t^{\nu-1} + \tau_h + \frac{l_{\mathrm{car}}}{v_{\max}^i}, t_{\mathrm{exit}}^{\nu-N^i} + N^i\tau_h \right\} \qquad \text{and} \\
t_{\mathrm{exit}}^\nu &= \max\left\{ t^\nu + \frac{L^i}{v_{\max}^i}, t_{\mathrm{exit}}^{\nu-1} + \tau_h + \frac{l_{\mathrm{car}}}{v_{\max}^i} \right\}.
\end{aligned}
\tag{3.14}
$$

Equation (3.14) is derived from a simple car-following relationship which yields a triangular flow-density relationship. It assures that there is a minimum time separation τ_h between vehicles, and that the effective vehicle length l_{car} is respected. Within the model delays propagate with a finite speed which is reached due to the coupling between the entry and exit times of consecutive cars. Recall that delays are propagated upstream instantaneously in standard queueing models. The model displays stable jams. This can basically be traced back to the second term in the expression for the entry time t^ν of equation (3.14). The jams propagate backwards with speed l_{car}/τ_h.

Simple implementation of capacity constraints

A simple stochastic microscopic queueing model meeting capacity constraints can be implemented in the following way:

A link i is spatially characterised by its length L^i and storage capacity N^i. Its dynamic properties are given by the free-flow speed $v_{\max}^i$ and the maximum

Figure 3.4 **Left**: Global FDR of the simple queueing approach FAST-LANE. **Right**: Space-time plot a the system initialised with one traffic jam.

capacity $q_{\max}^i$ at its downstream end. If a car enters a link at time t, a leaving time $t + L^i/v_{\max}^i$, which corresponds to the free-flow travel time, is assigned to it. The state of each link is updated in discrete time steps Δt. Vehicles are kept in a priority queue, in order to process only such cars for which the intended leaving time is already elapsed. FIFO is used as queueing discipline.

In each time step a certain number of cars, whose waiting time in the queue exceeds the calculated travel time, is passed to an outgoing queue. The number of cars that can leave a link during the time interval, given by Δt, is constrained by the link's capacity and the storage capacity of the next link. The capacity is modelled as random variable with mean $q_{\max}^i$ because in reality the outflow of a link fluctuates over time. If more cars than the link capacity arrive, a queue starts to build which may spill backwards through the network. To put it differently, due to the capacity restraints and finite storage capacities of the links, the service rate of an upstream server is influenced by a full queue downstream.

The model was introduced in [59, 60], and is implemented in the traffic simulation tool FASTLANE (*FAst Simulator for Traffic in LArge NEtworks*) [185] in order to solve the DTA problem by simulation. One of its major features is its computational efficiency (see also [27]) which allows the computation of traffic flows in large networks, still being microscopic and dynamic. Its input is a set of drivers with specific *trips*, *i.e.*, individual departure times and known routes, and calculates the travel times for all drivers using the network simultaneously.

In [59] the model was compared to microscopic car-following models for a bottleneck situation with excellent results. For the same situation its adaptability in respect to the computation of vehicular emissions was investigated in [51]. It was found that a detailed emulation of the dynamic effects at the bottleneck (*i.e.*, during the buildup of the queue) is necessary in order to achieve high accuracy.

A good approximation in comparison of the SKM was achieved by subdividing the link in front of the bottleneck into several segments. However, it turned out in further investigations that the test used in [51, 59] succeeded because of the very special situation used for the comparison: a two-lane road with a one-lane bottleneck at its end which is the queueing scenario per se.

Figure 3.4 illustrates the shortcomings of the simple queueing model FAST-LANE. To obtain the FDR the model is simulated on a closed loop, composed of identical segments with $L^i = 100\,m$. The system is initialised with one dense traffic jam at different global densities. As one can see in the figure, the speed of backward travelling jam waves is not modelled properly. Therefore, there is no high-density branch with negative slope present in the fundamental diagram. Jams do not run backwards but stick at the position where they were created. The reason for this is that a vehicle leaving the queue at its downstream end opens up a new space at the upstream end without any lag (*cf.* section 3.1.1).
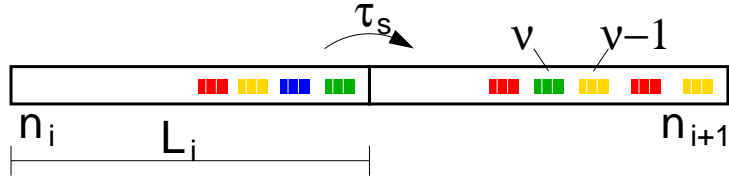
3.2   General approach based on time-headways (μ-Queue)

In the previous section a detailed review of approaches to traffic flow modelling is given, all based, in principle, on queueing theory. The discussion focused on their abilities with regard to the requirements given at the beginning of the chapter, namely,

- the modelling of traffic states distinct from each other.

- the distinction of individual car-driver-units.

- the usage of a preferably efficient implementation, *i.e.*, based on large spatial units and time steps.

It can be concluded from the above discussion of the models that it is necessary to account for service rates depending explicitly on the conditions of queues downstream, in addition to the dependence on the state inside the queue. Moreover, it became clear that a major drawback is related to the fact that a perturbation emerging at the downstream end of a queue reaches its upstream end instantaneously. In contrast, it is observed that the velocity of perturbations is finite in traffic flow and depends strongly on the traffic state. A proper approach, therefore, has to consider the lag between the emergence of a perturbation and its arrival at the upstream end of a queue.

The macroscopic models [35, 75] as well as the microscopic one [126] account for these effects using different approaches, however, the principles behind are similar and basic. They, therefore, play as well an important role within the new approach introduced in the following, although it is derived through a completely

Figure 3.5 Sketch of two consecutive segments and their parameters. A waiting time τ_s^i is imposed at the exit of each segment which depends on the state of both segments.

different line of thought. For the sake of completeness, note that similar ideas have also been put forward by a number of researchers, *cf.* [117] and references therein, which use a macroscopic framework (so called Markovian traffic flow models), and [142].

3.2.1 Dynamical equations

In the following model each link of length L_{link} is divided into a sequence of segments $i = 0, 1, .., I$. Each segment possesses a finite length L^i, such that $\sum_{i=0}^{I} L^i = L_{\mathrm{link}}$ (see also figure 3.5). Upon entering a segment i at time t^ν, any car ν gets assigned a proposed leaving time

$$t_{\min}^\nu = t^\nu + t_{\mathrm{tr}}(n^i, L^i, v_{\max}^i, \dots). \tag{3.15}$$

$v_{\max}^i$ is the maximum speed on the segment (*resp.* the link), and $t_{\mathrm{tr}}(\cdot)$ is the travel time which in general depends on the number of cars already inside the segment n^i. However, as observed in [60], the detailed form of the travel time function seems to be not very important as long as the flow constraints are modelled properly. Therefore,

$$t_{\mathrm{tr}} = L^i / v_{\max}^i \tag{3.16}$$

is used, independent of n^i.

When the time $t_{\min}^\nu$ is elapsed, the car ν can be transmitted into the next segment (or link of its path), provided

- some capacity constraint is obeyed at the downstream end of the segment.
- there is enough space on the destination segment $i + 1$.

If n^{i+1} denotes the current number of cars inside the destination segment and N^{i+1} its storage capacity, the latter condition means $n^{i+1} < N^{i+1}$. The storage capacity is calculated by

$$N^i = \lfloor \rho_{\max}^i L^i N_{\mathrm{lanes}}^i \rfloor, \tag{3.17}$$

with N_{lanes}^i, ρ_{max}^i being the number of lanes in the segment and the maximum density, respectively. For a one lane road and a homogeneous fleet of cars with length $l^\nu = l_{\text{car}}$, the relation $N^i = \lfloor L^i/l_{\text{car}} \rfloor$ holds.

In addition to the constraint that there has to be at least one site free in the destination segment, cars have to obey flow constraints in order to get a reasonable model for traffic flow. Let Q_{s}^i be the the maximum flow which the segment i can sustain given a specific traffic situation s. This capacity can be represented in terms of time-headway τ_{s}^i between two cars. Since the flow is $q = 1/\tau_h$, this capacity constraint is written down as an additional waiting time

$$\tau_{\text{s}}^i = 1/Q_{\text{s}}^i, \tag{3.18}$$

Thus, τ_{s}^i denotes the waiting time between the car $\nu - 1$ and the car ν under consideration. If car $\nu - 1$ left the segment i at $t_{\text{exit}}^{\nu-1}$, then car ν is not allowed to leave that segment earlier than time $t \geq t_{\text{exit}}^{\nu-1} + \tau_{\text{s}}^i$ (see figure 3.5).

In order to complete the model τ_{s}^i has to be defined. In FASTLANE (*cf.* section 3.1.3) this parameter is chosen to be constant (apart from fluctuations). As seen before, the downstream front of a jam stays fixed in that case. The right strategy to include a finite speed of perturbations can be motivated in the following way: Suppose the first car of an otherwise full segment $i + 1$ leaves this segment at a certain time. In reality the free site or hole (in physical parlance) generated in this way needs a certain time to reach the upstream segment. A car that tries to enter from upstream has to wait until the hole reached it. The corresponding waiting time is proportional to the number of cars inside the the segment where the hole was generated. In consequence, it is straightforward to assume
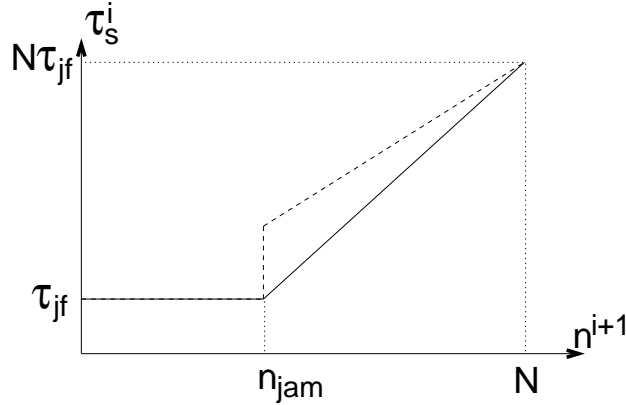
$$\tau_{\text{s}}^i \propto n^{i+1}. \tag{3.19}$$

This effect plays a prominent role if the two adjacent segments are in the congested state.

A simple approach for τ_{s}^i, which incorporates this idea, is given by the equations

$$\tau_{\text{s}}^i = \begin{cases} \max\left\{\tau_{\text{ff}}, n^{i+1}\tau_{\text{jf}}\right\} & \text{if} \quad n^i > n^{i+1} \\ \max\left\{\tau_{\text{ff}}, n^{i+1}\tau_{\text{jj}}\right\} & \text{if} \quad n^i \leq n^{i+1}, \end{cases} \tag{3.20}$$

where τ_{ff}, τ_{jf}, τ_{jj} are model parameters (see below). They can be regarded as state-dependent service rates. Equation (3.20) is able to generate stable backward propagating jams in the periodic system and, furthermore, describes properly simple traffic situations in open systems [22]. However, problems occur with respect to the realisation of high inflows with OBC. Therefore, a more general form is used in the following.

Figure 3.6 Function $f(n^{i+1}, tjj)$, equation (3.22), that determines the waiting time for the transition between two congested segments. **Dashed**: $\tau_{jj} = \tau_{jf}$. **Solid**: τ_{jj} as given in (3.24).

To this end, the behaviour of the waiting time τ_s^i is determined by a function depending on the states of the two neighbouring segments i and $i + 1$. In order to distinguish between free flow (f) and congestion (j) a parameter n_{jam}^i is introduced, and a segment i is called to be jammed if $n^i \geq n_{jam}^i$. In consequence, a general version of the queueing model has four additional parameters, besides n_{jam}^i, that describe the waiting time function τ_s^i. The parameters are named quite descriptive τ_{ff}, τ_{fj}, τ_{jf}, and τ_{jj}, where the indices denote the state of the upstream and downstream segment, respectively. The equation for τ_s^i then reads

$$\tau_s^i = \begin{cases} \tau_{ff} & \text{if} \quad n^i < n_{jam}^i \quad \text{and} \quad n^{i+1} < n_{jam}^{i+1} \\ \tau_{fj} & \text{if} \quad n^i < n_{jam}^i \quad \text{and} \quad n^{i+1} \geq n_{jam}^{i+1} \\ \tau_{jf} & \text{if} \quad n^i \geq n_{jam}^i \quad \text{and} \quad n^{i+1} < n_{jam}^{i+1} \\ f(n^{i+1}, \tau_{jj}) & \text{if} \quad n^i \geq n_{jam}^i \quad \text{and} \quad n^{i+1} \geq n_{jam}^{i+1} \end{cases} \tag{3.21}$$

In principle, the function $f(n^{i+1}, \tau_{jj})$ reflects (3.19) and is further specified by a linear relationship,

$$f(n^{i+1}, \tau_{jj}) = m\, n^{i+1} + b. \tag{3.22}$$

For simplicity, $m = \tau_{jj}$ is chosen and the axis intercept b is fixed to

$$b = N^{i+1} \left(\tau_{jf} - \tau_{jj} \right), \tag{3.23}$$

i.e., $f(N^{i+1}) \equiv N^{i+1}\, \tau_{jf}$ (see figure 3.6). Depending on the choice of τ_{jj} different model behaviours are obtained.

Given $\tau_{\mathrm{jj}} = \tau_{\mathrm{jf}}$, the function simply yields $f = \tau_{\mathrm{jf}}\, n^{i+1}$. Investigations show that the model displays stable jams if $\tau_{\mathrm{jf}} > \tau_{\mathrm{ff}}$. The mechanism behind will be discussed below but leaping ahead, due to equation (3.23), τ_{jf} determines the velocity of jams.

If $\tau_{\mathrm{jj}} \neq \tau_{\mathrm{jf}}$, the ratio of the two parameters determines the flow of quasi-homogeneous states at intermediate densities, not changing the mechanism of jams in the model. The choice

$$\tau_{\mathrm{jj}} = \frac{N-1}{N-n_{\mathrm{jam}}}\, \tau_{\mathrm{jf}} \tag{3.24}$$

leads to $f(n_{\mathrm{jam}}) = \tau_{\mathrm{jf}}$. It is worth saying that the straight line given by f becomes steeper, *i.e.*, flows increase at intermediate densities if τ_{jj} increases. The choice $m = 1/\tau_{\mathrm{jj}}$ would have been more intuitive but is numerically unfavourable. Equation (3.24) is an upper bound for τ_{jj} in respect to reasonable traffic flow behaviour.

In principle, the function τ_{s}^{i} can be made more complicated by taking care of the system's history. For example, at the end of a large jam, the jam occupies only part of a segment. In this case, the relation $\tau_{\mathrm{fj}} = \tau_{\mathrm{ff}}$ applies approximately. If the inflow into this segment is smaller than its outflow this may no longer be valid, because the jam front may finally travel backward within the segment. However, this happens rarely. So, to keep this model simple, this effect will be ignored.

Note that it may play a role if the segments in use become fairly long. In that case it may happen for specific traffic situations, that a microscopic simulation would yield a substructure, *e.g.*, with a jam in the middle of a segment. This is not modelled by this approach. In order to capture this, the concept of moving waiting queues has to be introduced. Macroscopically, this has been done in the models invented in [94, 95]. It would be an interesting task to transform that into the microscopic approach suggested here. However, segment lengths of several $100\,m$ are used in other (macroscopic) models as well and can, therefore, be assumed to be fairly uncritical.

Furthermore, testing the model with real data shows that it seems to be sufficient for most purposes to work with just two parameters, $\tau_{\mathrm{ff}} = \tau_{\mathrm{fj}}$ and $\tau_{\mathrm{jf}} = \tau_{\mathrm{jj}}$. Nevertheless, it is hypothesised that a microscopic queueing model with this four parameters can be used to mimic any of the microscopic simulation models currently under discussion (*cf.* section 2.1) with only slight adaptations of the parameters. This does not include, however, models that claim to describe synchronised flow [91, 96, 105].

The model will be referred to as μ-Queue (microscopic queueing model) in this work. In order to distinguish the number of virtual parameters, the following notation is used:

μ_1-Queue $\quad$ $n_{\text{jam}} = N$. The only parameter is τ_{ff} and the model is a deterministic version of FASTLANEif a parallel update scheme is used.

μ_2-Queue $\quad$ $\tau_{\text{fj}} = \tau_{\text{ff}}$ and $\tau_{\text{jj}} = \tau_{\text{jf}}$. Besides n_{jam}, the parameters are τ_{ff} and τ_{jf}.

μ_3-Queue $\quad$ $\tau_{\text{fj}} = \tau_{\text{ff}}$, the other three τ_{xx} are parameters.

μ_4-Queue $\quad$ All τ_{xx} are parameters.

Frequently, μ-Queue will only refer to the variants of the model which display backward propagating jam wave, *i.e.*, excluding μ_1-Queue. The meaning should be clear from the context.

3.2.2 Implementation of the model

In the following, the properties of the μ-Queue model are investigated. Due to the fact that the waiting times of each queue not only depend on its own state but also on the conditions downstream, the model cannot be treated with the analytical results of queueing theory [65]. Therefore, discussion is in parts done by means of computer simulation. For this purpose, periodic boundary conditions are used in this chapter. Open boundary conditions and street networks are discussed in the following one.

In order to get started, a one-lane loop of fixed length L_S is used which is divided into a sequence of I segments, all with equal length L. Moreover, because only one type of vehicle is used, the storage capacity N and maximum velocity v_{max} are as well fixed constants. The segments are implemented using FIFO as queueing discipline.

Initial conditions

Three different initial conditions are used in the following, namely,

homogeneous system , *i.e.*, each segment contains the same number of cars n_{hom} at the beginning of the simulation. The cars are positioned with equal spacings. The homogeneous state will be preserved, depending on the update procedure, because the model is formulated in a deterministic way. The total number of cars in the system N_S equals $I \cdot n_{\text{hom}}$.

quasi-homogeneous system , *i.e.*, all segments are initialised randomly with either $n_{\text{hom}} - 1$, n_{hom} or $n_{\text{hom}} + 1$ cars. Thus, the global density equals the one in the homogeneous case, but the occupancy of the segments may change during the simulation.

congested system , *i.e.*, one or two compact jams with N_S cars are put on the system.

Update procedure

After the initialisation of the system, the state of the segments is updated either in discrete time steps of size Δt or event-driven. The conditions which have to be met for a car to be able to leave a segment are the same in all update procedures. A car ν is allowed to pass the downstream end of a segment at time t, if

$$
\begin{aligned}
t &\geq \max\left\{t_{\min}^{\nu}, t_{\text{exit}}^{\nu-1} + \tau_{\text{s}}^{i}\right\} \qquad \text{and} \\
n^{i+1} &< N^{i+1}
\end{aligned}
\tag{3.25}
$$

hold.

In the case of discrete time steps, the following three update schemes have to be distinguished:
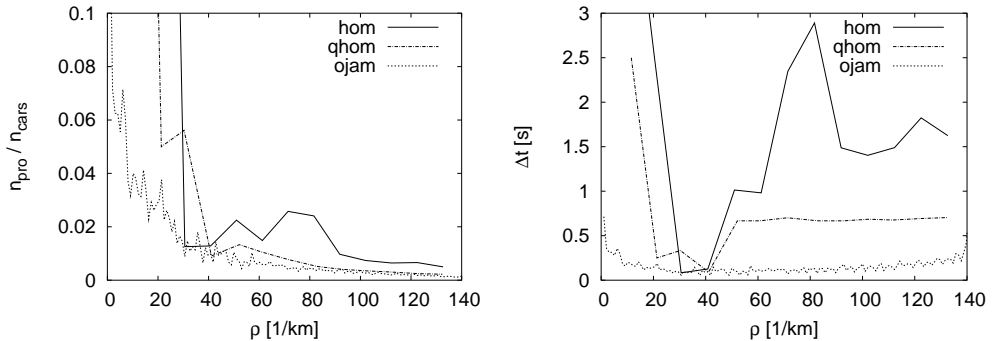
parallel update The update is divided into two sub-steps. In the first one, it is determined for all segments if there is a car to leave it, according to (3.25). If there is a leaving car, a new time-headway τ_{s}^{i}, equation (3.21), is assigned to the segment. In the second sub-step, all cars leaving a segment are moved to the next one. Due to the splitting each segment has to be touched twice per update.

sequential update In the sequential update, each segment has only to be touched once. The segments are processed in a fixed order and the complete update is done in one, *i.e.*, the checking for condition (3.25), the movement and the assignment of τ_{s}^{i}. However, the sequence of processing the segments has an influence on the development of a given traffic state and unmeant situations may arise.

shuffled update The procedure equals the sequential update, but the sequence of processing the segments is shuffled in each time step.

Since the values for realistic parameters τ_{xx} are of order seconds, the temporal discretisation has to be chosen smaller than $1\,s$ (in general $\approx 0.1\,s$). For such small time steps, the shuffled and parallel update yield similar results and properties of the model. This was explicitly checked for the μ-Queue model by means of simulations. However, with respect to the simulation of large networks over a long time period (*e.g.*, a day-to-day simulation) such small time steps sacrify numerical efficiency of the queueing approach. Recall that each link has to be updated at least once per time step. Moreover, the smaller the time steps are, the more *gridlocking* (see *p.* 127) becomes a problem. In contrast, a high temporal resolution is necessary with respect to emission modelling (*cf.* appendix B).

An **event-driven update** leads to a noticeable increase of numerical efficiency. Instead of using time steps explicitly, the temporal process is modelled as a sequence of events which take place at real-valued points in time. The leaving process of a car can be associated with an event. Because of FIFO conditions, only
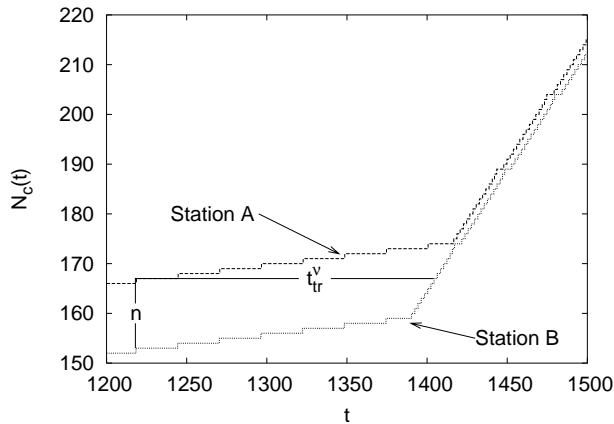
Figure 3.7 Performance of the event-driven update scheme over the system's density for different initial conditions. **Left**: Mean percentage of cars processed in each step of the update scheme. **Right**: Mean temporal increment Δt per step measured over the full simulation period.

the cars at the downstream ends of the segments have to be considered. They can be stored efficiently using a priority queue which gives back the current event. In appendix C the implementation of this idea is given as source code.

In order to test the computational performance of the event-driven scheme, a system consisting of 100 segments is initialised at different densities using different initial conditions. The μ_2-Queue model is used with $\tau_{\text{ff}} = 1.4\,s$ and $\tau_{\text{jf}} = 2.0\,s$. Figure 3.7 shows the advantages of the event-driven implementation. For (quasi-) homogeneous initial conditions the mean temporal increment per step is around $1\,s$ or even larger for most densities. Although this increment is considerably smaller for congested initial conditions, only 2% of the cars have to be updated in each step. Therefore, the performance is better compared to schemes using discrete time steps.

The different implementations were investigated with respect to their abilities to describe jam waves. For all schemes comparable behaviour was found. For certain sets of parameters (*e.g.*, μ_3-Queue with τ_{jj} given by (3.24) and $\tau_{\text{jf}} = 2\,s$) it was found that the event-driven update does not display stable jams for all initialisations with one jam whereas this was the case for the schemes base on discrete time steps. In regard to the μ-Queue model the discretisation of time leads to a stabilisation of the jam front, because leaving times are in consequence as well discretised.

Since the event-driven update is advantageous for network simulations and no time step, appropriate to the parameters, has to be chosen, this update scheme is exclusively used in the following. Note, however, that the conclusions on the model's dynamics are as well valid for the parallel and shuffled update schemes (given that an appropriate temporal discretisation is chosen).

Figure 3.8 Plot of $N_c(t)$-curves at two stations. Station B is located downstream of Station A. The vertical separation between the curves at time t gives the number of vehicles n between the stations. The travel time t_{tr}^{ν} of each car can be read immediately from the horizontal separation.

Measurements

In contrast to car-following models, the velocity of cars can not be measured at any point in time in the queueing approach but only at the moments where a car leaves a segment. This means, velocities as well as densities can only be determined with respect to a segment.

The only quantities that are given at each point in time are the number of cars that passed a segment during a specific time interval and their respective travel times. The number of cars that passed a segment can be used in a very descriptive way to visualise and compare data from multiple counting stations and to derive dynamic quantities about traffic flow. For this purpose, so called synchronised cumulative counts (or *N-curves*) are frequently used, see, *e.g.*, [26, 34, 130].

At the downstream end of each segment, the cumulative number of vehicles $N_c(t)$ that passed the segment is collected and the corresponding figure is the N-curve. If the counts at different segments (or stations) are initialised with the passage of a reference vehicle they become synchronised. In this case, the vehicle trip times are given by the horizontal separation between two curves, and vehicular accumulation by the vertical separation. The slope of the N-curve gives the average flow at a station. Thus, N-curves are used to define the measurements in the queueing system, *cf.* figure 3.8.

Local measurements are done with respect to a segment using the N-curves $N_c^{\mathrm{up}}(t)$ and $N_c^{\mathrm{down}}(t)$ at the upstream and downstream end of it, respectively. If

the sampling is done for intervals of size Δt_s the mean number of cars is given by

$$\langle n(t') \rangle = \frac{1}{\Delta t_s} \int_{z=t'}^{t'+\Delta t_s} \left(N_c^{\text{down}}(z) - N_c^{\text{up}}(z) \right) dz, \tag{3.26}$$

and the mean travel time (upon entering the segment) yields

$$\langle t_{\text{tr}}(t') \rangle = \frac{1}{n_\nu} \sum_{\{\nu : t^\nu \in [t', t'+\Delta t_s]\}} t_{\text{tr}}^\nu. \tag{3.27}$$

In (3.27) n_ν is the number of cars that passed the upstream end of the segment during the time interval $[t', t' + \Delta t_s]$. The dynamic quantities are calculated by means of

$$
\begin{aligned}
\langle \rho_{\text{loc}}(t') \rangle &= \frac{\langle n(t') \rangle}{L}, \\
\langle v_{\text{loc}}(t') \rangle &= \frac{\langle q_{\text{loc}}(t') \rangle}{\langle \rho_{\text{loc}}(t') \rangle} \quad \text{and} \\
\langle q_{\text{loc}}(t') \rangle &= \frac{1}{\Delta t_s} \left[N_c^{\text{down}}(t' + \Delta t_s) - N_c^{\text{down}}(t') \right].
\end{aligned}
\tag{3.28}
$$

Note that there may be intervals where no car can enter a segment due to complete congestion. In that case, the mean travel time, equation (3.27), is not defined. Given FIFO queueing discipline, the missing data points can be added such that

$$t' + t_{\text{tr}}(t') \leq (t' + \Delta t_s) + t_{\text{tr}}(t' + \Delta t_s) \tag{3.29}$$
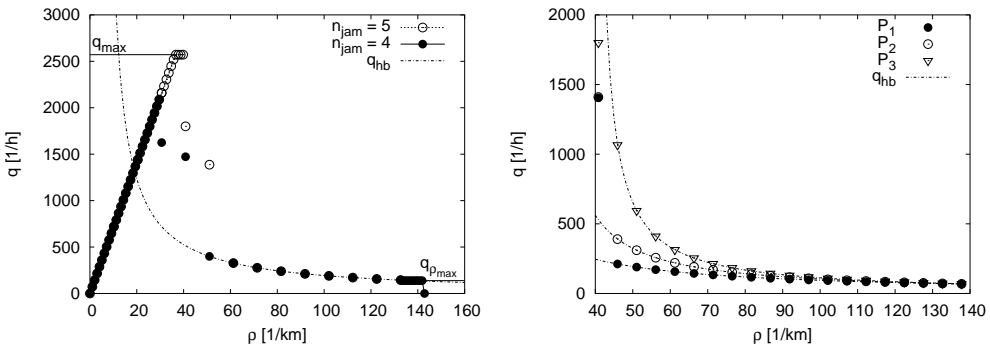
holds. It is worth saying that the sampling interval Δt_s has to be increased with increasing segment lengths. Furthermore note that the velocity is not determined by means of the average travel time, because this quantity is a sample over several sampling intervals, in contrast to the density and flow.

In the periodic system, also global measurements are used which are defined by

$$
\begin{aligned}
\langle \rho_{\text{glo}} \rangle &= \frac{N_S}{L_S}, \\
\langle v_{\text{glo}} \rangle &= \frac{\langle q_{\text{glo}} \rangle}{\langle \rho_{\text{glo}} \rangle} \quad \text{and} \\
\langle q_{\text{glo}} \rangle &= \frac{1}{t_{\text{end}} - t_{\text{start}}} \left[N_c(t_{\text{end}}) - N_c(t_{\text{start}}) \right]
\end{aligned}
\tag{3.30}
$$

over the simulation period $[t_{\text{start}}, t_{\text{end}}]$.

Note that there exist also methods which only use cumulative counts at discrete points in time in order to compute the dynamic quantities, see, *e.g.*, [42, 43, 136, 145].

Figure 3.9   Global FDR of the μ_3-Queue model with homogeneous initial conditions. The common parameters are $\tau_{ff} = \tau_{fj} = 1.4\,s$, $\tau_{jf} = 2\,s$, $v_{max} = 19.6\,m/s$. **Left**: Besides the parameter n_{jam}, the parameters $L = 98\,m$, $\tau_{jf} = \tau_{jj}$ and $N = 14$ are the same for both systems. The maximum flow q_{max} and the flow at $\rho_{glo} \approx \rho_{max}$ are given by (3.31) and (3.35), respectively. The high-density branch can be described by q_{hb}, as given by (3.34). **Right**: High density branch of three different parameter sets. The common parameters are $L = 196\,m$, $N = 28$ and $n_{jam} = 8$. For P_1, P_2 and P_3, the parameter τ_{jj} is $\tau_{jj} = 2, 2.4$ and $2.7\,s$, respectively.

3.2.3 Deterministic waiting times

The model is formulated in a deterministic way. Therefore, traffic jams are as well described deterministically and no spontaneous jam formation takes place. In the following, the stable traffic states of the model and their dependence on the parameters is discussed as well as a description of moving jams in the model is given. The discussion is done in most parts for the μ_3-Queue variant of the model but the arguments given also hold for the other ones (except for the μ_1-Queue which does not display backward travelling jam waves).

The homogeneous state

In order to discuss the homogeneous states of the μ-Queue model, a periodic system with $I = 100$ segments is used. Each system is initialised homogeneously at different densities. Before measurements are made, each initialisation is relaxed for $50000\,s$. Figure 3.9 shows the resulting FDR for different parameter sets. In contrast to the μ_1-Queue model[2], two branches, a low-density and a high-density branch, can clearly be distinguished.

The low-density branch is completely determined by the parameters τ_{ff}, v_{max} and n_{jam}. The maximum velocity defines the slope of that branch, and τ_{ff} gives

---

[2]Recall that this model is closely related with FASTLANE

in principle the maximum flow possible. However, depending on n_{jam} this maximum flow may not be reached. For initial conditions inside the density interval $(n_{\mathrm{jam}} - 1)/L \leq \rho_{\mathrm{glo}} \leq n_{\mathrm{jam}}/L$, there exist inhomogeneities in the system because the segments can be either in the free state or the congested one. Due to the model formulation, equation (3.21), this can lead to the formation of short jams as can be seen in figure 3.10[3]. In consequence, the maximum flow that can be reached by the system is given by

$$q_{\mathrm{max}} = \min\left\{ \frac{1}{\tau_{\mathrm{ff}}}, \frac{(n_{\mathrm{jam}} - 1)\, v_{\mathrm{max}}}{L} \right\}. \tag{3.31}$$

The high-density branch, $\rho_{\mathrm{glo}} \geq n_{\mathrm{jam}}/L$, can also be described analytically. The flow on that branch is mainly given by the waiting times τ_{s} at the downstream end of each segment, and independent of v_{max}. The latter is due to the fact that the free-flow travel time is considerably lower than the travel time in the congested state. Since τ_{s} is $\propto \langle n \rangle$ in the congested state and each car has $\langle n \rangle$ cars in front when entering a segment, the travel time is a quadratic function of the density. More precisely, due to the event-driven update procedure, a car that leaves a segment will find either n or $n - 1$ cars on the target segment ($n = \rho_{\mathrm{glo}} L$). Therefore, the mean waiting time yields $f(n - 0.5, \tau_{\mathrm{jj}})$, see (3.22). For the travel time in each segment, therefore,

$$t_{\mathrm{tr}}^{\mathrm{hb}}(\rho_{\mathrm{glo}}) = a_{\mathrm{hb}}\, \rho_{\mathrm{glo}}^2 + b_{\mathrm{hb}}\, \rho_{\mathrm{glo}} \tag{3.32}$$

holds, with

$$\begin{aligned} a_{\mathrm{hb}} &= \tau_{\mathrm{jj}}\, L^2 \\ b_{\mathrm{hb}} &= [N(\tau_{\mathrm{jf}} - \tau_{\mathrm{jj}}) - 0.5\,\tau_{\mathrm{jj}}]\, L. \end{aligned} \tag{3.33}$$

In (3.32) the units of ρ_{glo} and $t_{\mathrm{tr}}^{\mathrm{hb}}$ are $[1/m]$ and $[s]$, respectively. The flow of the congested homogeneous system then yields
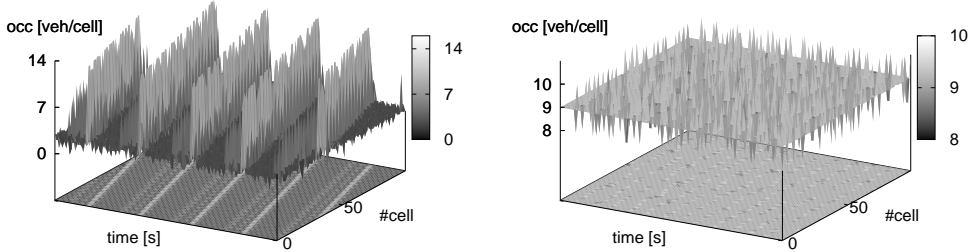
$$q_{\mathrm{hb}}^{\mathrm{hom}}(\rho_{\mathrm{glo}}) = \frac{\rho_{\mathrm{glo}}\, L}{t_{\mathrm{tr}}^{\mathrm{hb}}}. \tag{3.34}$$

Note that (3.32) is not true in case of a system that contains compact jams.

It is observed in figure 3.9 that the flow only vanishes exactly for $\rho_{\mathrm{glo}} = \rho_{\mathrm{max}}$. This stems from the fact that even though most segment may be completely filled with cars for most part of the sampling interval, there are still open spots in the

---

[3]Note that this effect is more pronounced within the event-driven update scheme compared to the parallel update. In the latter, the discrete time step leads to a synchronisation of the vehicles' movement.

Figure 3.10   Space-time plot of the μ-Queue model with homogeneous initial conditions. The plots show the last $10000\,s$ of the simulation. The parameters are $L = 98\,m$ $\tau_{\mathrm{ff}} = \tau_{\mathrm{fj}} = 1.4\,s$, $\tau_{\mathrm{jf}} = \tau_{\mathrm{jj}} = 2\,s$, $v_{\mathrm{max}} = 19.6m/s$, $N = 14$ and $n_{\mathrm{jam}} = 4$. **Left**: $\rho_{\mathrm{glo}} = 30km^{-1}$. **Right**: $\rho_{\mathrm{glo}} = 90km^{-1}$.

system. Therefore, a car still moves, if there is at least one place left in the destination segment. This flow is hence given by
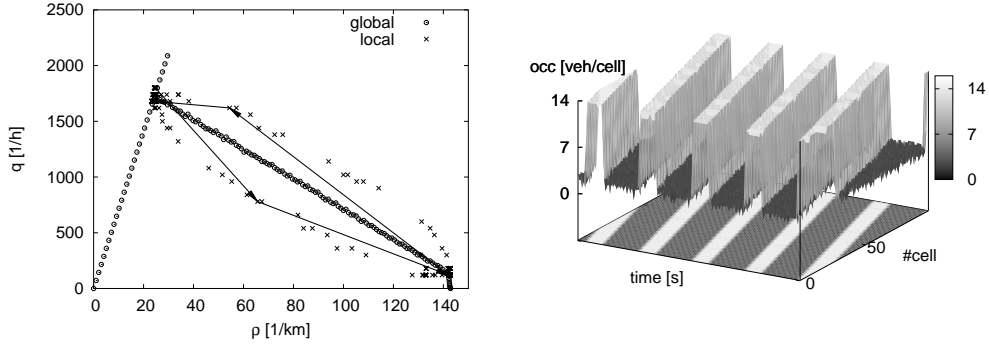
$$\frac{1}{q_{\rho_{\mathrm{max}}}} = \tau_{\mathrm{jj}}(N - 1) + N(\tau_{\mathrm{jf}} - \tau_{\mathrm{jj}}), \tag{3.35}$$

cf. equation (3.22).

The congested state

As intended, the μ-Queue model possesses stable jams moving backwards through the system. Figure 3.11 presents the fundamental diagram of a μ-Queue system which is initialised with one jam at different global densities. As one can see, this jam is not stable for densities lower than $(n_{\mathrm{jam}} - 1)/L$ and the system relaxes into the free-flow regime. However, for densities higher than $(n_{\mathrm{jam}} - 1)/L$, one clearly observes two states that are alternately measured by the virtual detector. The space-time plot of the system shows that these measurements correspond to a jam that moves backwards through the system. Moreover, one observes a capacity drop in the global FDR. The model's properties will be explored in more detail now with respect to jamming and the mechanism which stabilises the congested state.

The jams found in the model are compact , *i.e.*, $n \approx N$ holds for segments that are inside the congested region of the system. Their behaviour is described quantitatively in the sequel, starting with the velocity of the backward-moving downstream front of the jam. Having regard to the model's formulation this front

Figure 3.11 μ_2-Queue model with $L = 98\,m$ $\tau_{\text{ff}} = 1.4\,s$, $\tau_{\text{jf}} = 2\,s$, $v_{\max} = 19.6\,m/s$, $N = 14$ and $n_{\text{jam}} = 4$. The system consists of 100 segments and is initialised with one jam. **Left**: Global FDR and local measurements for a system initialised with 600 vehicles. The sampling interval is $\Delta t_s = 60\,s$. **Right**: The corresponding space-time plot shows the last $10000\,s$ of the simulation.

is given by means of segments and its velocity can be expressed by

$$v_{\text{jam}} = -\frac{L}{\tau_{\text{esc}}}. \tag{3.36}$$

τ_{esc} is the time, a completely filled segment needs to flush. Obviously, this time can be expressed by the waiting times τ^ν assigned to each car ν,

$$\tau_{\text{esc}} = \sum_{\nu=1}^{N} \tau^\nu \qquad \text{with } \tau^\nu \in \tau_s, \tag{3.37}$$

assuming that inside a jam segments are filled to their maximum storage capacity.

Given τ_{esc}, it is straightforward to calculated the number of vehicles found in the congested state according under stationary conditions. Since the *escape time* τ_{esc} determines the outflow from jam, this can be written as

$$q_{\text{out}} = \frac{\langle n_j \rangle}{\tau_{\text{esc}}} \approx \frac{N}{\tau_{\text{esc}}}. \tag{3.38}$$

$\langle n_j \rangle$ denotes the mean number of cars in a congested segment. The flow into the jam is written as

$$q_{\text{in}} = \frac{v_{\max}}{\langle h \rangle} \tag{3.39}$$

where $\langle h \rangle$ is the mean spatial headway between cars moving freely.

Let N_f, N_j be the total number of cars in free flow and congested state, respectively. Then, $N_S = N_f + N_j$ is the total number of cars in the system, and $\rho_{\mathrm{glo}} = N_S/L_S$ is the global density in a loop of length L_S. Assuming that there is only one compact jam of length L_j in the system, the following equation for $\langle h \rangle$ holds,

$$\langle h \rangle = \frac{1}{N_f} (L_S - L_j) - l_{\mathrm{car}}. \tag{3.40}$$

l_{car} is the length of a car. In the stationary state $q_{\mathrm{in}} = q_{\mathrm{out}}$, therefore, equating (3.38) with (3.39) yields

$$h_{\mathrm{eq}} = \frac{v_{\mathrm{max}}}{N} \tau_{\mathrm{esc}} \tag{3.41}$$

for the spatial headway in the stationary state. Together with (3.40) this leads to

$$h_{\mathrm{eq}} (N_S - N_j) = -l_{\mathrm{car}} (N_S - N_j) + L_S - L_j, \tag{3.42}$$

thus, the number of cars inside the jam yields
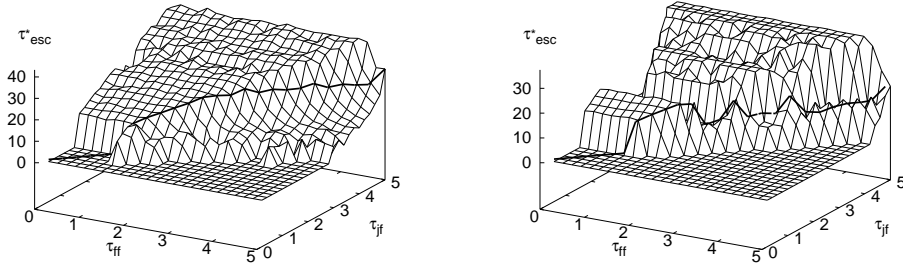
$$N_j = L_S \left(1 + \frac{L}{N h_{\mathrm{eq}}} \right) \rho_{\mathrm{glo}} - \frac{L_S}{h_{\mathrm{eq}}}. \tag{3.43}$$

Besides the dependence on the segment's parameters, the number of cars in the congested state is solely a function of the system density and system length. In consequence, the density ρ_{crit}, which gives the minimal global density where stable jams are found, is solely depending on the parameters of the μ-Queue model (*i.e.*, independent of the system length). It is given by

$$\rho_{\mathrm{crit}} = \frac{1}{h_{\mathrm{eq}} \left(1 + L/(N h_{\mathrm{eq}}) \right)}. \tag{3.44}$$

Note that $\rho_{\mathrm{crit}} \to \rho_{\mathrm{max}}$ for $\tau_{\mathrm{esc}} \to 0$ as one expects. Because the escape time τ_{esc} can scarcely be measured in a direct way, equation (3.44) is used instead for further numerical investigations. To this end, jams of different length are initialised in a periodic system which consists of 100 segments. The μ_2-Queue and μ_3-Queue model with $L = 98\,m$, $N = 14$, $n_{\mathrm{jam}} = 5$ and $v_{\mathrm{max}} = 19.6\,m/s$ are used. For varying parameters $(\tau_{\mathrm{ff}}, \tau_{\mathrm{jf}})$ and $(\tau_{\mathrm{ff}}, \tau_{\mathrm{jf}}, \tau_{\mathrm{jj}})$, respectively, each initialised system is simulated for $t_{\mathrm{rel}} = 100000\,s$ and it is determined in sequel whether the jam dissolved or not. As criterion, ρ_{crit} is defined to be the lowest density where there remain at least three consecutive segments with $n(t_{\mathrm{rel}}) = N$. The corresponding escape time τ_{esc}^* is calculated by (3.44).

The dependence of τ_{esc}^* on the parameters τ_{ff}, τ_{jf} and τ_{jj} is shown in figure 3.12. One can clearly distinguish between two regimes displaying stable *resp.* unstable

Figure 3.12 Escape time from jams versus τ_{ff} and τ_{jf}. The model shows two distinct regimes with a sharp change in the behaviour. The line $\tau_{\text{ff}} = \tau_{\text{jf}}$ is marked by the contour line. **Left**: μ_2-Queue model. Stable jams always exist for $\tau_{\text{jf}} \geq \tau_{\text{ff}}$. **Right**: μ_3-Queue model with τ_{jj} given by (3.24).

jams. As one expects, τ_{esc}^* increases with increasing τ_{jf}. Moreover, stable congested states in principle require $\tau_{\text{ff}} \leq \tau_{\text{jf}}$ which reminds on the slow-to-start behaviour known from microscopic car-following models, *cf.* section 2.2. Note that the values $\tau_{\text{esc}}^* \neq 0$ for $\tau_{\text{ff}} < \tau_{\text{jf}}$ stem from the fact that the function $f(n)$, equation (3.22), possesses a discontinuity $(n_{\text{jam}} - 1)\,\tau_{\text{jf}}$ which is large compared to τ_{ff}. Backward propagating clusters of cars are, therefore, still stable, however, the propagation speed is unrealistically high. For application purposes, these parameter sets do not yield reasonable models for traffic flow.

The fact that $\tau_{\text{ff}} \leq \tau_{\text{jf}}$ is necessary for stable jam propagation becomes more obvious in case of the μ_3-Queue model. If the maximum possible value for τ_{jj} is chosen according to (3.24), there are no stable jams for $\tau_{\text{ff}} > \tau_{\text{jf}}$.

For rather low values of τ_{ff} one finds an unexpected behaviour, namely, some kind of valley inside the $(\tau_{\text{ff}}, \tau_{\text{jf}})$ plane. Note that this behaviour of the escape time is explained by an observation done in the homogeneous system. If $\rho \approx n_{\text{jam}}/L$ there are always segments completely filled. Because of the choice for τ_{jj}, the short jams in the system may either be right stable or not. Thus, the probability to find a "stable" jam by the automatic detection is not zero for these densities. Indeed, the jams that were detected inside the observed valley are not compact and $\rho_{\text{crit}} \approx n_{\text{jam}}/L$ is found for the corresponding critical densities.

Besides the reduced outflow from jams, there is another property of the model that is important in respect to stable jams. Inside a jam the flow is very low due to the dependence of the additional waiting times on the number of cars inside segments downstream. This property was similarly observed in the SKM, *cf.* figure 2.3. As long as the waiting times are considerably higher than the time

a car needs to cross a free segment, the movement of the cars inside a jam is completely governed by (3.21). In this case the assumption on the escape time, equation (3.37), should hold.

In order to give a description of the mechanism that leads to stable jams in the μ-Queue model, a system with one jam that occupies several segments is considered. Assume that the segment $i + 1$ marks the downstream end of the jam and there is only one place left in that segment. Then, the waiting time imposed at the border between segment i and $i + 1$ is approximately $(N - 1)\,\tau_{\mathrm{jf}}$. Since for stable jams $\tau_{\mathrm{ff}} \leq \tau_{\mathrm{jf}}$ is required, all cars in segment $i + 1$ can leave the segment before another car will enter from segment i. Jams, therefore, move backward segment by segment. If this picture is right, the escape time at the density where jams become right stable yields

$$\tau_{\mathrm{esc}}^* = (N - n_{\mathrm{jam}})\,\tau_{\mathrm{jf}} + \tau_0. \tag{3.45}$$

Figure 3.13 shows τ_{esc}^* for fixed $\tau_{\mathrm{ff}} = 1.4\,s$ and different free-flow speeds. The values of τ_{esc}^* are determined by means of the critical density, equation (3.44), using the simulation method described above. The straight line shown in the figure is obtained by fitting all points of the curves τ_{esc}^* inside the regime of stable jams. Indeed, its slope is approximately $9 = (N - n_{\mathrm{jam}})$, *cf.* equation (3.45). The axis intercept τ_0 is independent of the free-flow speed but depends on τ_{ff} (not shown), however, the latter dependence is not very pronounced.
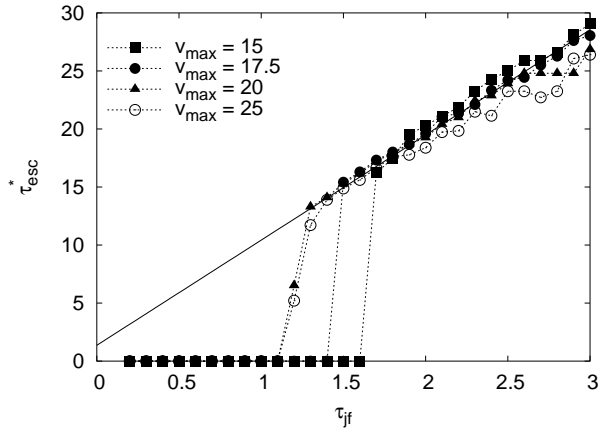
Unlike one may expect, $\tau_0 \ll n_{\mathrm{jam}}\tau_{\mathrm{ff}}$. This can be understood, recalling the mechanism of the jam's movement as given before. The finding that τ_0 is smaller than $n_{\mathrm{jam}}\tau_{\mathrm{ff}}$ means, that the movement "segment by segment" does not have to be given in a strict sense. In order to have stable jams it is already sufficient, that the cars inside a jam are either transmitted into an almost full segment or an almost free one. To put it differently, if τ_{jf} becomes to small with respect to τ_{ff} the information of the dissolving downstream front of the jam propagates backward too fast and leads to an almost instantaneous dissolution of the jam[4]. If the jam becomes unstable, the definition of escape time is obviously meaningless. That is why τ_{esc}^* drops sharply, as can be seen in figure 3.13.

Note that the propagation speed of jams is independent of v_{max} because the same it true for τ_0, which is a reasonable behaviour. The observation that the stable regime by means of τ_{jf} deepens fits as well into the given picture of jams in the μ-Queue model. The bigger v_{max} the better the assumption that the movement inside jams is entirely governed by the waiting time τ_{s} holds.

For jams of considerable size, *i.e.*, $\rho_{\mathrm{glo}} \gg \rho_{\mathrm{crit}}$, the jams move in fact "segment

---

[4]Note the similarity to traditional queueing approaches.

Figure 3.13   Escape time versus τ_{jf} for different free flow speeds at $\tau_{ff} = 1.4\,s$. The other parameters are $L = 98\,m$, $N = 14$, $n_{jam} = 5$. The model is the μ_3-Queue with τ_{jj} given by (3.24). The dependence of τ_{esc}^* in the stable regime is independent of v_{max} but with increasing v_{max}, the stable region by means of τ_{jf} deepens. The straight line is obtained by a fit of the points that lie in the regime of stable jams and is given by $f(\tau_{jf}) = 9.1\,\tau_{jf} + 1.36$, *cf.* (3.45).
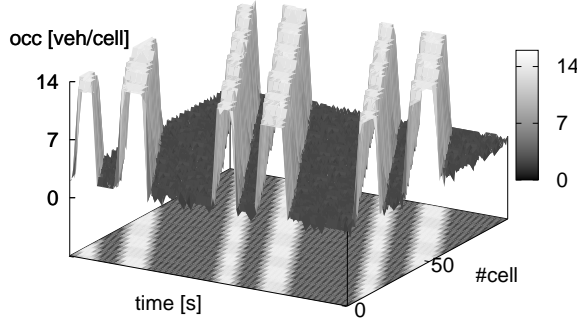
by segment". The slope of the high-flow branch is, therefore, given by

$$v_{jam}^{hb} = -\frac{L}{(N-1)\,\tau_{jf}}.$$ (3.46)
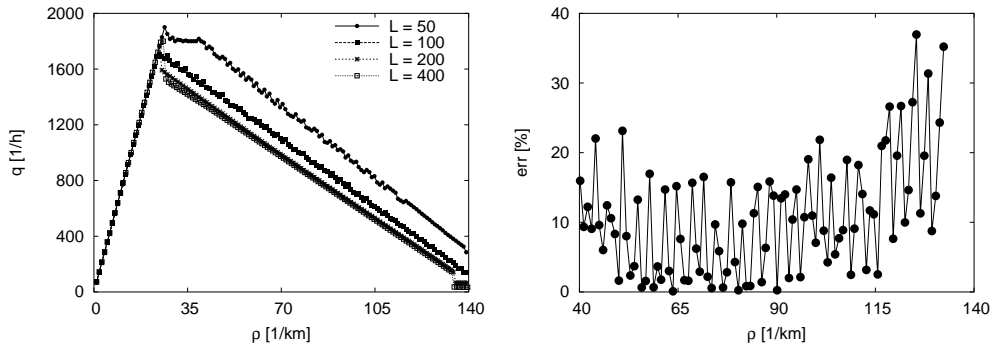
Before further properties of the model are discussed, just note, that the model is also able to show stable double-jam structures as have been found in real world observations [99]. The stability of such structures implies that the characteristic parameters of jams are robust which compares to empirical observations. In contrast to the simulations performed in [124] (using a LWR model) these structures are absolutely stable in the μ-Queue model, see figure 3.14.

Dependence on segment length

In order to be able to use the model for network simulations in an adjustable way, recall that each link of the network is decomposed into several segments. Thus, one aims to use as few segments as possible having numerical efficiency in mind. This means, segments should be as long as possible. However, in urban networks there are considerably short segment lengths predetermined. Therefore, the dependence of the model's behaviour on the segment length is investigated in the following.

Figure 3.14   The μ-Queue model shows stable, double-jam structures.


Figure 3.15   **Left**: FDR for systems with different segment lengths. **Right**: Discrepancy between the difference in the measured flows of the systems with $L = 100\,m$ and $L = 200\,m$ and the difference computed by (3.47).

For this purpose a periodic system of fixed length, $L_S = 10\,km$, is used varying the length L of the segments. For each density one compact jam is initialised, and the relaxation and measurements last for $50000\,s$ each. The storage capacity is computed by (3.17). The μ_2-Queue model is used with $\tau_{\mathrm{ff}} = 1.4\,s$ and $\tau_{\mathrm{jf}} = 2.0\,s$. The density $\rho_{\mathrm{jam}} = 40\,km^{-1}$ is chosen in order fix the parameter n_{jam} for the different systems. For very short segment lengths this leads to such small values for n_{jam} that the segments are always in the congested state. Therefore, n_{jam} is not allowed to become smaller than 3.

Table 3.1 summarises the findings for the globally measured FDR which are shown in figure 3.15. For all systems an excellent agreement between the slope of the high-density branch and (3.46) is found. The finding of mean flows at a specific density, distinct from each other, can as well be explained by the model's

L [m]	N	n_{jam}	v_{jam} [km/h]	Eq. (3.46) [km/h]	$q(\rho_{\mathrm{max}})$ [$1/h$]	Eq. (3.35) [$1/h$]
50	7	3	-14.95	-15	285	300
100	14	4	-13.75	-13.85	138.3	138.5
200	28	8	-13.12	-13.33	66.7	66.7
400	57	16	-12.96	-12.86	32.2	32.1
800	114	32	-12.95	-12.74	15.9	15.9

Table 3.1   Results for systems with different segment lengths. The corresponding flow-density relations are shown in figure 3.15. The agreement between the measured values for v_{jam} and $q(\rho_{\mathrm{max}})$ with the formulae derived for the model's behaviour is good.

properties. Since the flow at ρ_{max} is given by (3.35), the high-density branch can be described by

$$q^{\mathrm{hb}}(\rho) = -\frac{L}{(N-1)\,\tau_{\mathrm{jf}}}\,\rho + \frac{(N+1)}{(N-1)\,\tau_{\mathrm{jf}}}. \qquad (3.47)$$

Equation (3.47) allows for the calculation of the expected difference for the flows of systems with different segment lengths. This difference is compared to the differences found in simulation in figure 3.15. At intermediate densities ($\rho > \rho_{\mathrm{crit}}$) the agreement is fairly good. The oscillations stem from the fact, that the jam lengths adjust by means of segments in the model. As one may expect from the model properties, deviations from the approximation (3.47) increase for densities in the vicinity of ρ_{max}.

If N becomes small, *i.e.*, just a few cars fit into a segment, the definition of n_{jam} becomes meaningless. Simulation results advise that the segment length should not be chosen shorten than $L = 50\,m$. The model's behaviour still remains reasonable for short segments, however, due to the necessary lower bound introduced for n_{jam}, the plateau (which is already visible for $L = 50\,m$) deepens and the high-flow branch becomes numerically unstable.

Note that, due to (3.46) and (3.35), which determine the high-flow branch in principle, it is not possible to obtain a perfect agreement between the high-flow branches of two models with different segment lengths. If this is addressed, a good way is doing the adjustment by means of (3.46) only. In that case, the stability of jams remains unaffected increasing the segment length, however, there will remain discrepancy in the vicinity of ρ_{max}.

3.2.4   Remarks about waiting time distributions

The waiting times of the μ-Queue model (3.21) are deterministic. As a consequence, there are no spontaneous transitions from laminar to congested flow and vice versa under periodic boundary conditions. Moreover, the time-headway distributions of the model only show discrete peaks according to (3.21). Although the model is able to describe traffic states in the free flow and congested flow regime, it cannot be taken too serious from a pure microscopic perspective.
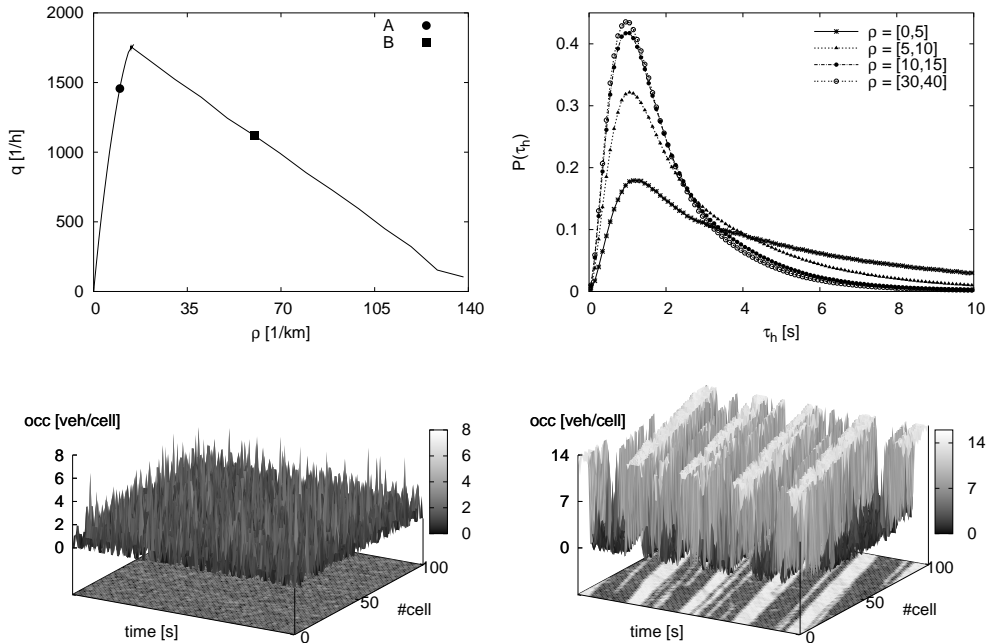
The following discussion gives an example, how waiting time distributions can be introduced into the μ-Queue model in order to obtain a more reasonable behaviour in respect to time-headways found in observations (*cf.* figure 2.2). This is done using a specific set of parameters, although the principles hold in general. The reason for this stems from the fact that appropriate parameters of the distributions used depend strongly on the parameters of the μ-Queue model. Moreover, if the noise is introduced at the border of two consecutive segments, which is certainly the favourable way in regard to the model's implementation, the fluctuation strength in the system becomes rather high. Because a simple way to determine the distribution's parameters in general from the system's parameters was not found, they have to be chosen carefully by means of simulations. Two distributions are used in order to introduce fluctuations into the model's dynamics, namely, a distribution for the free-flow velocities and one for the waiting times.

In traffic flow, cars do not drive all with the same maximum velocity. It is not very far fetched to assume that the velocities are Gaussian distributed around the speed limit given free-flow conditions. With respect to time-headways, however, one observes that short headways are suppressed and there is an exponential tail. An appropriate choice may be an Erlangian distribution whose density function is given by

$$p_{(a,m)}^{\text{erl}}(x) = \frac{x^{m-1} \exp\left(-x/a\right)}{(m-1)!\, a^m},\ 0 \leq x \leq \infty,\ a > 0,\ m \in \mathbb{N}^{>0}. \qquad (3.48)$$

Its mean value is $m\,a$ and its variance $m\,a^2$. The parameter a can be regarded as scale parameter and m as shape parameter. If $m = 1$, the Erlangian equals an exponential distribution. If $m \to \infty$, it becomes a symmetric distribution narrowly peaked around $m\,a$. In the following, the parameter of the Erlangian are $a = \tau_{\text{s}}^i$ and $m = 3$ which yield the properties stated above in respect to time-headway distributions observed in traffic flow. An easy implementation scheme of this distribution is given in appendix C.

Figure 3.16 shows simulation results of a periodic system using the μ_2-Queue model. System parameters are $L = 100\,m$, $N = 14$, $n_{\text{jam}} = 5$, $v_{\text{max}} = 25\,m/s$, $\tau_{\text{ff}} = 1.1\,s$ and $\tau_{\text{jf}} = 1.7\,s$. Free-flow speeds are Gaussian distributed with mean v_{max} and $\sigma_v = 5\,m/s$. Homogeneous and congested initial conditions are used.

Figure 3.16 **Top:** FDR of the simulated system (*left*). *On the right*, the time-headway distributions for different density regimes are shown.
Bottom: Space-time diagram of point A. The system was initialised by one jam (*left*). Space-time diagram of point B. The system was initialised with homogeneous conditions (*right*).

For all initial conditions with a global density in the low-density regime, free-flow states are eventually found. If the global density is within the high-density regime, there is eventually always a jam, independent from the initial conditions. This jam moves backwards through the system and is stable. Space-time diagrams of the two states found are shown in figure 3.16.

Instead of discrete values for the time-headways, as in the deterministic model, distributions are obtained that look more realistic. Within the low-density regime there exist very short headways. The distribution shows a sharp increase towards its maximum located at $\tau_h = 1\,s$ and an exponential tail for longer headways. Note, however, that the time-headway distributions do not become broader with increasing density. This is related with the mechanism of stable jams in the model which is not changed due to the introduction of noise. Jams still move "segment by segment" and, therefore, there always occur headways inside the interval $\left[\tau_{\mathrm{ff}}, \tau_{\mathrm{jf}}\right]$. Since their share is considerably high, the maximum of the distribution stays fixed at $\tau_h \approx \tau_{\mathrm{ff}}$, solely the tail of the distribution becomes longer with increasing

system's density. Within the stochastic implementation of the μ-Queue model, jams are no longer compact but show an internal structure, *i.e.*, there are also segments inside a jam with $n < N$.

It is emphasised that it is essential to use both distributions. If only the distribution for the velocities is used, one obtains already broad time-headway distributions instead of isolated peaks. But, time-headways smaller than τ_{ff} are still not present. On the other hand, if only the waiting times are computed by means of the Erlangian, the skewness of the time-headway distribution vanishes, *i.e.*, there is no longer a sharp increase at short time-headways as present in figure 3.16.
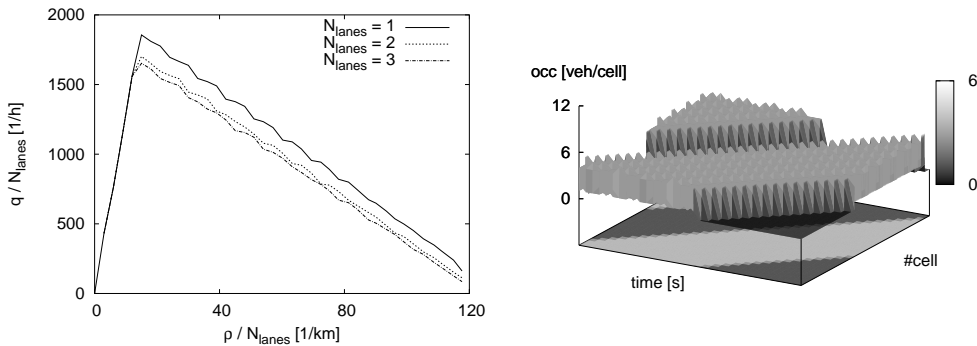
3.2.5   Aspects of multi-lane traffic

So far, only single-lane traffic is considered. However, with respect to a complete network-loading model, the effects of multi-lane traffic matter. Real traffic consists of non-homogeneous fleets of vehicles, and faster cars are able to pass slower ones. Highways, as well as arterials and main roads in urban networks, usually possess several lanes. Therefore, it is important to treat multi-lane roads in the queueing model. One difficulty in order to find simple rules modelling lane changes arises from the fact, that the lane usage distribution differs for highways and urban multi-lane roads [20, 29, 68, 122, 168].

Lane changes lead to the occurrence of strong correlations within velocity and flow measurements between neighbouring lanes which are observed in synchronised flow and wide moving jams [92, 140]. They, moreover, destabilise laminar flow [134]. If there is a strong asymmetry in the lane usage, as on German highways where overtaking on the right is prohibited, the lane-changing behaviour is responsible for the observed lane usage inversion [122, 168] (see also figure 3.18). It is still under discussion whether lane changes are just selecting rather than generating traffic states, or whether they give rise to states which just exist due to multi-lane effects [108]. Without doubt, multi-lane driving behaviour leads to a large variety of possible dynamical states [40] and plays an important role in the correct interpretation of measurements.

There exist several extensions of single-lane models in regard to multi-lane traffic which all depend strongly on the model's concept. If roads are represented based on individual lanes, one usually uses lane-changing rules in order to model lane usage, whereas the movement of densities or vehicles is still updated by means of the single-lane dynamics.

To this end, lane-changing and passing probabilities are frequently used in macroscopic traffic flow models [73, 129]. In microscopic car-following models behavioural rules for the lane change are often used [63, 80, 107, 135]. The lane-changing process is divided into two steps, namely, whether there is a reason to change the lane (*e.g.*, to pass a slower vehicle in front) and, if there is such
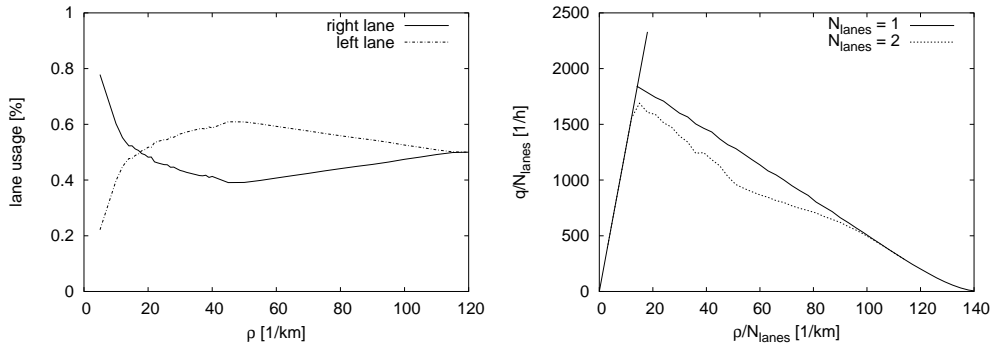
Figure 3.17 **Left**: Flow-density relations of the μ_2-Queue model with periodic boundary conditions and different number of lanes. The parameters are transformed according to (3.49). **Right**: Platoon of cars for the system with one lane. The leading car has a maximum velocity of $0.5 \cdot v_{\max}$. The global density equals $15\,km^{-1}$.

reason, whether the lane change is possible with respect to safety considerations (*e.g.*, not causing a collision). In order to avoid the implementation of such rules within the flow simulation, another approach is provided by the displacement of the determination of the lane usage into the route choice, *i.e.*, each vehicle drives along a pre-calculated route which specifies the path through the network together with the lanes to use along that path [126, 127].

Multi-lane traffic without passing

It is favourable within the framework of the μ-Queue model to treat multi-lane roads without changing the update procedure considerably. Although vehicles pass each other in free flow as well as dense traffic, the average behaviour of flow can be sufficiently described neglecting the passing of cars, given that the maximum velocity is restricted by speed limits such that individual maximum velocities of different vehicle types are of minor importance, *cf.* also figure 3.18. For example, on a two-lane urban road, all vehicles are forced to drive approximately $50\,km/h$ (at least in Germany) and most lane changes result from the followed route. Certainly, the different acceleration abilities of different vehicle types do have an impact on the driving dynamics, but such effects are not represented within the queueing model.

In this case, the developed framework can be used, changing solely the parameters of the model. Once, the parameters are determined for the one-lane situation

Figure 3.18 Simulation of a two-lane loop with the SKM and lane-changing. The number of cars is fixed to 1000 and a homogeneous fleet of cars is considered. Its parameters are $v_{\max} = 37\,m/s$, $a = 2\,m/s^2$, $b = 8\,m/s^2$, $l_{\mathrm{car}} = 7\,m$ and $\varepsilon = 1$. **Left**: Lane usage versus system density. Although there is a right lane preference, the left lane is used stronger for high densities (*lane inversion*). **Right**: Flow-density relation of the one-lane and two-lane loop.

(indicated by *), the parameters for the situation with N_{lanes} lanes chosen by

$$
\begin{aligned}
N &\leftarrow N^* N_{\mathrm{lanes}}, \\
n_{\mathrm{jam}} &\leftarrow n^*_{\mathrm{jam}} N_{\mathrm{lanes}}, \\
\tau_{\mathrm{xx}} &\leftarrow \tau^*_{\mathrm{xx}}/N_{\mathrm{lanes}},
\end{aligned}
\tag{3.49}
$$

lead to the same flow-density relation normalised per lane. Moreover, the stability of jams is not changed by this transformation. However, in regard to the event-driven update scheme, the average time increment will decrease with increasing number of lanes.

Figure 3.17 demonstrates this property of the model for a periodic system with $N_{\mathrm{lanes}} = 1, 2, 3$. The segment's parameters for $N_{\mathrm{lanes}} = 1$ are $L = 100\,m$, $v_{\max} = 36\,m/s, n_{\mathrm{jam}} = 5, N = 12$. The μ_2-Queue model is used with $\tau_{\mathrm{ff}} = 1.37\,s$ and $\tau_{\mathrm{jf}} = 2.0\,s$. If one aims to account for the fact that the flows on a two-lane highway are lower than twice the flows of the one-lane highway at a specific density, the parameters can easily be adjusted according to (3.49).

Passing of slow vehicles

As long as the maximum velocities of different vehicle types do not play a role, the averaged description without passing can be used. However, on highways without speed limit, slow vehicles as lorries will be passed by faster driving passenger cars.

Without the possibility of passing, platoons of cars build behind slow vehicles. Note that independent of the difference between the velocity of the leading car and the maximum velocity of cars trapped behind it, no backward propagating jams will arise in the μ-Queue model as long as the global density is in the free-flow regime, *cf.* figure 3.17.

A possible way to incorporate the passing of vehicles into the model is provided by the representation of each lane individually and the introduction of lane-changing rules. However, this would technically be quite difficult within the μ-Queue framework, because every time a vehicle is moved, the state of all neighbouring segments has to be considered. Therefore, a passing probability is introduced here. Apart from that, a multi-lane road is modelled in the way described before.

In order to get an idea how the passing probability should look like, the SKM is used as reference model. Lane-changes are modelled according to [113]. The update procedure of the SKM is amended by an additional set of rules which determines for each car whether the lane is changed or not. This rule set is applied before the speed update (2.6) is performed. A car will change its lane, if two conditions are fulfilled, namely, the change is favourable and safe:

> **if**   [(favourable($i \rightarrow j$)) **or** (rand $< p_{\text{change}}$)] **and** [safe($i \rightarrow j$)]
> **then**   change($i \rightarrow j$).
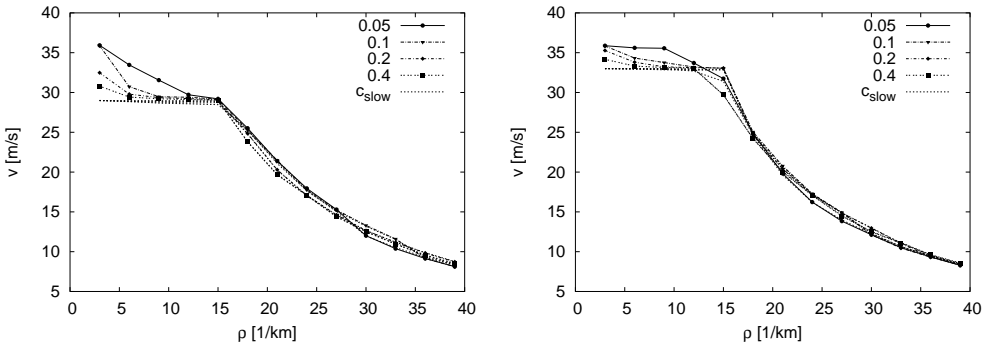
In the following, the upper index o indicates that the expression is evaluated at the other lane, *i.e.*, the lane a car may possibly change to. The expressions given in the above conditions are then given by

$$
\begin{aligned}
\text{congested} &= \left(v_{\text{safe}} < v_{\text{thresh}}\right) \quad \textbf{and} \quad \left(v^o_{\text{safe}} < v_{\text{thresh}}\right) \\
\text{favourable(right} \rightarrow \text{left)} &= \left(v_{\text{safe}} < v_{\text{max}}\right) \quad \textbf{and} \quad (\textbf{not } \text{congested}) \\
\text{favourable(left} \rightarrow \text{right)} &= \left(v_{\text{safe}} \geq v_{\text{max}}\right) \quad \textbf{and} \quad \left(v^o_{\text{safe}} \geq v_{\text{max}}\right)
\end{aligned}
$$

Moreover, passing on the right is prohibited, if the lanes are not in the congested state. For further details see [113].

Different two-lane systems with periodic boundary conditions and two vehicle types are simulated. Each simulation is done with 2000 vehicles and the fraction of slow vehicles is varied. The common parameters are $a = 2\,m/s^2$, $b = 8\,m/s^2$, $l_{\text{car}} = 7\,m$ and $\varepsilon = 1$. The maximum velocity for fast vehicles is $v_{\text{max}} = 37\,m/s$, for slow ones either $v_{\text{max}} = 34\,m/s$ or $v_{\text{max}} = 30\,m/s$. The parameters for the lane-changing rules are $v_{\text{thresh}} = 11.5\,m/s$ and $p_{\text{change}} = 0.01$. The mean velocity each vehicle type is able to achieve traversing the entire system is used as measurement.

Figure 3.19 shows the results. As can be seen, the fast vehicles are only able to achieve higher mean velocities than the slow ones inside the low-density regime.

Figure 3.19 Simulation of a two-lane loop with the SKM and lane-changing. Plotted is the mean velocity of fast cars at different global densities and different fractions of slow cars. c_{slow} gives the mean velocity of slow cars. **Left**: The maximum velocity of slow cars is $v_{\text{max}} = 30\,m/s$. **Right**: The maximum velocity of slow cars is $v_{\text{max}} = 34\,m/s$.
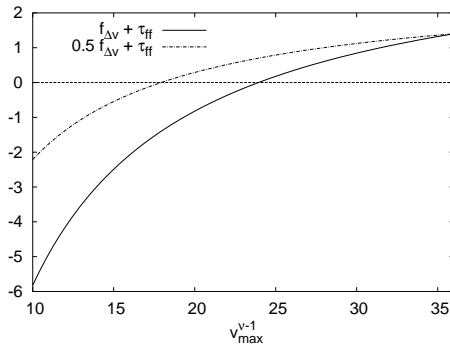
Although there are still successful passings within the high-density regime, there is no considerable difference between the mean velocity at densities $\rho > \rho_{\text{f}}$. Moreover, there are no high-flow states visible in figure 3.18 due to the de-stabilisation of flows by lane changes. In the low-density regime the slow vehicles drive with their maximum velocity, $v_{\text{max}} - \varepsilon a/2$.

With respect to the fast vehicles multiple dependencies determine their mean velocity. With increasing density their velocity decreases and approaches the velocity of the slow vehicles. The density where the difference in the velocities vanishes depends on the fraction of slow vehicles as well as on the difference between the respective maximum velocities. With increasing fraction of slow vehicles the difference between the mean velocities decreases more rapidly.

In order to mimic the properties of the above findings by means of a passing probability in the μ-Queue model, the following procedure is used. Each time a vehicle is received by a segment, it is decided whether it passes the vehicle in front, *i.e.*, the passing probability is defined with respect to segments. It is already clear at this point, that the parameters of such probability will strongly depend on the parameters of a segment. Therefore, its calibration is in general a difficult task.

Assume, a car ν with maximum velocity v_{max}^{ν} is driving behind a car $\nu - 1$ with $v_{\text{max}}^{\nu-1}$. The car ν is able to pass the car in front if the following conditions are met:

1. The following car is able to drive faster than the car in front, *i.e.*, $v_{\text{max}}^{\nu} > v_{\text{max}}^{\nu-1}$.

2. The time-headway between the two cars is small enough.

Figure 3.20 Representation of Δt_{exit}, equation (3.50), for a fast car with $v_{\text{max}} = 36\,m/s$ driving behind a slower one with maximum velocity $v_{\text{max}}^{\nu-1}$ ($\tau_{\text{ff}} = 1.4\,s$).

    3. A certain time interval elapsed since the last time where the car ν passed another one.
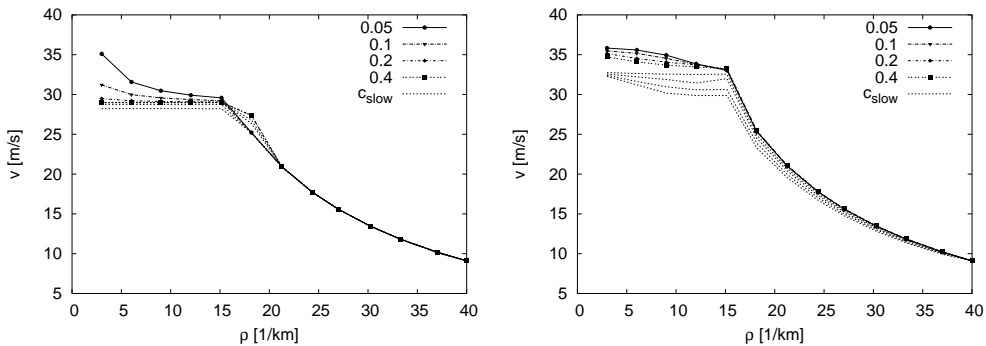
If the above conditions are met, the car ν passes the car in front with a probability depending on the density of the segment. If the segment is in the jammed state, the passing probability is set to zero.

    The conditions 2 and 3 need further elaboration. The second requirement is necessary to decide whether a passing effort is carried out at the time the following car enters the segment. Given $v_{\text{max}}^{\nu} > v_{\text{max}}^{\nu-1}$, the following condition for the difference between their exit times t_{exit} holds, due to to the dynamics of the μ-Queue model,

$$\Delta t_{\text{exit}} \equiv t_{\text{exit}}^{\nu} - t_{\text{exit}}^{\nu-1} \geq L \left(\frac{1}{v_{\text{max}}^{\nu}} - \frac{1}{v_{\text{max}}^{\nu-1}} \right) + \tau_{\text{ff}} \equiv f_{\Delta v} + \tau_{\text{ff}}. \qquad (3.50)$$

If a fast car drives behind a slow one, it will more and more approach until equality holds in (3.50). Because the movement of cars is deterministic, Δt_{exit} will in sequel not change as long as the traffic state persists. $\Delta t_{\text{exit}} < 0$ means that the fast car is able to reach the end of the segment before the slow one, if its motion would not be hindered. If the difference in the maximum velocities is quite small, however, Δt_{exit} never becomes negative, as one can see in figure 3.20. In order to allow the passing of the fast car anyhow, an interval for Δt_{exit} is defined where a passing attempt is carried out, namely, $\Delta t_{\text{exit}} \in [f_{\Delta v} + \tau_{\text{ff}}, c_{\Delta v}\, f_{\Delta v} + \tau_{\text{ff}}]$, where $c_{\Delta v}$ is a parameter (see figure 3.20).

    Before the third requirement is further explained, the passing probability is given. It should depend on the density to assure that in the jammed state the passing probability becomes zero. For simplicity, a linear function is used which

Figure 3.21   Simulation of a two-lane loop with the μ_2-Queue model
and passing. Plotted is the mean velocity of fast cars at different global
densities and different fractions of slow cars. c_{slow} gives the mean velocity
of slow cars. **Left**: The maximum velocity of slow cars is $v_{\max} = 29\,m/s$.
Right: The maximum velocity of slow cars is $v_{\max} = 33\,m/s$.

depends on the number of cars on the segment n,

$$p_{\text{pass}} = c_p \left(-c_m\, n + 1 \right). \qquad (3.51)$$

The parameters c_m and c_p are used in order to adjust the upper bound for the
density interval where passing can be carried out and the level of passing activity,
respectively. In the simulation, a random number η in the interval $[0, 1]$ is drawn
from a uniform distribution, and the passing attempt is successful if $\eta < p_{\text{pass}}$.

Already the conditions 1 and 2 together with (3.51) lead to a reasonable be-
haviour, namely, that the slow vehicles drive with their maximum velocity whereas
the velocity of the fast ones decreases with increasing density. However, the de-
pendence on the fraction of slow vehicles is not reproduced.

That is the reason why the third condition is introduced, namely, a certain
time interval has to be elapsed since the last passing of a car. If the last passing
happened at t_{lp}, no further passing attempts are allowed until $t > t_{\text{lp}} + c_{\text{lp}}\, n$. Again
c_{lp} is a parameter.

Figure 3.21 presents the results of the described procedure for passing within
the μ_2-Queue model. The simulations are all done with 2000 vehicles on a two-
lane loop and the density and the fraction of slow vehicles are varied. The max-
imum velocity of fast cars is $36\,m/s$. The other parameters with respect to one
lane are $L = 100\,m$, $N = 12$, $n_{\text{jam}} = 5$, $\tau_{\text{ff}} = 1.4\,s$ and $\tau_{\text{jf}} = 2.0\,s$. The adjust-
ment to two lanes is done by (3.49). The parameters for the passing algorithm are
$c_{\Delta v} = 0.9$, $c_m = 0.2$, $c_p = 0.5$ and $c_{\text{lp}} = 30\,s$.

The results compare quite good to the SKM (*cf.* figure 3.19). However, as
stated before, the multiple dependencies found in the SKM are not mimicked in

all details by the μ-Queue model. For example, the dependency on the fraction of slow vehicles is not as pronounced as in the reference system. If the difference in the maximum velocities is quite small, the movement of slow vehicles is more influenced as in the SKM. This is due to the dynamics of the μ-Queue model. Each time a slow vehicle is passed, it is penalised by an additional waiting time, since lanes are not treated separately as in the SKM.

The passing algorithm should therefore only be used with a small number of vehicle types. However, for many applications it is already sufficient to discriminate between passenger cars and lorries.

3.3 Application: Modelling of vehicular emissions

The development of the μ-Queue model is motivated, besides other reasons, by the computation of vehicular emissions in the framework of DTA. In the following, it is demonstrated that the model is well suited to calculate environmental impacts of traffic with high temporal and spatial resolution. As before, the SKM is used as a reference model. Because the generation of air pollutants as well as noise is strongly dependent on the vehicles' velocities (beside other dependencies), a detailed mapping of the dynamic situation is necessary on a microscopic level. The presented benchmarks are, therefore, not only important with respect to application purposes. They are, moreover, suited to investigate in how far the developed model is able to catch the dynamics of traffic states distinct from each other.
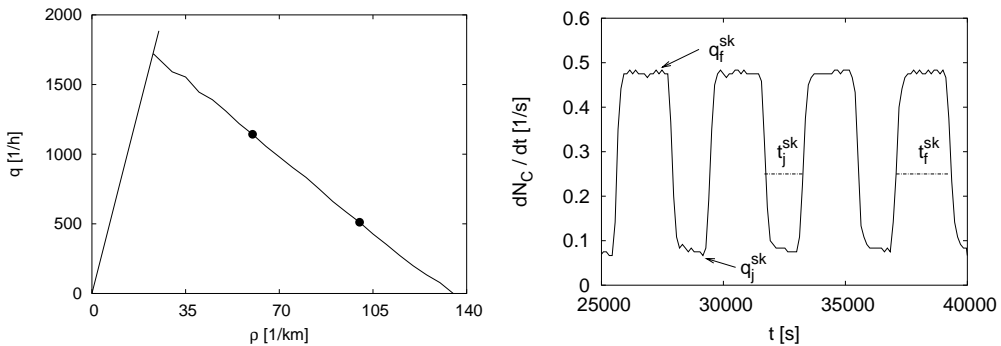
The transformation of the vehicles' dynamics into vehicular emissions is done by means of *emission factors*. The data source for these factors and the methods used to connect them with the two models are described in detail in appendix B. The appendix gives, moreover, further details with respect to the role of traffic flow models in the context of air-quality management systems.

3.3.1 Single-lane loop

The following presents simulation results of a periodic system with one lane. The different versions of the μ-Queue model are compared to simulation results of the SKM. Moreover, a method is introduced which can be used to calibrate the parameters of the queueing model.

The reference system

As experimental setup a loop is used which is always initialised by 1000 vehicles standing bumper to bumper. In order to model different global densities the system

Figure 3.22   **Left**: FDR of the reference system. The points indicate the system states which are used to calibrate the parameters of the μ-Queue model. **Right**: The derivative of the cumulative counts for a system with $\rho_{\text{glo}} = 60\,km^{-1}$. It is used to determine the parameters for the calibration process.

length L_{S} is varied. The parameters for the SKM used are

$$
\begin{array}{lll}
a = 2\ m/s^2 & b\ =\ 8\ \ m/s^2 & v_{\max}\ =\ 22\ \ m/s \\
\varepsilon\ =\ 1 & l_{\text{car}}\ =\ 7\ \ m & \tau = \Delta t = 1\ s.
\end{array}
$$

The corresponding FDR is shown in figure 3.22.

Calibration of parameters

Before simulation results of both models can be compared, the parameters of the queueing model have to be calibrated with respect to the reference system. The principle procedure can be described as follows [22]:

In a first step, one has to define certain measurements o_i which can be observed within the simulation. This can be, *e.g.*, the flow which is observed at a specific global density of the system. The measurements of the reference system, o_i^{r}, and the ones of the system which is calibrated, o_i^{c}, are used to define an *error measure* by means of relative errors, *i.e.*,

$$
\text{err} = \frac{1}{n_i} \sum_{i=1}^{n_i} \frac{\mid o_i^{\text{r}} - o_i^{\text{c}} \mid}{o_i^{\text{r}}}. \tag{3.52}
$$

 In a second step, the model is simulated with a certain set of parameters, and an algorithm is used to improve err by changing the set of parameters.

Since it is not possible for the queueing model to compute the Jacobi-matrix with respect to the parameters analytically, a direct search approach, the so called

Downhill-Simplex method [139] is used. This method does neither need to compute
derivatives nor does it need an explicit analytical formulation of the system to be optimised. A computer implementation is presented in [149]. The algorithm starts with a simplex in the n-dimensional parameter space which is in sequel transformed iteratively until a local minimum is found. Therefore, the procedure should be started with different initial configurations.

Instead of using the global FDR as measurements for the error function (3.52), the cumulative counts N_c are used here. One reason for this procedure is that they can easily be measured in both models without the need to determine a sampling interval in advance. Moreover, these functions contain information about the dynamics of both traffic states. The derivative of the cumulative counts according to time t immediately gives the flows q_f and q_j in free flow and inside a jam, respectively. Moreover, the temporal intervals t_f and t_j each of the two phases need to pass the virtual detector are used, see figure 3.22. All these measures can easily be detected in an automated way.

The four quantities are determined at two densities, $\rho = 60, 100 \, km^{-1}$. In order to deal with the stochastic nature of the SKM, averages over 30 simulation runs are used. Table 3.2 summarises the resulting measures.

ρ $[km^{-1}]$	q_f^{sk} $[s^{-1}]$	q_j^{sk} $[s^{-1}]$	t_f^{sk} $[s]$	t_j^{sk} $[s]$
60	0.47 ± 0.003	0.089 ± 0.003	2047 ± 302	1452 ± 219
100	0.45 ± 0.006	0.083 ± 0.002	327 ± 21	1914 ± 106

Table 3.2   Measures of the reference system for the calibration process.

Results of the μ-Queue model

The method described before is used to determine optimal parameters for μ-Queue model. In all simulations L is fixed to $100 \, m$. For the μ_2-Queue model, different parameters for $v_{\max}$, N and n_{jam} were tried. The best agreement was achieved for $v_{\max} = 21 \, m/s$. This fits surprisingly good to the free-flow speed of the SKM which is $\langle v \rangle = v_{\max}^{\mathrm{sk}} - \varepsilon a/2$. For N and n_{jam} the best agreement was found for $N = 12$ and $n_{\mathrm{jam}} = 5$, respectively. This corresponds to the measured density inside moving jams of the SKM which is 11.5 vehicles per $100 \, m$. Therefore, these parameters are as well used for the μ_3-Queue and μ_4-Queue during the calibration process. Table 3.3 summarises the parameters resulting from the calibration.
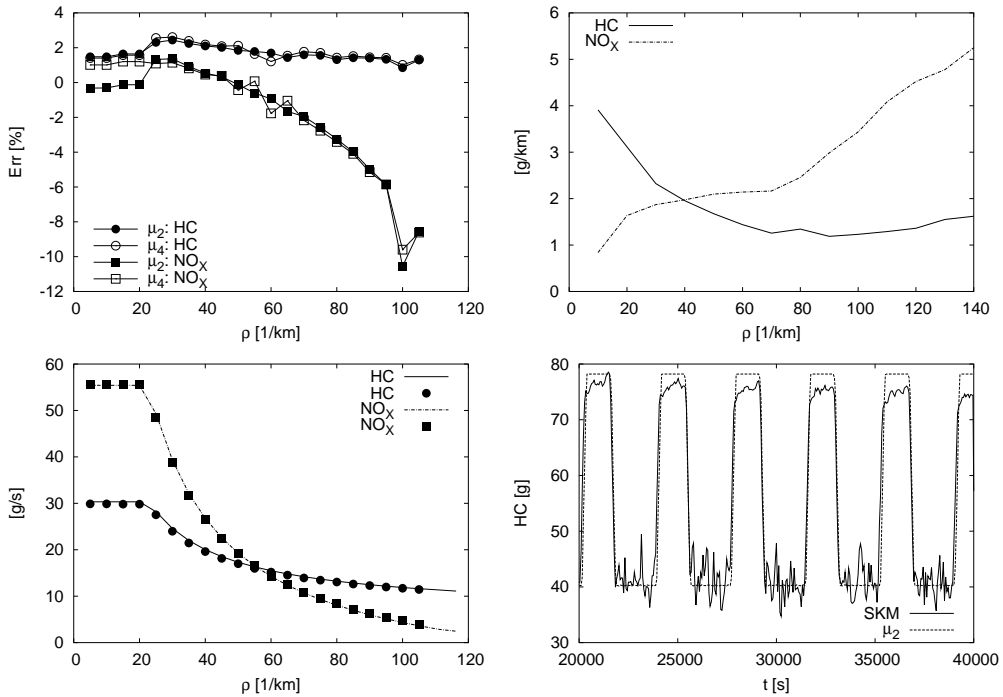
With respect to the total error, there is no considerable difference between all three model variants. For all systems, the agreement to the SKM is better for

	N	n_{jam}	$v_{\max}$ $[m/s]$	τ_{ff} $[s]$	τ_{fj} $[s]$	τ_{jf} $[s]$	τ_{jj} $[s]$
μ_2-Queue	12	5	21	1.538	1.538	2.070	2.070
μ_3-Queue	12	5	21	1.751	1.751	2.063	2.600
μ_4-Queue	12	5	21	1.205	1.675	2.163	3.052

	ρ $[km^{-1}]$	q_{f} $[s^{-1}]$	q_{j} $[s^{-1}]$	t_{f} $[s]$	t_{j} $[s]$	err
μ_2-Queue	60	0.472	0.053	2280	1500	
		0.005	0.401	0.114	0.033	0.138
	100	0.465	0.053	436	1848	
		0.034	0.360	0.334	0.0345	0.191
μ_3-Queue	60	0.481	0.052	2260	1420	
		0.023	0.415	0.104	0.022	0.141
	100	0.481	0.054	420	1800	
		0.069	0.354	0.284	0.060	0.192
μ_4-Queue	60	0.465	0.052	1989	1277	
		0.010	0.411	0.029	0.120	0.142
	100	0.468	0.053	420	1860	
		0.041	0.356	0.284	0.028	0.177

Table 3.3   Results of the calibration process of the μ-Queue model. In the upper part of the table the parameters are presented for which the best agreement to the SKM was found. In the lower part the resulting measures and the error corresponding to the SKM are given in detail.

$\rho = 60\,km^{-1}$ than for $\rho = 100\,km^{-1}$. This corresponds to the finding that the main contribution to the error stems from the flow inside a jam. This flow is considerably lower than in the corresponding SKM, which results from the difference in the mechanisms of both models to stabilise jams. Since the contribution of jams to the system's dynamics increases with increasing density, the agreement between both models decreases.

During the search process for an "optimal" parameter set one realises that the error function does not possess very pronounced optima. This is due to the fact that the parameter τ_{jf} plays a prominent role in regard of the model´s dynamics. As seen before, the speed of jam waves is primarily determined by this parameter. Thus, this parameter is almost the same within all three model variants. Once τ_{jf} is fixed, the possible range for the other parameters is restricted (*cf.* discussion in section 3.2), but within these ranges the parameters can be varied without causing considerable changes in the error function.

Figure 3.23 **Top**: *Left*: Relative difference of the total amount of emitted HC and NOx in the μ_2-Queue and μ_4-Queue depending on the density of the system. *Right*: Emission factors used for the calculations.
Bottom: Results of the μ_2-Queue model. *Left*: Total amount of emitted HC and NOx in the SKM (lines) and μ_2-Queue model (points) at different system densities. *Right*: Emission of HC over the simulation period at a fixed piece of road of length $1\ km$.

In the case of the μ_2-Queue model, τ_{ff} has to be chosen such that stable jams exist in the model. Moreover, the choice of τ_{ff} is not allowed to affect the movement of free-flowing vehicles in a way that the free-flow speed $v_{\max}$ can no longer be reached. However, as long as these two criteria are met, the exact value of τ_{ff} is of minor importance.

For the μ_3-Queue model, τ_{jj} is chosen independently of τ_{jf}. With increasing τ_{jj} the flow at intermediate densities increases as well (*cf.* figure 3.6). Therefore, it is possible to either increase τ_{ff} and τ_{jj}, or to decrease both parameters without changing the model's behaviour considerably. Again, the criterion has to be met, that the parameters guarantee stable jams.

A slight improvement can be achieved using the μ_4-Queue model. Here, the free flow and the approaching of the upstream jam front can be adjusted independently of each other. As one may expect, $\tau_{\mathrm{ff}} < \tau_{\mathrm{fj}}$.
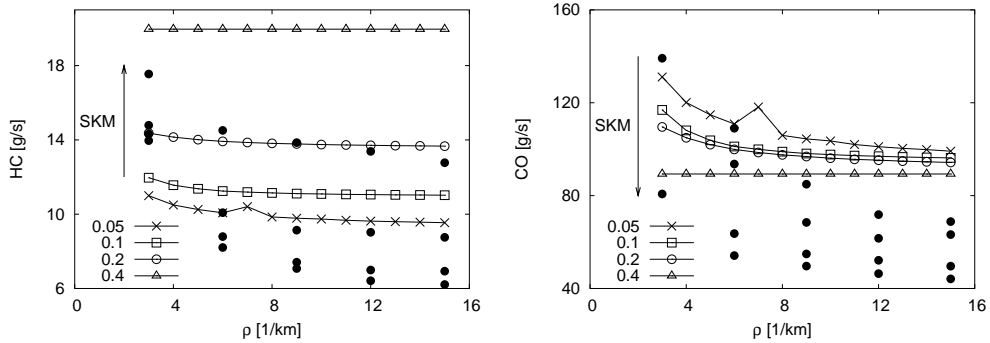
In the following the μ_2-Queue and μ_4-Queue are used to compare the computation of vehicular emissions to the SKM. Periodic systems at different densities are simulated for this purpose. After the initialisation of the system, it is simulated until stationarity is reached, and measurements are taken for a fixed temporal interval in the sequel. For each density one run is performed with the queueing model and several runs (30 at each density) are used for the SKM to get averaged values.

The results are presented in figure 3.23. For demonstration purposes, the pollutants hydrocarbons (HC) and nitrogen oxides (NOx) are chosen, due to their different velocity dependence. Whereas the amount of emitted NOx per kilometre increases with increasing velocity, HC behaves just the opposite. The dependence of the total amount of the two pollutants on the density is the same for both models. A more detailed comparison is possible using the relative differences. Over the full range of densities the amount of emitted HC compares better than the amount of NOx. This is due to the fact, that the velocity dependence of NOx is stronger than for HC, and therefore, deviations between the two models become more visible. At high densities the relative error of NOx increases, since the choice $N = 12$ (*i.e.*, $\rho_{\mathrm{max}} = 120\,km^{-1}$) strictly limits the storage capacity of a segment within the μ-Queue model whereas higher densities can partially be reached within the SKM. Note that the calibration of the μ-Queue model is done by means of two specific densities only, whereas the agreement between the two models is fairly good over the full range of densities. This also holds with respect to the temporal development of the emissions at a fixed location.

3.3.2   Multi-lane loop

The numeric experiment accomplished above is repeated for a periodic system with two lanes and two different types of vehicles, namely, passenger cars and lorries. Again, the SKM serves as reference system using the lane changing rules introduced in section 3.2.5. Note that it is to be expected that the two models do not compare as good as in the case of one lane (*cf.* discussion in the corresponding section).

Different two-lane systems with periodic boundary conditions and two vehicle types are simulated with the SKM in a first step. Each simulation is done with 2000 vehicles and the fraction of slow vehicles is varied. The common parameters are $a = 2\,m/s^2$, $b = 8\,m/s^2$, $l_{\mathrm{car}} = 7\,m$ and $\varepsilon = 1$. The maximum velocity for fast vehicles is $v_{\mathrm{max}} = 37\,m/s$, for slow ones $v_{\mathrm{max}} = 30\,m/s$. The parameters for the lane-changing rules are $v_{\mathrm{thresh}} = 11.5\,m/s$ and $p_{\mathrm{change}} = 0.01$. At each time step the current velocity of each car is transformed by means of emission factors. For fast vehicles emission factors of passenger cars are used whereas emission factors of lorries are used for the slow ones.

Figure 3.24   Total amount of emissions in the free flow regime for the μ_2-Queue model on a two-lane loop with passing. The fraction of lorries is varied from 0.05 to 0.4. The results of the SKM are inserted as single points, the arrow indicates the direction of increasing fraction of slow vehicles.

As queueing model, the μ_2-Queue version is used. which has already been compared to the SKM with respect to passing. The parameters are chosen similar to section 3.2.5, *i.e.*, $L = 100\,m$, $N = 12$, $n_{\mathrm{jam}} = 5$, $\tau_{\mathrm{ff}} = 1.3\,s$ and $\tau_{\mathrm{jf}} = 2.0\,s$ (with respect to one lane). The maximum velocity for fast and slow vehicles is $v_{\mathrm{max}} = 36\,m/s$ *resp.* $v_{\mathrm{max}} = 29\,m/s$. The passing probability is parameterised by $c_{\Delta v} = 0.9$, $c_m = 0.2$, $c_p = 0.5$ and $c_{\mathrm{lp}} = 20\,s$.

The comparison is focused on the free-flow regime, since vehicles can, otherwise, not realise their different maximum velocities. The results for the two pollutants hydrocarbons (HC) and carbon monoxide (CO) are presented in figure 3.24. They are chosen, because they show a different behaviour with respect to the composition of the vehicle fleet. The amount of HC increases with an increased fraction of lorries whereas the amount of CO decreases.

The dependence on the fraction of slow vehicles is well reproduced by the μ-Queue model. Also the dependence of the emission level on the density is reproduced, however, it is not as pronounced as in the SKM. This compares to the findings in section 3.2.5.

It can be concluded that the μ-Queue model is an appropriate approach to model vehicle fleets on a qualitative level. However, discrepancies exist on a quantitative level and deviations up to 50% are observed. For all simulations the emission level is lower in the SKM compared to the μ-Queue model. This is due to the fact that lane changes in the SKM force vehicles to slow down considerably, especially if a slow vehicle occupies the lane in front of a fast vehicle. Moreover, the explicit modelling of lane changes leads to stronger fluctuations in the velocities of the cars. In contrast, multi-lane traffic is modelled in an averaged way in

the μ-Queue model. Since in the regime of high velocities the emission factors strongly increase with the velocity, this leads to discrepancies between the two models and the level of emissions is lower in the SKM.

Same results are found for simulations with high densities (not shown), however, the deviations from the reference system become smaller. This is related to the fact, that velocity differences decrease in the congested state and passing is of minor importance. The dependency of the emission level of different pollutants on the fleet composition is as well reproduced for high densities. Note that the latter even holds if the μ-Queue model is used without passing.

3.4   Conclusion

This chapter aimed to introduce a vehicle-based traffic flow model based on queueing theory. To this end, a rather extensive review of known approaches in this context is given, in a first step. This is done in order to understand, what mechanisms are needed to reach a detailed description of traffic dynamics, and what is still missing. It is demonstrated that traditional approaches fail due to a missing coupling of the dynamics between consecutive queues. In consequence, there is no difference in the dynamics of the system in regard to free-flow and congested traffic conditions. Moreover, density perturbations are propagated upstream with infinite velocity and congested parts of such systems, therefore, dissolve from the upstream end in contrast to the findings in real traffic.

The new model approach (μ-Queue model) uses coupled queueing segments and is formulated based on time-headways between consecutive cars, *i.e.*, taking a microscopic perspective. The introduced waiting times at the end of a segment, represented as FIFO queue, can be regarded as state-dependent service rates. In contrast to traditional approaches, this dependence additionally accounts for the conditions downstream of the segment. As a consequence, the speed of perturbations is different in upstream and downstream direction, and the model allows for the dynamic description of backward-propagating wide moving jams.

Numerical investigations demonstrate, that the μ-Queue model possesses two different traffic states, homogeneous and congested flow. Within the deterministic model's formulation, there are no transitions between these states, given periodic boundary conditions. Introducing distributions for the waiting times and velocities, transitions between the states occur, and it is even possible to obtain a reasonable behaviour in regard to time-headway distributions observed in street traffic.

The relation between the properties of the model's states and its parameters is explored and an analytical description of the flow-density relation is given within the deterministic approach. The conditions necessary in order to obtain stable

jams are identified and the mechanism of moving jams within the approach is explained in detail.

Due to the exclusive local interactions within the introduced event-driven implementation of the μ-Queue model, a very efficient update scheme is obtained which allows for the simulation of large networks. In regard to applications, it is further demonstrated that multi-lane traffic can as well be described. The question of parameter calibration is further addressed, comparing the dynamics of the μ-Queue model to the SKM. To summarise the results, the new approach is well able to reproduce the dynamics of jams as well as the environmental impacts (by means of computing the emission of primary air-pollutants) in regard to the microscopic car-following model, needing considerably less numerical efforts at the same time.

Network Flows And Traffic Assignment

4.1   Open boundary conditions

In the previous chapter, a new formalism of a microscopic queueing model was introduced and its abilities with respect to the modelling of traffic dynamics were investigated using periodic boundary conditions. It is shown that the μ-Queue model possesses two traffic states, distinct from each other, and its dynamics concurs very well with the dynamics of the more detailed car-following model (SKM). Because the model is intended to be used in the network loading step of traffic assignment, the investigation of the model's abilities in regard to open boundary conditions is a mandatory step.

   As seen in the discussion of the SKM (section 2.4), open boundary conditions do not change the bulk states of the model in principle but affect the state selection. Depending on the effective inflow and outflow at the boundary, a certain traffic state is stabilised. Because the theory of open boundaries can be formulated in a rather general way, *i.e.*, without taking into account the details of the particular model's dynamics *resp.* on a mesoscopic level [67, 109, 148], similar results are expected within the μ-Queue model. That is indeed what is found. However, one also finds effects that stem from the fact that in the deterministic version of the model there is no intrinsic transition from laminar to congested flow. This point is further discussed in the following.

4.1.1   Implementation of open boundaries

Before results of the μ-Queue model are discussed, a short description of the implemented boundary conditions is given. Again, the parameters α and β are used to control the inflow and outflow, respectively.

In the SKM both rules, *i.e.*, at the entry and the exit of the system, have a stochastic nature. In the deterministic μ-Queue model, however, a stochastic implementation of the rule at the entry makes no sense. Independent of the virtual insertion of cars, the time-headways of the first segment in the system always obey equation (3.21) and details of the implemented rule are evened out. Therefore, a very simple rule is appropriate for the entry. Each time a car is inserted into the system, a new car is created at the entry, and a time-headway of size $1/\alpha$ is assigned to it.

The outflow from the open system is determined by the right boundary. Two strategies for the removal of cars from the system can be distinguished:

- The first strategy is similar to the one used for the SKM. A small system with N_β segments is linked to the open system. In order to change the outflow, a velocity restriction is imposed given by $v_\beta = v_{\max}\beta$.

- The second strategy uses a blockade at the right boundary which either lets an arriving vehicle pass or not. The blockade is simply switched on with a probability $(1 - \beta)$.
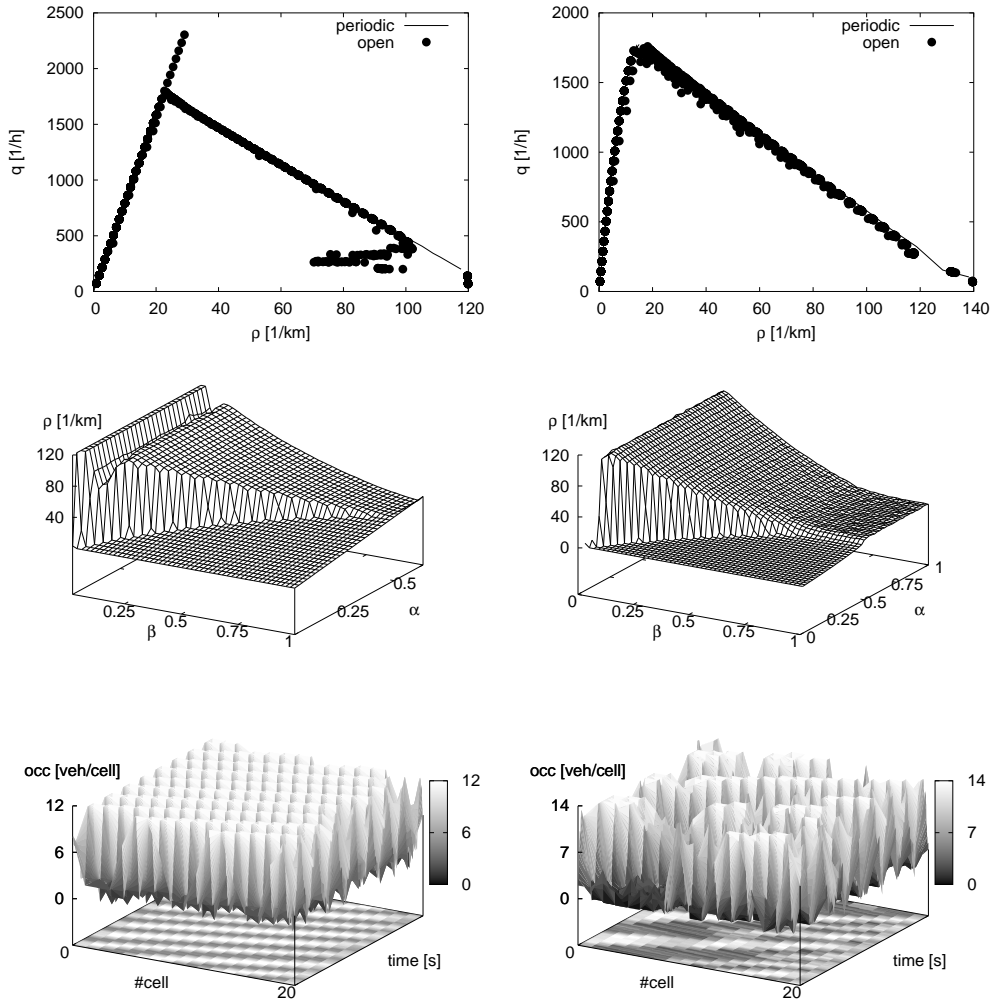
4.1.2   Phase diagram of the μ-Queue model

Simulations of the open system are made with the deterministic and stochastic μ_2-Queue model. The system consists of 100 segments, each of length $L = 100\,m$. The (α, β)-plane is screened with step size 0.02. Each system is relaxed for 10^6 time steps before measurements start. After that time all systems are in the stationary state where the inflow equals the outflow. Measurements are averages over 10^6 time steps as well.

The parameters of the deterministic μ_2-Queue model are $v_{\max} = 22\,m/s$, $N = 14$, $n_{\mathrm{jam}} = 4$, $\tau_{\mathrm{ff}} = 1.4\,s$ and $\tau_{\mathrm{jf}} = 2.0\,s$. The parameters for the stochastic version of the model are $v_{\max} = 25\,m/s$, $N = 14$, $n_{\mathrm{jam}} = 5$, $\tau_{\mathrm{ff}} = 1.1\,s$ and $\tau_{\mathrm{jf}} = 1.7\,s$. Free-flow speeds are Gaussian distributed with mean $v_{\max}$ and $\sigma_v = 5\,m/s$. For the distribution of the waiting times an Erlangian, equation (3.48), is used with $m = 3$. Figure 4.1 summarises the results for both models, using the second strategy to control the exit of the system.

The deterministic μ-Queue model completely reproduces the FDR of the periodic system. In contrast to the SKM (*cf.* section 2.4), states which lie on the high-flow branch only exist for undisturbed right boundaries, *i.e.*, $\beta = 1$. Therefore, no high-flow phase is present in the phase diagram of the open system. The phase diagram is only shown up to $\alpha = 0.65$, because the maximum flow is reached at this point. A further increase of α is, therefore, without effect. Due to the insertion strategy, the inflow then simply equals the outflow from jam.

Additionally, one observes system states which do not lie on the high-flow

Figure 4.1   Shown are the FDR, the density over the (α, β)-plane and a space-time diagram within the high-density phase. The striped patterns that were found in the SKM also exist in the μ_2-Queue model. The right boundary is implemented by a blockade which is turned on with probability $(1 - \beta)$.
Left: Deterministic μ_2-Queue model. The space-time diagram is done for $(\alpha, \beta) = (0.5, 0.2)$.
Right: Stochastic version of the μ_2-Queue model. The space-time diagram is done for $(\alpha, \beta) = (0.6, 0.4)$.

branch of the periodic system (if initialised with a jam). These states correspond to the FDR of the periodic system if homogeneous initial conditions are used. The
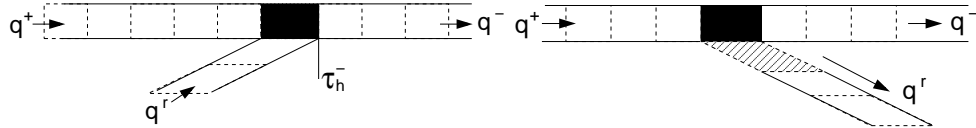
observations are not in contradiction to the theory of open boundary conditions, in particular, they do not contradict the extremal principle (2.33). They simply show that the μ-Queue model possesses two different states, the laminar and the congested one, and that there is no intrinsic mechanism which triggers a transition between them. Therefore, there is a non-vanishing probability that the boundary flows stabilise the homogeneous state. Noticeably, this is not an effect of the deterministic insertion strategy but happens for specific values of β. This can clearly be seen in the phase diagram. A possible explanation for this effect is that for these values a synchronisation between the temporal headways inserted at the entry and the headways generated at the exit occurs.

The findings are independent of the strategy chosen at the exit of the system. The only difference is that one observes more states, which correspond to the periodic system with homogeneous initial conditions, if the exit is controlled by a speed reduction. In that case, the influence of the right boundary is, therefore, weaker than for the case of using a blockade at the exit. This can easily be understood. Just changing the maximum velocity at the exit does not necessarily changes the time-headways between two consecutive vehicles. In combination with the deterministic insertion strategy, homogeneous patterns in the system are stabilised. In contrast, the usage of a random blockade truly changes the time-headways between arriving cars.

In the case of the stochastic μ-Queue model, the observed behaviour is similar to the deterministic μ-Queue model. As one may expect, system states vanish, which correspond to the periodic system with homogeneous initial conditions. There is no more high-flow branch, neither for the periodic nor for the open system. This is due to the fact that the implementation of waiting time distributions (*cf.* section 3.2.4) leads to rather strong fluctuations in the system. High-flow states therefore break down immediately.

The phase diagrams of the open system are qualitatively the same for both implementations. There exist two phases, distinct from each other. If the system's density is chosen as order parameter, one finds again that the phase transition between the high-density and low-density phase is of first order (*cf.* section 2.4). Even the particular microscopic structure, the striped pattern, is found in the high-density phase. In the case of the deterministic μ-Queue model this structure is very regular and each jam reaches the system's entry. In contrast, the jams that arise in the stochastic μ-Queue model either dissolve before reaching the entry or grow along their way through the system until the entry is reached. This compares well to the findings made in the SKM.

Recall, that the existence of boundary induced phase transitions is also found in real traffic situations [140, 147], as well as the striped pattern is similar to structures found in observations [76, 93, 173]. Therefore, the results demonstrate that the μ-Queue model truly improves the modelling of traffic dynamics and the

Figure 4.2   Sketch of an on-ramp (*left*) and an off-ramp (*right*). The black rectangle symbolises the node of the network, the dashed lines the segments which compose the link. At the on-ramp an additional time-headway τ_h^- is introduced in order to assure the maximum capacity of the leaving link. At the off-ramp an additional storage segment (striped rectangle) decouples the ramp from the main road.
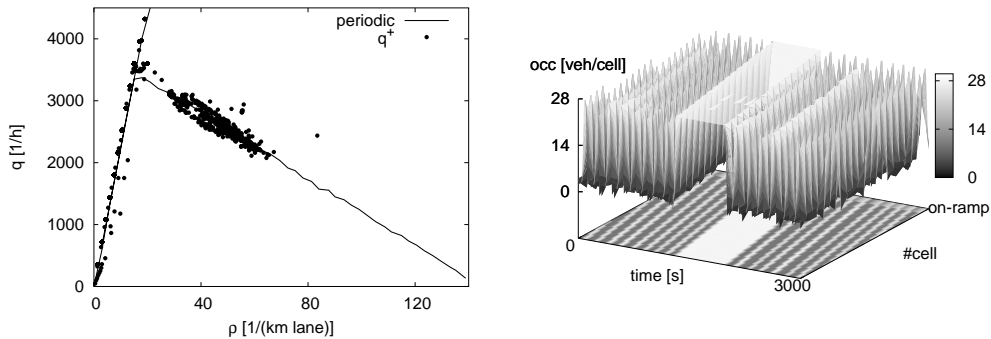
influence by dynamic bottlenecks (as one finds at on- and off-ramps) compared to traditional approaches by queueing theory. For example, the μ_1-Queue model shows a complete different behaviour with respect to dynamic bottlenecks. As long as the inflow is lower than the current capacity of the exit, one obtains a low-density phase. The system states lie on the free-flow branch of the corresponding periodic system. Otherwise, if the inflow exceeds the capacity of the exit for a certain period, a queue builds which stays fixed at the exit. The entry of the system remains unaffected until the queue spreads over the complete system. However, at the moment where the capacity restraint is removed the system recovers very quickly and vehicles leave the queue with maximum flow. Therefore, traditional queueing models tend to overestimate the throughput at bottlenecks.

4.1.3   Merges and diverges

Open boundaries play an important role in real traffic networks. Merges and diverges introduce stochastic boundary conditions (depending on the arriving and leaving flows) which yield bottlenecks, *i.e.*, capacity reductions. Traffic streams are affected by passing the bottleneck and from a practical point of view, it is important to have models that are able to predict reliably the things that matter, *i.e.*, bottleneck behaviour and queue dynamics [8, 39]. Therefore, it is shown in short, how merges and diverges can technically be modelled in the queueing approach. Moreover, the behaviour of the μ-Queue model is discussed qualitatively. Leaping ahead, it is shown, that the μ-Queue model is able to reproduce the properties of traffic streams at network nodes (including their dynamics) without major changes in its implementation.

On-ramps

The simplest merge is given by *on-ramps*, *i.e.*, a network node (intersection) with indegree 2 and outdegree 1. Usually an on-ramp is composed of a main road and
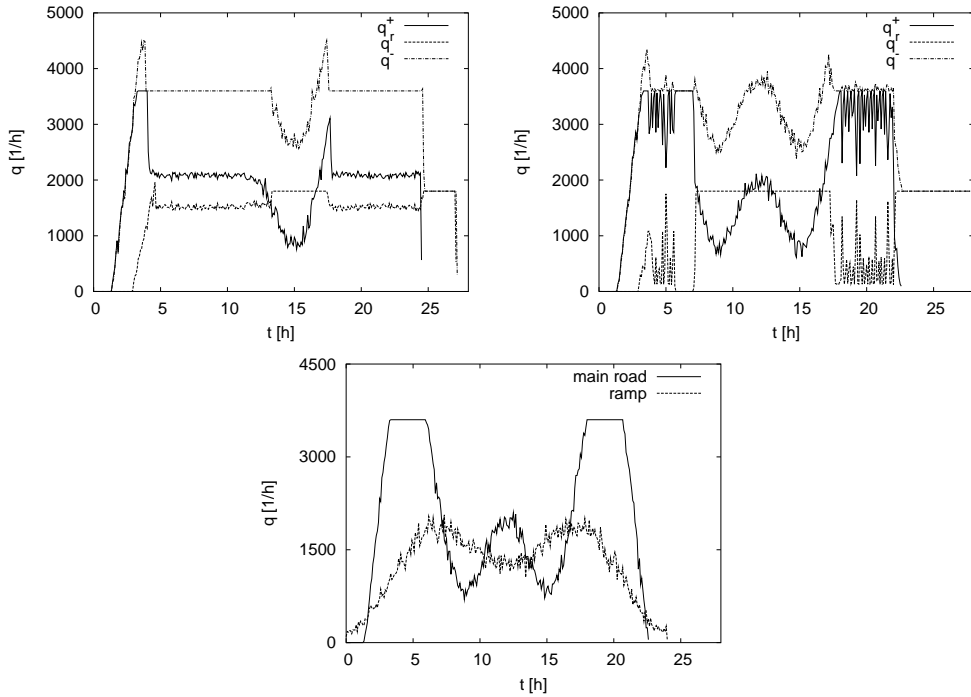
Figure 4.3 Simulation results of an on-ramp (figure 4.2) for different flows q^+, q^r. **Left**: System states on the approaching main road. Measurements are samples over $5\,min$. As long as the intersection's capacity is not exceeded, free-flow conditions are found. Otherwise, jams are created at the intersection which move backward through the system. **Right**: In the regime of congestion, the striped pattern is found again, which emerges at the intersection. A traffic jam, which is generated downstream the intersection, simply travels through this pattern. The striped pattern recovers immediately after the jam has passed the on-ramp.

a side road which is connected via the ramp. The leaving link may additionally have a capacity different from the incoming ones. If its capacity is lower than the capacity of an incoming link, it has to be assured that the flow into the leaving link does no exceed its capacity.

Recall, that in the event-driven implementation of the μ-Queue model (*cf.* appendix C), waiting times are passed between two consecutive segments (*i.e.*, the last segment of an incoming link and the first segment of the leaving one in this case). This is done in order to yield an efficient implementation of the model. Doing so, the compliance with the capacity of the incoming links is always assured. However, the incoming links do not have mutual information about their current outflows. If the sum of their capacities exceeds the capacity of the leaving link τ_{ff}^-, this capacity may not be respected. Therefore, supplementary time-headways τ_h^- are introduced at the entry of each link, which yield $\tau_h^- = \tau_{\mathrm{ff}}^-$. Additionally, these headways are disturbed randomly in order to introduce capacity fluctuations at network nodes. This is done by means of a Gaussian distribution $\mathcal{N}$, *i.e.*, $\tau_h^- = \tau_{\mathrm{ff}}^- + \sigma_\tau \mathcal{N}(0,1)$. Note, that the headways at the entry of each link only affect the incoming flows if their sum exceeds τ_{ff}^-. The principle geometry is sketched in figure 4.2. Further note, that the following results do not change in principle, if deterministic values for τ_h^- are used.

In order to demonstrate, that the behaviour of the on-ramp implementation

Figure 4.4 Flow over time for the approaches of the on-ramp, q^+ and q^r, and the leaving link q^-. The demands are given by (4.1) (*bottom*). **Top left**: μ_1-Queue model. **Top right**: μ_2-Queue model.

compares to reality, the open-boundary experiment is repeated. The main road is implemented as a two-lane road without passing and its parameters are $v_{\max} = 31, m/s$, $N = 14$, $n_{\mathrm{jam}} = 5$, $\tau_{\mathrm{ff}} = 1.6\,s$ and $\tau_{\mathrm{jf}} = 2.0\,s$. The ramp possesses one lane with parameters $v_{\max} = 22, m/s$, $N = 14$, $n_{\mathrm{jam}} = 5$, $\tau_{\mathrm{ff}} = 1.3\,s$ and $\tau_{\mathrm{jf}} = 2.0\,s$. The inflows to both links, q^+ and q^r, are varied from zero up to the corresponding maximum inflow.

There are two important causality regimes which should at least be reproduced by the on-ramp [36]. Either the flow on both approaches is dictated by conditions upstream, *i.e.*, both approaches are flowing freely. Or, both approaches are congested due to the intersection's lack of capacity *resp.* to congestion downstream, *i.e.*, the flow on both approaches is dictated by conditions downstream. In the first case density waves move forwards, whereas density waves move backwards in the second case. Indeed, this behaviour is found for the on-ramp as one can see in figure 4.3.

The generation and dissolution of queues as well as their interplay at the bottleneck are essential in order to yield an usable network model. In reality flows are usually time-dependent. Therefore, the behaviour of the μ-Queue model is

discussed in short for time-dependent inflows. For this purpose a full day period T is simulated and the inflows are parametrised as

$$
\begin{aligned}
q^+(t) &= 0.55 - 0.45 \left(\cos \frac{4\pi t}{T} + \cos \frac{6\pi t}{T} \right) \\
q^r(t) &= 0.35 - 0.45 \left(\cos \frac{2\pi t}{T} + \cos \frac{4\pi t}{t} \right).
\end{aligned}
\tag{4.1}
$$

The results for the μ_1-Queue and μ_2-Queue model are shown in figure 4.4.

The dynamics of the μ_1-Queue model is rather basic. At the moment where there is a considerable flow at the on-ramp, the capacity of the main road breaks down. A queue builds on both links approaching the intersection and the total capacity of the leaving link is shared. During the formation and dissolution of the queues at the intersection, the leaving flow is constant. The on-ramp strongly affects the flow on the main road during the peak period. After the system recovered during the period of lower inflows this behaviour is repeated.

In contrast, the μ_2-Queue model covers more of the dynamics given by the inflows (4.1). Here, the inflows also share the capacity of the leaving link, however, in a more subtle way. During the first peak period on the main road, the inflow to the system from the on-ramp is suppressed to a lower level compared to the μ_1-Queue model. As well, the main road does not reach its maximum capacity. During the period of lower demand, the system recovers and the flows correspond to the dynamics of the inflows. The flow from the ramp equals the outflow from jam during the following period, because the complete ramp is in the congested state. The behaviour of the second peak period resembles the first one.

Note that the two models behave completely different with respect to the main road and the ramp. In the μ_1-Queue, the flow at the end of the simulation stems from the demand which could not be served on the main road whereas it is just the opposite in the μ_2-Queue model. Further note that all drivers pass the system at an earlier point in time in the μ_1-Queue model. This results show once more the flaw of traditional queueing approaches (as the μ_1-Queue) with respect to traffic simulation, namely, that information about the traffic state downstream is not transferred upstream.

Finally note that the introduced concept of τ_h^- is also important for the modelling of crossings (network nodes *resp.* intersections with outdegree > 1). Moreover, it can be used to represent traffic lights. To this end, however, the τ_h^- of different leaving links have to be synchronised.

Off-ramps

The simplest diverge is given by *off-ramps*, *i.e.*, a network node with indegree 1 and outdegree 2. As for the on-ramp, an off-ramp is usually composed of a
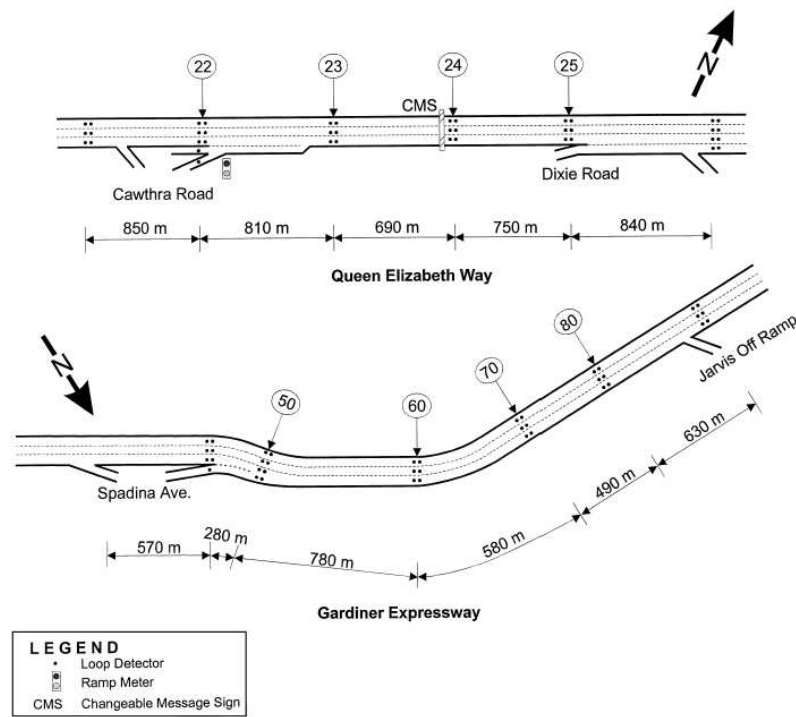
main road and a side road which is connected via the ramp. A sketch is given in figure 4.2.

The throughput at an off-ramp strongly depends on the directions which are chosen by the passing vehicles. As long as the percentage of cars which leave the main road is small, the traffic flow along the main road is not affected. However, if this demand exceeds the capacity of the off-ramp, a queue starts to build. With increasing number of queued vehicles at the off-ramp, there is a transition from the regime of undisturbed flow on the main road to the regime of an effective bottleneck which governs the movement of all vehicles approaching the intersection.

In principle, this behaviour is reproduced by the event-driven implementation of the μ-Queue model. However, due to the strict FIFO queueing discipline on each link, the influence of side roads at intersections is too strong. It is observed, that the capacity of the main road is in general even adjusted to the lower capacity of the ramp before the storage capacity of the ramp is completely utilised. Therefore, an additional *storage segment* is introduced in front of the off-ramp with a vanishing travel time. At its downstream end this segment is coupled to the off-ramp in the usual way. However, at its upstream end it does not transmit time-headways according to the capacity of the ramp but τ_{ff} of the main road. Doing so, one reaches the effect, that the flow on the main road is only affected by the off-ramp, if the storage capacity of the ramp is completely allocated. By calibration of the storage capacity of the additional segment the point of transition between undisturbed and affected flow on the main road can even be calibrated. Note that the introduction of additional storage segments is also mandatory for the implementation of crossings. Otherwise, the outgoing link with the smallest capacity governs the throughput of all incoming links.

4.2 Comparison to real world measurements

In order to use the μ-Queue model as a component of traffic assignment, it is worth to investigate the model's abilities to reproduce dynamic situation which are found in measurements. Moreover, the model's parameter have to be determined such that the properties of the network under discussion are recovered. For this purpose, an appropriate procedure is the use of real world measurements (if available) in an algorithm for the *calibration* of parameters. In principle, the approach is similar to the calibration process used in section 3.3, which is repeated in short here: The model is started with an initial set of parameters and the simulation results are compared to the findings in the measurements. To this end an error function has to be defined. In a second step an algorithm is used to improve the resulting error by changing the parameter set. Again, the Downhill-Simplex method [139, 149] is used here.

Figure 4.5   Sketch of the two freeway sites which are used for the comparison to real world measurements. The figure is taken from [25].

For the comparison to measurements and the demonstration of the calibration procedure, observations from two freeway bottlenecks in and near Toronto, Canada, are used. The two locations are illustrated in figure 4.5. The two sites have been featured in previous studies of capacity [18, 25]. The detectors are labelled in the figure. The detectors on Queen Elizabeth Way record counts, occupancies and time mean speeds in each lane over $30\,s$ intervals. The detectors on the Gardiner Expressway collect the same measurements over intervals of $20\,s$ duration.

4.2.1   Single-lane traffic

Because detectors are usually placed on major roads, there are hardly measurements for single-lane traffic. Therefore, multi-lane traffic data is used which is scaled down to a single lane. This is described in the following. The comparison is done for two data sets (D1,D2) which were taken at the Gardiner Expressway and the detectors 50 through 80 are used.

Detector 50 is used to fix the boundary conditions at the entry of the system. The cumulative counts, which can easily be calculated by the given data sets, are

added up over intervals of $2\,min$. In order to scale the inflow down to one lane, the cumulative counts are simply divided by the number of lanes.

The right boundary is controlled by means of measured velocities (*cf.* the first rule at the exit given in section 4.1). This is done for two reasons. The first one is due to the data sets. During the evaluation of the cumulative counts, inconsistencies are detected, namely, that the number of vehicles between two detectors exceeds the maximum density during several periods. Recall that the difference between the cumulative counts of two detectors gives the number of cars between them (see *p.* 74). The second reason is due to the down-scaling of the inflow into the system.

As input for the control of the right boundary either detector 70 (`G1`) or 80 (`G2`) are used. In the first case `G1`, detector 60 is used to determine the error done by the simulation. In the second case `G2`, the error is averaged using detector 60 and 70. The error at each detector is given by

$$\mathrm{err} = \frac{1}{n_i} \sum_{i=1}^{n_i} \frac{\mid v_i^{\mathrm{obs}} - v_i^{\mathrm{sim}} \mid}{v_i^{\mathrm{obs}}}, \tag{4.2}$$
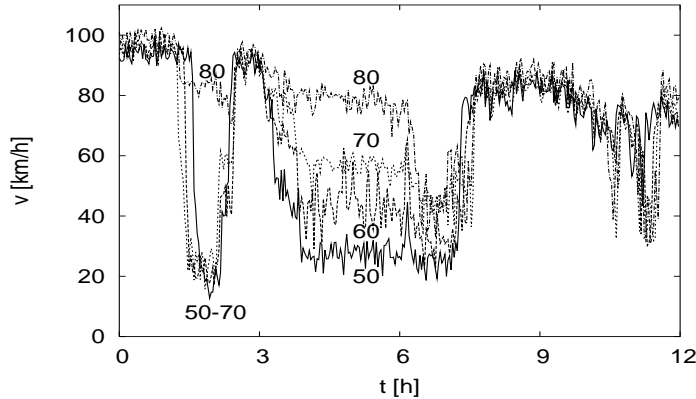
with v_i^{obs}, v_i^{sim} being the velocities observed and simulated, respectively. n_i is the number of sample points which are taken on $2\,min$ intervals.

The dynamic situation which is observed at Gardiner Expressway is rather interesting. At this location, one frequently finds a dynamic bottleneck which is located approximately one kilometre downstream of the on-ramp at detector 50, see figure 4.6. Besides the fact that the road possesses a slight curve in vicinity of the location where the bottleneck arises, there are no further disturbances of the traffic stream [18]. The dynamic situation is similar for both data sets which are used in the following. Note that the existence of the bottleneck is almost invisible at detector 80.

The calibration process is done for the μ_1-Queue and μ_4-Queue model using both data sets (`D1`, `D2`). The segment length is fixed to $100\,m$. The results are presented in Table 4.1.

With respect to the μ_1-Queue model one can clearly see that it is not able to reproduce the dynamic situation at all. At the exit a queue start to grow and the simulated velocity is virtually constant. The parameters adjust in a way, that the mean velocity equals the measured velocity during the period of the breakdown. This demonstrates once more, that the missing of backward travelling jam waves in traditional queueing approaches leads to a wrong description of dynamic traffic situations.

In contrast, the μ_4-Queue model achieves very good agreement with the observations. Except for the (`G2`,`D2`) simulation, the overall calibration error is rather small. As already noted before (see figure 4.6), the bottleneck of the system is
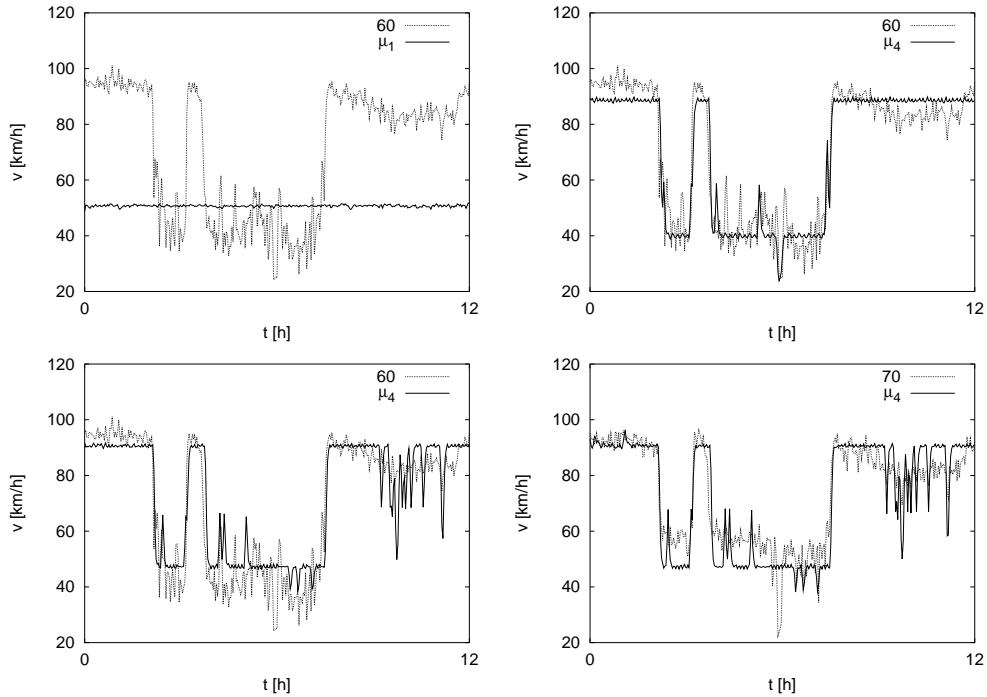
Figure 4.6   Measured velocities at detector 50 through 80 on Gardiner Expressway (`D2`). An active bottleneck exists between detector 60 and 70 which is almost invisible at detector 80. The dynamic situation in `D1` is similar, however, the breakdown at detector 80 is more pronounced.

			N	n_{jam}	v_{max} $[m/s]$	τ_{ff} $[s]$	τ_{fj} $[s]$	τ_{jf} $[s]$	τ_{jj} $[s]$	err_{cal}	err_{val}
G1	D1	μ_1	14	-	14.08	0.84	-	-	-	0.355	-
G1	D2	μ_1	14	-	12.6	2.16	-	-	-	0.383	-
G1	D1	μ_4	13	2	24.61	1.79	2.64	2.91	2.72	0.093	0.104
G1	D2	μ_4	11	3	23.03	1.22	1.85	1.76	1.67	0.139	0.16
G2	D1	μ_4	12	2	25.17	1.9	1.72	2.21	2.07	0.116	0.164
G2	D2	μ_4	14	2	26.4	1.84	3.55	2.07	1.92	0.221	0.342

Table 4.1   Results of the calibration process of the two data sets (`D1`,`D2`) on Gardiner Expressway. Either the exit is controlled by the velocities measured at detector 70 (`G1`) or at detector 80 (`G2`). Besides the calibration error err_{cal} also the validation error err_{val} is given. The latter one results, if the obtained parameter sets are mutually exchanged.

located upstream from detector 80. Therefore, the measurements taken there do not contain the complete dynamic situation. Thus, it is not surprising that the error is lower in `G1` compared to `G2`. Figure 4.7 illustrates the resulting velocities over time for the first data set (`D1`).

The resulting parameters further reflect that the simulated period is mainly governed by congestion. Therefore, the values for n_{jam} are very small. Moreover, the values determined for τ_{jj} are always smaller than τ_{fj}. According to the definition of the waiting times in congestion (3.22) this means that the flows inside jams are rather small. This may also be connected with the finding that the μ-Queue

Figure 4.7   **Top**: Simulation results with data set D1 for simulation setup G1. One clearly sees, that the μ_1-Queue model is not able to reproduce the dynamic situation at all (*left*). In contrast, the μ_4-Queue model compares very well to the observed traffic situation (*right*).
Bottom: Simulation results for the same data set and simulation setup G2 with the μ_4-Queue model.

model is less sensible with respect to boundary conditions controlled by velocities compared to a control by cumulative counts[1].

Besides the error of the calibration step, the validation error is also given in Table 4.1. This error results, if the parameter sets are mutually exchange, *i.e.*, the parameters found for the first data set are applied to the second one and vice versa. It is clear that the validation error is higher than the calibration error. However, it is still small enough here, in order to yield an appropriate description of the dynamic situation. With respect to the calibration of different links in a network, it should, therefore, be possible, to obtain parameter sets generally valid by means of comparison to just a few traffic situations.

	N	n_{jam}	v_{max} $[m/s]$	τ_{ff} $[s]$	τ_{fj} $[s]$	τ_{jf} $[s]$	τ_{jj} $[s]$	$\mathrm{err}_{\mathrm{cal}}$	$\mathrm{err}_{\mathrm{val}}$
Q1	12	2	27.56	1.79	2.14	2.87	3.35	0.041	0.054
Q2	14	2	28.9	1.64	2.01	2.73	3.07	0.042	0.043

Table 4.2   Results of the calibration process with the two data sets on Queen Elizabeth Way using the three lane version of the μ_4-Queue model without passing. Parameters are given with respect to one lane. Recall, they have to be transformed by means of (3.49). The dynamic situations of the two data sets are not such distinct from each other as in the case of Gardiner Expressway. This explains, why the validation error is only slightly higher than the calibration error.

4.2.2 Multi-lane traffic
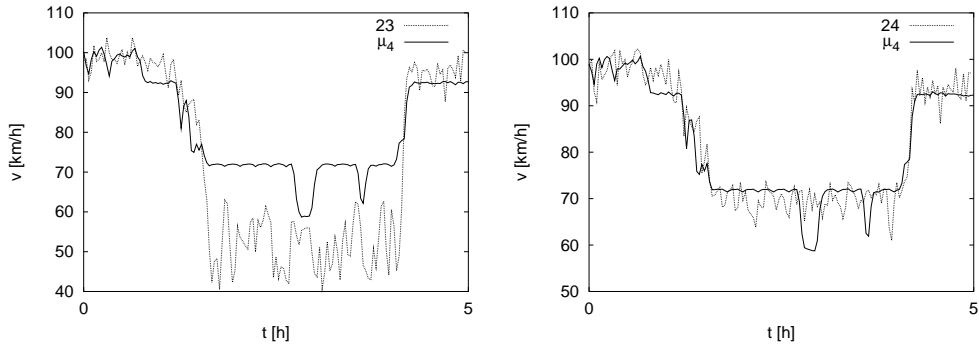
Two data sets from Queen Elizabeth Way (Q1,Q2) are used to investigate the abilities of the μ-Queue model with respect to multi-lane traffic. The location is illustrated in figure 4.5. The entry of the simulated system is placed at detector 23, the exit lies at detector 25. Again, cumulative counts are used to determine the inflow to the system. The measured velocities at the exit are used to control right boundary conditions. The error function (4.2) is evaluated at detector 24.

Again, good agreement is found. The parameters from the optimisation step are given in Table 4.2. The μ_4-Queue model is used with three lanes without passing. Figure 4.8 shows the comparison between measured velocities at the detectors 23, 24 and the simulated values. The velocities at station 24, which are used for the calibration process, are reproduced very well.

The obtained results for single-lane traffic and multi-lane traffic are truly encouraging to use the queueing model in the framework of dynamic traffic assignment, because it is quite able to reproduce dynamic situations found in real traffic. Moreover, they underline the necessity of having backwards moving jam waves included in the model's dynamics in order to be a meaningful model for traffic flow.

---

[1]This control of the exit compares to the random blockade used in section 4.1.

Figure 4.8 Simulation results for the data set Q1. The measured velocities at the entry of the system are lower than the simulated ones. This may be related to the existence of the on-ramp in the real world situation.

4.3 Dynamic Traffic Assignment

The continuous increase of traffic demand together with the limited possibility of a further increase of road infrastructure forces the authorities to develop methods which allow for a more efficient usage of existing road capacities. Besides other objectives, the instruments of ITS (Intelligent Traffic System) focus on an optimal distribution of traffic demand by providing information about the traffic conditions in a network and introduction of certain ITS measures. Traffic assignment can be seen as one principal component of ITS, since it allows the testing and evaluation of ITS measures before they are implemented in practice [127]. Moreover, it can be used for the prediction of traffic conditions in short-term (*e.g.*, [177]). Further examples for issues which can be addressed by traffic assignment can for example be found in [3, 6, 184].

A traffic assignment model predicts route choice, network flows, link travel times and route travel costs on a given transportation network with a given travel demand. The latter one might either be static (*e.g.*, reflecting the rush-hour period) or dynamic. Due to its importance, there exist a wide variety of approaches to traffic assignment which go along with conceptually different understandings about it. Therefore, some short comments about the concept are made in the following before the framework is presented, which uses the queueing model introduced above.

4.3.1 Static vs. dynamic traffic assignment

A majority of approaches concerning traffic assignment tackle the problem from a mathematical point of view using optimisation techniques. In principle, a model

for traffic assignment consist of three parts: conservation of flow, route choice criteria (usually user equilibrium or system optimum) and a model of flow behaviour or propagation within individual links.

The models aim to compute the route choice in a traffic network which results from a given travel demand. The network is defined by means of a directed graph $\mathcal{G} = (\mathcal{N}, \mathcal{A})$ with nodes $\mathcal{N}$ and arcs $\mathcal{A}$. The travel demand is represented as trips between nodes $r, s \in \mathcal{N}$ (which are called origin and destination nodes, respectively). In order to define an objective function to be optimised, these models are based on an assumption of the route [2] choice. A widely used route choice model is provided by Wardrop's first principle [181]: All used routes (for a specific pair (r, s)) have equal costs and no unused route has a lower cost. The state, which results from the optimisation assuming this principle, is referred to as *user equilibrium*.

The simplest treatment of the problem is given by neglecting all temporal dependencies, *i.e.*, the travel demand and the arc flows are static. In this case, the distribution of the travel demand over the network can, *e.g.*, be described as convex optimisation problem [17], which is solved numerically [57, 60, 176]:

$$\min z(\mathbf{x}) = \sum_{a \in \mathcal{A}} \int_0^{x_a} \tau_a(x) dx \tag{4.3}$$

subject to

$$
\begin{aligned}
\sum_{r,s} \sum_{p \in \mathcal{P}_{rs}} f_p^{rs} \delta_{a,p}^{rs} &= x_a & \forall a \\
\sum_{p \in \mathcal{P}_{rs}} f_p^{rs} &= d_{rs} & \forall r, s \\
f_p^{rs} &\geq 0 & \forall p, r, s.
\end{aligned}
\tag{4.4}
$$

The notation is taken from [60]. x_a is the flow over arc a and $\tau_a(x)$ gives the associated costs (usually travel times). Further, f_p^{rs} is the flow on path $p \in \mathcal{P}_{rs}$, where $\mathcal{P}_{rs}$ is the set of all path from r to s. Finally, d_{rs} is the travel demand from r to s, and the function $\delta_{a,p}^{rs}$ equals one or zero if arc a is part of path p or not, respectively.

In order to have a unique solution (with respect to arc flows) in the optimisation problem, one usually chooses strictly monotonic increasing and strictly convex link cost functions $\tau_a(x)$. For example, the travel time function (3.4) is of that kind.

Due to the existence of efficient solution techniques, the static approach to traffic assignment is widely used by civil engineers for planning purposes. However, it is rather obvious, that the static description is not sufficient with respect to the

---

[2] A route between r and s is simply a path in the network which starts at r and ends at s.

inherent dynamic nature of traffic. Static approaches are neither able to describe the situation in a congested network nor the exceeding of capacities during rush hour. The assumption that the travel time on a link is a monotonically increasing function of the link flow is, moreover, violated in practice. For all flow levels below capacity there are two corresponding travel time values [132]. Another major shortcoming stems from the fact that the flows on routes sharing a common arc always interact. In reality drivers on different routes may use a link at different times. These shortcomings matter in particular in regard to ITS applications.

Therefore, dynamic assignment models take time dependencies explicitly into account. It is still possible to formulate an optimisation problem for the dynamic case [151, 166], but the computation of solutions becomes infeasible for networks of sizes that matter in practice [60]. The different approaches uses distinct methods to describe the problem and differ in the assumptions which are made to obtain time-dependent cost functions on the links of the network [2, 23, 87, 143]. However, their focus is more on the mathematical description of route choice than on a realistic description of traffic flow. Many of them address the question of the existence and the uniqueness of a solution rather than the aspects of applicability to real world problems.

4.3.2 Simulation-based traffic assignment

The approaches discussed above can be seen as models for route choice which are enhanced by a very simple description on link flows by means of travel time functions. However, due to the interactions of the individual drivers during their travel through the network, the route choice and travel times are strongly coupled: The route choice is based on travel times and the travel times result from the route choice. Therefore, it is necessary to have a model for link flows which reproduces the dynamic findings of traffic flow.

In order to improve the quality of the computed assignment of a given travel demand, traffic flow simulation can be used. Either, a static assignment model is enhanced by an appropriate description of traffic flow (*e.g.*, [58, 157, 163]) or an existing flow model is extended by a model for route choice (*e.g.*, [54, 59, 171]). The following focuses on the latter approach.

It is convenient to refer to two main components of a *simulation-based traffic assignment* procedure, namely the *route choice mechanism* and the *network loading*. The latter is the method used to represent the evolution of the traffic flow over the links of the network once the route choice has been determined. The typical simulation approach is a systematic relaxation via a variant of the following procedure [27]:

1. Make some initial guess for the routes.

2. Execute all route plans simultaneously in a microscopic traffic simulation (*network loading*).

3. Readjust some or all of the routes using the knowledge from the network loading (*route choice*).

4. Restart with the second step until a certain criterion for the relaxation progress is met.

The assignment which results from the iterative relaxation procedure can be interpreted as imitating drivers' adaption over time to changes in network topology or control. The latter includes the implementation of ITS measures.

The procedure has much in common with the relaxation methods for static assignment. Instead of using link cost functions, a network loading model performs the task to determine the objective function. By doing so, one looses the mathematical knowledge (*e.g.*, about the existence and uniqueness of the solution). In the simulation-based assignment the convergence and the stability of the algorithm can usually not be proven. However, one gains a realistic description of traffic dynamics which is essential with respect to the usability in real world applications.

Network loading model

In principle, every traffic flow model can be used for the network loading step of the simulation based traffic assignment, if traffic dynamics is reproduced on an appropriate level. In particular, queue spillovers and distinct traffic states have to be taken into account, since they have a considerable influence on the quality of the resulting assignment [37, 111]. Moreover, depending on the level of disaggregation of the travel demand, the modelling should be based on individual car-driver units which are able to travel along their individual routes.

Therefore, the microscopic car-following model and the queueing approach introduced in this work are both appropriate models in this context. Since the relaxation process usually needs several iterations until a sufficient level of convergence is reached, the network loading (as well as the route choice) should be computationally fast. In this respect, the queueing approach is favourable compared to the car-following model. In the latter one, each car has to be processed several times during its movement along a link, whereas this has to be done only once for each segment in the queueing approach. Computational studies show, that the queueing model can gain a factor of 10 to 100 according to the real time ratio compared to the car-following approach [27, 154]. Hence, the μ-Queue model is used for the network loading step in the following.

Note that the deterministic version of the μ-Queue model is used. The findings for open boundary conditions show that the model displays boundary induced phase transitions. Because in the network each intersection represents an open boundary, traffic streams will cross, merge and diverge there, building the mechanism for congestion. Moreover, due to individual paths and trip startings in the travel demand, the model will hardly be found in laminar flow conditions over the full simulation period.

Route choice model

In the route choice step the information from the network loading step is used to readjust the current route choices of the simulated drivers. There are many variations with respect to the route choice model (*e.g.*, [12, 47, 60, 127, 171]). They differ in the fraction of routes which are re-planned, in the number of routes known to each driver, or the usage of a deterministic and a probabilistic route choice. The procedure used in the following is introduced in [60]. Although a detailed description of the algorithm is not attempted here, the assumptions and properties of this route choice model are presented briefly. The notation is taken from the original publication [60]. It is based on individual *trips*, which are characterised by an origin, a destination and a departure time.

For each trip (or driver) a set $\mathcal{P}$ of routes between the origin and destination is known. A probability distribution $p : \mathcal{P} \to \mathbb{R}_+$ with $\sum_{r \in \mathcal{P}} p(r) = 1$ is associated with each trip. r is a specific route from the set $\mathcal{P}$. Additionally, a learned or perceived travel time $t_{\mathrm{tr}}(r)$ is known for each $r \in \mathcal{P}$. The set of routes can, *e.g.*, be initialised by means of fastest paths computed in the empty network.

In the network loading step a specific route s is chosen from $\mathcal{P}$ according to p. After the network loading, the route travel time from the simulation step $t_{\mathrm{tr}}^{\mathrm{sim}}(s)$ and the time-dependent link travel times are known. These are used in order to update the travel time known for each trip by application of

$$
\begin{aligned}
t_{\mathrm{tr}}(s) &\leftarrow t_{\mathrm{tr}}^{\mathrm{sim}}(s) \\
t_{\mathrm{tr}}(r) &\leftarrow \beta t_{\mathrm{tr}}^{\mathrm{dij}}(r) + (1 - \beta) t_{\mathrm{tr}}(r) \qquad \forall r \in \mathcal{P} \setminus s.
\end{aligned}
\tag{4.5}
$$

β is a parameter and $t_{\mathrm{tr}}^{\mathrm{dij}}(r)$ is the travel time of route r calculated from the time-dependent link costs.

In a following step the route set $\mathcal{P}$ is possibly extended by a new route, if there exist faster paths in the network than the ones contained in $\mathcal{P}$. Finally, based on the travel times (4.5), the different routes are compared with each other (introducing an additional small noise) and the probability distribution of each trip is adjusted such that

  - the probability of choosing a route which has a low travel time increases.

   - the probability of choosing a route which has a high travel time decreases.

For further details the reader is referred to [59, 60].

The route choice model is a stochastic one, *i.e.*, all noise of the simulation is moved into the distribution of the routes. This leads to the fact that the algorithm does not converge in a strict sense. A measure for convergence is therefore given by means of the distribution of choice probabilities [89, 132]. If the system is relaxed to a sufficient level, this distribution becomes stationary. An easy measure to determine the relaxation level is provided by means of average route travel times. The equilibrium which is achieved is called *stochastic user equilibrium*.

The route choice procedure should be used with route sets $\mathcal{P}$ which contain more than one element. Otherwise it is known that the process tends to produce oscillations in the route choices or becomes unstable [60].

Within the described procedure different routes for a specific origin-destination pair are evaluated according to their travel time. This is done by means of fastest path which are computed using a time-dependent implementation of Dijkstra's shortest path algorithm [46]. The basic version of the algorithm can easily be extended to address particularities of road networks as turning restrictions, additional waiting times at nodes etc. (*e.g.*, [48, 69, 144]). Since in each iteration up to several million paths have to be computed, it is important to use efficient implementations of the algorithm [83, 186]. With respect to time-dependent fastest path the sampled link travel times $t_{\mathrm{tr}}^{\mathrm{link}}$ (sampled on intervals of size Δt) from the network loading step have to fulfill FIFO-conditions, *i.e.*, for each link

$$t + t_{\mathrm{tr}}^{\mathrm{link}}(t) \leq (t + \Delta t) + t_{\mathrm{tr}}^{\mathrm{link}}(t + \Delta t) \tag{4.6}$$

has to be satisfied. In that case, the time-dependent implementation of Dijkstra's algorithm gives the optimal solution and possesses the complexity of the static variant [1]. Since the queueing model fulfills FIFO, the same holds for the travel times on the links.

4.4   Application: Environmental impact modelling

The following presents simulation results with respect to air pollution which are obtained by means of the DTA framework introduced in the last section. Two intentions are followed. On the one hand, the differences of the μ_1-Queue and μ_4-Queue model are further discussed. On the other hand, an example is given for the applicability of the framework.

This is done using both, results of the new model implementation as introduced in this work and results of a collaborative work with meteorologists from

the University of Cologne[3]. This collaboration was part of the Collaborative Research Centre SFB419 [164] supported by the German Research Foundation (DFG) which investigated environmental problems of industrialised regions. In particular, the computation of emission inventories due to street traffic is an important part of an air-quality management system which was developed within this project. Air pollutants from street traffic are of particular importance due to their high contribution to the total emission level and their high temporal variability. Strategies to reduce the local impact of pollution, therefore, have to include the management of traffic streams. In order to investigate the effects of certain reduction measures, such a model system is able to support the decision process. A sketch of the introduced model chain is given in figure B.1. In appendix B the role of traffic flow modelling in the area of air-quality systems and the methodology to map traffic dynamics to emissions is further presented.

The results of the previous sections show that the μ_1-Queue model possesses deficits with respect to the modelling of traffic dynamics. One, therefore, expects, that the μ_4-Queue model leads to better results with respect to emission modelling (*cf.* section 3.3). Nevertheless, in order to give some examples on measures to control traffic, FASTLANE[4] is used here, presenting results from the collaborative work within the SFB419 [164, 165]. During the project time, FASTLANE has been the model of choice and a lot of efforts have been made to calibrate the model chain using this model. Because the project ended in 2002 and several people were involved, this cannot be repeated here. As long as comparisons are made between a reference situation and a scenario computed with the same model, the usage of FASTLANE should not be seriously erroneous.

4.4.1 Data sources

The project focused on the area of the city of Cologne. The data sources, which were used in the project with respect to the traffic simulation, stem entirely from the project "stadtinfoköln" [169] and were generated by the "Institut für Stadtbauwesen, RWTH Aachen". The data set contains the main road network of the city of Cologne including the highway ring which encloses the area of the city (*cf.* figure 4.10). Besides the traffic which is generated by inhabitants, the highway ring is a main traffic node in Germany with a high fraction of transit traffic. More-

---

[3]Institute for Geophysics and Meteorology, and Rhenish Institute for Environmental Research (EURAD Project).

[4]Recall that FASTLANE can be regarded as the implementation of the μ_1-Queue model using a parallel update scheme and randomly fluctuating capacities. Because the time step used for the simulations with FASTLANE was very small ($\Delta t = 3\,s$), it behaves rather similar to the μ_1-Queue model. It is denoted in any case presented here, whether FASTLANE or the μ_1-Queue model is used.

over, due to the high number of workplaces inside Cologne, there is also a high fraction of commuter traffic which loads the road infrastructure.

The data about the network contains informations about the number of lanes, speed limits, maximum capacity and a classification into road classes. For each road class, flow-density relations are given, which are used to calibrate the parameters of the μ-Queue model *resp.* FASTLANE.

In order to compute traffic assignments, *origin-destination relations* (or origin-destination matrices) are necessary. The sources of traffic described above have to be included in these relations to obtain realistic traffic loads. Moreover, for the project, which addressed simulations with a high temporal and spatial resolution, these relations have to be highly disaggregated in space (*i.e.*, the number of origin-destination pairs with respect to network nodes has to be high) and time (*i.e.*, the relations have to be specified for temporal short intervals). These requirements are met by the given data set. The methods used to obtain the relations are described in detail in [155]. General approaches for the generation of time-dependent origin-destination flows can, *e.g.*, be found in [7, 16, 179].

The resulting data base consists origin-destination relations for each day of week which give the number of trips between traffic zone. These traffic zones are spatially fine grained. For each day, the relations are furthermore sliced in intervals of one hour. For the purpose of the DTA model, the original relations were further temporally disaggregated in order to obtain trips which are specified by a starting time, a starting node and an ending node. The traffic load for each day of week contains up to two million individual trips.

4.4.2   Experiences from the assignment step

Network representation

In regular, digital road maps are obtained from ordinary maps using algorithms for image processing. Frequently, these algorithms come in trouble to resolve relations between arcs and nodes at complex intersections. Many relations resulting from the image processing have to be adjusted by hand (*resp.* in a half-automated way) to obtain a meaningful representation for the simulation model.

The following case appears rather often: In the original network representation, road links are given as arcs between nodes, however, turning restrictions are not specified. This leads to unwanted effects, especially at highway interchanges. If the interchange is approached from a specific direction, there are always four possibilities to change to a target direction, instead of one (which is the case in reality). It is quite clear that, in consequence, a proper modelling of throughputs at an interchange is not possible. This is also true for other kinds of intersections.

For the case of the Cologne network, a complete revision of all relations between arcs and nodes would have been to time consuming. Therefore, only the most important intersections were revised, including the complete highway ring. Turning restrictions were introduced by means of node expansion (*e.g.*, [48]).
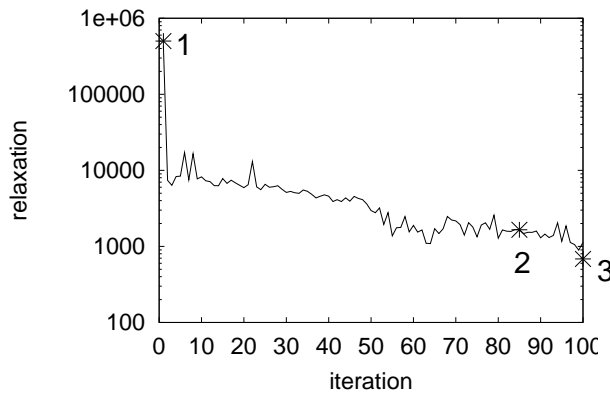
Gridlocks

In reality there are mainly two peak periods for the traffic demand over the day, namely, the morning peak when people are on their way to work and the evening peak where traffic flows in reversed direction. During these periods, certain parts of the network are usually in the regime of *saturation*, that is where congestion occurs. In this regime, the network loading step is very sensible to the degree of relaxation reached already *resp.* to the number of trips contained in the origin-destination relations. This is due to the fact that spillovers past merges can lead to gridlock on ring roads and on other parts of networks with closed loops (which are frequent in urban traffic networks). For example, a slight increase in a feasible origin-destination flow in such network can result in a situation where all traffic remains stuck in the network [37].

In the case where gridlock occurs, the network loading step will not terminate, if there is no mechanism to flush the complete network. This was introduced in the DTA framework used in the project in the following way: If the number of cars in the network exceeds a certain threshold, or there are still cars in the network at the end of the simulated period, the storage capacities of all segments are set to infinity. By this, the network loading step can be terminated in a proper way, *i.e.*, travel times are known for all links in the network (which are, of course, very high for the links which were locked).

Nevertheless, the travel times which are sampled after the gridlock occurred in the network are in principle useless. With respect to the relaxation process, one observes, that the point in time at which the network becomes locked shifts to later times from iteration to iteration. However, the number of iterations can be very high before a net-loading step is obtained without gridlock.

In order to decrease the number of iterations in the relaxation process, the storage segments introduced in section 4.1.3 can be useful. The iteration process is started with a rather high storage capacity of these segments. After a small number of iteration steps (which has to be determined for the specific problem) the storage capacity is decreased from iteration to iteration, step by step. By doing so, one possibly even achieves that no gridlock occurs at all. In any case, it is achieved that the drivers in the simulation learn alternative routes right from the beginning of the relaxation process. This procedure was chosen in the project and it was found, that the number of iterations could indeed be lowered considerably. Moreover, one observes that the average number of cars in storage segments decreases very

Figure 4.9   Illustration of the relaxation process. Plotted is the level of relaxation (sum of all travel times) against the iteration steps. The line gives the relaxation process of a workday (reference day). If the number of trips contained in the corresponding origin-destination relations is increased by 5% the first iteration yields a level of relaxation which is indicated by point 1. If the same relation is initialised recycling the routes from the assignment of the reference day, the first iteration immediately reaches point 2. If only the distribution of trip starting times is changed and the routes are recycled, the first iteration reaches immediately point 3.
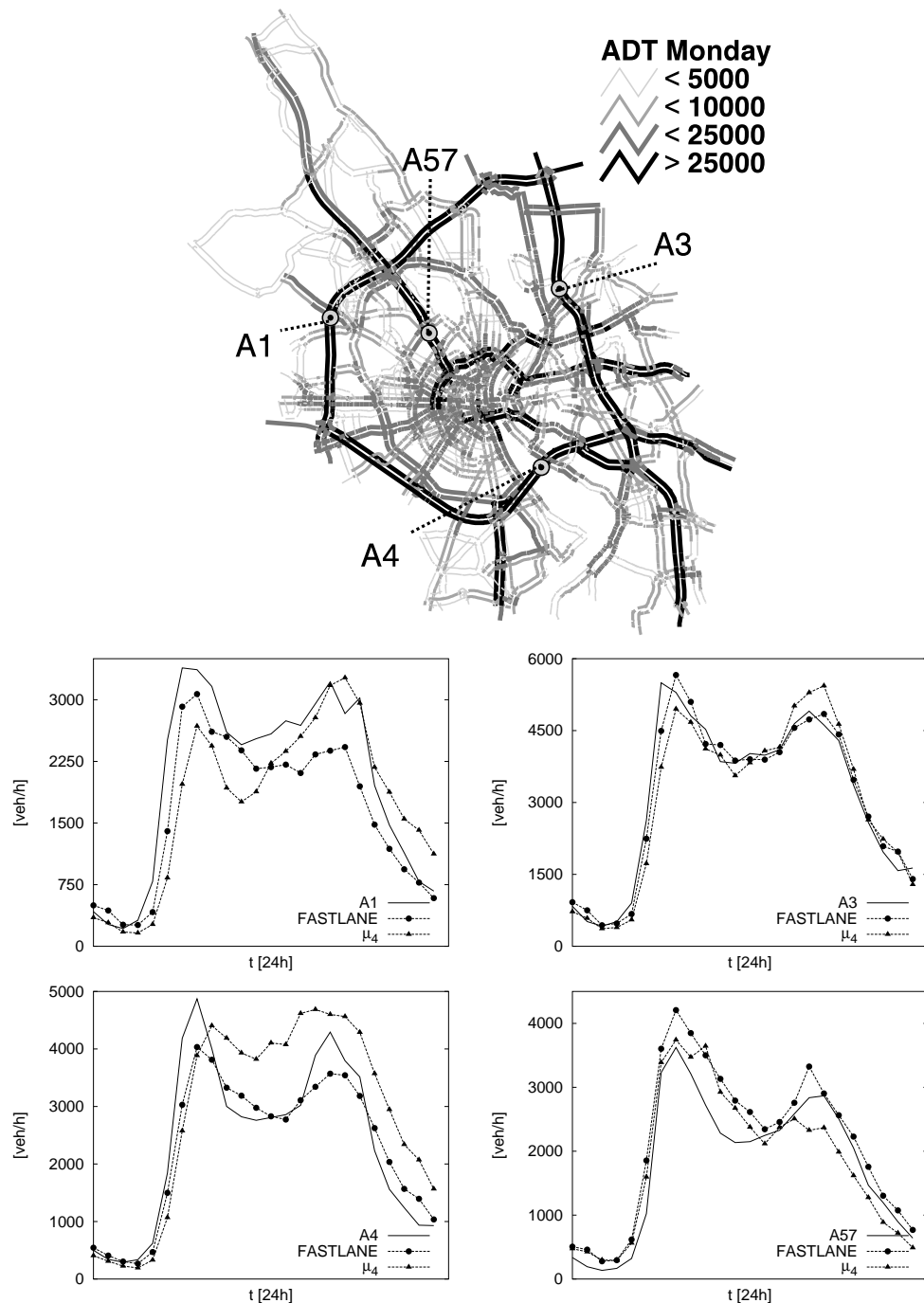
fast due to the readjustment of the routes.

Recycling of routes
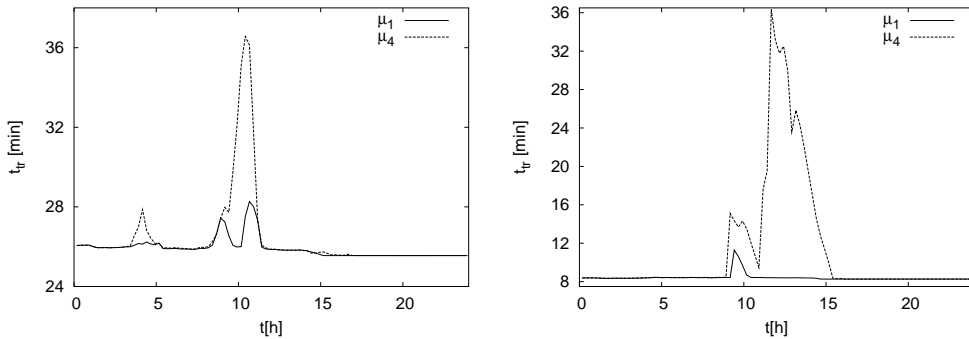
In the project, many assignments had to be computed, namely, for different scenarios, and for each day of week within each scenario. Regarding traffic counts, it is known, that traffic volumes and routes do not differ too much between workdays [102]. If the fraction of commuter traffic is quite high, this sounds quite natural. If the assignment of a workday has been computed, this can be used to initialise the route choice for the assignment of other days. Figure 4.9 shows that one can indeed save a considerable number of iterations by this procedure.

4.4.3   Results of the reference scenario

The following shows simulation results of the assignment of Monday, comparing the μ_1-Queue model *resp.* FASTLANE with the μ_4-Queue model. Since the information about the iteration process has not been stored in the project (where FASTLANE was used) and different computer architectures were used, this cannot be compared to the new model here. However, the new implementation of the

Figure 4.10   Average daily traffic volumes computed for Monday with FASTLANE. The four plots on the bottom show comparisons between simulation results of FASTLANE *resp.* the μ_4-Queue model and counts from traffic detectors.

Figure 4.11   Travel times of specific routes over daytime which result from the μ_1-Queue model and the μ_4-Queue model. **Left**: Route along the highway ring. **Right**: Route passing the inner city of Cologne.
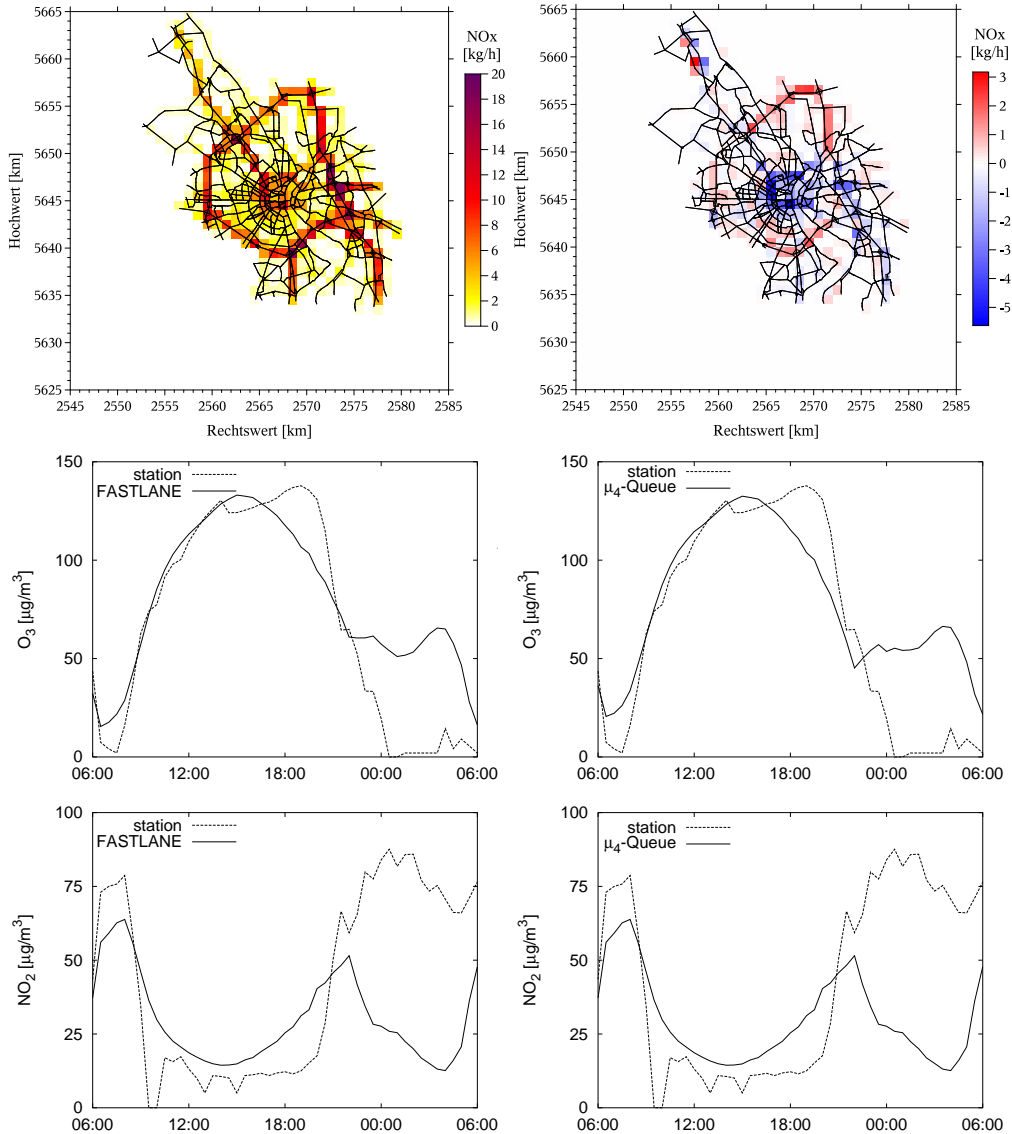
model with the event-driven update scheme yields a real-time ratio around 100 (on an Intel XEON 900 MHz).

Figure 4.10 shows the resulting assignment of FASTLANE with respect to average traffic volumes on Monday. One clearly sees the strong load on the highway ring and arterials roads. Comparison with traffic counts from detectors (which are averages over several Mondays) show that the model is able to reproduce the time-of-day dependent traffic loads with respect to its dynamic and volume. The results for the μ_4-Queue model are similar with respect to average traffic volumes. This is partially due to the observation, that it is rather difficult to find reasonable path alternatives different from the optimal path [132].

However, with respect to route travel times there are differences between both approaches. In order to demonstrate this, the resulting assignment of the μ_4-Queue model is used. Given this route choice, the network loading step is repeated with the μ_1-Queue model and travel times along the routes are compared with each other. The travel times for a route along the highway ring and a route passing the inner city are shown in figure 4.11. Whereas the travel time function over day is rather flat in the case of the μ_1-Queue model, the μ_4-Queue model shows a considerable increase of the travel times within certain periods of the day. This difference in the behaviour is due to the fact, that the μ_1-Queue tends to overestimate throughputs at bottlenecks and does not reproduce traffic dynamics in a right way.

Note that computations were made for all weekdays without changing the parameters of the network. The results obtained at different days all compare well with traffic counts, which shows that the parametrisation of the network used is robust.

Figure 4.12 shows results with respect to the computation of air pollution. The

Figure 4.12 **Top**: Emission inventories of NOx computed with the results of the assignment of Monday. On the *right*, the emission inventory of FASTLANE is shown. On the *left*, the difference between the emissions from the μ_4-Queue model and FASTLANE are presented.
Middle/Bottom: Comparisons between the *immissions* (*i.e.*, after the computation using the complete model chain, figure B.1) stemming from simulation and field-measurements. Results of FASTLANE are shown on the *left*, the ones of the μ_4-Queue model on the *right*. For further details the reader is referred to [161].

emission inventories are computed using FASTLANE and the μ_4-Queue model. The emission inventories of both models show a similar spatial structure which is due to the relation between the amount of emitted pollutants and traffic volumes. Recall that the assignments yielded similar results. With respect to the quantitative emission level, differences are found , however, because the traffic dynamics in both approaches is distinct from each other. Moreover, comparisons between results of simulations with the complete model chain (figure B.1, *i.e.*, after the transport and transformation of the primary pollutants by chemical reactions) and field-measurements are shown. Besides the emission inventory due to street traffic further sources of air pollutants are included in the calculations.

The comparison shows that the variation over day is well reproduced although there are still quantitative differences. Due to the complexity of the model chain it is not possible to trace back deviations to a single model part. Investigations of the model chain by means of sensibility studies however show, that without taking into account the emissions of traffic results of that quality cannot be obtained [78, 161].

4.4.4 Remarks about scenario computations

The following results stem from the works within the SFB419 [165]. They are all computed by means of FASTLANE[5]. Therefore, conclusions are only made by means of comparisons between the different scenarios. The computations presented above serve as a reference. The following scenarios are used:
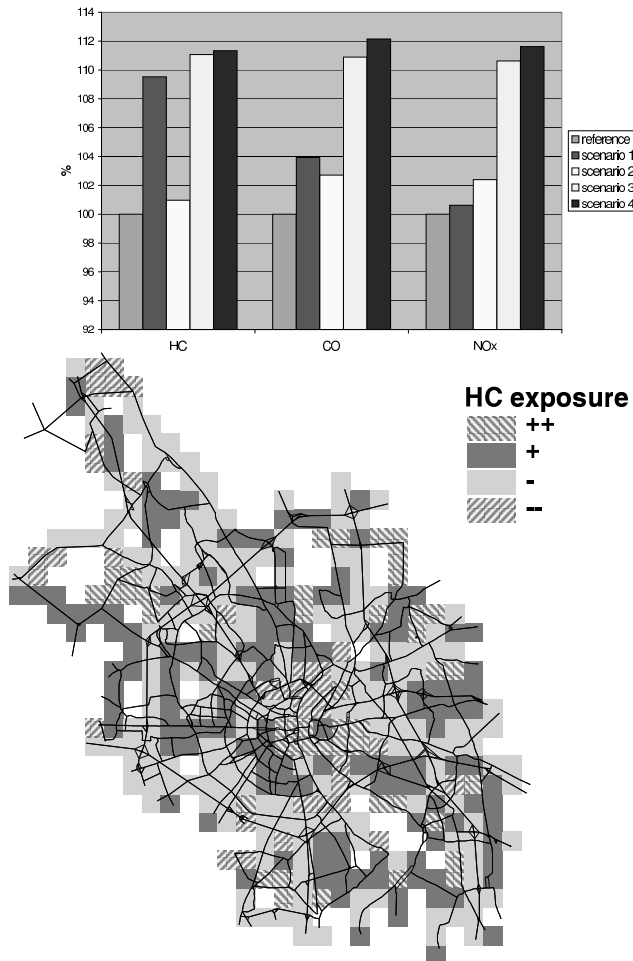
1. In order to keep traffic away from the inner city, the two bridges that cross the river Rhine are closed for traffic. Moreover, the speed limit is lowered by $20\,km/h$ on all roads which are not highways.

2. Equals scenario 1, however, no speed limit reduction is applied.

3. Increase of traffic volumes by 15%.

4. The traffic demand equals scenario 3. Additionally, the highway ring around Cologne is enlarged to have entirely three lanes per driving direction.

Figure 4.13 shows the total amount of emitted pollutants by traffic. In all scenarios, one observes an increase of the emission level, although this increase is partially rather small.

Despite the fact, that a complete closing of the two bridges in the inner city of Cologne is rather impractical[6], Scenario 1 and 2 are made in order to investigate the effect of measures to relocate traffic streams. Because drivers, which have to cross the Rhine, are forced to take longer routes (note that the origin-destination flows remain unchanged), the increase of total emission is unavoidable. However,

---

[5]Recall the connection to the μ_1-Queue model.
[6]One could think about road-pricing to reduce their usage.

Figure 4.13 **Top**: Total emission of hydrocarbons (HC), carbon monoxide (CO) and nitrogen oxides (NOx) for the different scenarios defined in the text. **Bottom**: Comparison of the spatial distribution of emitted HC between scenario 1 and the reference. $(++, +)$ means that the emission level is decreased by $(> 20\%, \leq 20\%)$ in scenario 1 compared to the reference. $(--, -)$ means that the emission level is increased by $(> 20\%, \leq 20\%)$ in scenario 1 compared to the reference.

as figure 4.13 shows, the spatial distribution of primary pollutants changes. Since in the inner city the number of people, which is exposed to the primary pollution, is rather high, this redistribution may lead to local improvement of the situation. However, in order to rate the impact situation, an integrated approach has to be used, which relates the population density with the immission inventories [66].

The results further show two problems in respect to the investigation of reduction scenarios. If relocation of traffic streams is addressed without changing the origin-destination relation, it is clear that one only achieves a spatial redistribution of emissions. However, traffic management strategies do have an impact on the behaviour of people planning their mobility. In principle, models of DTA should therefore be coupled to models which establish a connection to activity planning behaviour (*e.g.*, [82, 171]). This was not possible in the project presented here.

The other problem is related to the velocity dependence of emission factors (*cf.* appendix B). With respect to scenario 1 and 2 one observes that in the first scenario the amount of HC and CO is increased rather strong (due to the speed reduction), whereas it is just the opposite for the second scenario. The message is, that a certain measure may be positive with respect to one pollutant, but worsens the situation with respect to another one. Note that these arguments are purely on the level of emission inventories. The resulting impact after taking into account the meteorology may show different results.

Finally, the findings with respect to scenario 3 and 4 should be commented in short. Probably, one may expect that, due to the improved flow conditions on the highway ring in scenario 4, emissions should be lowered. However, one observes a further increase compared to scenario 3. The reason stems from an an effect which can be observed rather often. Due to the improved traffic conditions on the highway ring more drivers use it. Each of them reduces its individual travel time and accepts longer routes by this.

4.5   Conclusion

Whereas there are no transitions between the states of the deterministic μ-Queue model in periodic systems, phase transitions occur using open boundary conditions. The complete phase diagram of the μ-Queue model is derived. Two phases are found, namely, the low-density *resp.* the high-density phase, and the boundary induced phase transition between them is of first order. A high-flow phase in the sense of section 2.4 is not present in the model, however, high-flow states exist for undisturbed flows at the right boundary. The microscopic structure of striped patterns is retrieved, according with the ones found in the SKM. These findings do not change if the stochastic version of the model is used.

The sensitivity of the model in regard to the implementation of boundary conditions is discussed, leading to an appropriate representation of merges and diverges necessary for the simulation of street networks. It is shown that the model behaves reasonable in the presence of dynamic bottlenecks. The focus on real world applications is further complemented by the comparison to measurements stemming from distinct traffic situations. The results show that the μ-Queue model

is suitable in order to reproduce dynamic traffic situations and allows for the calibration of the model's parameters by means of observations.

The μ-Queue model is implemented as part of a simulation-based dynamic traffic assignment, undertaking the task of the network loading step. This framework is applied to simulate street traffic in the area of the city of Cologne. Besides the discussion about practical aspects of the model's application within this framework, it is shown that the approach is well applicable to large-scale simulations of several million individual trips, being numerically efficient. The differences between the μ-Queue model and FASTLANE *resp.* μ_1-Queue model are further demonstrated, showing that the latter approach tends to overestimate throughputs at bottlenecks and does not reproduce traffic dynamics properly.

Finally, examples of scenario computations in regard to environmental impacts of street traffic on air-quality are given, however, by means of FASTLANE. To this end, the presented framework is embedded into a model chain which additionally includes further sources of emission and computes the transport and transformation of air pollutants, due to chemical processes. The results show that it is essential within such approach to include emission inventories of traffic which have a high temporal and spatial resolution. Moreover, it becomes clear, that the explicit modelling of traffic demand and integrated impact assessment, both not included in the above model chain, is necessary in order to explore valuable measures aiming to improve the impact situation.

Chapter
5

Summary

This work focuses on the investigation of vehicle-based models of traffic flow motivated by its use within dynamic traffic assignment and the computation of environmental impacts by street traffic. In particular, the abilities of different approaches in regard to the inherent dynamic of traffic flow is addressed. The following summarises the main results of this work, more detailed discussions are presented at the end of each chapter.

In the first part of this work, the dynamics of an already known microscopic car-following model (SKM,[112, 113]) is investigated. A classification of the model's behaviour in regard to the stability of high-flow states [131] is presented. It is shown, that within the parameter regime where structure formation is observed, the high-flow states are stable against intrinsic fluctuations of the model, given that the braking ability does not become too high. Moreover, the outflow from jam is shown to be stable within this parameter regime. The model is extended by an anticipatory driving strategy, and it is shown that this mechanism further stabilises high-flow states and allows for very short time-headways as found in observations. The inner working of this mechanism is explained by means of numerical and analytical results. The investigations on open boundary conditions show that the model fulfills an extremal principle [109, 148]. The complete phase diagram of the SKM, including the extension by anticipation, is derived and the nature of the phase transitions is investigated. It can be concluded that the occurrence of a high-flow phase and the present microscopic structures (striped pattern) are generic for microscopic car-following models which exhibit a branched flow-density relation and phase separation.

In the second part of this work, a new approach (μ-Queue model) based on queueing theory is introduced. Within this approach coupled queues are used and service rates are implemented by means of time-headways between cars. The introduced waiting times can be regarded as state-dependent service rates which account for the conditions downstream of the queue, in contrast to traditional approaches from queueing theory. It is shown that the new approach is, in con-

sequence, able to describe the dynamics of backward-propagating wide moving jams. The relation between the properties of the model's states and its parameters is explored and an analytical description of the flow-density relation is given. The mechanism of moving jams is explained in detail. The introduced event-driven implementation of the μ-Queue model yields a very efficient update scheme which allows for its usage within the framework of simulation-based traffic assignment in large networks.

Comparisons between the dynamics of the μ-Queue model and the SKM demonstrate that the new approach is well able to reproduce the dynamics of jams as well as the environmental impacts by means of computing emissions, needing considerably less numerical efforts compared to the SKM.

The investigations of open boundary conditions and the comparison to measurements complete the discussion of the μ-Queue model. It is shown that even the deterministic version of the model displays boundary induced phase transitions between laminar and congested flow. The microscopic structure of the observed phases concur with the ones found in the SKM. Moreover, the comparison to measurements further demonstrate that even multi-lane traffic can approximately be treated with this approach.

Finally, the application of the model in the context of the computation of environmental impacts of street traffic is demonstrated. To this end, simulation results of the network of Cologne are given. The properties of the μ-Queue model with respect to traffic assignment is further discussed as well as examples for the computation of scenarios aiming an improvement of the impact situation are given. The results show that it is essential within the modelling of air quality to include emission inventories of traffic which have a high temporal and spatial resolution. It is demonstrated that the new approach is able to meet these requirements.

Basic concepts of queueing theory

Queueing theory is a branch of operations research which explores the relationships between the demand on a service system and the delays suffered by the users of that system. On the one hand, one tries to *simplify* the description by disregarding details that are considered superfluous. On the other hand, *approximations* are used in order to transform incomplete data into mathematical quantities. In the following the basic concepts are discussed in short, and important notations are introduced. The discussion follows [65, 120].

In queueing theory, a service system is described as a queue together with a service device. Customers, jobs or requests are assumed to arrive with a specific *arrival rate* λ and they are processed with a certain *service rate* μ. If the arrival rate exceeds the service rate for a certain period, delays occur and requests experience an additional waiting time before being processed. Usually, there is not infinite space but a restricted *storage capacity* in front of the service. One distinguishes the queue and service capacity, which are the maximum number of requests that solely fits into the queue and in both, service facility and queue, respectively. In order to allow a mathematical description, assumptions about the distribution of the service and arrival rate are made, as well as the storage capacities are fixed to a specific value. The parameters of a queueing system are specified by the *Kendall notation* `A/B/m/K/P` with

A	interarrival time distribution,
B	service time distribution,
m	number of server,
K	storage capacity of the system (default $= \infty$) and
P	customer population (default $= \infty$).

As distributions,

$$
\begin{array}{ll}
M & \text{Markovian (exponential),} \\
E_r & \text{Erlangian,} \\
D & \text{deterministic or} \\
G & \text{general distribution}
\end{array}
$$

are generally used.

In order to complete the system's definition, one has to specify the *queueing discipline*, *i.e.*, the order of processing the request in the queue. Usually one either uses *FIFO* or *LIFO*, *i.e.*, first-in-first-out or last-in-first-out disciplines, respectively.

Although one uses a simplified description and approximations by means of the above distributions, closed form expressions for the expected *waiting time* W or the number of requests Q_L (*queue length*) in the system can, in the majority of cases, only be given for equilibrium conditions.

M/M/1-queue

Let p_k be the probability to find k requests in the system. If requests arrive with rate λ and are further processed with rate μ, the following balance equations hold in statistical equilibrium,

$$
\begin{aligned}
\lambda p_0 &= \mu p_1 \\
(\lambda + \mu)p_i &= \lambda\, p_{i-1} + \mu\, p_{i+1} \qquad i \geq 1.
\end{aligned}
\tag{A.1}
$$

Adding these equations for different i yields

$$
p_i = (1 - \eta_q)\eta_q^i \qquad i = 0, 1, 2, ..,
\tag{A.2}
$$

where $\eta_q = \lambda/\mu$ is the *utilisation* of the queue. $\sum_{i=0}^{\infty} p_i = 1$ is used in order to derive (A.2).

The number of requests in the system then yields

$$
\langle Q_L \rangle = \sum_{i=0}^{\infty} i\, p_i = \frac{\eta_q}{1 - \eta_q},
\tag{A.3}
$$

the average time spent in the system yields

$$
\langle W \rangle = \sum_{i=0}^{\infty} \left(\frac{i+1}{\mu} \right) p_i = \frac{1}{\mu\,(1 - \eta_q)}.
\tag{A.4}
$$

As one can easily see,

$$
\langle Q_L \rangle = \lambda \langle W \rangle
\tag{A.5}
$$

holds. Equation (A.5) is known as *Little's formula* which holds in general [65].

M/G/1-queue

In the following, the average queue length is derived for service rates that are generally distributed with mean $1/\mu$ and variance σ^2. The derivation follows [120].

In the case of the M/M/1-queue, the system is completely described by the number of users in the system, *i.e.*, the knowledge about this number is sufficient to describe the complete history of the system, as far as the future is concerned. Therefore, one can immediately state that the probability of completing a service within the next time interval Δt is equal to $\mu \Delta t$, independent of the past. In contrast, using a M/G/1-queues, this probability also depends on how long ago the service began to the request that is currently receiving service.

There are several different approaches to describe the stationary state of a M/G/1-queue. The simplest one uses the trick of focusing attention on certain specific instants in time, so called *epochs*. At these instants the knowledge about the number of requests in the system is sufficient in order to specify its current state. An epoch is given by the instant t_i at which the server completed the service of a request i.

In order to proceed, three random variables are introduced, namely,

N the number of requests in the system instantaneously after the instant t_{i-1},

R the number of new requests that arrive at the system during the service time of the request i and

N' the number of request in the system instantaneously after t_i.

For these variables

$$N' = N + R - 1 + \delta \tag{A.6}$$

with

$$\delta = \begin{cases} 0 & \text{if} \quad N > 0 \\ 1 & \text{if} \quad N = 0 \end{cases} \tag{A.7}$$

holds. If $f(s)$ is the probability distribution function for the service time S of the requests, the expected values for R and R^2 yield

$$\begin{aligned} \langle R \rangle &= \int_0^\infty \langle [R|s] \rangle f(s) ds \\ &= \lambda \langle S \rangle = \frac{\lambda}{\mu} \end{aligned} \tag{A.8}$$

$$\begin{aligned} \langle R^2 \rangle &= \int_0^\infty \langle [R^2|s] \rangle f(s) ds \\ &= \lambda^2 \langle S^2 \rangle + \lambda \langle S \rangle = \lambda^2 \left(\sigma^2 + \frac{1}{\mu^2} \right) + \frac{\lambda}{\mu}. \end{aligned} \tag{A.9}$$

Squaring (A.6) and taking the expected value yields

$$2 \langle N \rangle \langle 1 - R \rangle = \langle R^2 \rangle - 2 \langle R \rangle + 1 + \langle \delta \rangle \langle 2R - 1 \rangle. \tag{A.10}$$

Since in equilibrium $\langle N' \rangle = \langle N \rangle$ holds, $\langle \delta \rangle = 1 - \eta_q$ the expected number of requests in the system is

$$\langle Q_L \rangle = \eta_q - \frac{\eta_q^2 + \lambda^2 \sigma^2}{2(1 - \eta_q)}. \tag{A.11}$$

Equation (A.11) is also known as *Pollaczek-Khintchine formula* which is used in section 3.1.1.

Oversaturated queues

Obviously, the equations (A.3) and (A.11) become invalid in the case of oversaturated queues, $\eta_q \to 1$. In that case, a deterministic description of queueing can be applied [183]. If one assumes that requests arrive and depart regularly with rates λ *resp.* μ, the mean number of requests waiting for service is given by
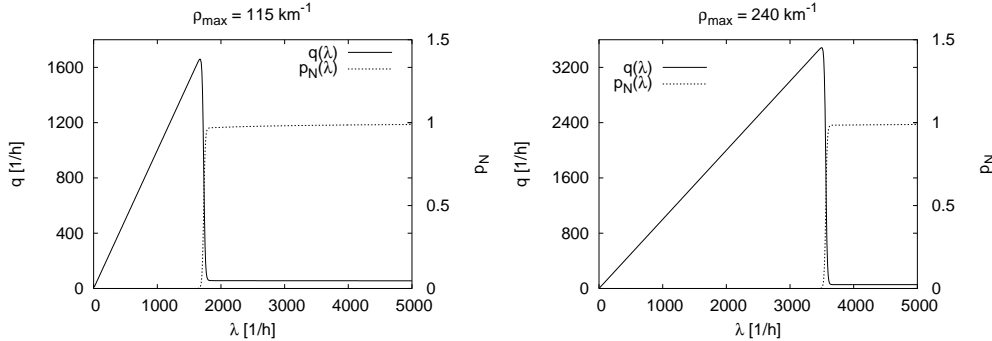
$$Q_L(t) = Q_L^0 + (\lambda - \mu)\, t = Q_L^0 + \mu(\eta_q - 1)\, t, \tag{A.12}$$

where Q_L^0 is the queue length at $t = 0$. The average waiting time W per request for those, that arrived during the period $(0, t)$, can be expressed as

$$
\begin{aligned}
W(t) &= \frac{1}{\lambda\, t} \int_{Q_L^0}^{Q_L^0 + \lambda t} \left(\frac{Q_L}{\mu} - \frac{Q_L - Q_L^0}{\lambda} \right) dQ_L \\
&= \frac{Q_L^0}{\mu} + \frac{t}{2}(\eta_q - 1).
\end{aligned}
\tag{A.13}
$$

State-dependent queues

Observations of street traffic show that the vehicles' speed on a road segment is strongly influenced by the the current density. To put this in terms of queueing theory, the service rate is dependent on the utilisation of the queue. Therefore, it is straightforward to give up the assumption of fixed service rates, using state-dependent rates instead. The basic idea of state-dependent queues is demonstrated using a traffic flow model, introduced in [84]. Traffic flow is described in terms of M/G/N/N queues, *i.e.*, the storage capacity of a queue is limited by N and there are N service stations. Each vehicle, that arrives at the queue, is assigned to a free service station whose service rate depends on the number of vehicles already in the queue.

Figure A.1 Flow versus λ for the linear model (A.14). The parameters are $L = 1600\,m$, $v_{\max} = 24\,m/s$. If the inflow λ exceeds a certain threshold λ^*, the segment becomes completely blocked. Shown are the relations for $\rho_{\max} = 115\,km^{-1}$ and a fictitious value $\rho_{\max} = 240\,km^{-1}$.

In order to construct the model for traffic flow, it is further necessary to assume a relationship $v(\rho)$ between the density and mean travel speeds. In [84] a linear and an exponential model are assumed (parameters of the functions are fitted according to empirical observations). For simplicity, only the linear model,

$$v(n) = \frac{v_{\max}}{N}\left(1 + N - n\right), \tag{A.14}$$

is discussed. n and N are the current number of vehicles inside a road segment and the storage capacity of the segment, respectively.

Each road segment is then modelled as a queue with N service channels. Arrivals of vehicles are assumed to be independent of the state of the queue (rate λ), whereas the service time follows a general distribution whose mean depends on n. This dependency is given by $f(n) = v(n)/v_{\max}$. For the state probabilities

$$p_n = \left[\frac{(\lambda\,L/v_{\max})^n}{n!\,f(n)f(n-1)\cdots f(2)f(1)}\right] p_0, \tag{A.15}$$

holds, where p_0 is given by $\sum_{i=0}^{N} p_n \equiv 1$ [30]. Combining (A.14) and (A.15) the probabilities p_n yield

$$p_n = \left[\frac{(\lambda\,L/v_{\max})^n}{\prod_{j=1}^{n} j\left(\frac{1+N-j}{N}\right)}\right] p_0 \tag{A.16}$$

and

$$p_0^{-1} = 1 + \sum_{i=1}^{N}\left[\frac{(\lambda\,L/v_{\max})^i}{\prod_{j=1}^{i} j\left(\frac{1+N-j}{N}\right)}\right]. \tag{A.17}$$

The state probabilities p_n can be applied to calculate performance measures for the queueing system, *e.g.*, the balking probability p_N and the throughput $q = \lambda\left[1 - p_N\right]$ (see figure A.1).

In order to examine the performance of a network, each of its queues has to be studied independently by the analytical equations (A.16) and (A.17). The description of blocking, that occurs between queues, makes further model refinements necessary. It is straightforward to implement a network (or a single link as well) by simulating M/G/C/C state-dependent queues. However, as stated in [84], this takes an excessive amount of CPU time even for a single queue.
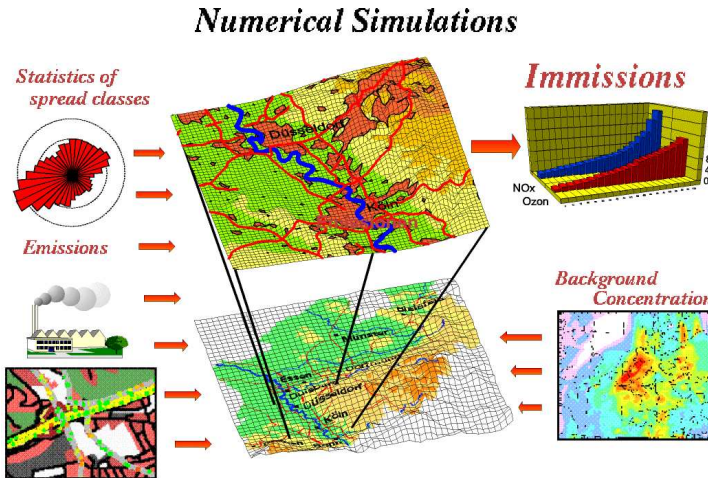
Computation of vehicular emissions

The need of air-quality management systems

Without doubt air quality can be seen to be one main indicator for the quality of life in urban areas. Although several administrative attempts were made in recent years to reduce the emission of air pollutants, the ongoing increase of energy consumption counteracts these steps. Besides industry and domestic log fire emissions, one main polluter of air is street traffic. Granted, limits for specific car emissions will be lowered due to legislation, but traffic still has an increasing impact on the environment as a result of its rapid growth in daily volumes. Politicians are forced to find solutions to this situation and, therefore, *air-quality management systems* are building up in industrial conurbation areas.

The highly variable character of traffic emissions and the fact that many of these emissions undergo chemical reaction processes during their journey through the atmosphere, inhibits an exclusively observational quantification of emissions. For that reason the effect of air pollutants can more profitably be estimated by a combination of emission inventories, models of atmospheric dynamics and air chemistry. These model systems have to integrate the information about different originators of air pollutants and treat their movement and transformation on different scales. In the Collaborative Research Center SFB419 [164] supported by the German Research Foundation (DFG) the μ_1-Queue model *resp.* FASTLANE was integrated into a model chain which is presented in figure B.1. The simulation environment was focused to gain a high spatial and temporal resolution at a local scale, *i.e.*, the area of the city of Cologne, including the possibility to work out the effects of possible reduction strategies by means of scenario computation. The presentation of results from this project are out of the scope of this work. Interested readers are referred to [49, 50, 125, 162, 165].
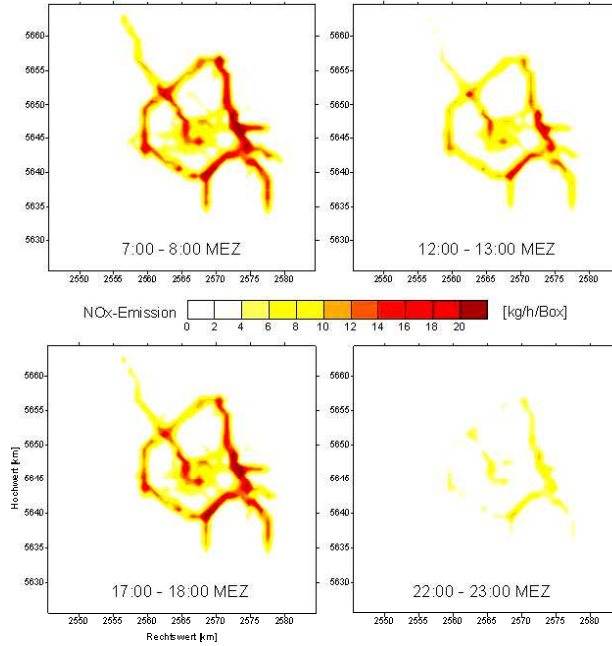
Figure B.1   Components of an air-quality management system used in [164]. Emission inventories at the local scale are calculated at high spatial and temporal resolution. In particular, vehicular emissions are calculated with the μ-Queue model.

The role of traffic flow models

As already stated above, traffic represents one of the largest sources of *primary air pollutants*. In order to achieve an appropriate description of the impact situation, emission inventories of vehicular emissions are indispensable [19, 128, 152]. For this purpose simulation models determining the effects of street traffic on air pollution are particularly valuable, since usually there are no emission measurements covering a whole urban area. The same holds for dynamic information about the traffic situation in the network. Knowing the travel demand however, either from traffic counts or from statistical methods (*e.g.*, [177] for the city of Cologne), the computation of flows through individual links of the network are possible by means of traffic assignment (*cf.* section 4.3).

It is a fact that the amount of emitted pollutants by traffic is not only dependent on mean traffic loads but strongly dependent on dynamic effects like jamming and single vehicular dynamics. In order to cover these strong temporal dependencies the models of choice have to provide such dynamic information to be able to serve as emission inventories for high resolution meteorological simulations. Microsimulation models that work on the level of individual vehicles can fulfil this requirement. For the μ-Queue model this has been demonstrated in [51] for a special traffic situation and, in more general, in section 3.3. In addition, they are suitable for scenario calculations to evaluate reduction strategies since changes in infrastructure, traffic composition and demand or route choice behaviour are

Figure B.2 Emission inventory for NOx during a typical workday around the city of Cologne [50].

effortless to build in. An example for such an emission inventory, which was computed in the SFB419, is given in figure B.2.

Mapping dynamic traffic states to vehicular emissions

The SKM and the μ-Queue model, presented in this work, simulate traffic streams and one obtains dynamical informations as the vehicle speed. Note that this observable is quantified differently in the two models. In the SKM the velocity of each car is known at each time step, whereas these are determined with respect to segments in the latter case. In order to transform the velocities into the amount of emitted pollutants, tables relating the two quantities are needed. These are called *emission factors* ef.

Used data bases

The following description of the used data base follows partially [66].

The emissions of air pollutants for single vehicles depend on the vehicle characteristics, the operation mode of the vehicle, the driving situation and the environmental conditions at a given moment. The baseline data for the determination of road vehicle emissions is generally gained by measuring the emission behaviour

of a representative vehicle in a laboratory setting by simulating specific driving conditions. These sets of measurements are usually aggregated either by estimating a functional relationship (*e.g.*, the German recommendations for economic assessment of road infrastructure investments (EWS) [56, 180]) or by clustering the data into typical driving situations (*e.g.*, the Workbook on Emission Factors for Germany and Switzerland (HBEFA) [15, 70]).

The EWS has the advantage, that the full functional relationship on the vehicle's velocity v is given for a specific vehicle type veh and pollutant pol,

$$\mathrm{ef}_{\mathrm{pol,veh}}(v) = \begin{cases} (c_0 + c_1 v^2 + c_2/v) & \text{for } v > 20 km/h \\ \min\{c_s, (c_0 + c_1 v^2 + c_2/v)\} & \text{for } v \leq 20 km/h, \end{cases} \qquad \text{(B.1)}$$
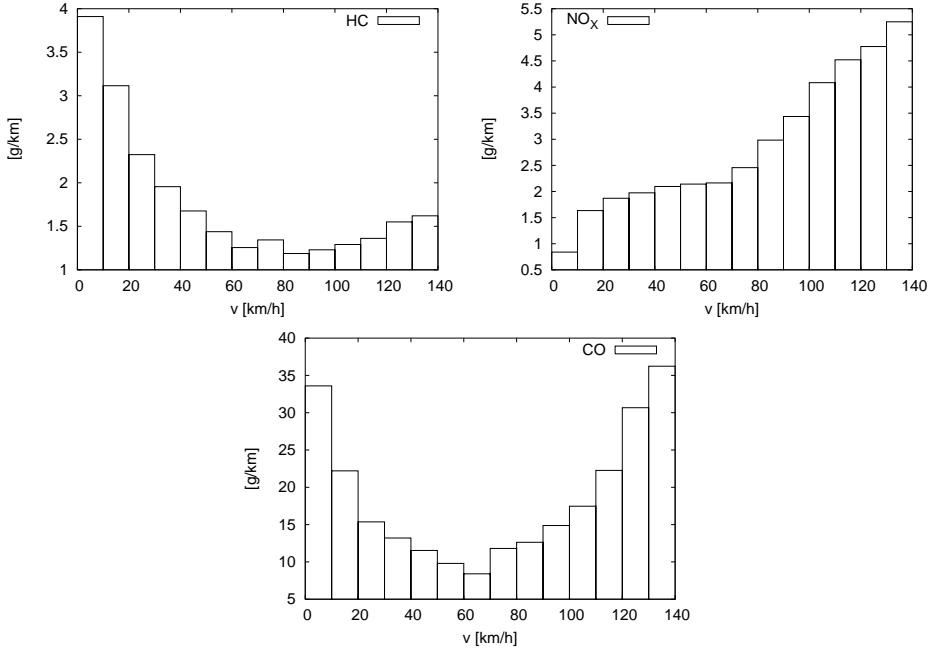
with parameters c_0, c_1 and c_2 for free flow and parameter c_s for stop-and-go traffic. The units of ef are $[g/(km\,veh)]$. These parameters are differentiated by vehicle type and pollutant. A reduction factor is applied for each pollutant in order to take account of advanced pollution reduction technologies. The total emission of a specific pollutant is computed by summation over all vehicles and network sections. However, with respect to simulations which are based on individual trips, one has to know the vehicle types.

If the latter information is not known or modelled explicitly, the HBEFA provides a useful database. The emission factors are given for specific traffic situations, and an aggregation is provided which takes into account the composition of the vehicle fleet with respect to a certain year. Moreover, if more information on the fleet are available, the emission factors can be used on the level of emission concepts or vehicle types (similar to the EWS). The emission factors are provided for the warm operation mode, and additional surcharges due to temperature, cold start and volatility emissions can be considered. With respect to scenario simulations, it is of special interest that the development of the vehicle fleet is forecasted until 2020.

The emission factors used in this work are based on the HBEFA. In the data base, the emission factors are given for traffic situations which are characterised by a mean speed (beside other dependencies). In order to obtain an effortless mapping between the velocity and the amount of emission, the different traffic situations are aggregated into bins of size $10\,km/h$. Figure B.3 shows the emission factors of three different pollutants, namely, hydrocarbons (HC), nitrogen oxides (NOx) and carbon monoxide (CO). One can clearly see that the functional behaviour is rather different for the distinct pollutants, and their amount strongly depends on velocity.

Implementation aspects

The transformation of velocities into emissions is straightforward in the SKM. At each time step, the current velocity of each vehicle is known. By multiplication

Figure B.3 Emission factors for different kind of pollutants as discrete function of velocity. As one can see, the amount of emission is strongly dependent on the vehicle's velocity. Moreover, the functional shape is rather different for each pollutant.

of the velocity with the corresponding emission factor, one obtains the amount of emission per time step. All one has to do, is to sum up the contributions of all cars.

In the μ-Queue model, a slightly different procedure has to be used, because velocities are only known per sampling interval and segment. In order to determine the emission factor, the mean velocity during a sampling interval according to equation (3.28) is used. To account for the fact that cars may stay in a segment for several sampling intervals, the entry and exit time for each car is additionally sampled. The total duration of a stay in a segment is then distributed to the corresponding sampling intervals. The total emission per sampling interval inside a segment is then given by the sum of all these contributions multiplied with the corresponding emission factor.

The above procedure is appropriate, if all vehicles are treated as representing the vehicle fleet. In the case, where distinct vehicle types are used, it is, furthermore, necessary to sample the mean velocity of each vehicle type. In that case, equation (3.27) is evaluated separately for each vehicle type.

Event-driven update scheme

The following program shows the event-driven update scheme as used for the μ-Queue model. The code has been simplified, but contains all methods necessary to understand the principle procedure. The declaration of public methods is omitted. The implementation is a one-lane system with periodic boundary conditions. The system is initialised with one compact jam.

```
typedef unsigned int uint;
typedef double real;
enum State {Free,Jam,Full};
const real segment_length = 98.0;  // [m]
const real segment_speed  = 19.6;  // [m/s]
const real segment_tauff  = 1.4;   // [s]
const real segment_taufj  = 1.4;   // [s]
const real segment_taujf  = 2.0;   // [s]
const real segment_taujj  = 2.0;   // [s]
const uint segment_njam   = 4;     //
const real car_length     = 7.0;   // [m]

template<class T>
T max(T& t1, T& t2)
{
  if (t1 > t2)
    return t1;
  return t2;
};
class CarComp{
public:
  bool operator() (Car* c1, Car* c2){
    return (c1->get_tEvent()>c2->get_tEvent());
  };
};

/*********************************************/
```

```cpp
class Car{
  real get_tEvent()                 {return tEvent;};
  uint get_id()                     {return id;};
  Segment* at_segment()             {return seg;};
  void update_tEvent(real t)        {tEvent = t;};
  void update_segment(Segment* s) {seg=s;};
private:
  uint id;         // car ID
  Segment* seg;    // car at segment
  real tEvent;     // next event
};

Car::Car(uint _id, Segment* _seg, real _tEv)
  : id(_id), seg(_seg), tEvent(_tEv){};

/***********************************************/

class Segment{
public:
  State get_state()    {return state;}
  uint  get_index()    {return index;}
  void  set_tb(real t){t_block = t;};
private:
  vector<Car*> cars;
  State         state;
  real          length, speed, tau_ff, tau_fj, tau_jf, tau_jj;
  uint          n_jam, capacity, index;
  real          t_block;
};

Segment::Segment(real _l,real _v, real _tff, real _tfj,
                 real _tjf, real _tjj, uint _njam, uint _index)
  : length(_l), speed(_v), tau_ff(_tff), tau_fj(_tfj),
    tau_jf(_tjf), tau_jj(_tjj), n_jam(_njam), index(_index)
{  state = Free;
   capacity = static_cast<uint>(_l/car_length);
   t_block   = -1.0; };

inline bool
Segment::initialise(Car* c, real pos)
{
  if (cars.size() < capacity){
    real trt = (length-pos)/speed;
    c->update_tEvent(trt);
    cars.push_back(c);
    if (cars.size() < n_jam)
      state = Free;
    else if (cars.size() < capacity)
      state = Jam;
```

```
    else
      state = Full;
    return true;
  }
  return false;
}

inline Car*
Segment::send(Car* tc,Segment* next,real time)
{
  if (time < t_block){
    tc->update_tEvent(t_block);
    return tc;
  }
  cars.pop_back();
  if (cars.empty()){
    state = Free;
    t_block = max(time + tau_ff,t_block);
    return NULL;
  }
  Car* lc = cars.back();
  real tb = next->get_timeheadway(state);
  t_block = max(t_block,time+tb);
  lc->update_tEvent(max(lc->get_tEvent(),t_block));
  if (cars.size() < n_jam)
    state = Free;
  else
    state = Jam;
  return lc;
};

inline Car*
Segment::receive(Car* tc, real time)
{
  if (cars.empty()){
    state = Free;
    if (n_jam <= 1)
      state = Jam;
    real tleave = max(time+length/speed,t_block);
    t_block = tleave;
    tc->update_tEvent(tleave);
    tc->update_segment(this);
    cars.push_back(tc);
    return tc;
  }
  else{
    real tleave = time+length/speed;
    tleave = max(cars[0]->get_tEvent()+tau_ff,tleave);
    tc->update_tEvent(tleave);
```

```cpp
    tc->update_segment(this);
    cars.insert(cars.begin(),tc);
    if (cars.size() < n_jam){
      state = Free;
    }
    else if (cars.size() < capacity){
      state = Jam;
    }
    else{
      state = Full;
    }
    return NULL;
  }
}

inline real
Segment::get_timeheadway(State predState)
{
  if (predState != Free){
    if (state == Free){
      return tau_jf;
    }
    else{
      real m = tau_jj;
      real b = capacity * (tau_jf-m);
      real zw = m * cars.size() + b;
      return zw;
    }
  }
  else{
    if (state == Free){
      return tau_ff;
    }
    else{
      return tau_fj;
    }
  }
};

inline Car*
Segment::first_car()
{
  if (cars.size() == 0)
    return NULL;
  uint lix = cars.size()-1;
  return cars[lix];
}

/***********************************************/
```

```
class Loop
{
private:
  vector<Segment*> segment;
  Loop* from;
  Loop* to;
  priority_queue<Car*,std::vector<Car*>,CarComp> cars;
};

Loop::Loop(uint _seg)
{
  for (uint s=0; s<_seg;s++){
    Segment* new_segment =
            new Segment(segment_length,segment_speed,
                        segment_tauff,segment_taufj,
                        segment_taujf,segment_taujj,
                        segment_njam,s);
    segment.push_back(new_segment);
  }
  from = this;
  to   = this;
};

inline uint
Loop::initialise(uint nCars)
{
  real x = -car_length;
  for (uint c = 0; c < nCars; c++){
    x += car_length;
    uint s = static_cast<uint>(x/segment_length);
    real xi = x-s*segment_length;
    Car* nc = new Car(c,segment[s],0);
    segment[s]->initialise(nc,xi);
  }
  for (uint s = 0; s < segment.size(); s++){
    Car* nc = segment[s]->first_car();
    if (nc){
      cars.push(nc);
    }
  }
  return nCars;
};

inline real
Loop::simulate(real tMax)
{
  Car* tz = cars.top();
  real time = tz->get_tEvent();
```

```
  vector<Car*> process;
  while (time < tMax){
    while((cars.size() > 0) &&
          (cars.top()->get_tEvent() <= time)){
      process.push_back(cars.top());
      cars.pop();
    }
    real next_to_leave = cars.top()->get_tEvent();
    for (uint i = 0; i < process.size(); i++){
      Segment* on_segment = process[i]->at_segment();
      Segment* to_segment = next_segment(on_segment);
      if (to_segment->get_state() != Full){
        Car* insert_car = on_segment->send(process[i],
                                           to_segment,
                                           time);
        if (insert_car){
          cars.push(insert_car);
        }
        if (insert_car != process[i]){
          insert_car = to_segment->receive(process[i],time);
          if (insert_car){
            cars.push(insert_car);
          }
        }
      }
      else{
        process[i]->update_tEvent(next_to_leave);
        cars.push(process[i]);
      }
    }
    process.clear();
    time = cars.top()->get_tEvent();
  }
  return time;
};

inline Segment*
Loop::next_segment(Segment* s)
{
  uint on_index = s->get_index();
  if (on_index < (segment.size()-1)){
    on_index++;
    return segment[on_index];
  }
  else{
    return to->first_segment();
  }
};
```

```
inline Segment*
Loop::first_segment()
{
  return segment[0];
};

/*********************************************/

int main()
{
  uint maxNoCar = 600;
  uint maxNoSeg = 100;
  real maxTime  = 50000.0;
  Loop simulation(maxNoSeg);
  simulation.initialise(maxNoCar);
  real tstart = simulation.simulate(maxTime);
  return 0;
}
```

Implementation of Erlangian distribution

Thanks to Peter Wagner.

```
real erlang(real a, int m) {
  real x = 1.0;
  real r = 0.0;
  for (int k=1; k<=m; k++){
    r = 0.0;
    while ((r==0.0) || (r==1.0))
      r = drand48();
    x *= r;
  }
  return (-a*((real) log(x))/(1.0*m));
}
```

Glossary of Notation

Bibliography

[1] R. Ahuja, T. Magnanti, and J. Orlin. *Network Flows*. Prentice Hall, Englewood Cliffs, New Jersey, 1993.

[2] T. Akamatsu. An efficient algorithm for dynamic traffic assignment with queues. *Tranportation Science* **35**(4):389–404, 2001.

[3] H. Al-Deek, A. Khattak, and P. Thananjeyan. A combined traveler behavior and system performance model with advanced traveler information systems. *Transportation Research A* **32**(7):479–493, 1998.

[4] T. Antal and G. Schütz. Asymmetric exclusion process with next-nearest-neighbor interaction: Some comments on traffic flow and a nonequilibrium reentrance transition. *Phys. Rev. E* **62**(1):83–93, 2000.

[5] C. Appert and L. Santen. Boundary induced phase transitions in driven lattice gas with metastable states. *Phys. Rev. Letters* **86**(12):2498–2501, 2001.

[6] R. Arnott, A. Palma, and R. Lindsey. Does providing information to drivers reduce traffic congestion? *Transportation Research A* **25A**(5):309–318, 1991.

[7] K. Ashok. *Estimation and prediction of time-dependent origin-destination flows*. PhD thesis, Massachusetts Institute of Technology, 1996.

[8] V. Astarita, K. Er-Rafia, M. Florian, M. Mahut, and S. Velan. A comparison of three methods for dynamic network loading. *Transportation Research Records* **1771**:179–190, 2001.

[9] M. Bando, K. Hasebe, K. Nakanishi, and A. Nakayama. Analysis of optimal velocity model with explicit delay. *Phys. Rev. E* **58**:5429–5435, 1998.

[10] M. Bando, K. Hasebe, A. Nakayama, A. Shibata, and Y. Sugiyama. Structure stability of congestion in traffic dynamics. *Japan Journal of Industrial and Applied Mathematics* **11**(2):203–223, 1994.

[11] M. Bando, K. Hasebe, A. Nakayama, A. Shibata, and Y. Sugiyama. Dynamical model of traffic congestion and numerical simulation. *Phys. Rev. E* **51**:1035–1042, 1995.

[12] J. Barceló and J. Casas. Heuristic dynamic assignment based on microscopic traffic simulation. In *9th Meeting of the Euro Working Group on Transportation, Bari, Italy*, June 2002. See www.aimsun.com/documents.html.

[13] R. Barlovic, T. Huisinga, A. Schadschneider, and M. Schreckenberg. Open boundaries in a cellular automaton model for traffic flow with metastable states. *Phys. Rev. E* **66**(046113), 2002.

[14] R. Barlovic, L. Santen, A. Schadschneider, and M. Schreckenberg. Metastable states in cellular automata for traffic flow. *European Physical Journal B* **5**:793, 1998.

[15] U. Becker and F. Richter. Die neuen Emissionsfaktoren für den Straßenverkehr: Was können Sie damit tun und was dürfen Sie damit keinesfalls tun? *Straßenverkehrstechnik* :578–585, 11/1998.

[16] K. Beckmann and G. Rindsfüser. Dynamic estimation of transportation demand: Solutions - Requirements - Problems. In W. Brilon and et.al, editors, *Traffic and Mobility - Simulation, Economics and Environment*, pages 15–34. Springer, 1999.

[17] M. Beckmann, C. McGuire, and C. Winsten. *Studies in the economics of transportation*. Yale University Press, New Haven, 1956.

[18] R. Bertini and M. Cassidy. Some observed queue discharge features at a freeway bottleneck downstream of a merge. *Transportation Research A* **36**(8):683–697, 2002.

[19] C. Borrego, O. Tchepel, N. Barros, and A. Miranda. Impact of road traffic emissions on the air quality of the Lisbon region. *Atmospheric Environment* **34**(27):4683–4690, 34.

[20] M. Brackstone and M. McDonald. The microscopic modelling of traffic flow: Weaknesses and potential developments. In D. W. et al., editor, *Traffic and Granular Flow*, pages 151–165. World Scientific, 1996.

[21] M. Brackstone and M. McDonald. Car-following: a historical review. *Transportation Research F* **2**:181–196, 1999.

[22] E. Brockfeld, R. D. Kühne, P. Wagner, and A. Skabardonis. Towards a benchmarking of microscopic traffic flow models. In *Proceedings of TRB 2003 Annual Meeting (CD-ROM)*, 2003. to be published in Transportation Research Records 2003.

[23] M. Carey and E. Subrahmanian. An approach to modelling time-varying flows on congested networks. *Transportation Research B* **34**:157–183, 2000.

[24] M. Cassidy. Bivariate relations in nearly stationary highway traffic. *Transportation Research B* **32**:49–59, 1998.

[25] M. Cassidy and R. Bertini. Some traffic features at freeway bottlenecks. *Transportation Research B* **33**:25–42, 1999.

[26] M. Cassidy and J. Windover. Methodology for assessing dynamics of freeway traffic flow. *Transportation Research Records* **1484**:73–79, 1995.

[27] N. Cetin and K. Nagel. Parallel queue model approach to traffic microsimulations. In *Proc. of Swiss Transportation Research Conference*, 2002.

[28] R. Chandler, R. Herman, and E. Montroll. Traffic dynamics: Studies in car following. *Operations Research* **6**:165–184, 1958.

[29] G. Chang and Y. Kao. An empirical investigation of macroscopic lane-changing characteristics on uncongested multilane freeways. *Transportation Research A* **25**:375–389, 1991.

[30] J. Cheah and J. Smith. Generalized M/G/C/C state dependent queueing models and pedestrian traffic flow. *Queueing Systems* **15**:365–386, 1994.

[31] S. Cheybani, J. Kertesz, and M. Schreckenberg. Nondeterministic Nagel-Schreckenberg traffic model with open boundary conditions. *Phys. Rev. E* **63**:016108, 2001.

[32] S. Cheybani, J. Kertesz, and M. Schreckenberg. Stochastic boundary conditions in the deterministic Nagel-Schreckenberg traffic model. *Phys. Rev. E* **63**:016107, 2001.

[33] D. Chowdhury, L. Santen, and A. Schadschneider. Statistical physics of vehicular traffic and some related systems. *Physics Reports* **329**(4-6):199–329, 2000.

[34] B. Coifman. Improved velocity estimation using single loop detectors. *Transportation Research A* **35**(10):863–880, 2001.

[35] C. Daganzo. The cell transmission model: A dynamic representation of highway traffic consistent with the hydrodynamic theory. *Transportation Research B* **28**(4):269–287, 1994.

[36] C. Daganzo. The cell transmission model, Part II: Network traffic. *Transportation Research B* **29B**(79-93), 1995.

[37] C. Daganzo. Queue spillovers in transportation networks with a route choice. *Transportation Science* **32**(1):3–11, 1998.

[38] C. Daganzo. The lagged cell transmission model. In *Proc. of 14th ISTTT Symposium*, pages 81–106, 1999.

[39] C. Daganzo. Remarks on traffic flow modeling and its applications. In W. Brilon and et.al, editors, *Traffic and Mobility - Simulation, Economics and Environment*, pages 105–116. Springer, 1999.

[40] C. Daganzo. A behavioral theory of multi-lane traffic flow: Part I: Long homogeneous freeway sections, Part II: Merges and the onset of congestion. *Transportation Research B* **36**:131–169, 2002.

[41] C. Daganzo, M. Cassidy, and R. Bertini. Possible explanations of phase transitions in highway traffic. *Transportation Research A* **33**:365–379, 1999.

[42] D. Dailey. Travel-time estimation using cross-correlation techniques. *Transportation Research B* **27**(2):97–107, 1993.

[43] D. Dailey. A statistical algorithm for estimating speed from singe loop volume and occupancy measurements. *Transportation Research B* **33**:313–322, 1999.

[44] K. Davidson. A flow-travel time relationship for use in transportation planing. In *Proceedings of the Australian Road Research Board*, volume 3, pages 183–194, 1966.

[45] B. Derrida, M. Evans, V. Hakim, and V. Pasquier. Exact solution of a 1D asymmetric exclusion model using a matrix formulation. *J. Phys. A* **26**(7):1493–1517, 1993.

[46] E. Dijkstra. A note on two problems in connection with graphs. *Numerical Mathematics* **1**:269–271, 1959.

[47] DYNASMART. See www.dynasmart.com.

[48] N. Eissfeldt. Kürzeste vs. schnellste Wege in digitalen Straßenkarten. Diplomarbeit, Fernuniversität Hagen, 2003.

[49] N. Eissfeldt, M. Luberichs, and F.-N. Sentuc. Investigating emissions of traffic by simulation. In E. Kerckhoffs and M. Snorek, editors, *Proceedings of ESM 2001, Modelling and Simulation*, pages 961–965. Society for Computer Simulation International, 2001.

[50] N. Eissfeldt, M. Luberichs, and F.-N. Sentuc. A breath of fresh air. *Traffic Technology International* :76–80, Aug/Sep 2002.

[51] N. Eissfeldt and R. Schrader. Calculation of street traffic emissions with a queueing model. *Journal of Computational Technologies* **7**:5–15, 2002.

[52] N. Eissfeldt and P. Wagner. Effects of anticipatory driving in a traffic flow model. *European Physical Journal B* **33**:121–129, 2003.

[53] M. Evans, N. Rajewsky, and E. Speer. Exact solution of a cellular automaton for traffic. *Journal of Statistical Physics* **95**(1/2):45–96, 1999.

[54] M. Fellendorf and P. Vortisch. Integrated modeling of transportation demand, route choice, traffic flow and traffic emissions. In *Proceedings of TRB 2000 Annual Meeting (CD-ROM), Washington*, 2000.

[55] T. Fliessbach. *Statistische Physik*. Spektrum, Akademischer Verlag, 1995.

[56] Forschungsgesellschaft für Straßen- und Verkehrswesen, Empfehlungen für Wirschaftlichkeitsuntersuchungen an Straßen. Aktualisierung der RAS-W 86,Köln, 1997.

[57] M. Frank and P. Wolfe. An algorithm for quadratic programming. *Naval Research Logistics Quarterly* **3**:95–110, 1956.

[58] M. Friedrich, I. Hofsäß, and et. al. Umlegung zeitlich differenzierter Nachfragematrizen. In *Berichte des Institus für Stadtbauwesen der RWTH Aachen, Band 69*, pages 99–107, 2000.

[59] C. Gawron. An iterative algorithm to determine the dynamic user equilibrium in a traffic simulation model. *Int. Jrn. Mod. Phys. C.* **9**(3):393–407, 1998.

[60] C. Gawron. Simulation-based traffic assignment. Dissertation, Universität zu Köln, 1998. See www.zaik.uni-koeln.de/~paper.

[61] J. Gier and B. Nienhuis. Exact stationary state for an asymmetric exclusion process with fully parallel dynamics. *Phys. Rev. E* **59**(5):4899–4911, 1999.

[62] P. Gipps. A behavioural car following model for computer simulation. *Transportation Research B* **15**:105–111, 1981.

[63] P. Gipps. A model for the structure of lane-changing decisions. *Transportation Research B* **20**(5):403–414, 1986.

[64] H. Greenberg and A. Daou. The control of traffic flow to increase the flow. *Operations Research* **8**:524–533, 1960.

[65] D. Gross and C. Harris. *Fundamentals of Queueing Theory*. John Wiley & Sons, New York, 3 edition, 1998.

[66] A. Gühnemann, P. Wagner, and N. Eissfeldt. Intelligent transport management by integrated dynamic traffic simulation and impact assessment. In *Selected Proceedings from the 9th World Conference on Transport Research (CD-ROM)*. 9th World Conference on Transport Research (WCTR), Seoul, 2001, Pergamon, 2003.

[67] J. Hager, J. Krug, V. Popkov, and G. Schütz. Minimal current phase and universal boundary layers in driven diffusive systems. *Phys. Rev. E* **63**:056110, 2001.

[68] F. Hall and T. Lam. The characteristics of congested flow on a freeway across lanes, space and time. *Transportation Research A* **22**:45–56, 1988.

[69] S. Hasselberg. Some results on heuristical algorithms for shortest path problems in large road networks. Dissertation, Universität zu Köln, 2000. See www.zaik.uni-koeln.de/~paper.

[70] Handbuch Emissionsfaktoren des Straßenverkehrs. Version 1.2, on behalf of the Swiss ministry of environment, forestry and agriculture Bern and the German envirionmental agency Berlin, in German, 1999.

[71] D. Heidemann. A queueing theory approach to speed-flow-density relationships. In J.-B. Lesort, editor, *Transportation and Traffic Theory - Proceedings of the 13th International Symposium on Transportation and Traffic Theory*, pages 103–118. Elsevier Science, 1996.

[72] D. Heidemann. A queueing theory model of nonstationary traffic flow. *Transportation Science* **35**(4):405–412, 2001.

[73] D. Helbing. *Verkehrsdynamik*. Springer, 1997.

[74] D. Helbing. Traffic and related self-driven many-particle systems. *Review of Modern Physics* **73**(4):1067–1141, 2001.

[75] D. Helbing. A section-based queueing-theoretical traffic model for congestion and travel time analysis. *Physics A* **36**:L593–598, 2003.

[76] D. Helbing, A. Hennecke, and M. Treiber. Phase diagram of traffic states in the presence of inhomogeneities. *Phys. Rev. Lett.* **82**(21):4360–4363, 1999.

[77] D. Helbing and M. Treiber. Gas-kinetic-based traffic model explaining observed hysteretic phase transition. *Phys. Rev. Lett.* **81**:3042–3045, 1998.

[78] A. Hennig. Sensitivitätsstudien zur Erstellung von Schadstoffklimatologien. Diplomarbeit, Universität zu Köln, 2002.

[79] R. Herman and K. Gardels. Vehicular traffic flow. *Scientific American* **6**:35–43, 1963.

[80] P. Hidas. Modelling lane changing and merging in microscopic traffic simulation. *Transportation Research C* **10**:351–371, 2002.

[81] D. Huang. Stochastic exclusion processes with extended hopping. *Phys. Rev. E* **64**:036108, 2001.

[82] ILUMASS - Integrated Land-Use Modelling and Transportation System Simulation. See www.ilumass.de.

[83] R. Jacob, M. Marathe, and K. Nagel. A computational study of routing algorithms for realistic transportation networks. *ACM Journal of Experimental Algorithms* **4**, 1998. Article No.6.

[84] R. Jain and J. Smith. Modeling vehicular traffic flow using M/G/C/C state dependent queueing models. *Transportation Science* **31**(4):324–336, 1997.

[85] S. Janz. Mikroskopische Minimalmodelle des Straßenverkehrs. Diplomarbeit, Universität zu Köln, 1998.

[86] R. Jiang and Q. Wu. Cellular automata models for synchronized traffic flow. *Journal of Physics A* **36**:381–390, 2003.

[87] D. Kaufman, J. Nonis, and R. Smith. A mixed integer linear programming model for dynamic route guidance. *Transportation Research B* **32**(6):431–440, 1998.

[88] C. Kayatz. Stability analysis of traffic flow models. Master's thesis, ETH Zürich, 2001.

[89] T. Kelly and K. Nagel. Relaxation criteria for iterated traffic simulations. *Int. Jrn. Mod. Phys. C.* **9**(1):113–132, 1998.

[90] B. Kerner. Experimental features of self-organization in traffic flow. *Phys. Rev. Lett.* **81**:3797–3800, 1998.

[91] B. Kerner. The physics of traffic. *Phys. World 8/99* :25–30, 1999.

[92] B. Kerner. Complexity of synchronized flow and related problems for basic assumptions of traffic flow theories. *Networks and Spatial Economics* **1**:35–76, 2001.

[93] B. Kerner. Empirical macroscopic features of spatio-temporal traffic patterns at highway bottlenecks. *Phys. Rev. E* **65**:046138, 2002.

[94] B. Kerner, H. R. an M. Aleksic, and A. Huang. Verfolgung und Vorhersage von Verkehrsstörungen auf Autobahnen mit 'ASDA' und 'FOTO' im online-Betrieb in der Verkehrsrechnerleitzentrale Rüsselsheim. *Straßenverkehrstechnik* **10**, 2000.

[95] B. Kerner, H. R. an M. Aleksic, A. Huang, and R. Lange. Online automatic tracing and forecasting of traffic patterns. *Traffic Engineering and Control* **42**:345–350, 2001.

[96] B. Kerner and S. Klenov. Cellular automata approach to three-phase traffic theory. *J. Phys. A* **35**:9971–10013, 2002.

[97] B. Kerner and P. Konhäuser. Cluster effect in initially homogeneous traffic flow. *Phys. Rev. E* **48**:R2335–R2338, 1993.

[98] B. Kerner and P. Konhäuser. Structure and parameters of clusters in traffic flow. *Phys. Rev. E* **50**(1):54–83, 1994.

[99] B. Kerner and H. Rehborn. Experimental features and characteristics of traffic jams. *Phys. Rev. E* **53**:R1297–R1300, 1996.

[100] B. Kerner and H. Rehborn. Experimental properties of complexity in traffic flow. *Phys. Rev. E* **53**:R4275–R4278, 1996.

[101] B. Kerner and H. Rehborn. Experimental properties of phase transitions in traffic flow. *Phys. Rev. Lett.* **79**(20):4030–4033, 1997.

[102] M. Kleinhans. Klassifikation von Verkehrsdaten mit Clusterverfahren. Diplomarbeit, Universität zu Köln, 2002.

[103] W. Knospe. Synchronized traffic - Microscopic modeling and empirical observations. Dissertation, Universität Duisburg, 2002.

[104] W. Knospe, L. Santen, A. Schadschneider, and M. Schreckenberg. Towards a realistic microscopic description of highway traffic. *J. Phys. A* **33**:L477–485, 2000.

[105] W. Knospe, L. Santen, A. Schadschneider, and M. Schreckenberg. Human behavior as origin of traffic phases. *Phys. Rev. E* **65**:015101(R), 2002.

[106] W. Knospe, L. Santen, A. Schadschneider, and M. Schreckenberg. CA-models for traffic flow: How do they reproduce the reality. to be submitted, 2002.

[107] W. Knospe, L. Santen, A. Schadschneider, and M. Schreckenberg. A realistic two-lane traffic model for highway traffic. *Journal of Physics A* **35**:3369–3388, 2002.

[108] W. Knospe, L. Santen, A. Schadschneider, and M. Schreckenberg. Single-vehicle data of highway traffic: Microscopic description of traffic phases. *Phys. Rev. E* **65**(056133), 2002.

[109] A. Kolomeisky, G. Schütz, E. Kolomeisky, and J. Straley. Phase diagram of one-dimensional driven lattice gases with open boudaries. *J. Phys. A* **31**:6911–6919, 1998.

[110] M. Koshi, M. Iwasaki, and I. Ohkura. Some findings and an overview of vehicular flow characteristics. In *Proceedings of the 8th International Symposium on Transportation and Traffic Theory*, pages 403–426. Elsevier,Amsterdam,Toronto, 1983.

[111] H. Koutsopoulos and M. Habbal. Effect of intersection delay modeling on the performance of traffic equilibrium models. *Transportation Research A* **28A**(2):133–149, 1994.

[112] S. Krauß. Towards a unified view of microscopic traffic flow theories. In M. Papageorgiou and A. Pouliezos, editors, *IFAC Transportation Systems 1997*, volume 2, pages 941–946, 1997.

[113] S. Krauß. Microscopic modeling of traffic flow: Investigation of collision free vehicle dynamics. Dissertation, Universität zu Köln, 1998. See www.zaik.uni-koeln.de/~paper.

[114] S. Krauß, P. Wagner, and C. Gawron. Continuous limit of the Nagel-Schreckenberg model. *Phys. Rev. E* **54**:3707–3712, 1996.

[115] S. Krauß, P. Wagner, and C. Gawron. Metastable states in a microscopic model of traffic flow. *Phys. Rev. E* **55**:5597–5602, 1997.

[116] J. Krug. Boundary-induced phase transitions in driven diffusive systems. *Phys. Rev. Lett.* **67**:1882–1885, 1991.

[117] C.-J. Lan and G. Davies. Empirical assessment of a Markovian traffic flow model. *Transportation Research Records* **1591**:31–37, 1997.

[118] C.-J. Lan and G. Davis. Real-time estimation of turning movement proportions from partial counts on urban networks. *Transportation Research C* **7**:305–327, 1999.

[119] M. Larraga, J. del Rio, and A. Schadschneider. New kind of phase separation in a CA model with anticipation. *J. Phys. A* , 2004. in press.

[120] R. Larson and A. Odoni. Urban Operations Research. See web.mit.edu/urban_or_book/www/book/.

[121] W. Leutzbach. *Introduction to the Theory of Traffic Flow*. Springer, 1988.

[122] W. Leutzbach and F. Busch. Spurwechselvorgänge auf dreispurigen BAB-Richtungsfahrbahnen. Technical report, FA. 1.082G81H des BMV, Karlsruhe, 1984.

[123] M. Lighthill and J. Whitham. On kinematic waves. I. Flow movements in long rivers. II. A theory of traffic flow on long crowded roads. *Proc. Royal. Soc. A* **229**:281–345, 1955.

[124] W. Lin and H. Lo. A theoretical probe of a German experiment on stationary moving traffic jams. *Transportation Research B* **37**:251–261, 2003.

[125] M. Luberichs, F.-N. Sentuc, N. Eissfeldt, and et. al. Modelling urban air pollution based on dynamic traffic simulation. In W. Dabbert, editor, *Transport and Air Pollution*, page 8 pp. NCAR, Boulder, Colorado, 2001.

[126] M. Mahut. *Discrete flow model for dynamic network loading*. PhD thesis, Université de Montréal, 2000.

[127] M. Mahut, M. Florian, and N. Tremblay. Space-time queues and dynamic traffic assignment: A model, algorithm and applications. In *TRB* 82nd *Annual Meeting Compendium of Papers (CD-ROM)*, 2003.

[128] C. Mensink, I. de Vlieger, and J. Nys. An urban transport emission model for the Antwerp area. *Atmospheric Environment* **34**(27):4595–4602, 2000.

[129] P. Michalopoulos and Y. Yamauchi. Multilane traffic flow dynamcis: Some macroscopic considerations. *Transportation Research B* **18**(4/5):377–395, 1984.

[130] J. Munoz and C. Daganzo. Fingerprinting traffic from static freeway sensors. See www.ce.berkeley.edu/Programs/Transportation/Daganzo/ Article_Intellimotion2000.pdf, 2002.

[131] K. Nagel, C. Kayatz, and P. Wagner. Breakdown and recovery in traffic flow models. In Y. S. et al., editor, *Traffic and Granular Flow 2001*, pages 141–153. Springer,Heidelberg, 2001.

[132] K. Nagel, M. Rickert, P. Simon, and M. Pieck. The dynamics of iterated transportation simulations. Technical report, LA-UR 98-2168, 1998. See http://transims.tsasa/lanl.gov.

[133] K. Nagel and M. Schreckenberg. A cellular automaton model for traffic flow. *J. Physique* **2**:2221–2229, 1992.

[134] K. Nagel, P. Wagner, and R. Woesler. Still flowing: Old and new approaches to traffic flow and traffic jam modelling. *Operations Research* **51**(5), 2003.

[135] K. Nagel, D. Wolf, P. Wagner, and P. Simon. Two-lane traffic rules for cellular automata: A systematic approach. *Phys. Rev. E* **58**(2):1425–1437, 1998.

[136] D. Nam and D. Drew. Automatic measurements of traffic variables for intelligent transportation systems applications. *Transportation Research B* **33**:437–457, 1999.

[137] A. Namazi. Boundary induced phase transitions in a traffic flow model with metastable states. Diplomarbeit, Universität zu Köln, 2001.

[138] A. Namazi, N. Eissfeldt, P. Wagner, and A. Schadschneider. Boundary-induced phase transitions in a space-continuous traffic model with non-unique flow-density relation. *European Physical Journal B* **30**:559–570, 2002.

[139] J. Nelder and R. Mead. A simplex method for function minimisation. *Computer Journal* **7**:308–313, 1965.

[140] L. Neubert, L. Santen, A. Schadschneider, and M. Schreckenberg. Single-vehicle data of highway traffic: A statistical analysis. *Phys. Rev. E* **60**(6):6480–6490, 1999.

[141] G. Newell. A simplified theory of kinematic waves in highway traffic. Part I: General theory. Part II: Queueing at freeway bottlenecks. Part III: Multidestination flows. *Transportation Research B* **27**(4):281–313, 1993.

[142] G. Newell. A moving bottleneck. *Transportation Research B* **32**:531–538, 1998.

[143] Y. Nie, M. Zhang, and L. Der-Horng. Models and algorithms for the traffic assignment problem with link capacity constraints. *Transportation Research B* **38**(4):285–312, 2004.

[144] S. Pallottino and M. Scutella. Shortest-path algorithms in transportation models: classical and innovative aspects. In P. Marcotte and S. Nguyen, editors, *Equilibrium and advanced transportation modelling*, pages 245–281. Kluwer Academic Press, 1998.

[145] K. Petty, P. Bickel, J. Jiang, and et.al. Accurate estimation of travel times from single-loop detectors. *Transportation Research A* **32**(1):1–17, 1998.

[146] L. Pipes. An operational analysis of traffic dynamics. *J. Appl. Phys.* **24**(3):274–281, 1953.

[147] V. Popkov, L. Santen, A. Schadschneider, and G. Schütz. Empirical evidence for a boundary-induced phase transition. *J. Phys. A* **34**:L45–L52, 2001.

[148] V. Popkov and G. Schütz. Steady-state selection in driven diffusive systems with open boundaries. *Europhys. Lett.* **48**(3):257–263, 1999.

[149] W. Press, S. Teukolsky, W. Vetterling, and B. Flannery. *Numerical Recipes in C*. Cambridge University Press, 1992. chapter 10.

[150] N. Rajewsky, L. Santen, A. Schadschneider, and M. Schreckenberg. The asymmetric exclusion process: Comparison of update procedures. *J. Stat. Phys.* **92**(1/2):151–194, 1998.

[151] B. Ran and D. Boyce. *Modeling Dynamic Transportation Networks*. Springer, 2nd edition edition, 1996.

[152] A. Reynolds and B. Broderick. Development of an emission inventory model for mobile sources. *Transportation Research D* **5**:77–101, 2000.

[153] P. Richards. Shockwaves on the highway. *Opns. Res.* **4**:42–51, 1956.

[154] S. Rosswog, C. Gawron, S. Hasselberg, R. Böning, and P. Wagner. Computational aspects in traffic simulation problems. *Future Generation Computer Systems* **17**(5):659–665, 2000.

[155] S. Ruhren and H. Mühlhans. Zeitlich feinteilige Verkehrsnachfrageermittlung im Rahmen einer netzweiten Kurzfristprognose von Verkehrszuständen. In *Tagungsbericht HEUREKA 02,Karlsruhe, Forschungsgesellschaft für Strassen- und Verkehrswesen (FGSV), Köln*, 2002.

[156] L. Santen. Numerical investigations of discrete models for traffic flow. Dissertation, Universität zu Köln, 1999.

[157] W. Schnabe and D. Lohse. *Grundlagen der Straßenverkehrstechnik und der Verkehrsplanung*, volume 2. Verlag für Bauswesen, Berlin, 1997.

[158] G. Schütz. Exactly solvable models for many-body systems far from equilibrium. In C. Domb and J. Lebowitz, editors, *Phase Transitions and Critical Phenomena*, volume 19. (Academic Press, New York), 2000.

[159] G. Schütz and E. Domany. Phase transitions in an exactly soluble one-dimensional exclusion process. *Journal of Statistical Physics* **72**:277–296, 1993.

[160] T. Schwerdtfeger. Makroskopisches Simulationsmodell für Schnellstraßennetze mit Berücksichtigung von Einzelfahrzeugen (DYNEMO). Dissertation, Universität Karlsruhe, 1987.

[161] F.-N. Sentuc. Der Einfluss lokaler Verkehrsemissionen auf die Immissionssituation im Großraum Köln. Dissertation, Universität zu Köln, 2004.

[162] F.-N. Sentuc, N. Eissfeldt, M. Luberichs, and et.al. Investigating the impact of traffic based emissions on urban air pollution with a nested model system. In *Proceedings of the 4th Symposium on the Urban Environment*, pages 225–226, Norfolk,Virginia (USA), 2002. American Meteorological Society.

[163] D. Serwill. DRUM - Modellkonzept zur dynamischen Routensuche und Umlegung. Dissertation,RWTH Aachen, 1994.

[164] SFB 419, Environmental problems of industrialised regions: scientific solution strategies and socio-economic implications. See www.uni-koeln.de/sfb419.

[165] SFB 419, Ergebnisberich 1999-2001 und 2002 des SFB 419. [164], 2001.

[166] Y. Sheffi. *Urban transportation networks: Equilibrium analysis with mathematical programming methods*. Prentice Hall, Englewood Cliffs, New Jersey, 1985.

[167] M. Spahn. Reisezeiten im Nagel-Schreckenberg-Modell mit VDR und weiteren eindimensionalen Verkehrsflussmodellen auf einer offenen Kante. Diplomarbeit, Humboldt-Universität zu Berlin, 2002.

[168] U. Sparmann. Spurwechselvorgänge auf zweispurigen BAB-Richtungsfahrbahnen. *Forschung Straßenbau und Straßenverkehrstechnik* **Heft 263**, 1978.

[169] stadtinfoköln. See www.stadtinfokoeln.de/.

[170] B. Tilch and D. Helbing. Evaluation of single vehicle data in dependence of the vehicle-type, lane and site. In D. H. et al., editor, *Traffic and Granular Flow 1999*, pages 333–338. Springer, 2000.

[171] TRANSIMS. TRansportation ANalysis and SIMulation System. See http://transims.tsasa.lanl.gov/.

[172] M. Treiber and D. Helbing. Memory effects in microscopic traffic models and wide scattering in flow-density data. *Phys. Rev. E* **68**:046119, 2003.

[173] M. Treiber, A. Hennecke, and D. Helbing. Congested traffic states in empirical observations and microscopic simulations. *Phys. Rev. E* **62**(2):1805–1824, 2000.

[174] J. Treiterer and J. Myers. The hysteresis phenomenon in traffic flow. In D. Buckley, editor, *Proc. 6th Internat. Sympos. on Transportation and Traffic Theory*, pages 13–38, Sydney,Australia, 1974. Elsevier, New York.

[175] N. Vandaele, T. V. Woensel, and A. Verbruggen. A queueing based traffic flow model. *Transportation Research D* **5**(2):121–135, 2000.

[176] A. Vildósola-Engelmayer. Berechnung des Benutzeroptimums in Verkehrsnetzen mit Hilfe des Frank-Wolfe-Algorithmus. Diplomarbeit, Universität zu Köln, 1998.

[177] S. von der Ruhren, K. Beckmann, N. Eissfeldt, J. Gräfe, H. Mühlhans, and P. Wagner. Simulationsbasierte Kurzfristprognose von Verkehrszuständen im Rahmen von stadtinfoköln - Methodik, Umsetzung, Erfahrungen. In

Tagungsdokumentation (CD-ROM) 19. Verkehrswissenschaftliche Tage. TU Dresden, September 2003.

[178] P. Wagner, 2002. private communication.

[179] P. Wagner and K. Nagel. Microscopic modelling of travel demand: The home-to-work problem. In *TRB* 78nd *Annual Meeting, Paper No. 990919*, 1999.

[180] C. Walther. Geschwindigkeiten und Schadstoffemissionen des motorisierten Straßenverkehrs in innerörtlichen Netzen auf der Grundlage der EWS-Berechnungsvorschriften. *Straßenverkehrstechnik* :19–25, 1 2000.

[181] J. Wardrop. Some theoretical aspects of road traffic research. In *Proceedings of the Institute of Civil Engineers*, volume 1, pages 325–378, 1952.

[182] R. Wiedemann. Simulation des Straßenverkehrsflusses. Schriftenreihe des Instituts für Verkehrswesen, Heft 8, Universität Karlsruhe, 1974.

[183] W. Wong, S. Wong, and C. Tong. Sheared delay formulae for the TRAN-SYT traffic model: a review and calibration. *Transport Reviews* **23**(1):1–20, 2003.

[184] H. Yang and S. Yagar. Traffic assignment and signal control in saturated road networks. *Transportation Research A* **29**(2):125–139, 1995.

[185] ZAIK. Traffic Simulation Group. See www.zaik.de/AFS/traffic.

[186] F. B. Zhan. Three fastest shortest path algorithms on real road networks: Data structure and procedures. *Journal of Geographic Information and Decision Analysis* **1**(1):69–82, 1997. See http://publish.owo.ca/~jmalczew/gida_1/Zhan/Zahn.htm.

[187] H. Zhang. A note on highway capacity. *Transportation Research B* **35**:929–937, 2001.

Index

Deutsche Zusammenfassung

Ohne Zweifel ist auf unseren Straßen eine ständige Zunahme der Verkehrsmengen zu beobachten. Und ein Ende dieser Entwicklung ist angesichts der prognostizierten Zunahme von Güter- und Geschäftsverkehr nicht absehbar. Bereits die heutigen Verkehrsmengen übersteigen vielerorts die vorhandene Straßenkapazität, insbesondere in Ballungsräumen. Die resultierenden Engpässe führen zu Staus. Diese sind nicht nur ein Ärgernis für die direkt Betroffenen, sondern verstopfte Straßen führen zu volkswirtschaftlichen Kosten und beeinflussen Mensch und Umwelt. Aufgrund finanzieller und platzmäßiger Beschränkungen lässt sich dieser Situation nicht allein durch einen weiteren Ausbau der Verkehrsinfrastruktur begegnen. Vielmehr sind Strategien gefragt, die eine effizientere Nutzung existierender Kapazitäten erlauben, beispielsweise durch die Umverteilung von Verkehrsströmen und die Beeinflussung des individuellen Mobilitätsverhaltens.

Die Instrumente intelligenter Transportsysteme (ITS) versuchen eine Umverteilung von Verkehrsströmen unter anderem durch aktuelle Informationen über den Netzzustand und aktive Steuerungsmaßnahmen zu erreichen. In diesem Zusammenhang spielen Simulationsmodelle des Straßenverkehrs eine wichtige Rolle, um auf Basis lokaler Messungen eine netzweite Beschreibung des Verkehrszustandes zu erhalten. Solche Modelle erlauben es zudem, Maßnahmen, die im Rahmen von ITS eingesetzt werden sollen, bereits im Vorfeld zu testen und hinsichtlich ihrer Wirksamkeit zu bewerten. Die dynamische Verkehrsumlegung (DTA) bildet hierbei einen methodischen Rahmen, mit dem sich viele solcher Fragestellungen betrachten lassen. DTA dient dazu, die Routenwahl, Netzflüsse und Reisezeiten einer gegebenen Verkehrsnachfrage in einem Verkehrsnetz zu bestimmen. Auch hier spielen Verkehrsflussmodelle eine wichtige Rolle.

Modelle des Verkehrsflusses müssen insbesondere in der Lage sein, die dynamischen Eigenschaften von Verkehr und von Engpässen richtig wiederzugeben. Spielen für die Fragestellung Aspekte wie die individuelle Routenwahl und die Beeinflussung individuellen Fahrverhaltens eine Rolle, ist darüber hinaus ein mikroskopischer Modellansatz vorteilhaft. Das gilt insbesondere auch für die Betrachtung von Umweltwirkungen des Straßenverkehrs, da die Schadstoffemissionen von Fahrzeugen nicht allein von mittleren Verkehrsmengen abhängen, sondern stark durch dynamische Erscheinungen wie Staus und die Einzelfahrzeugdy-

namik bestimmt sind.

An diesem Punkt setzt die vorliegende Arbeit an. Im Rahmen einer Zusammenarbeit mit Meteorologen der Universität zu Köln [164] sollte ein Modellkette aufgebaut werden, mit der sich Luftbelastungen unter besonderer Berücksichtigung des Straßenverkehrs berechnen lassen (s.a. Appendix B). Zu Beginn des Projekts war geplant, die Berechnung der verkehrsbedingten Schadstoffkataster mit Hilfe einer zweistufigen Modellkette folgendermaßen zu realisieren: Im ersten Schritt wird das Routenwahlverhalten einer gegebenen Verkehrsnachfrage mit Hilfe von DTA berechnet. Das dabei verwendete Verkehrsflussmodell basiert auf einem Warteschlangenansatz [59, 60]. In einem folgenden Schritt werden die Schadstoffkataster mit Hilfe eines sehr detaillierten mikroskopischen Fahrzeugfolgemodells (SKM, [112, 113]) berechnet. Dies geschieht auf Basis der im vorherigen Schritt berechneten Routen.

Das beschriebene Vorgehen bringt jedoch Schwierigkeiten mit sich. So ist es nicht ausreichend, die Netzwerkparameter für jedes Modell isoliert an den realen Gegebenheiten zu kalibrieren. Obwohl dies für sich genommen schon einen erheblichen Aufwand darstellt, müssen vielmehr die Parameter beider Modelle derart aufeinander abgestimmt sein, dass dynamische Engpässe und auftretende Staus gleichartig in beiden Modellen abgebildet sind. Dies ist insbesondere für Verkehrnachfragen nahe der Netzkapazität von Bedeutung. Ist dieser Abgleich nicht erfüllt, führen beispielsweise *gridlocks* zu Inkompatibilitäten zwischen beiden Ansätzen.

Es ist in diesem Falle naheliegend, zu versuchen, die Emissionen des Verkehrs direkt im Schritt der DTA zu berechnen, um den zweistufigen Modellierungsansatz zu umgehen. Untersuchungen des in der DTA verwendeten einfachen Warteschlangenmodells zeigen jedoch, dass die Dynamik von Verkehrszuständen nicht hinreichend wiedergegeben wird. So existieren beispielsweise keine rücklaufenden Staus und die Flüsse an Engpässen werden tendenziell überschätzt. Weitere Untersuchungen zeigen, dass diese Probleme praktisch in allen Warteschlangenansätzen zur Modellierung von Verkehrsflüssen auftauchen, die auf klassischer Warteschlangentheorie basieren (s.a. Appendix A).

Das vornehmliche Ziel der vorliegen Arbeit ist es, diese Probleme aufgreifend, einen neuen Ansatz für die einzelfahrzeugbasierte Verkehrsflussmodellierung mit Hilfe von Warteschlangenansätzen zu entwickeln (μ-Queue Modell). Dieser soll in der Lage sein, die Dynamik verschiedener Verkehrszustände detailliert wiederzugeben ohne dabei die für DTA notwendige hohe numerische Effizienz zu verlieren.

Neben dieser Zielsetzung steht in der Arbeit die Untersuchung dynamischer Eigenschaften mikroskopischer Verkehrsmodelle im Vordergrund. Diese sind nicht nur aus Anwendungssicht von Bedeutung, sondern ihr Verständnis ist auch aus physikalischer Sicht spannend, lässt sich Verkehr doch als komplexes System vie-

ler wechselwirkender Teilchen im Ungleichgewicht auffassen. In diesem Zusammenhang gibt es viele offene Fragen, die mit dem Verständnis der Mechanismen verknüpft sind, die für den Zusammenbruch von fließendem Verkehr verantwortlich sind. Um die Schwachstellen momentan verwendeter Modell zu verstehen und die wesentlichen Modellbestandteile im Hinblick auf gemessene Daten zu identifizieren, ist ein tiefes Verständnis der Dynamik solcher Modelle entscheidend. Einige dieser Fragen werden im Rahmen dieser Arbeit anhand des SKM und des neu eingeführten Warteschlangenansatzes betrachtet.

Das mikroskopische Fahrzeugfolgemodell SKM steht hierbei im ersten Teil der Arbeit (Kapitel 2) im Vordergrund. Diese Modell wurde bereits ausführlich in [113] untersucht und die hier gemachten Untersuchungen stellen Ergänzungen dar. Neben der Untersuchung der Verteilung von Zeitlücken und der *optimal-velocity*-Kurve innerhalb des Modells beziehen sich diese auf die Modellklassen des SKM, einer Modellerweiterung um antizipatives Fahren und das Verhalten unter offenen Randbedingungen.

Innerhalb des SKM lassen sich verschiedene Modellklassen anhand des dynamischen Modellverhaltens unterscheiden. Im Parameterbereich, in dem das Modell Strukturbildung zeigt, wird eine Neuklassifizierung des Modellverhalten anhand neuerer Arbeiten zur Klassifikation stochastischer Verkehrsflussmodelle [88, 131] vorgenommen. Im Gegensatz zu Modellen die auf Zellularautomaten beruhen, besitzt das SKM Hochflusszustände, die stabil gegenüber modellimmanenten Fluktuationen sind. Es wird zudem gezeigt, dass ein Übergang zu metastabilen Hochflusszuständen auftritt, wenn das Bremsvermögen im Modell gegen Unendlich läuft. Entgegen der Annahmen der Originalarbeit [113] existieren solche Hochflusszustände immer, solange die Fluktuationsstärke nicht zu groß wird. Für die übliche Parametrisierung $\varepsilon = 1$ der Fluktuationsstärke εa sind diese Hochflusszustände praktisch im gesamten Parameterbereich mit Strukturbildung existent. Unabhängig von der Stabilität der Hochflusszustände, findet man für alle Parametrisierungen (mit $\varepsilon = 1$) mit Strukturbildung einen stabilen Ausfluss aus dem Stau.

Antizipation stellt eine wichtige Modellkomponente mikroskopischer Fahrzeugfolgemodelle im Hinblick auf die Wiedergabe empirischer Messungen dar. Diese Fahrstrategie wird hier in das SKM mittels Übernächste-Nachbar-Wechselwirkung eingeführt. Die Auswirkungen dieser zusätzlichen Modellkomponente auf die Dynamik des Modells wird mit Hilfe von Simulationen und analytischen Rechnungen untersucht. Es wird gezeigt, dass Antizipation zu einer Stabilisierung der Flüsse in dichtem Verkehr führt und eine Abbildung der empirisch gefundenen sehr kurzen Zeitlücken ermöglicht. Die übrigen Eigenschaften der Modelldynamik bleiben dabei praktisch unverändert. Der dahinter liegende Mechanismus koppelt drei aufeinander folgende Fahrzeuge und die zwei zugehörigen Zeitlücken sind dabei antikorreliert. Diese Ergebnisse lassen sich auch auf andere

Fahrzeugfolgemodelle, die mit Antizipation arbeiten, übertragen. Die im Rahmen dieser Betrachtungen durchgeführte Untersuchung der Fixpunkte des SKM zeigt, dass diese sehr stabil sind. Infolge ist zu erwarten, dass eine deutliche Modellmodifikation notwendig ist, um mit diesem Modell synchronisierten Verkehr abbilden zu können.

Die Untersuchung des SKM in beiden Modellvarianten unter offenen Randbedingungen zeigt, dass dieses ein Extremalprinzip [109, 148] erfüllt. Dieses stellt in sehr allgemeiner Weise eine Verbindung zwischen den Eigenschaften des periodischen und offenen Systems her. Das SKM besitzt neben der Freifluss- und Stauphase eine Hochfluss-Phase. Die mikroskopische Struktur dieser Phasen hat große Ähnlichkeit mit gemessenen Strukturen [76, 93, 173]. Es werden geeignete Randbedingungen eingeführt, die zusätzlich eine Untersuchung der Phasenübergänge ermöglichen. Es zeigt sich, dass der Übergang zwischen der Freifluss- und Stauphase erster Ordnung ist, die Übergänge in die Hochflussphase sind von zweiter Ordnung. Für beide Modellvarianten wird das vollständige Phasendiagramm angegeben. Die hier gemachten Ergebnisse lassen in Kombination mit [13] den Schluss zu, dass das abgeleitete Phasendiagramm und die mikroskopische Struktur der Phasen generisch für mikroskopische Fahrzeugfolgemodelle sind, die Hochflusszustände und Phasenseparation zeigen.

Im zweiten Teil der Arbeit wird ein neuer Ansatz zur fahrzeugbasierten Modellierung von Verkehrsfluss mit Hilfe von Warteschlangen vorgestellt. In Kapitel 3 zeigt die ausführliche Untersuchung bestehender Ansätze zunächst, dass die fehlende Kopplung zwischen aufeinanderfolgenden Warteschlangen dazu führt, dass verschiedene Verkehrszustände nicht existieren und Dichtefluktuationen mit unendlicher Geschwindigkeit stromaufwärts weitergegeben werden. Infolge dessen lösen sich Staus im Gegensatz zur Realität in solchen Modellen von hinten auf.

In dem neuen Ansatz (μ-Queue Modell) wird diese Kopplung eingeführt und die Fahrzeugbewegung von Warteschlange zu Warteschlange wird mit Hilfe von Zeitlücken beschrieben, wobei mit dem FIFO-Prinzip gearbeitet wird. Die hierbei verwendeten Wartezeiten am Ende einer jeden Warteschlange können als zustandsabhängige Servicezeiten der Warteschlange aufgefasst werden. Im Gegensatz zu klassischen Ansätzen, berücksichtigt diese Servicezeit nicht nur den Zustand innerhalb der Warteschlange selbst, sondern auch den Zustand ihres Nachfolgers. Infolge ist die Ausbreitungsgeschwindigkeit von Dichtefluktuation in Vorwärts- und Rückwärtsrichtung unterschiedlich und das Modell erlaubt die Abbildung rückwärtslaufender Staus.

Numerische Untersuchungen des μ-Queue Modells zeigen, dass es zwei verschiedene Verkehrszustände besitzt, homogenen und gestauten Fluss. Die deterministische Formulierung des Modells zeigt keine Übergänge zwischen diesen beiden Zuständen unter periodischen Randbedingungen. Werden jedoch Wartezeitverteilungen und Geschwindigkeitsfluktuationen eingeführt, treten solche Übergänge

auf und es lassen sich realitätsnahe Zeitlückenverteilungen simulieren.

Die Untersuchungen des Modellverhaltens stellen eine analytische Beschreibung der Fluss-Dichte-Relation für das deterministische μ-Queue Modell her. Zudem lassen sich Bedingungen an die Modellparamter herleiten, die stabile Staus erlauben. Der dem Modell zugrunde liegende Mechanismus der Bewegung von Staus wird ferner ausführlich untersucht und dargestellt.

Es wird eine ereignisorientierte Implementation des μ-Queue Modells präsentiert, deren numerische Effizienz die Verwendung des Modells zur Simulation großer Netzwerke erlaubt. Im Hinblick auf die Anwendung wird gezeigt, dass sich der Modellansatz sowohl auf Mehrspurverkehr übertragen lässt, als auch, dass die Modellierung von Schadstoffemissionen mit hoher räumlicher und zeitlicher Auflösung möglich ist.

Die sich in Kapitel 4 anschließende Untersuchung des μ-Queue Modells unter offenen Randbedingungen dient unter anderem der Vorbereitung von Netzwerksimulationen im Rahmen von DTA. Im Fall offener Ränder werden Phasenübergänge sogar zwischen den Verkehrszuständen des Modells in der deterministischen Formulierung gefunden. Das komplette Phasendiagramm des μ-Queue Modells, sowohl in der deterministischen als auch der stochastischen Formulierung , wird abgeleitet. In beiden Fällen findet man Phasen, deren mikroskopische Struktur denen im SKM ähneln. Zudem erlauben die Untersuchungen Rückschlüsse auf die Sensibilität des Modells hinsichtlich verschiedener Implementationen von Randbedingungen. Aus diesen lassen sich geeignete Elemente, wie Auf- und Abfahrten ableiten, die für die Repräsentation realer Straßennetzwerke verwendet werden können. Neben dieser theoretischen Betrachtung des Modells, werden Vergleiche mit gemessenen Verkehrssituationen unter offenen Randbedingungen durchgeführt. Hierbei wird eine sehr gute Übereinstimmung zwischen den Daten und der Modelldynamik erzielt.

Die Arbeit schließt mit der Einbettung des neuen Warteschlangenansatzes in einen simulationsbasierten Ansatz der DTA. Simulationen des Stadtgebietes von Köln werden verwendet, um die praktische Anwendbarkeit des Modells zu demonstrieren. Das Modell erlaubt die Berechnung des Routenwahlverhaltens von mehreren Millionen Einzelfahrten in akzeptabler Rechenzeit. Neben dem Aspekt der Verkehrsumlegung liegt der Schwerpunkt auf der Berechnung von Szenarien, die eine Veränderung der Belastungssituation durch Luftschadstoffe zum Ziel haben. Dazu wird sich der zu Beginn angesprochenen Modellkette bedient. Die Ergebnisse zeigen, dass das Modell in der Lage ist, Emissionskataster von hoher zeitlicher und räumlicher Auflösung zu berechnen, wie sie für die meteorologischen Modelle zur Beschreibung von Luftqualtität benötigt werden.

-

Danksagung

Erklärung

Ich versichere, daß ich die von mir vorgelegte Dissertation selbständig angefertigt, die benutzten Quellen und Hilfsmittel vollständig angegeben und die Stellen der Arbeit – einschließlich Tabellen, Karten und Abbildungen –, die anderen Werken im Wortlaut oder dem Sinn nach entnommen sind, in jedem Einzelfall als Entlehnung kenntlich gemacht habe; daß diese Dissertation noch keiner anderen Fakultät oder Universität zur Prüfung vorgelegen hat; daß sie – abgesehen von unten angegebenen Teilpublikationen – noch nicht veröffentlicht worden ist sowie, daß ich eine solche Veröffentlichung vor Abschluß des Promotionsverfahrens nicht vornehmen werde.

Die Bestimmungen dieser Promotionsordnung sind mir bekannt. Die von mir vorgelegte Dissertation ist von Prof. Dr. Rainer Schrader und Priv.-Doz. Dr. Andreas Schadschneider betreut worden.

Teilpublikationen

N. Eissfeldt and R. Schrader, Calculation of street traffic emissions with a queueing model, *Journal of Computational Technologies*, **7**:5-15, 2002

N. Eissfeldt, M. Luberichs and F.-N. Sentuc, A breath of fresh air, *Traffic Technology International*, 76-80, Aug/Sep 2002

A. Namazi, N. Eissfeldt, P. Wagner and A. Schadschneider, Boundary-induced phase transitions in a space-continuous traffic model with non-unique flow-density relation, *European Physical Journal B*, **30**:559-570, 2002

N. Eissfeldt and P. Wagner, Effects of anticipatory driving in a traffic flow model, *European Physical Journal B*, **33**:121-129, 2003.

Lebenslauf

Persönliche Daten

Name	Nils Gustaf Eissfeldt
Adresse	Sülzburgstraße 170, 50937 Köln
geboren am	27.07.1972 in Aachen
Staatsangehörigkeit	deutsch
Familienstand	verheiratet, zwei Kinder

Schulbildung

1978 - 1982	Grundschule in Richterich, Aachen
1982 - 1991	Kaiser-Karls-Gymnasium in Aachen

Zivildienst

08/1991 - 10/1992	Malteser Hilfsdienst in Aachen

Studium

11/1992 - 09/1998	Studium der Physik, Abschluß Diplom-Physiker
1992 - 1993	TU München
1993 - 1994	RWTH Aachen
1994 - 1995	Université de Paris-Sud
1995 - 1997	RWTH Aachen, Studentische Hilfskraft am Institut für theoretische Physik B und am 1. Physikalischen Institut der RWTH Aachen
1997 - 1998	Forschungszentrum Jülich
10/1999 - 11/2003	Wirtschaftswissenschaftliches Zusatzstudium für Naturwissenschaftler an der Fernuniversität Hagen, Abschluß Diplom-Wirtschaftsphysiker

Berufstätigkeit

01/1999 - 06/2004	Wissenschaftlicher Mitarbeiter am Zentrum für Angewandte Informatik (ZAIK), Arbeitsgruppe Faigle/Schrader, Universität zu Köln